# Volants thermiques cryogéniques liquide vapeur pour applications spatiales

Josiana Prado Afonso

UNIVERSITÉ DE GRENOBLE

# THÈSE

Pour obtenir le grade de

## DOCTEUR DE L'UNIVERSITÉ DE GRENOBLE

Spécialité : **Mécanique des Fluides, Procédés, Énergétiques**

Arrêté ministériel : le 6 janvier 2005 -7 août 2006

Et de

## DOCTEUR DE L'UNIVERSIDADE NOVA DE LISBOA

Spécialité : **Génie Physique**

**préparée dans le cadre d'une cotutelle entre l'*Université de Grenoble* et *l'Universidade Nova de Lisboa***

Présentée par


## Josiana PRADO AFONSO


Thèse dirigée par **Bernard ROUSSET** et **Grégoire BONFAIT**
codirigée par **Ivan CHARLES et Isabel CATARINO**

préparée au sein des **SBT, Grenoble** dans **l'École Doctorale IMEP2**
et au sein du **CEFITEC, FCT** dans l'**Universidade Nova de Lisboa**

# Volants thermiques cryogéniques liquide vapeur pour applications spatiales

Thèse soutenue publiquement le **7 de juin de 2013**
devant le jury composé de :

**Mr Jorge PAMIES TEIXEIRA**
Professeur à l'Universidade Nova de Lisboa, Président
**Mr Marcel TER BRAKE**
Professeur à l'Université de Twente, Rapporteur
**Mr António AMORIM**
Professeur à l'Universidade de Lisboa, Rapporteur
**Mr José REBORDÃO**
Professeur à l'Universidade de Lisboa, Membre
**Mr Bernard ROUSSET**
Ingénieur chercheur au CEA Grenoble, Membre
**Mr Grégoire BONFAIT**
Professeur à l'Universidade Nova de Lisboa, Membre
**Mr Ivan CHARLES**
Ingénieur chercheur au CEA Grenoble, Membre
**Mme Isabel CATARINO**
Professeur à l'Universidade Nova de Lisboa, Membre

# Declaration

**Towards Cryogenic Liquid –Vapor Energy Storage Units for space applications**

# Acknowledgements

For this thesis, I received help from many people and their influence is noticeable in the contents of this thesis.

First of all, I would like to thank Prof Bonfait and Prof Isabel for the opportunity they gave me, back in 2007, to take part in the research at the cryogenic lab at CEFITEC/UNL, where I started out as a researcher.

I would like to acknowledge the help and support received during my thesis in Portugal.

Regarding my stay in Grenoble, I want to thank the Dr Girard , the head of the Service de Basses Temperatures of CEA and Dr Duband, the head of the cryocoolers and space cryogenics group) for having welcomed me.

I could never thank enough for the support provided by Dr Charles, who over almost the past three years has not only helped me, providing all the necessary technological and scientific information, but also gave me all his support whenever I needed it.

Mention has to be made of the help given by Dr Rousset, who, despite not being near my working place, was always ready to provide his scientific support whenever I needed clarification.

Concerning my thesis report, I would like to thank my four supervisors and I would like to say how obliged I feel for all the time, patience and accuracy provided and showed by Dr Charles and Dr Rousset, who despite the distance were always available to help me either on phone or by email.

I would like to thank:

Dr Gully for the conversation we had about heat transfer in the porous media with diphasic helium and for his great help in developing the model presented in the thesis.

Alexandre Coynel for his availability and help at the lab, mainly with the set-up and solve technical problems.

Dr Prouve for his willingness and availability to solve a leakage problem in the set-up and to continue the experiment when I had to go back to Portugal.

All people of the Service de Basses Temperatures for making me feel at home during the stay at their lab and for the excellent working environment. I thank all the people who spent their time teaching me their know-how and helped me.

Large thanks to all the members of the jury who agreed to assess this work.

To cabinet colleagues in Portugal and Grenoble: Daniel, Diogo and Aurélia, who allowed for moments of relaxation during experiments.

To all my friends from Portugal and Grenoble who walked with me this academic path, who shared joys, sadness, victories and moments of stress. A special word of gratitude goes to Patricia, Adérito, Angela -my good confidents.

I want to thank my mother and my sister, who, although far away, were always there to encourage me in bad times and congratulated me in good times. I also thank David for his availability to help me.

Special thanks to several Institutions for their support::

- To Fundação da Ciência e da Tecnologia for giving me a PhD scholarship (SFRH/BD/60357/2009) and a financial support for the project "Cryogenic Temperature Stabilizers" (PTDC/EME-MFE/101448/2008),

- To European Space Agency for the project "Low-temperature Energy Storage Unit for 20K-80K applications", European Space Agency (ESA), No 21879/08/NL/CBI
- To CEA-Grenoble/Service de Basses temperatures, Grenoble, France;
- To CEFITEC, and the Physics Department of Faculdade de Ciência e Tecnologia of Universidade Nova de Lisboa, Portugal.

Thanks to everyone who participated in this remarkable experience of my life!

# Sumário

O desenvolvimento de criorrefrigeradores e de sensores cada vez mais sensíveis, torna interessante usar unidades de armazenamento de energia (Energy Storage Unit-ESU) e desligar o criorrefrigerador para funcionar num ambiente sem vibrações. Em particular para as aplicações espaciais, seria também útil, utilizar um ESU para evitar sistemas criogénicos sobredimensionados para atenuar as flutuações de temperaturas devidas às variações de carga térmica. Em ambos os casos, a deriva de temperatura deve manter-se limitada para manter o bom desempenho dos detectores.

Nesta tese, ESUs utilizando o calor latente associado à mudança líquido-vapor como reservatório de energia foram estudados. A fim de limitar a deriva de temperatura, enquanto se mantém de tamanho reduzido a célula a baixa temperatura, uma solução possível consiste em dividir o ESU em dois volumes: uma célula a baixa temperatura acoplada ao dedo frio do criorrefrigerador mediante um interruptor térmico conectado a um volume de expansão à temperatura ambiente para reduzir o aumento de temperatura que ocorre durante a evaporação do líquido. Para diminuir ainda mais a deriva de temperatura, foi testado uma nova ideia que consiste na introdução de uma válvula entre os dois volumes a fim de controlar a pressão na célula. Para tornar o ESU independente da gravidade e assim adaptado às aplicações espaciais, os efeitos da capilaridade foram utilizados usando um material poroso na célula. Neste caso, as experiências revelam resultados inesperados referentes ao armazenamento de energia e à diferença de temperatura entre o líquido e as paredes.

Para descrever as modificações térmicas devidas ao meio poroso, uma célula com paredes laterais pouco condutoras foi construída e testada com hélio. Após uma caracterização completa fora das condições de saturação (condução, convecção), esta célula foi utilizada para experiências com e sem meio poroso, aquecida na parte superior ou na parte inferior com diferentes fluxos de calor e para várias temperaturas de saturação. Em paralelo, um modelo que descreve a resposta térmica de uma célula contendo líquido e gás num meio poroso aquecido na parte superior (“contra a gravidade”) foi desenvolvido. Os resultados obtidos foram utilizados como referência ao modelo que se baseia no equilíbrio de três forças: a força de capilaridade, a força da gravidade e perda de carga induzida pelo escoamento do líquido.

**Palavras-chave**: unidades de armazenamento de energia, azoto, azoto, hélio, transferência de calor, meio poroso, capilaridade.

# Résumé

Avec le développement des réfrigérateurs cryogéniques mécaniques et des capteurs de plus en plus sensibles, l'emploi d'un volant thermique (**E**nergy **S**torage **U**nit ou ESU) doit permettre de stopper temporairement le cryoréfrigérateur et de fonctionner en l'absence de vibration. L'utilisation d'un ESU limite également la nécessité de surdimensionner le système cryogénique pour absorber les éventuelles surcharges thermiques transitoires; ce qui est particulièrement utile pour les applications spatiales. Dans tous les cas, la dérive en température doit rester limitée pour garantir la bonne performance du détecteur.

Dans cette thèse, des ESUs basés sur la chaleur latente associée au changement de phase liquide-vapeur ont été étudiés. Afin de limiter la dérive en température, tout en maintenant un volume réduit pour la cellule à basse température, une solution possible consiste à séparer l'ESU en deux volumes: une cellule à basse température reliée au doigt froid du cryoréfrigérateur à travers un interrupteur thermique et un volume d'expansion à la température ambiante permettant de réduire l'augmentation de température liée à l'évaporation du liquide. Pour diminuer encore la dérive en température, une nouvelle amélioration a été testée avec de l'azote: elle consiste en la mise en place d'une vanne commandée entre les deux volumes permettant de contrôler la pression de la cellule froide (remplie d'azote liquide-vapeur). De plus, un matériau poreux a été introduit à l'intérieur de la cellule pour rendre l'ESU indépendant de la gravité et donc approprié aux applications spatiales. Dans ce cas, les expériences révèlent des résultats inattendus concernant le stockage d'énergie et la différence de température entre le liquide et les parois.

Pour caractériser l'influence des milieux poreux sur les transferts thermiques d'un volant thermique liquide-vapeur chauffé, une cellule dédiée avec des parois latérales non conductrices a été construite et testée avec de l'hélium diphasique liquide-vapeur. Après caractérisation complète de cette cellule en dehors des conditions de saturation (conduction, convection), des expériences ont été effectuées avec ou sans milieu poreux, en chauffant la cellule en haut ou en bas de la cellule et pour différents flux de chaleur et températures de saturation. En parallèle, un modèle décrivant la réponse thermique d'une cellule contenant liquide et vapeur avec un milieu poreux chauffée en haut (contre la gravité) a été mis en œuvre. L'ensemble des données a ensuite été utilisé comme référence pour ce modèle qui repose sur un équilibre de trois forces: la force de capillarité, la force de gravité et la perte de pression induite par l'écoulement du liquide.

**Mot-clés** : volant thermique, azote, hélium, transfert de chaleur, milieu poreux, capillarité.

# Abstract

With the development of mechanical coolers and very sensitive cryogenic sensors, it could be interesting to use Energy Storage Units (ESU) and turn off the cryocooler to operate in a free micro vibration environment. An ESU would also avoid cryogenic systems oversized to attenuate temperature fluctuations due to thermal load variations which is useful particularly for space applications. In both cases, the temperature drift must remain limited to keep good detector performances.

In this thesis, ESUs based on the high latent heat associated to liquid-vapor phase change to store energy have been studied. To limit temperature drifts while keeping small size cell at low temperature, a potential solution consists in splitting the ESU in two volumes: a low temperature cell coupled to a cryocooler cold finger through a thermal heat switch and an expansion volume at room temperature to reduce the temperature increase occurring during liquid evaporation. To obtain a vanishing temperature drift, a new improvement has been tested using two-phase nitrogen: a controlled valve was inserted between the two volumes in order to control the cold cell pressure. In addition, a porous material was used inside the cell to turn the ESU gravity independent and suitable for space applications. In this case, experiments reveal not fully understood results concerning both energy storage and liquid-wall temperature difference.

To capture the thermal influence of the porous media, a dedicated cell with poorly conductive lateral wall was built and operated with two-phase helium. After its characterization outside the saturation conditions (conduction, convection), experiments were performed, with and without porous media, heating at the top or the bottom of the cell with various heat fluxes and for different saturation temperatures. In parallel, a model describing the thermal response for a cell containing liquid and vapor with a porous medium heated at the top (“against gravity”) was developed. The experimental data were then used as a benchmark for this model based on a balance of three forces: capillarity force, gravity force and pressure drop induced by the liquid flow.

**Keywords:** Energy storage units, nitrogen, helium, heat transfer, porous media, capillarity

# List of Contents

# List of Figures

# List of tables

# List of Variables

| | |
|---|---|
| C | specific heat |
| Q | heat |
| L | latent heat |
| m | mass |
| $T_{ER}$ | temperature of enthalpy reservoir |
| $T_{liq}$ | temperature inside the cell |
| $T_{top}$ | temperature on the top end of the cell |
| $T_{bottom}$ | temperature on the bottom end of the cell |
| $Q_{para}$ | parasitical energy |
| $U_{cell}$ | internal energy |
| $h_{vapor}$ | enthalpy vapor |
| $P_{sat}$ | saturation pressure |
| $T_{sat}$ | saturation temperature |
| $P_{fill}$ | filling pressure |
| $T_{PC}$ | pre-cooling temperature |
| $T_F$ | Functional or final temperature |
| $P_F$ | Functional or final pressure |
| $P_{min}$ | minimal pressure |
| t | time |
| $P_{ESU}$ | pressure inside the cell |
| $P_{EXP}$ | pressure in the expansion volume |
| n | number of moles evaporated |
| $T_{\text{cold finger}}$ | temperature of cold finger |
| Z | compressibility factor |
| $\rho$ | density |
| E | energy |
| $u_f$ | specific internal energy at initial temperature |
| $u_i$ | specific internal energy at final temperature |
| V | volume |
| Cv | volumetric specific heat capacity |
| $\sigma_{stress}$ | stress |
| D | diameter |
| $t_{hic}$ | thickness of cell wall |
| $T_I$ | initial temperature of energy storage unit |
| σ | surface tension |
| Ø | diameter capillaries |
| $\rho_{liq}$ | liquid density |
| $\rho_{vap}$ | vapor density |
| h | capillary height |
| $l_c$ | capillary length |
| R | Thermal resistance |
| $Ra_l$ | Rayleigh number |
| $P_r$ | Rayleigh number |

| | |
|---|---|
| $Nu$ | Nusselt number |
| $\mu$ | dynamic viscosity |
| $C_p$ | specific heat |
| $\lambda$ | thermal conductivity of the liquid in the cell |
| $L_c$ | characteristic length |
| $T_h$ | temperature of the hot surface |
| $T_c$ | temperature of the cold surface |
| $\beta$ | volume coefficient of expansion |
| $A_s$ | area of the cell |
| k | permeability |
| H | height of cell |
| $\lambda^*$ | effective thermal conductivity |
| $Cp_l$ | specific heat capacity of liquid |
| $C_{HS}$ | conductance of heat switch, |
| A | section of the cell |
| $\varepsilon$ | porosity of ceramic |
| $\alpha$ | part of liquid that is stored inside the ceramic |
| r | radius pore |
| $E_{origin}$ | accessible energy at the y-intercept. |
| $E_{acess}$ | accessible energy |
| $E_{theor}$ | theoretical energy |
| $H_{en}$ | enthalpy |
| $\Delta P_{cap}$ | capillary pressure |
| $\Delta P_g$ | gravitational force |
| $\Delta P_{FL}$ | pressure drop induced by liquid flow |
| $\Delta P_{FV}$ | pressure drop induced by vapor flow |
| $U_L$ | filtration velocity of liquid |
| $U_V$ | filtration velocity of vapor |
| $D_{vol-L}$ | volumetric flow rate |
| $V_{cell}$ | volume of cell |
| $\dot{Q}$ | load heat |
| $\dot{m}$ | mass flow rate |
| g | gravity acceleration |

Acronyms

| | |
|---|---|
| ESU | Energy Storage Unit |
| CTSU | Cryogenic Thermal Energy Storage Unit |
| TSU | Thermal Storage Unit |
| PCM | phase change material |
| SEM | Scanning electron microscope |

# Introduction

The latest advances in spatial missions require cryogenic systems that provide to very sensitive sensors a low (e.g. from 50 mK to 100K) and a stable temperature to very sensitive sensors and, as far as possible, without vibration generation [1–4].

To reach the low temperature, a cryostat filled with liquid and/or a cryocooler are used. However, both systems have some disadvantages: the cryostat has a finite lifetime (for instance, the 2400 liters helium reservoir of Herschel satellite will be depleted this year) and the cryocooler, even with the Pulse Tube developments, generate vibrations due to the expansion-compression processes inherent to their operation and due to moving parts on the compressor side [5]. In some cases, these vibrations are incompatible with the very sensitive sensors needed for high precision measurements. A potential solution for this problem would be to stop the cryocooler during the measurements [6–8]; however this would lead to a rapid increase of the sensor temperature. To reduce this temperature increase, it is possible to couple the detection stage to an Energy Storage Unit (ESU) which is a system able to store the parasitical heat load and the heat dissipated by the sensors itself in order to maintain the sensors at low temperature in a totally vibration-free environment. Let us note that such systems have also ground applications for any system using regenerative cryocooler and requiring a negligible vibration level. Such an ESU can also be useful to maintain a stable temperature by absorbing the heat bursts released by sensors [2][9] or, integrated in a cryogenic chain, adsorbing the heat bursts occurring during regeneration phase of adsorption or adiabatic demagnetization refrigerator [10].

To store thermal energy at low temperature, the sensible heat of materials with high specific heat or the latent heat associate to fluid phase changes can be used. To facilitate its integration in a cryogenic system, the ESU shall be as small as possible, and, as usual for space applications, it has to be as light as possible. This requirement leads to minimization of the mechanical support sections which helps reducing the heat leaks coming through. Furthermore the space application ESU must be insensitive to the gravity effect.

The ideal energy storage system would not have any temperature drift during the energy storage phase of operation. The ESUs using the triple point of pure systems are then the best candidates for stability but unfortunately such system can only work for limited discrete temperatures and cannot be employed below 13.8 K (the hydrogen triple point). An alternative solution was imagined and tested during this thesis consists in using a system that allows the evaporation of liquid at constant temperature by using a pressure control. This controlled solution has some advantages: the working temperature can be a priori chosen as far as it corresponds to a temperature on the saturation line of a cryogenic liquid. It is shown in this thesis that such systems compete favorably when compared with a triple point solution in energy capacity per cold volume unit. The ESUs with two phase fluid need to incorporate porous media to confine the liquid inside the cell [3][6][9]. However this porous media has to be chosen properly, pore diameter and void fraction being some of the issues to be solved. Thermal response of such system has been poorly studied and both data and theory are still lacking: fulfilling this lack is one of the goals of this thesis.

This thesis is organized in four chapters. In the first chapter, a review of the state of the art about the existing low temperature ESUs is presented. This section is divided using the different types of storage techniques.

The second chapter is about original ESUs that used the latent heat associated to nitrogen liquid-vapor transition. Two systems are presented: the first one is a simple liquid-vapor enthalpy reservoir while the second one is equipped with a temperature control. These two kinds of ESUs were designed and built during the thesis are able to store 4.0 kJ between 75.7 K – 80.8 K and 1.5 kJ at 81 K respectively using the two-phase liquid-vapor nitrogen. Each ESU consists of a nitrogen reservoir, coupled to a cryocooler's cold finger by a gas-gap switch. The energy is absorbed by the latent heat due to liquid evaporation along the saturation curve. To reduce the temperature drift of the low temperature reservoir during the heat absorption phase, this reservoir is connected to an expansion volume at room temperature (dual volume configuration). This second volume is used in order to limit the rise of the pressure and consequently limit the rise of the temperature while following the saturation line. The temperature drift versus the energy absorbed is an important feature of an ESU, because it can be a serious inconvenient for some particularly sensitive application. One way to decrease this temperature drift is to use a larger expansion volume. Another new possibility is to keep the saturated pressure fixed (and also the saturated temperature) at the required set point value. This control of pressure is the main novelty of the second kind of ESU built and tested here. The whole system is pumped (by liquefaction during cooling down) below the required pressure and a valve is introduced between the cold reservoir and the expansion volume. During the transient load, the aperture of the valve is controlled to adjust the pressure drop between the two volumes in order to keep the set point pressure inside the cold reservoir. The control can only be made until the expansion volume reaches the saturation pressure.

If designed for space applications, the ESU must be insensitive to gravity. The use of an adequate porous media is required: this media should be as light as possible, have only open pores with a typical size insuring a capillary height roughly equal to the dimension of the cell for ground demonstration. Porous ceramic was chosen and tests revealed some unexpected behaviors. The presence of ceramic enhances the wall heat transfer in the boiling regime. Furthermore, below a certain liquid quantity in the cell, the cell wall and the fluid becomes progressively thermally decoupled. This issue will be studied by using a dedicated cell that is described in the fourth chapter.

In the third chapter, the study on the sizing of a single volume ESU using helium that absorbs 300 J between 4.5 K and 4.7 K is presented as well as the reason leading to the choice of helium. The coupling of this kind of ESU with an adsorption refrigerator was studied for the SPICA mission (2021) as a potential solution to increase the duty cycle of the one shot sub-kevin coolers [11]. This ESU will use the latent heat associated to the liquid gas transition of helium. A sensitivity study to initial temperature and temperature drift was carried out to see the impact on the ESU design. Beyond thermodynamics, the cell thickness is calculated in order to obtain a first approximation of the weight of such a system. A porous medium was also proposed to turn the ESU insensible to gravity. But in this case where the drift of temperature is quite small ($\approx 0.2$ K), the heat transfer between the cell wall (where the heat load is applied) and the fluid confined in the pores should be excellent. As previously mentioned, the thermal heat transfer in presence of ceramic exhibits an unexpected behavior. A dedicated experimental set-up was developed to allow a better understanding of the capillarity effect in the porous media and characterize the heat transfer. This is the subject of the last chapter

The fourth chapter presents the mentioned experimental set-up as built to collect experimental data and analyze the influence of the porous media on heat transfer. Tests at different saturation temperature (2.55 K, 3.55 K and 4.65 K) and with different heat flux were performed and analyzed. Different ceramic and cell heights have been investigated. The experimental setup consists in a cylindrical low temperature cell connected to a very large expansion volume at room temperature. The function of the expansion volume is to keep the low temperature as constant as possible in order to maintain the helium properties almost constant during the measurements. The top and the bottom of the cell are thermally connected mainly through by the fluid with the goal of studying the effect of capillarity: the lateral wall is

built in thin stainless steel and not in a high thermal conductivity material as it would be the case for spatial applications. First of all, the cell was fully characterized outside liquid-vapor equilibrium; thermal conductivity measurements have been performed with and without the ceramic inside the cell. Natural convection inside the cell was also studied using a heater on its bottom and helium gas inside. To keep subcooled liquid inside the cell, the cold finger was connected to the top of the cell. In the following tests, this connection was dismantled and the cold finger was linked to the cell bottom. A thermal heat switch is used to couple the experimental cell to the cold source during condensation being decoupled during thermal characterization. Heat flux was applied either on the top or on the bottom of the cell to check the gravity influence. Furthermore, the fluid temperature was varied to analyze the dependence of the effects to the surface tension and density. Finally, a second cell with twice the height of the first one was also tested. Results showed the same surprising heat transfer behavior as in liquid-vapor nitrogen ESU. However a new phenomenon was observed: The accessible storage energy depends on the level of the applied power: the higher the power the lower the accessible storage energy. So, a phenomenological model able to describe this unexpected ESU thermal behavior when the power is applied at the top of the cell (anti gravity tests) was developed and benchmarked against the experimental results. This model is based on a balance of three forces: capillarity force, gravity force and pressure drop induced by the liquid flow. The results obtained help to predict the performance of an ESU with two phase fluid when heat is applied.

# Chapter 1: Thermal Energy Storage Unit

An Energy Storage Unit (ESU), also called Cryogenic Thermal Energy Storage Unit (CTSU) or Thermal Storage Unit (TSU) consists in a system able to store thermal energy in order to be used as a temporary cold source [6] or as a thermal buffer to attenuate temperature fluctuations due to heat bursts [2]. Incorporating an ESU may minimize the cryocooler's size, weight, peak input power and increase the cryocooler's lifetime [4].

The combined cryocooler-ESU system is ideal to store the heat generated by the sensor for some period of time while the cryocooler is stopped. This provides a cryogenic environment free of any vibration and electromagnetic noise produced by cryocooler compressors.

## 1.1 Types of storage techniques for ESU

The mains goal of a thermal ESU is then to store the maximum energy in a determined range of temperature in a small and light volume.

There are two types of physical effects that can be used for such ESU: using the specific heat of materials or using latent heat associated to a liquid-vapor, solid-vapor, solid-liquid or solid-solid phase transition of cryogens:

- In the first type, a material with high specific heat (C) is chosen in order to absorb the heat (Q) by a small temperature T increase of the material without involving any first order phase transition: $\Delta T = Q/C$. The higher the heat capacity, the smaller the temperature increases. At low temperature (typically, $T < 30$ K), the specific heat of the material is usually low, then to improve this storage capability, materials with specific heat anomaly are preferred. Such specific heat anomalies occur during magnetic phase transitions such as paramagnetic to magnetic order (ferromagnetic, antiferromagnetic, ferrimagnetic orders). These transitions are of second order and exhibit a peak in C(T).
- In the second type, the heat is stored by transformation of a phase into another. At low temperature, the typical phase changes are solid ↔liquid, solid ↔vapor, liquid ↔vapor and solid↔solid. On contrary to magnetic transitions, these phase changes are of first order and lead to a latent heat L (of fusion, of sublimation, of vaporization, respectively). During a transformation of an infinitesimal mass quantity dm from a phase to another, an energy $Q = L\,dm$ is absorbed. If pressure is kept constant, the transformation occurs at constant temperature. If the system is closed (constant mole number), the phase transformation is usually accompanied by a pressure increase and then, on the coexistence line, by a temperature increase. However, on a triple point of a pure substance (solid, liquid and vapor, for instance), simultaneous coexistence of three phases leads to a phase transformation occurring at constant temperature (Gibbs' phase rule) and pressure.

Two designs of latent heat ESU can be distinguished upon the number of volumes involved: single volume and dual volume. In the single volume design, all the working fluid is stored in the low temperature cell whatever the temperature. The high filling pressure at room temperature, necessary to obtain a non neglectable condensed phase quantity at low

temperature, leads to an increase of the wall thickness and the corresponding cell weight. The design is simple and can be relatively compact.

A dual volume ESU consists in a cell at low temperature connected to a storage tank at room temperature Figure 1.1 [2]. In this configuration, the filling pressure is lower than in a single volume for a given working fluid mass and the energy reservoir becomes lighter and smaller than in a single volume. Some volumetric studies are summarized in Table 1.1 that can help on a trade-off between both configurations [2]. However, this double volume solution has as a main inconvenient: the increase of the total volume of the system and the need for plumbing between the low temperature and the room temperature vessels.

Some publications on the subject are summarized in next subsections (1.2, 1.3 and 1.4). These publications are divided according to the different types of storage technique used.

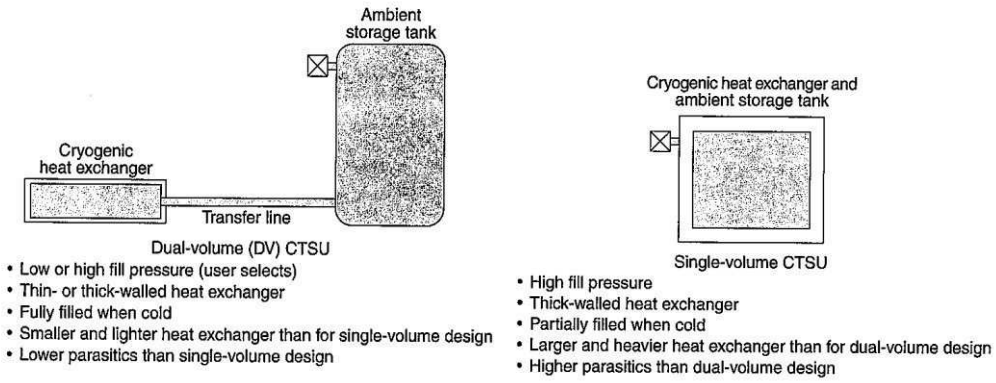


**Figure 1.1: Single and dual volume ESU [2].**

**Table 1.1: Comparison between single volume and dual volume system [2]. "PCM" stands for Phase Change Material.**

| Requirements | | | | Single-Volume Results | | | Dual-Volume Results | | |
|---|---|---|---|---|---|---|---|---|---|
| Oper. Temp. | PCM | Energy Storage (J) | PCM Mass (g) | Minimum Heat Exchanger Core Void Volume at 34.5 MPa Fill Pressure ($cm^3$)[a] | Minimum Spherical Heat Exchanger Total Core Diameter (cm)[b] | Spherical Shell Thickness for 103.4 MPa Shell Material (cm)[c] | Minimum Heat Exchanger Core Void Volume at 3.45 MPa Fill Pressure ($cm^3$)[a] | Minimum Spherical Heat Exchanger Total Core Diameter (cm)[b] | Spherical Shell Thickness for 103.4 MPa Shell Material (cm)[c] |
| 25 | Ne | 5000 | 305 | 1081 | 16.0 | 2.7 | 243 | 9.8 | 0.16 |
| 35 | $N_2$ | 5000 | 568 | 1439 | 17.6 | 2.9 | 653 | 13.6 | 0.23 |
| 54 | $O_2$ | 5000 | 360 | 797 | 14.5 | 2.4 | 283 | 10.3 | 0.17 |
| 57 | $NF_3$ | 5000 | 235 | 234 | 9.6 | 1.6 | 153 | 8.4 | 0.14 |
| 63 | $N_2$ | 5000 | 195 | 493 | 12.3 | 2.1 | 224 | 9.5 | 0.16 |
| 83 | Ar | 5000 | 168 | 298 | 10.4 | 1.7 | 118 | 7.7 | 0.13 |
| 90 | $CH_4$ | 5000 | 86 | 381 | 11.3 | 1.9 | 205 | 9.2 | 0.15 |

[a]Ideal gas assumed.
[b]$r_D$ = relative density core = 0.5, 100% fill.
[c]Safety factor of 2.

## 1.2 Sensible heat ESU

In this section, some published examples of ESU using the high specific heat of a material are presented.

### 1.2.1 ESU at 20 K using lead

Due to this relatively low Debye temperature, the lattice specific heat of lead is still relatively large compared to other materials and then was previously used for an ESU build and tested to store 36 J between 10 K and 20 K in CEFITEC (Universidade Nova de Lisboa) [7][8]. In Figure 1.2 is shown the specific heat of lead compared to other usual material frequently used in cryogenics.

This device is composed by an energy reservoir (ER) and a heat switch. The ER is a cylindrical copper container (19 mm depth; 30/28 Outer/inner diameter) (Figure 1.3) built with a cylindrical copper rod at its core in order to promote temperature homogeneity. Total mass of copper is 46 g. Inside the copper container 10 $cm^3$(113 g) of lead was melted at 380 ºC to ensure a good contact between copper and lead. The heat switch connects the ER with the cryocooler. The heat switch is used to manage the thermal conduction between its two extremities.

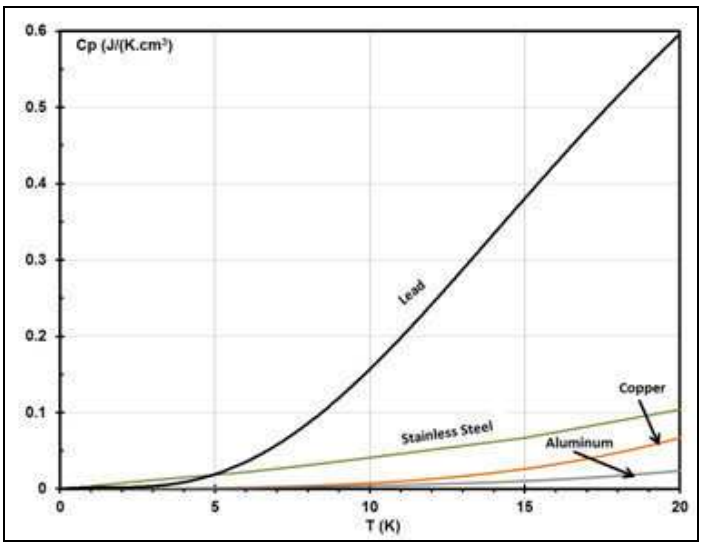


**Figure 1.2: Specific heat of lead and other usual material frequently used in cryogenics as a function of temperature.**

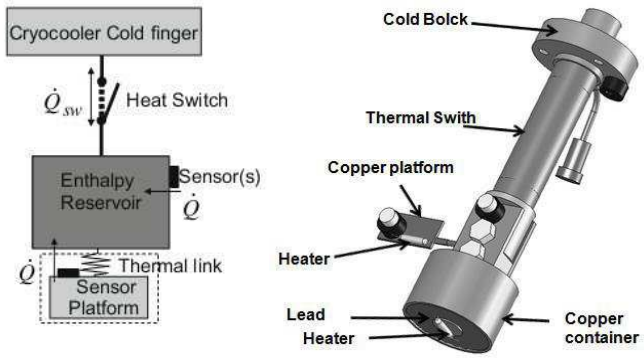


**Figure 1.3: Schema (left), and 3D view (right) of ESU composed by enthalpy reservoir and thermal switch [7].**

A heating resistor was attached on the ER to apply an external heat load during the tests. In Figure 1.4, is shown a test result when 4.6 mW was applied to the lead ER. During one hour, the ESU stored 36 J between 11 K and 20 K in a vibration-free environment. The thermal diffusion time is 0.1 s and 10 s at 10 K and 20 K respectively, much shorter than the experimental time.

One way to avoid the temperature drift and to maintain the temperature constant at 20 K was explored by a weakly coupled copper platform, temperature controlled, that uses the reservoir as a cold source.

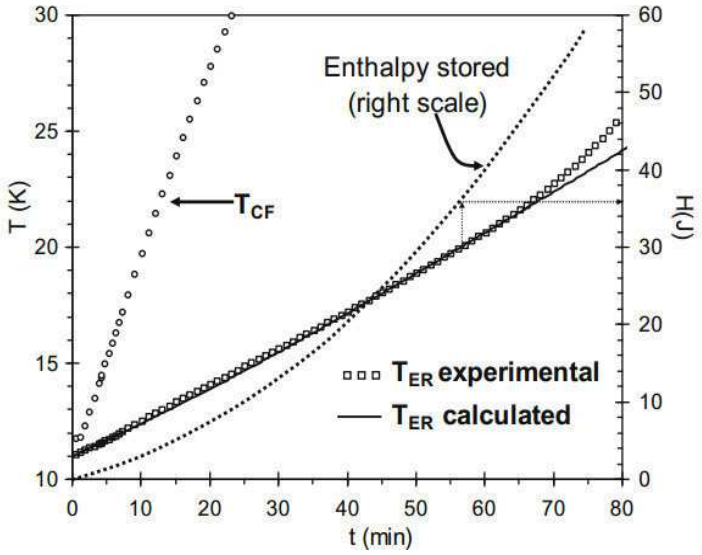


**Figure 1.4: The variation of enthalpy reservoir ($T_{ER}$) calculated (solid line) and experimental (squares) when 4.6 mW was applied. The $T_{CF}$ represents the cold finger temperature of the cryocooler. The dotted line represents the enthalpy stored (right axis) in the enthalpy reservoir between T and 11 K [7].**

### 1.2.2 ESU at 6 K using $Gd_2O_2S$

Another sensible heat ESU was built in CEFITEC. This device uses spheres of $Gd_2O_2S$ (GOS) to store energy between 3 K and 6 K [12][8]. This ceramic material has a high heat capacity peak at 5.2 K (see Figure 1.5) due to a paramagnetic-antiferromagnetic phase transition. The enthalpy reservoir was dimensioned to store 36 J between 3 K and 6 K.

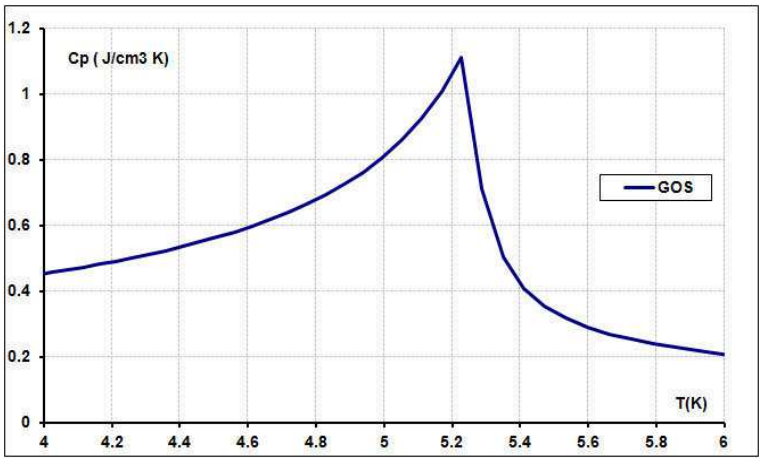


**Figure 1.5: Specific heat of GOS as a function of temperature.**

A copper recipient (38.5 $cm^3$) was built to contain the 24.6 $cm^3$ of spheres of GOS with a copper rod at the centre to improve the temperature homogeneity (Figure 1.6). To ensure the spheres thermalisation, helium (100 kPa at room temperature) was introduced in the recipient as exchange gas. This container was indium sealed by a brass lid.

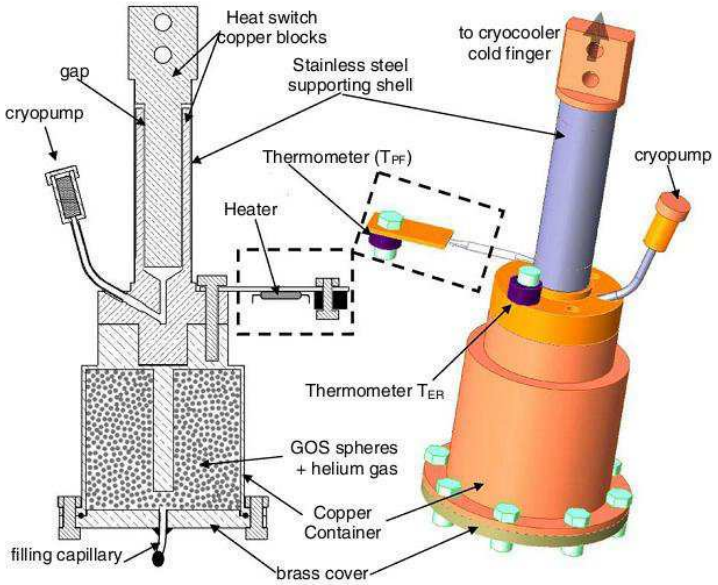


**Figure 1.6: Cross section (left) and 3D view (right) of ESU composed by enthalpy reservoir and thermal switch [12].**

This enthalpy reservoir was attached to the cold finger of a cryocooler through a heat switch. Thermometers and heaters were thermalized to the copper container. Two different tests were performed. In the first test, the thermal load of 10 mW was applied directly on the reservoir. Between 3 K and 6 K the ESU stored 25.8 J, significantly lower than expected. Several reasons that explain this discrepancy are presented elsewhere [12].

In a second experiment, the heater was attached to a weakly coupled platform. During this test, the cryocooler is stopped and the platform temperature is maintained controlled at 6 K during 51 min. The ESU absorbed 24.8 J. In both cases, the ESU is used as a vibrationless cold source.

### 1.2.3 Ball Aerospace ESU at 15 K using lead

The Ball Aerospace company built a Hybrid 10 K Cryocooler [13].This machine is a combination of the Joule Thomson cooling stage (reaching 10 K) with a Stirling precooler (reaching 15 K). A TSU (Thermal Storage Unit) that consists of 200 g of lead is mounted on the pre-cooling stage at 15 K. This stage is maintained at a temperature 5 K higher than the sensor temperature (10 K). The choice of this 15 K temperature for pre-cooling is justified by the fact that this is an efficient temperature to start a helium Joule-Thomson cooler. Also, at 15 K, the TSU absorbs more energy than at 10 K due to the specific heat that decreases with decreasing temperature. This system for cooling the sensor at 10 K increases the helium mass flow of the J-T loop to absorb the load at 10 K during a high heat load. The TSU function is to absorb the peak load at 15 K generated by the J-T system when the flow increases. The good results obtained allowed creating an efficient 10 K cryocooler with variable capability that is easily integrated.

### 1.2.4 ESU tandem arrangement using TSU at 40 K (Copper) and TSU at 15 K (helium).

Another machine based in the concept of a Joule Thomson associated to a multistage Gifford Mac Mahon precooler was developed by the Redstone Engineering Consulting Inc. and the Air Force Research Lab [14](Figure 1.7). Two TSU were coupled at two places on the precooler: one at 40 K and the other at 15 K. These TSU improve the efficiency of the

cryocooler in adsorbing peaks under variable load. The first TSU (40 K) consists of a simple copper plate that stores energy by sensible heat. However, it also allows sizing the heat exchangers in low load conditions, significantly reducing their sizes and complexities.

The second TSU (15 K) consists of a small pressure vessel filled with charcoal adsorbent connected to the high-pressure side of the J-T stage. The use of charcoal as an adsorbent allows improving volumetric heat capacity of helium concentrated gas. In Table 1.2, it is possible to see features and benefits of the charcoal TSU.

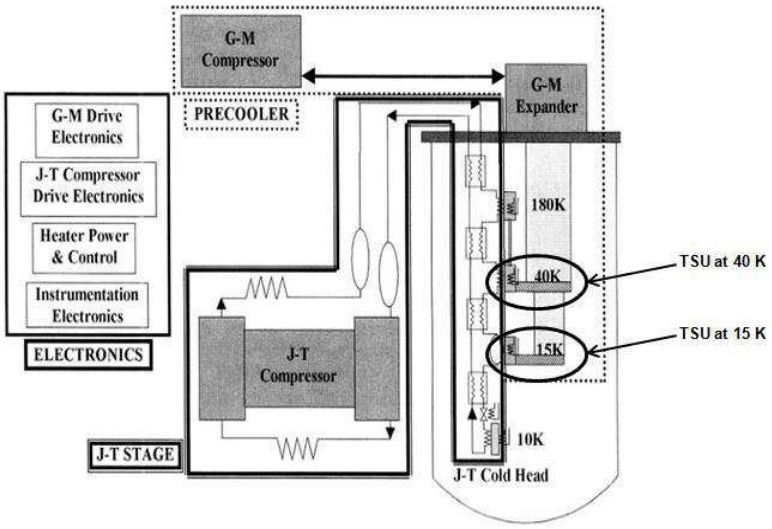


**Figure 1.7: Schematic of 10 K Cryocooler adapted from [14].**

**Table 1.2: Features and benefits of the charcoal TSU [14].**

| FEATURES | BENEFITS |
|---|---|
| Works at temperatures below 14K, as well as higher temperatures | Provides TSU solution for very low temperatures where there was no solution previously |
| Maintains constant sensor temperature as heat load varies | Temperature control is needed for good sensor performance |
| Averages heat load on cryocooler | Minimizes cryocooler input power, size and weight, heat rejection penalties on spacecraft |
| Allows large TSU temperature variation when installed in flow loop | Simplifies TSU thermal design; minimizes TSU size and weight; and simplifies cooling system physical packaging |
| Allows remote placement of TSU when installed in flow loop | Improves integration of cooling system and sensor; simplifies physical packaging; and facilitates redundancy of cooling system |

When the temperature in the TSU increases, the charcoal releases helium which flows through the J-T stage. This helium flow induces a cooling effect that counterbalances the heating from the increased flow rate. This way, the TSU and the precooler temperatures increase slowly which allows the system to maintain the sensor temperature at 10 K for a longer time.

A more detailed study of a TSU at 15 K [15] was made. This TSU has a toroid shape which allows a good integration in the J-T loop and the pre-cooler (GM). The interior is filled with several layers of copper screens and charcoal. The experience with and without TSU was performed. The impact of the charcoal mass and its location were also studied (in high-pressure and low-pressure sides of cold head). Analyzing the Figure 1.8, we may conclude that the position at the low pressure side is more interesting because for the same quantity of charcoal the peak cooling capacity is higher.

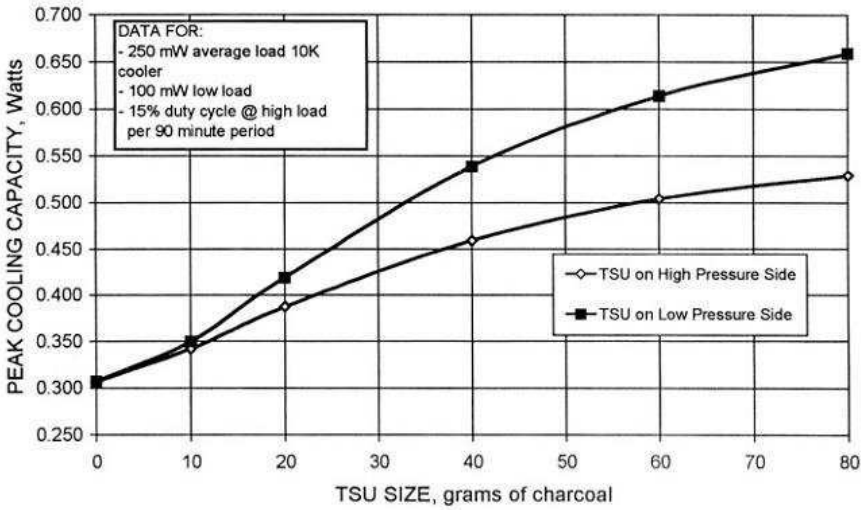


**Figure 1.8: J-T stage peak cooling power capacity for the JT with TSU placed in the high and low pressure lines [14].**

## 1.3 Triple Point

The system introduced is this section works at the triple point of a pure fluid and absorbs at constant temperature heat loads using the latent heat involved in phase transitions (mainly solid to liquid) .

### 1.3.1 Nitrogen Triple point - ESU at 63 K

**Lockheed ESU at 63 K .**

To maintain the sensor temperature at 63 K under a varying heat load, a Thermal Storage Unit was built and tested by Lockheed [9]. This TSU used the nitrogen triple point to store 17 kJ. This device is a single sphere of aluminium with a 22.5 cm diameter and with aluminium foam inside (Figure 1.9). The charging pressure was 130 bars at room temperature, with thermal cycling performed at 200 bars and rupture test at 460 bars.

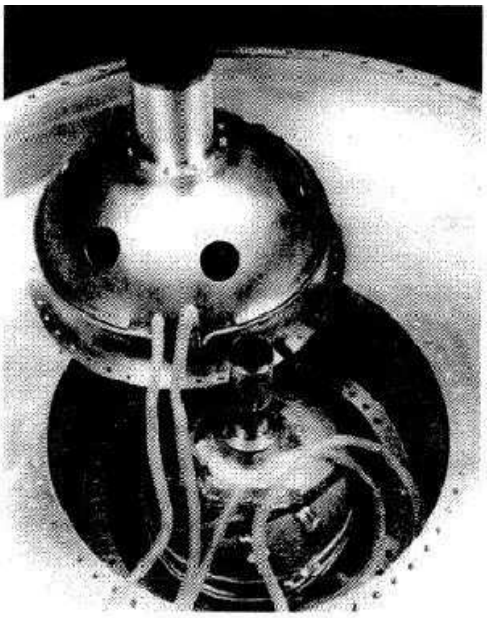

**Figure 1.9: Photograph of the aluminium TSU [9].**

This TSU, containing 0.656 kg of nitrogen, has two temperature sensors coupled to the top and the bottom hemispheres of the tank. Tests were made with different heat loads, the result for the 0.5 W is presented in Figure 1.10 [9]. In this test, 17 kJ was the thermal capacity according to the nitrogen mass introduced into the TSU. Comparing the initial and final temperatures there is a difference of 0.5 K. This difference increases with the applied load. This temperature drift is due to the phase transformation that happened far away from the wall cell, inside the foam. And as the aluminium foam is not a very good thermal conductor, and the thermometer and heaters were mounted on the outside of the cell, the heat is better transferred through the wall cell than in the foam/nitrogen combination. This way, the temperature measured on the cell drifted over time.

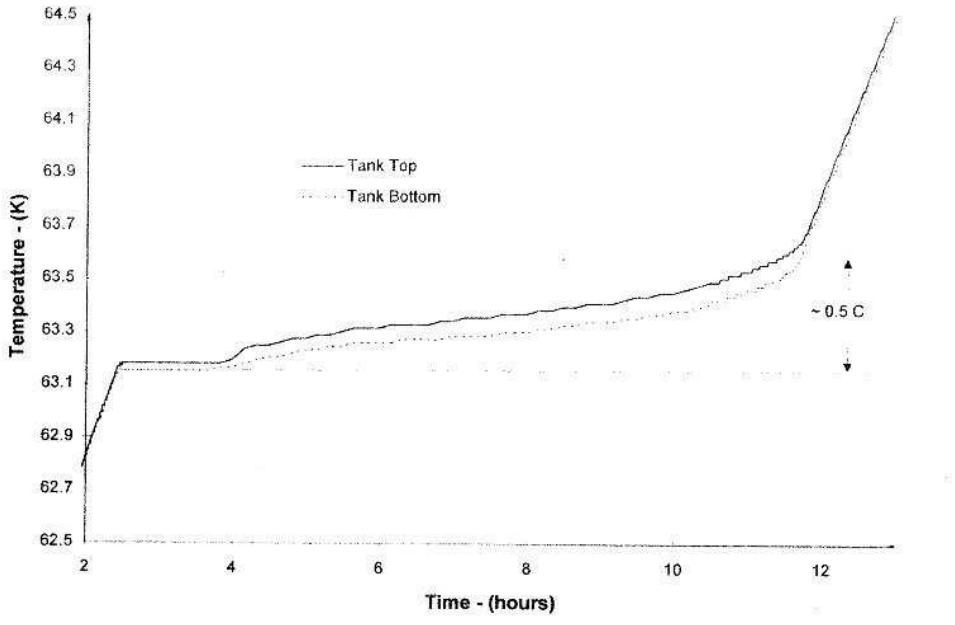


**Figure 1.10: Temperature evolution of TSU for the 0.5 W [9].**

**Twente University TSU at 63 K**

In order to avoid electromagnetic interferences and vibrations induced by the cryocooler, a TSU was considered to maintain a SQUID (Superconducting Quantum Interference Device) at constant temperature after stopping the cryocooler (Twente University, FHARMON project, NL) [6]. This SQUID requires to be operated below 77 K with maximum variation of about 0.1 K. So, one solution is to use the nitrogen triple point (63.5 K) device.

This system is composed by a TSU connected to a cryocooler by a heat switch. During measurements, the heat switch isolates the TSU from the stopped cryocooler. The power required for the sensor is 0.5 W for 10 hours (18 kJ).

The TSU was built to store 54 kJ (1.5 W for 10 hours). This corresponds to 2.1 kg of nitrogen. Highly porous alumina was used to retain nitrogen liquid against gravity. The dimensions of the TSU are 19 cm of diameter and 22.5 cm in height. A structure of the energy reservoir is shown in Figure 1.11. This structure was made in which layers of copper and porous material alternate, thus establishing a good thermal contact between the nitrogen and the casing of the TSU.

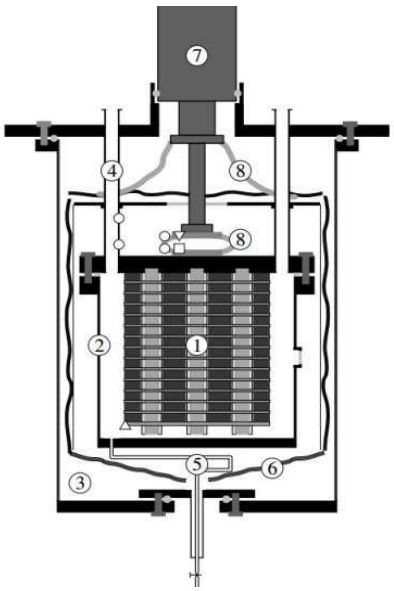


(1) Core of the TSU with alternating layers of copper and porous material;
(2) TSU container;
(3) vacuum space;
(4) three stainless-stell support tubes;
(5) drainpipe;
(6) Multilayer Insulation supported by a plate attached to the support tubes;
(7) cooler;
(8) braided copper cables connect the first stage to the three tubes and the second stage to the TSU. The symbols indicate the positions of sensors: ○ thermocouples to measure gradients over tube and copper cable; □ heater; ∇ diode; Δ thermocouple and diode.

**Figure 1.11: Schematic of the Twente TSU [6].**

The TSU is connected to a room temperature at a filling/evacuation system of the fluid so it is never subjected to high pressure. Experiments (without heat switch) at different heat loads were carried out. When the applied load is not too high, the temperature drifts very slowly. For example in Figure 1.12, when 2.5 W are applied the temperature drift is about 0.5 K after ≈ 6.5 h. During the beginning of the solid melting, the temperature drifts are always very small. At the end of the melting, significant temperature differences can occur in localized points and decrease with the heat loads (less than 2 K with 18 W).The experiments showed that the final TSU capacity was 25 kJ whereas 30 kJ were expected: this energy lack is explained by liquid loss during the filling procedure.

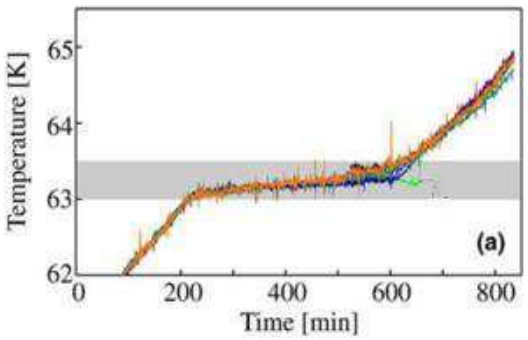


**Figure 1.12: Temperature evolution of TSU for the 2.5 W adapted from [6].**

### 1.3.2 TSU at 14 K using the hydrogen triple point

Service de basses temperature - CEA recently built a TSU working at the triple point of hydrogen (14 K) and storing 10 J [16]. The TSU is composed by two parts: a copper block with thin slots (≈ 100 µm) and stainless steel cap that fits on the base enclosing an empty volume that will be filled by hydrogen gas (Figure 1.13). To store 10 J, a volume of 22.2 $cm^3$ of liquid hydrogen was required. Slots allow both increased thermal contact between the cell and the fluid and the confinement of the liquid by capillary effect. The liquid trapped in the slots becomes solid after cooling. The liquid and the solid confinement make the cell insensitive to gravitational orientation.

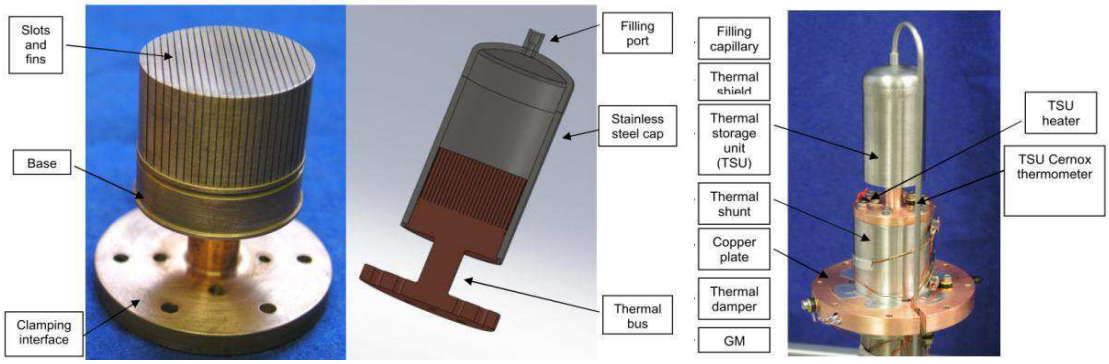


**Figure 1.13: The thermal bus (first), complete cold unit (second), Thermal Storage Unit mounted on the second stage of the Gifford Mac Mahon [16].**

This TSU was tested in two ways. In the first test, the cell was connected to an expansion volume of 1.9 l at room temperature with 1.2 bar. This cell was maintained at 13.8 K during 100 s storing 10.14 J (100 mW was applied for ≈ 100 s). In these tests, the temperature drifted only 10 mK in 100 s. This temperature drift increases when the applied heat load is higher; with 500 mW applied the drift is 30 mK. A similar behaviour has been verified when the cell unit was working against gravity, i.e the filing port is aligned with gravity, which demonstrates the possibility to use this kind of cell for space missions.

In the second test, an expansion volume at room temperature was used, so it was necessary to fill the cell with 80 bars at room temperature to get the same 10.14 J.

In both test configurations, the TSU could store the same energy (Figure 1.14). However, the expansion volume at room temperature connected to the cell drastically decreases filling pressure.

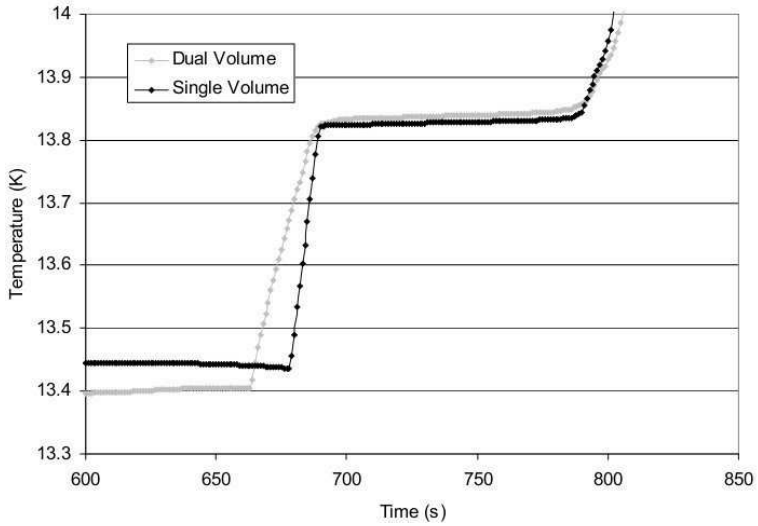


**Figure 1.14: Temperature evolution in dual and single volume configuration, with 100 mW of applied thermal load 100 mW [16].**

## 1.4 Dual phase

The ESUs presented in this section use phase transitions such as melting, vaporization, sublimation or crystal structure realignment, for energy storage.

### 1.4.1 BETSU at 120 K using Solid –Liquid transition of methylpentane

Brilliant Eyes Thermal Storage Unit (BETSU) was developed and flown on the shuttle flight STS-62 in March 1994 [17]. This unit worked at 120 K by melting 35 g of 2 - methylpentane with 3 % acetone added to minimize supercooling effect. The BETSU weight 1.5 kg with 0.9 kg for the aluminium fins matrix. Aluminium fins improve the thermalisation between the container and the phase change material (PCM). The BETSU design satisfies the requirements for its operation, as can be seen in Table 1.3.

**Table 1.3: BETSU design requirement [17].**

| Description | Requirement | Performance | Verification method |
|---|---|---|---|
| PCM refer. temp. | 120 ± 1 K @ 1 W for 1500 J | 119 ± 2.0 K @ 1 W for 1500 J | Test |
| Min. storage capacity | 1500 J | 2500 J latent (>3000 J total) | Test |
| Min. storage efficiency | 60% | 100% | Test |
| Max. rate | 4 W | 4 W | Test |
| Sensor accuracy | ±0.1 K | ±0.1 K | Test |
| $Q$-meter accuracy | ±0.05 W @ 1 W (5%) | ±0.03 W @ 1 W (3%) | Test |
| Max. TSU weight | 7.0 kg | 0.9 kg can (1.5 kg TSU) | Inspection |
| Max. PCM can $L/D$ | 0.5 | 0.5 | Inspection |
| Max. PCM volume | 1000 $cm^3$ | 54 $cm^3$ | Inspection |

A trade-off study was performed to analyse the weight and cost benefits of the BETSU and concluded that BETSU allows reducing 100 times the cooling system weight in comparison with a system without BETSU. Another trade-off study was performed which compared the BETSU to a single – phase sensible heat device (SHD). In Figure 1.15 it is possible to see the weight ratio of equivalent copper, aluminium 6061 and magnesium in function of allowable

temperature rise. For example, this BETSU weights 7 times less that the lighter SHD, for an allowable temperature rise of 3 K.

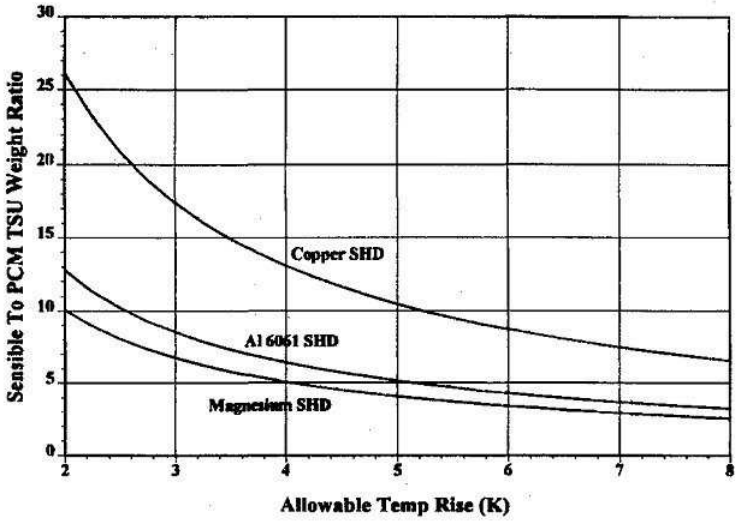


**Figure 1.15: Weight ratio of metallic sensible heat to phase change device in BETSU, as a function of allowable temperature rise [17].**

### 1.4.2 CTSU at 35 K using Solid-Solid transition of nitrogen

A dual volume Cryogenic Thermal Storage Unit (CTSU) was developed using nitrogen solid(α)-solid(β) transition at 35 K (latent heat = 9 J/g) and partially tested in shuttle flight STS-95 [18]. The goal was to reduce the power demand on the mechanical cooler and to reduce temperature fluctuation on the cooled element.

This CTSU consists of an aluminium 6063 heat exchanger connected to a storage tank by a capillary tube. The heat exchanger is composed by two drilled-hole 6063 aluminium halves welded together (Figure 1.16). The heat exchanger was installed between the cold finger of a mechanical cooler and the beryllium interface to the payload play. This system was filled with 22.4 bars representing a mass of 630 g of nitrogen, having an energy storage capacity of 5670 J. The TSU was submitted to a heat load fluctuation from 0.7 to 3.7 W and allowed limiting the temperature variation to 0.01 K/min. Figure 1.17 illustrates additional system details.

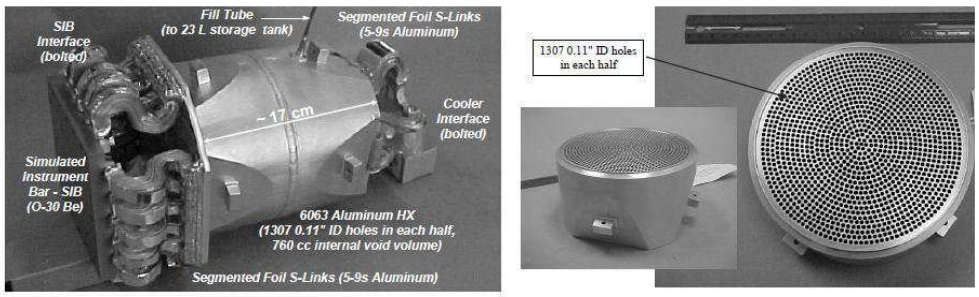


**Figure 1.16: Photographs of the DV-CTSU (right) and heat exchanger (left) [19].**


**Figure 1.17: The complete system for the solid N2 TSU[19].**

### 1.4.3 ITSU at 35 K using the Liquid-Vapor transition of neon

The Ball Aerospace and the Redstone Engineering developed a hybrid cooler for cooling infrared imaging systems under variable loads [20]. Hybrid machines consist of a fluid circulation J-T system and a pre-cooling system linked by an Internal Thermal Storage Unit (ITSU) (see Figure 1.18). The circulating fluid is neon, its liquid-vapor transition allowing maintaining the focal plane at 35 K.

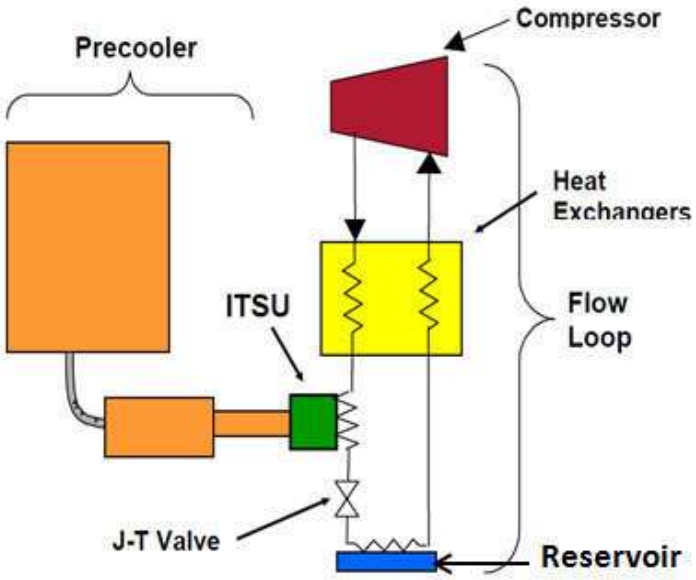


**Figure 1.18: Schema of the hybrid cooler with an internal Thermal Storage Unit [15].**

When the load is applied on the reservoir, liquid neon is evaporated. This gas is recompressed and redirected to the ITSU where it is condensed. When it is necessary to absorb load energy in the tank, liquid of ITSU flows through a Joule Thomson valve that regulates the flow. This way the tank's temperature is kept constant.

### 1.4.4 CRYOTSU at 60 K using the Solid –Solid transition of nitrogen trifluoride

A 60 K double volume Cryogenic Thermal Storage Unit called CRYOTSU unit was embarked in October 1998 on STS-95 flight for AFRL customer [3]. It was developed by Swales/AFRL/NASA Goddard to absorb the wide heat load variation during the high peak of the duty cycle while keeping the cryocooler specifications for an average heat load.

The requirements for this TSU are as found in Table 1.4.

**Table 1.4: Requirements for the 60 K Thermal Storage Unit [3].**

| TSU Operating Parameter | Performance Requirement |
|---|---|
| Operating Temperature | 55-65 K |
| Energy Storage Capacity | 6000 J |
| Temperature Stability | +/- 0.5 K |
| Weight | < 3.5 kg |
| Volume | < 1500 cc |
| Focal Plane Heat Load | 1-5 W,3 W avg |
| Focal Plane Interface Material | Beryllium |
| Gravity Environment Functionality | 1-G and 0-G |

The first material chosen for use in this TSU was the nitrogen trifluoride which undergoes an energetic solid-solid transition (21.3 J/g) at 56.6 K. This material has 2-3 times the energy storage capacity as nitrogen for the same filling pressure.

During this project, two different TSU prototypes were studied to build the flight model.

The first TSU built for this work, Figure 1.19, consists of an aluminium block with 176 internal drilled holes (3.2 mm diameter x 57.2 mm) to improve thermalisation [1]. Despite of $NF_3$ being the best solution, experimental tests was performed with other PCM (nitrogen, freon-22, air and nitrogen trifluride). Experimental conditions and results are summarized in Table 1.5.

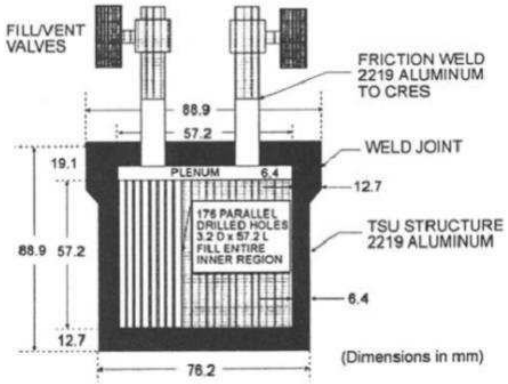


**Figure 1.19: Design of TSU [1].**

**Table 1.5: Experimental condition for PCM characterization tests [1].**

| PCM Tested | TSU Fill Pressure (MPa) | MW (kg/kmol) | Fill Mass* (kg) | PC Energy (kJ/kg) | Energy Storage (kJ) | Expected PC Temp (K) and Type |
|---|---|---|---|---|---|---|
| Nitrogen | 20.7 | 28 | 0.0235 | 25.7 | 0.604 | 63.2, melt |
| Freon-22 | Two-phase | 86.5 | 0.0758 | unknown | unknown | 59, s-s |
| Air | 13.8 | 29 | 0.0162 | 23.1** | 0.374 | 59, melt |
| $NF_3$ | 7.58 | 71 | 0.0218 | 21.3 | 0.464 | 56.7, s-s |

* TSU internal volume = 99.75 cc; ** Weighted average of $N_2$, $O_2$ values

The second built TSU benefits from the experience of the first, improving its performance [3][21][22]. Aiming to increase the energy storage and the thermal stability while reducing the total weight and volume the dual-volume design was adapted. To decrease the supercooling of $NF_3$ one solution is to increase the core surface. So, an aluminium foam core (40 ppi, 40 % relative density) was used as heat exchanger.

The design of the flight 60 K TSU is a dual volume as illustrated in Figure 1.20. Cryogenic temperature heat exchanger weighs 2.1 kg and needs 282 g of $NF_3$ to stock 6000 J with a temperature stability of 0.2 K. The heat exchanger volume has a beryllium shell to ensure direct mounting of focal plane on TSU. The aluminium foam was brazed to the ends-cap. The

spherical storage volume at room temperature is made in titanium and was designed to contain an internal pressure up to 6.9 bars.

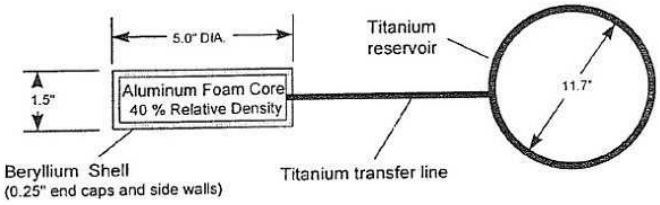


**Figure 1.20: Schema of Flight CTSU [3].**

Despite of this exhaustive on $NF_3$ the final 60 K CTSU uses nitrogen. Nitrogen has a lower heat capacity performance than the solid-solid transition of $NF_3$, but it was preferred for being non-toxic. Such final Figure 1.21 design is composed of a hermetically-sealed, dual-volume, beryllium and large room temperature stainless steel vessel of 16.7 liters that contains nitrogen [23]. The TSU is a beryllium disk of 15 cm, 5 cm height perforated with holes of 2.8 cm of dry mass 1 kg. It has a volume of 140 $cm^3$ and filled at 6.1 bars to hold a 0.118 kg of nitrogen.

The theoretical energy storage capacity of the flight CTSU is 2960 J and allows maintaining the temperature stability at approximately ± 0.25 K. Zero-g environment had no discernible impact on CTSU [24].

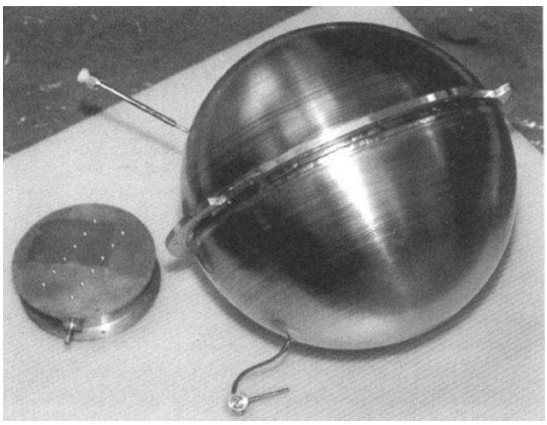

**Figure 1.21: Photograph of the triple point CTSU with stainless steel vessel [23].**

### 1.4.5 TSU between 4 - 90 K using different fluids

The Special Research & Development Bureau for cryogenic Tecnologies (SR & DB) developed cryocoolers with associate TSU in order to increase lifetime (up to 10-20 years) and temperature stability (± 0.5 K) of their cryogenic cooling systems [4]. In this work, the TSU are called cold accumulators. These accumulators allowed also the decrease vibration and electromagnetic interference.

Eight systems with J-T or Stirling cryocooler coupled to cold accumulators were tested. Cold accumulators absorb energy between 4-90 K using phase transitions of nitrogen, argon, deuterium or neon. In Table 1.6 it is possible to see details of these systems.

**Table 1.6: Thermal parameters and lifetime of SR & DB cryocoolers for the 4-90 K temperature range with melting-freezing, evaporation- condensation, and solid-solid transition accumulators [4].**

| No. | Temp-erature K | Temp-erature stability K | Design useful load W | Peak cooling capacity W | Relative cooling cycle duration | Accum-ulator fluid | Compressor type | Compressor fluid | Cooling life-time, years | Peak power consumption W | Meanday power consumption W | Cryocooler Type |
|---|---|---|---|---|---|---|---|---|---|---|---|---|
| 1 | 84 | 0.2 | 2-3 | 40 | 0.08 | Melt. Ar | Oil-free, ball sus-pended piston, lifetime 1 year | $N_2$ + $CH_4$ + $C_2H_6$ + $C_3H_8$ + $C_4H_{10}$ | 3-5 | 1000 | 80 | Mixture J-T |
| 2 | 84-90 | 0.5 | 0.5-1.5 | 15 | 0.04-0.1 | Melt. Ar | Same | Same | 3-5 | 500 | 20-50 | Mixture J-T |
| 3 | 35-40 | 0.3 | 0.6-3.2 | 8.0 | 0.11 | Solid $N_2$ | Same | Gaseous Ne | 3-5 | 1000 | Total 400 | Ne J-T |
| | 85-90 | 0.5 | 2.3 | 28.0 | 0.24 | Melt. Ar | Same | Mixture | | 1000 | | Mixture J-T |
| 4 | 25-30 | 0.2 | 0.7 | 8.5 | 0.11 | Melt. Ne | Same | Gaseous $H_2$, Ne | 3-5 | 1400 | Total 450 | Ne J-T + $H_2$ J-T |
| | 85-90 | 0.5 | 2.0-4.5 | 28.0 | 0.25 | Melt. Ar | Same | Mixture | | 1000 | | Mixture J-T |
| 5 | 5-10 | 0.2 | 0.1-0.5 | 0.5 | 0.2 | - | Same | Gaseous He | 5-10 | 500 | Total 1150 | He J-T |
| | 20-25 | 0.3 | 2.0 | 3.0 | 1 | Melt. $D_2$ | Linear, diaphragm suspended | Same | | 1050 | | Split-Stirling (USA) |
| 6 | 65 | 0.5 | 0.1-0.5 | 4 | 0.1-0.2 | Melt. $N_2$ | Oil-free, ball suspended piston, lifetime 1 year | Same | 5 | 150 | 15-30 | Split-Stirling |
| 7 | 77 | 0.01 | 0.01-0.1 | 12-15 | 0.025 | Liquid $N_2$ | Same | $N_2$ + $CH_4$ + $C_2H_6$ + $C_3H_8$ + $C_4H_{10}$ | 20 | 1000 | 25 | Mixture J-T |
| 8 | 87 | 0.01 | 0.01-0.1 | 15-20 | 0.02 | Liquid Ar | Same | Same | 20 | 1000 | 30 | Mixture J-T |

Aiming to develop cryocooler with accumulators for the range of 4 K -150 K the set of fluids with correspondent phase change characteristics are summarized in Table 1.7.

**Table 1.7: Some prospective cryogenic accumulator fluids for the 4-150 K temperature range [4].**

| No. | Accumulator fluid | Phase change temperature, K | Type of a phase change | Phase change energy, kJ/kg |
|---|---|---|---|---|
| 1 | Helium-4 | 4.2 | Evaporation-condensation | 20.9 |
| 2 | Hydrogen | 13.8 | Melting - freezing | 58.0 |
| 3 | Deuterium | 18.7 | Melting - freezing | 48.9 |
| 4 | Neon | 24.6 | Melting - freezing | 16.6 |
| 5 | Nitrogen | 35.6 | Solid-solid | 8.2 |
| 6 | Oxygen | 54.4 | Melting - freezing | 13.9 |
| 7 | Nitrogen trifluoride | 56.7 | Solid-solid | 21.3 |
| 8 | Nitrogen | 63.2 | Melting - freezing | 25.7 |
| 9 | Carbon monooxide | 68.1 | Melting - freezing | 29.9 |
| 10 | Nitrogen | 77.3 | Evaporation-condensation | 199.1 |
| 11 | Argon | 83.8 | Melting - freezing | 29.4 |
| 12 | Propane | 85.5 | Melting - freezing | 80.0 |
| 13 | Argon | 87.3 | Evaporation-condensation | 163.2 |
| 14 | Ethane | 90.3 | Melting - freezing | 95.5 |
| 15 | Methane | 90.7 | Melting - freezing | 58.7 |
| 16 | Krypton | 115.9 | Melting - freezing | 19.5 |
| 17 | N.Buthane | 134.9 | Melting - freezing | 75.4 |

- Melting –freezing correspond to the triple points.

### 1.4.6 ESU between 20 K and 80 K using heat capacity of solid water.

To use High Temperature Superconductors (HTS) in magnetically levitated vehicles (maglev), they must stay below ≈ 50 K to allow high magnetic field generation. A solution to maintain the HTS between 20 K and 50 K during one full day without using a cryocooler in the vehicle is to attach the magnetic coil to an adequate thermal system able to store the heat released by the HTS coil and by other parasitical heat source [25]. In this temperature range, the relatively high specific heat and thermal conductivity of water ice indicate that its use as storage medium can be a quite good solution. One experimental apparatus was mounted as represented in Figure 1.22. A copper block (9.28 kg) was used to mimic the HTS in a one-third-scale of the on-board magnet for maglev vehicles. Without water ice, the system drifts from 20 K to 50 K in 6 h whereas attaching only 1 kg of solid water allows extending this duration by 2 hours.

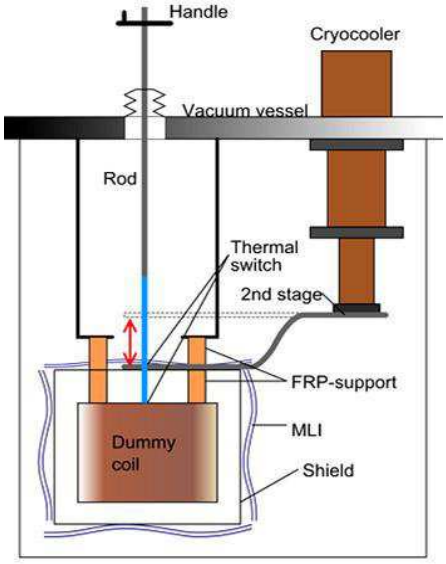


**Figure 1.22: Schema of the experimental apparatus [25].**

### 1.4.7 ESU between 65 K -80 K using Liquid-Vapor transition of nitrogen

The energy storage units built in CEFITEC (during my master thesis) allow keeping a hypothetical sensor at low temperature in a vibration-free environment while temporarily stopping the cryocooler. This liquid $N_2$ system used the latent heat of the liquid to vapor transformation of nitrogen as main energy absorber.

The ESU consists in an enthalpy reservoir and a heat switch. The enthalpy reservoir (38.5 $cm^3$) is made of copper with a brass cover indium sealed. It was thermalized to the cold finger of a 4 K Gifford Mac Mahon cryocooler by a gas-gap heat switch using nitrogen as a conducting gas. A small cryopump was used in order to toggle between the conducting (ON) and isolating (OFF) states of the heat switch.

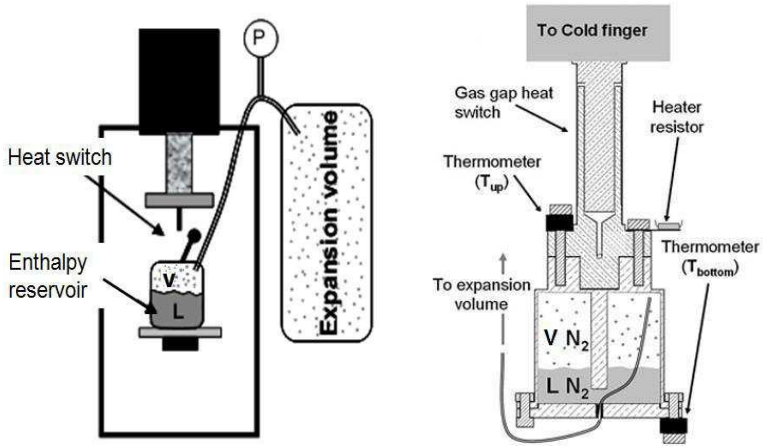


**Figure 1.23: Schema of the experimental set-up [26].**

On the top of the enthalpy reservoir was thermalized a thermometer to measure the container temperature as well as a heating resistor to mimick the sensor dissipation.

After condensing nitrogen into the reservoir, the heat switch is used to decouple the cell from the cryocooler cold finger. A constant heating power is applied leading to liquid evaporation along the saturation curve, the ESU mode started. If the enthalpy reservoir containing the cryogenic fluid is closed, this vapor formation would lead to a strong pressure increase: the temperature would rise quite rapidly as long as the liquid and vapor coexist. To reduce this temperature increase, the reservoir was connected by a capillary to an expansion volume at room temperature, limiting the pressure augmentation. The pressure in the expansion volume was measured: as long as liquid and vapor coexist in equilibrium thermodynamic, this pressure can be transformed in temperature by the correspondence P-T on the saturation curve and used to determine the temperature inside the cell ($T_{liq}$ ).

Using a 6 liters expansion volume filled with 1.95 bar at room temperature, this ESU is able to store up to 3720 J along a 65 K to 83.5 K temperature drift during the ESU mode. Figure 1.24 shows the temperature evolution of the cell with 1 W as constant heating power applied. The red curve displays an artificial drift of the temperature of cold finger. At $t \approx 64$ min, the temperature $T_{top}$ starts to increase faster indicating that there is no more liquid in the cell, and by the same time, the temperature as measured by the pressure exhibits a plateau as there is no more liquid in the cell.

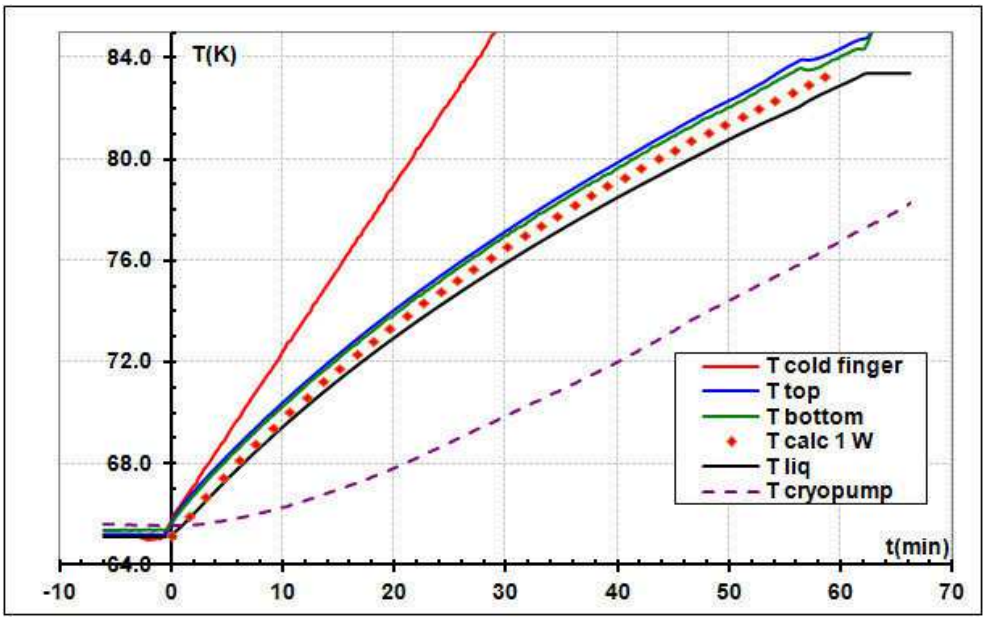


**Figure 1.24: Temperature drift for the liquid N2 ESU mode (1 W applied) starting at T≈ 65 K with a filling pressure of 1.95 bar [26].**

In order to compare experimental temperature drift $T_{liq}(t)$ with the one expected from the system, a numerical simulation was carried out. Knowing all the volumes of the system and the filling pressure at room temperature, the number of moles in the whole system can be determined. Knowing the density of the fluid at low temperature and the $P_{sat}(T)$ allows us to calculate the number of condensed moles in the liquid phase.

Using the first law of thermodynamics for an open system (the low temperature cell), the necessary heat Q for rising the temperature from $T_n$ to $T_{n+1}$ (temperatures at time t and $(t+\Delta t)$, respectively), can be calculated as:

$$Q = \Delta U_{cell} - h_{vapour}\Delta n \quad + C_{cell}\Delta T \tag{1.1}$$

which discretizes as:

$$Q \quad (T_{n+1}, T_n) + Q_{para}(T_{n+1}, T_n) = \\ U_{cell}(T_{n+1}) - U_{cell}(T_n) - \big(n \quad (T_{n+1}) - n(T_n)\big)h_{vapor}(T_n) + C_{cell}(T_{n+1} - T_n) \tag{1.2}$$

In this expression, the term $Q(T_{n+1}, T_n) = \dot{Q}\,\Delta t$ represents the heat entering into the system between $T_n(t)$ and $T_{n+1}(t+\Delta t)$ due to the applied Joule heating; this energy is called accessible energy. $Q_{para}(T_{n+1}, T_n)$ is the parasitical energy received by the system due to the temperature difference between the cell and the cold finger through the stainless steel support of the switch (OFF state) and due to radiation (a rather pessimistic value of 0.5 for emissivity was used in calculating the form factor for two concentric cylinders). The sum of accessible energy and parasitical energy is called the experimental energy. $U_{cell}$ is the total internal energy of the working fluid (liquid and vapor) existing in the cell, $h_{vapor}$ is the molar enthalpy of the vapor and n is the molar amount of fluid in the cell; $C_{cell}$ is the total heat capacity of the cell housing. The value of $T_{n+1}$, after each increment can be calculated and the T(t) drift entirely determined using the initial conditions as unique parameters.

These iterative calculations were made using a programmed worksheet and software was written in Java. The calculated temperature drift is plotted in Figure 1.24 ($T_{calc}$-solid symbols) for a charge pressure of 1.95 bar in the 6 liters expansion volume. The theoretical energy and experimental energy results agree within 5 % and are discussed in the literature [26].

The main inconvenient of this ESU is the temperature drift that still exists while the heating power is absorbed.

## 1.5 Conclusion

A bibliographic review of existent systems constructed to accumulate thermal energy for different cryogenic applications in order to reduce the temperature drift has been presented:

- The solid state ESUs uses high heat capacity to limit the temperature rise and are limited to relatively high temperature as specific heat of material decreases with temperature or near a specific heat anomaly (mainly due to a magnetic phase transition) at low temperature.
- The triple point ESUs absorbs a heat input maintaining a constant temperature as long as the three phases coexist. Systems were presented in two configurations: simple and dual volume. The dual volume is used in order to decrease the filling pressure and the thickness of the cell walls. Such ESUs are limited to temperature where a triple point can be found.
- The dual phase ESUs uses the latent heat involved in a liquid –vapor transition to absorb energy. One advantage of the liquid –vapor dual phase ESU is that the liquid-vapor latent heat $L_{L\text{-}V}$ is significantly higher than that corresponding to the solid-liquid transition at the triple point. For example, for $N_2$, $L_{L\text{-}V} \approx 200$ J/g whereas $L_{S\text{-}L} \approx 26$ J/g.

An expansion volume is necessary to avoid rapid temperature increase during the ESU-mode.

Facing the state of art, the work being presented in this thesis is joining some novel contributions:

The dual phase ESUs creates at CEFITEC is a new system that has a big potential: it stores energy in a quite compact cell at low temperature connected to an expansion volume at room temperature. As this system is very recent, it is necessary to test better the concept and this way will be possible investigate the physical and technology problem that appearing. For example the drift of temperature while the energy is absorbed can be an inconvenient for determine applications.

In the next chapter, it will be described two solutions to reduce this temperature drift. As this system stores energy without vibration, with or without drift of temperature, it is possible to use it for spatial applications, for example, to keep at constant temperature sensors whatever their power dissipation. The devices integrated in spatial systems must be insensitive of gravity. To turn the liquid-vapor ESU working whatever the gravity direction or in absence of gravity, the cell was filled with a porous medium to retain the liquid. It will be also described how this solution solved the gravity issue and can enhance the heat exchange. It will be also shown that, for low liquid fraction in the cell, this heat exchange becomes progressively very poor.

# Chapter 2: Energy Storage Unit of Liquid- Vapor Nitrogen

In section §1.4.7 an ESU working around between 65 K and 83.5 K is described. It consists mainly in a low temperature cell able to store energy while the cryocooler is stopped without significant temperature increase thanks to latent heat of liquid nitrogen evaporation. This work was developed during a master thesis [27] and upgraded as a part of this current PhD work. During the first year of my PhD, this work was updated using the same or similar experimental set-up with the three following goals:

- to decrease the temperature drifts and/or an increase the stored energy during the ESU mode. This objective was reached by using a 24 liters expansion volume.
- to avoid temperature drift during the ESU mode by installing a control pressure system in the circuit. This modification turns this ESU directly comparable to the triple point ESU.
- to turn the system insensible to gravity in order to be used in space environment. The capillarity effects in a porous ceramic were used to confine the liquid inside the low temperature cell.

In this chapter, the modifications done to fulfil these goals and the tests performed are presented and discussed.

## 2.1 Liquid-Vapor Enthalpy Reservoir (without ceramic)

Tests similar to those shown in the section §1.4.7 with the expansion volume of 24 liters were performed. Then, the experimental set-up and modus operandi are presented in more details.

### 2.1.1 Experimental set-up

The experimental set-up was the same as used in section §1.4.7 with an expansion volume of 24 liters instead of 6 liters. The schema and a picture of the low temperature cell are shown in Figure 2.1. The low temperature cell of ≈ 38.5 $cm^2$ was attached to the cold finger of a 4 K Gifford Mac Mahon cryocooler[1] through a gas gap heat switch using nitrogen as exchange gas (Figure 2.1). At room temperature expansion volume of 24 liters was connected by ¼" tubes and by a capillary to the low temperature cell.

[1] This cryocooler is over dimensioned for the temperature range in this study. Nevertheless it was available in the lab facilities.

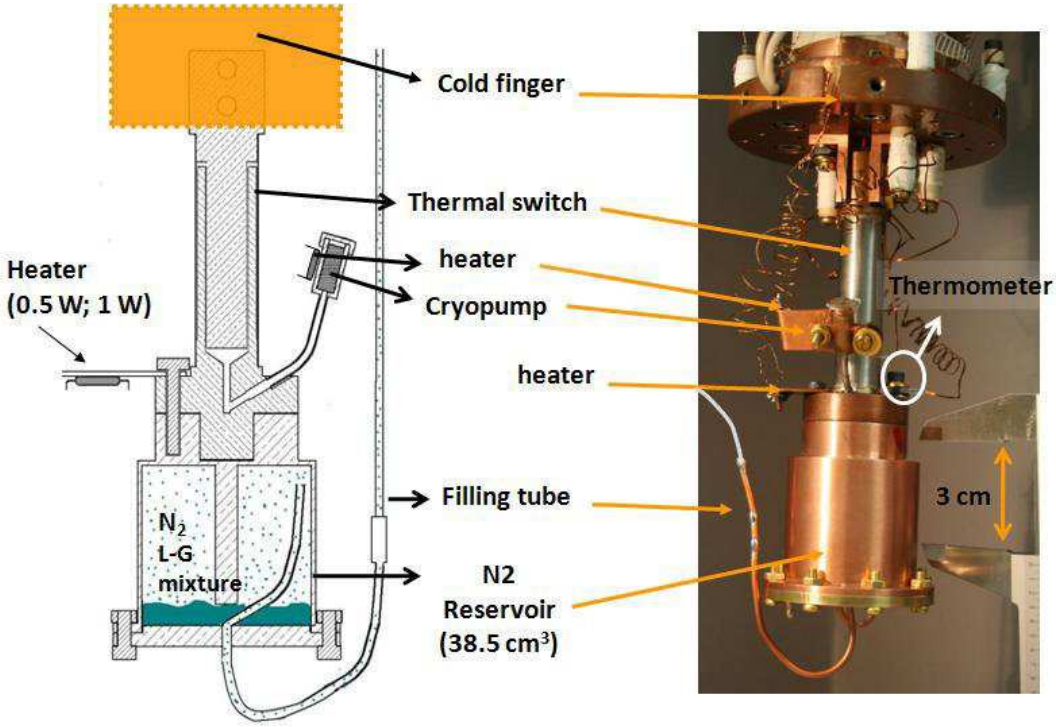


**Figure 2.1: Low temperature experimental set-up. The enthalpy reservoir (reservoir of nitrogen) of ≈ 38.5 cm$^3$ was attached to the cold finger by a gas gap heat switch.**

The gas gap heat switch

The gas gap heat switch (Figure 2.2) used in this experiment was already described and tested with various gases [28][29]. In our case, nitrogen gas was used as exchange gas. The switch consists of two concentric copper blocks maintained separated by a 100 μm gap thanks to a thin stainless steel cylindrical support (≈100 μm thick). The gas management is obtained by a small adsorption pump containing activated charcoal. If the cryopump is cooled down below ≈90 K, the charcoal adsorbs almost completely the gas existing in the gap and the conduction through the residual gas (molecular regime) is very low: In this case, the thermal conduction mainly takes place only along the thin stainless steel support (OFF state, conductance ≈ 1 mW/K at T ≈ 80 K). On heating up the cryopump (temperature above ≈130 K), the adsorbed gas is released to the gap, the thermal conduction (viscous regime) occurs mostly through the 100 μm gas layer separating the two copper blocks (ON state, conductance ≈ 85 mW/K at T ≈ 80 K with nitrogen in viscous regime). During all these experiments, the switch was filled with 200 mbar of nitrogen at room temperature and sealed.

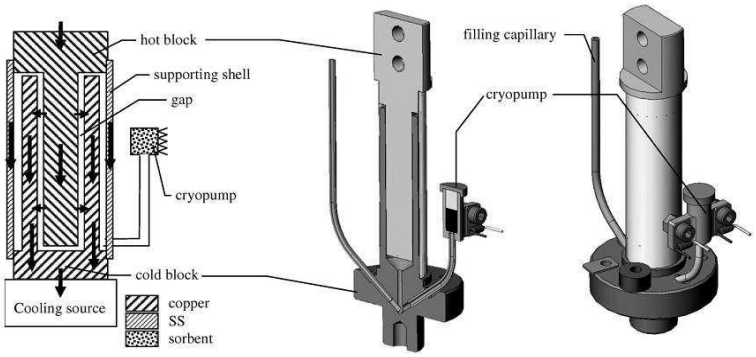


**Figure 2.2: Schema of principle( left) and cross section (middle) and 3D view (right) of a gas-gap switch with adsorption pump[28].**

Reservoir

The enthalpy reservoir (Figure 2.1 ) is made of copper (126 g) with a brass cover (63 g). The copper cylindrical recipient has a copper rod (diameter = 5 mm) at the centre to promote the temperature homogeneity. The cell was hermetically sealed with the brass cover fixed by screws and an indium o-ring.

For gas exhaust, a copper capillary passed through the brass cover with its extremity located at the top of the cell to avoid liquid expulsion during the pressure increase. The other end is connected to a 530 mm long stainless steel capillary (2 mm and 1.5 mm as outer and inner diameters). When the hot and cold ends of this capillary are at 300 K and 60 K respectively, 7.38 mW reaches the reservoir. This parasitical heat load is much smaller than the applied heat loads used for the tests (typically 1 W).

The cell temperature was measured by two thermometers thermalized on the top and bottom part (brass cover) of the cell ($T_{top}$ and $T_{bottom}$, respectively).

A 0-20 bars pressure sensor, mounted in a manifold at room temperature, was used to measure the pressure in the cell during the experiments. Along the saturation line, the pressure can be converted in temperature, allowing measuring the temperature ($T_{liq}$) of the vapor-liquid interface inside the cell. The conversion of the gas pressure in temperature is obtained using the ($P_{sat}$, $T_{sat}$) data for the saturation line given by the REFPROP® program [30]. A small electronic resistor was attached on the top part of the cell as a heat source ($\dot{Q}$) using Joule effect.

### 2.1.2 Modus operandi

The modus operandi is illustrated in Figure 2.3.

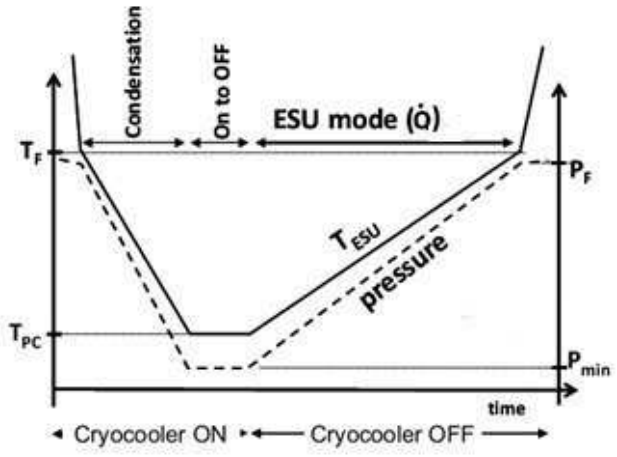


**Figure 2.3: Schema of timing of operation.**

With the whole system (expansion volume and low temperature cell) at room temperature, it is filled with $N_2$ gas at a pressure $P_{fill}$ (referred as filling pressure in the following) allowing the calculation of the total enclosed amount that will be maintained constant during all the experiment. In the first phase, the cryocooler is turned on, with the heat switch in the high conductance state ("ON" state) and the cell is cooled down to the pre-cooling temperature $T_{PC}$. For real systems, $T_{PC}$ would be very close of the cryocooler base temperature.

During the cooling, when the pressure and the temperature of the gas correspond to a point on the saturation curve ($T_F$, $P_F$) ("F" stands for "Functional" or "Final"), the gas begins to condense in the low temperature cell. Beyond this point, further cooling leads to an increase of the liquid quantity into the cell and to a pressure decrease, the low temperature cell acting as a pump for the expansion volume. When the pre-cooling temperature is reached, the pressure in the whole system is minimal ($P_{min}$) and corresponds to the saturation pressure at $T=T_{PC}$ .The knowledge of cell pressure (or temperature), of expansion and cell volumes and of vapor and

liquid densities along the saturation curve allows the determination of the amount of liquid and vapor during all this process.

When the temperature $T_{PC}$ is reached, the switch can be toggled to the OFF state (2nd phase) to thermally decouple the ESU from the cold finger. At this temperature, the amount of liquid in the cell determines the maximum energy stored by the ESU. Once this state is reached, the ESU is ready to work, the cryocooler can be stopped and a certain heating power leads to liquid evaporation (3nd phase, ESU mode). In most cases of the experiments shown below, the cryocooler's cold finger temperature was swept in order to simulate a natural warming after turning OFF the cryocooler. Temperature and pressure were recorded up to total liquid evaporation and because the gas is stored in the finite expansion volume, the pressure in the system increases slowly, and so does the temperature. When the liquid totally disappears (at $T_F$, $P_F$), the heat becomes to be stored only by the sensible heat of the container. So, the temperature drifts increase much faster. The ESU must then be recycled.

### 2.1.3 Results

This section displays typical experimental results for an ESU-mode using a 24 liters expansion volume and 1 W heating power. Such experimental data, with a cell volume completely open, are useful to compare with ESU-mode results obtained with the same experimental conditions but with the cell filled by a porous material (next sections).

Figure 2.4 displays the temperature drift during a test using the expansion volume of 24 liters and a filling pressure of 1.52 bar (1.47 moles in the whole system). The cold finger's temperature was controlled at 75 K and the reservoir was cooled down to $T_{PC} = 75.7$ K corresponding to an initial liquid filing of ≈ 60% (≈ 22.8 $cm^3$). At t=0 s, the initial pressure in the whole system is 0.83 bar corresponding to a temperature $T_{liq}$ of 75.7 K, in good agreement with the temperature as measured by the two other thermometers (75.9 K and 75.8 K). A constant heating power (1 W) is applied to the cell at t=0. As already explained, to simulate the stopping of the cryocooler, the cold finger's temperature is swept at a rate of 0.3 K/min (red curve). The green curve ($T_{top}$) and the blue curve ($T_{bottom}$) represent the temperature drift as measured by respective thermometers whereas the black curve is the temperature calculated from the pressure ($T_{liq}$). The temperatures measured in top and in bottom of the cell are very close indicating that there is no significant temperature gradient along the cell.

However, the temperature difference between the cell walls ($T_{top}$ and $T_{bottom}$) and the fluid ($T_{liq}$) increases from less than 1 K at the beginning of the ESU mode up to 1.5 K at its end(t ≈ 65.7 min). This temperature difference, $\Delta T$ can be explained by heat transfer across the nitrogen liquid/cell wall interface that becomes more difficult as the liquid evaporates due to reduction of liquid-solid area. Using the expression for the nucleating boiling regime $\frac{\dot{Q}}{A} \approx 500(\Delta T)^{2.5}$ where the factor 500 (that depends of surface orientation) have the following units $W.m^{-2}.K^{-2.5}$ [31] and A is the wetted cell area where occurs the liquid-solid heat transfer, it is possible to calculate an approximate value for $\Delta T$. In our condition with 1 W applied, and 60 % of liquid inside the cell (35.3 $cm^2$ of wetted area) the $\Delta T$ calculated is 0.8 K, in the same order of magnitude than that measured during the experiment. The Figure 2.4 displays the experimental $\Delta T = T_{bottom} - T_{liq}$) versus the percentage of liquid in the cell. This $\Delta T$ is compared to the results given by the expression for nucleate boiling for two different values of the factor (500 and 300). In these calculations, the bottom area (≈ 10 $cm^2$) is considered always wetted whereas the cylindrical area decreases proportionally to the liquid fraction.

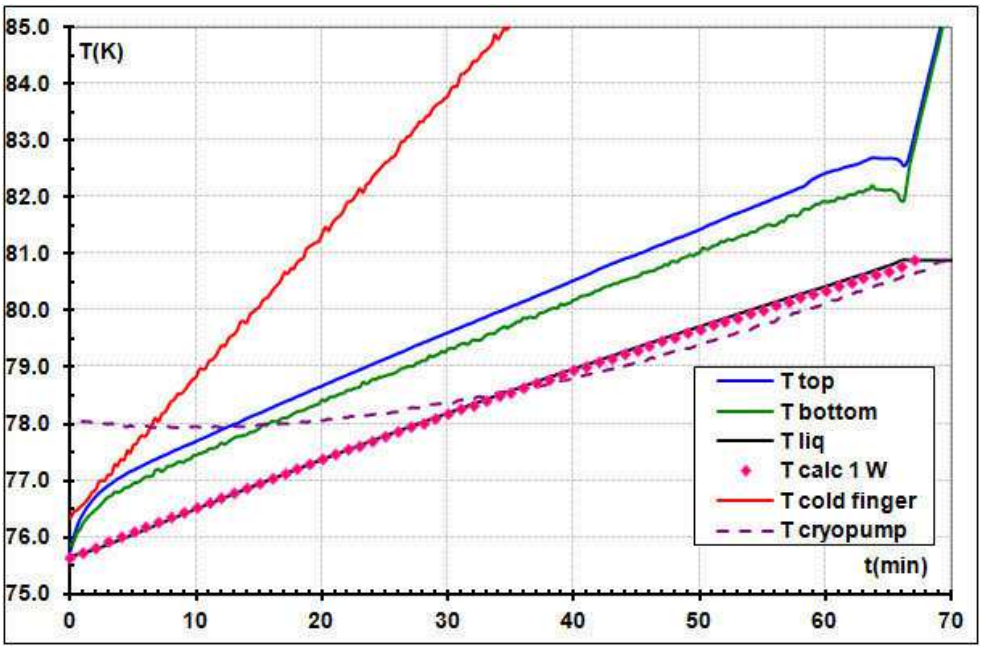


**Figure 2.4: Temperature drift for an ESU mode (1 W applied) starting at $T_{PC}$= 75.7 K with a filling pressure of a 1.5 bar, an expansion volume of 24 liters and cryocooler heating up at 0.3 K/min.**

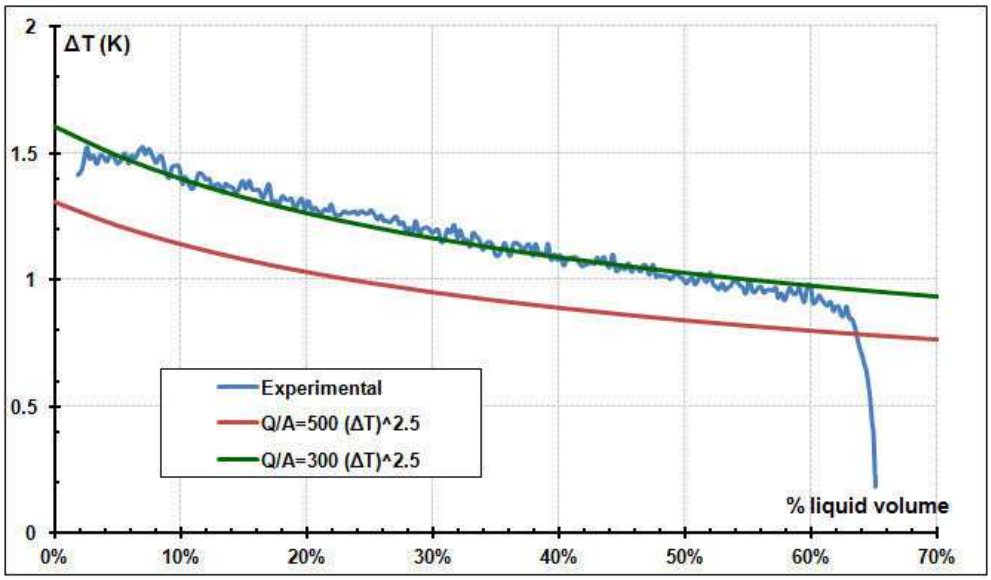


**Figure 2.5: The *ΔT* as a function of percentage of liquid volume for the case 1 W applied.**

For t ≈ 65.7 min, the $T_{top}$ and $T_{bottom}$ start to increase faster and the temperature as measured by the pressure stabilizes indicating that no more liquid exists in the cell and then the pressure stops to increase: the pressure can no longer be used as thermometer. After that time, there is no more liquid in the cell and all energy is absorbed by heat capacity of the cell wall and of the gas, but since heat capacities are rather low, the temperature increases faster than before.

During this ESU mode, the whole system stored an experimental energy of ≈ 4080 J between 75.7 K and 80.8 K (i.e. the energy dissipated by the electrical heater added to the parasitical heat losses).

The pink curve is the temperature as calculated by the Excel worksheet $T_{calc}(t)$ (using the equation the first law of thermodynamic for open systems (equation (1.2)) and takes into account the parasitical heat flowing through the heat switch as well as the radiation losses between the low temperature cell and the thermal shield thermalized to the cold finger(a rather pessimistic value of 0.5 for emissivity was used for all parts). Theoretical and experimental results agree within 5 % as well as the results obtained in previous test with the 6 liters

expansion volume [27]. This discrepancy can be explained by two ways. First, the heating power effectively dissipated on the reservoir is lower than that measured at room temperature, 2 % difference being due to resistance of the wires. In second the overheating of the heater ($\approx 2$ cm$^2$) up to 200 K causes dissipation by radiation that can lead to a correction of about 3 % for the effective heating power transmitted to the cell.

These results, compared with those of Figure 1.24 (6 liters as expansion volume, $\approx$ 3700 J stored between 65 K and 83.5 K), showed clearly that a large expansion volume allows storing the same energy within the same low temperature cell volume but with a temperature drift significantly reduced. Let us note that to store this same energy (4 kJ) within this same temperature range using a sensible heat ESU, it will be necessary $\approx 3.5$ kg of copper ($\approx 400$ cm$^3$) or 2.2 kg of aluminum ($\approx 830$ cm$^3$).

## 2.2 Liquid-Vapor Enthalpy Reservoir (with ceramic)

To turn the system insensitive to gravity, the low temperature cell was filled with one piece of porous medium fitting the cell dimensions. Tests with 6 liters expansion volume and 24 liters expansion volume were performed. To verify the gravity effect, tests with an "upper output" for the gas connected to the expansion volume are compared with test using a "bottom output". These tests are discussed.

### 2.2.1 Experimental set-up/modus operandi

To avoid expelling liquid instead of gas during the ESU mode, the system described in previous section can only work in one orientation with respect to the gravity: the capillary end must be in the gas -in the upper part of the cell- at any time, the gravity forcing to maintain the liquid phase in the bottom part of the cell. This is a serious inconvenient for the integration of such a system in spatial applications where it must work in any orientation and in microgravity environment. So, to turn this ESU insensitive to gravity, an $Al_2O_3$ ceramic foam (void volume of ≈92 %, pore size ≈ 60-50 μm), Procelit P160 (see Figure 2.6) manufactured by RATH [2], was fitted in the cell. In this kind of porous media, the capillary effects are stronger than gravity, so the liquid is retained in the ceramic independently of the gravity direction. A ceramic similar to this one was recently successfully used in Herschel satellite to confine $^3$He [32].

In a first approximation, the capillary height, the maximum height that a liquid is able to climb in a capillary tube, can be approximately calculated using cylindrical tubes with a diameter that equal to average pore size. Between 64 K and 84 K the capillary height is estimated between 8 cm and 12 cm (see Figure B.4). This problem is discussed studied in more detail in Chapter 4:.

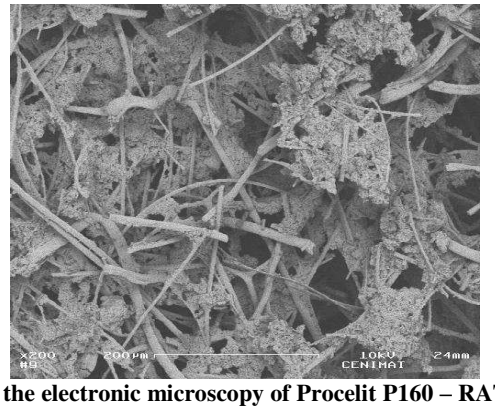


**Figure 2.6: Photography of the electronic microscopy of Procelit P160 – RATH ( photographic record- UNL/FCT/CENIMAT)**

[2] Ceramic P160, Rath GmbH, Hafnerstraße 3, A-3375 Krummnußbaum, Austria

To test if the system becomes gravity independent without rotating the cryocooler, the low temperature cell was slightly modified in order to allow the fluid to be exhausted by the bottom part of the cell (Figure 2.7). Tests were firstly performed with the upper output connected to the expansion volume and the bottom output blocked. Afterwards, same tests were performed with the upper output blocked and the bottom output connected to the expansion volume (anti-gravity configuration, Figure 2.7). Thus, the comparison of the results in these two configurations is a good way to test the gravity effect.

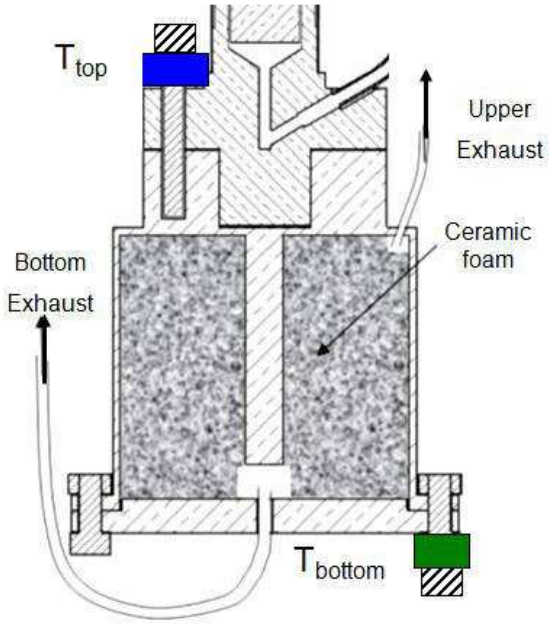


**Figure 2.7: Low temperature cell with ceramic foam and the two exhausts.**

### 2.2.2 Results

#### 2.2.2.1 Expansion Volume of 6 liters

The temperature drifts during an ESU mode with and without ceramic filling, using the upper exhaust (bottom exhaust blocked) are display in Figure 2.8. In the same figure are also plotted the results of Figure 1.24 obtained in the same initial conditions but without ceramic. During this test, the system uses the expansion volume of 6 liters, was filled with 1.95 bars (≈0.45 mole corresponding to ≈ 38 % and ≈ 35 % of liquid fraction with ceramic and without ceramic respectively), the pre-cooling temperature, $T_{PC}$, was 65 K and 1 W was applied during the ESU-mode.

As it can be seen in the Figure 2.8, the ceramic introduced some differences in the experimental results. For t < 46.5 min, the temperature difference between the liquid-gas interface ($T_{liq}$) and the thermometers ($T_{top}$ and $T_{bottom}$) decreases with ceramic $\Delta T$<0.3 K, whereas it can reach 1.5 K without ceramic. This reduction of the temperature difference could be explained by an increase of the contact area between the liquid and the cell walls: in such a case, the ceramic being in contact with the cell walls and due to the capillarity/wetting effects, liquid nitrogen would wet a large area of the cell leading to a decrease of the thermal contact resistance. Also is possible than the ceramic in contact with the cell walls can increase the number of active nucleation site, so the rate of bubbles formed increases improving the heat transfer.

For t ≥46.5 min, (liquid fraction below ≈13% full symbol in Figure 2.8) for the cell with ceramic (solid lines), $T_{top}$ and $T_{bottom}$ start to increase in relation with $T_{liq}$, reaching $T_{top}$= $T_{bottom}$ = 86 K whereas $T_{liq}$ = 82 K at t= 60 min. In the end of evaporation, this temperature difference reached more than 9 K. This behaviour can be explained if a quantity of liquid is retained in small pores without a continuous path of liquid to reach the cell walls. In such a case, the cell walls are no more wetted. As the ceramic is a bad thermal conductor and turns difficult gas convection, this liquid becomes strongly thermally isolated and can stay inside the ceramic at a significantly lower temperature than that measured on the wall.

To identify the point where the difference between the cell temperature ($T_{top}$, $T_{bottom}$) and the temperature of the liquid - vapor interface starts to increase, a fit of $T_{top}(t)$ between 0 min and 45 min was traced. The point where the curve of $T_{top}$ and the fit intercept is the red point. This method was used in all graphs to identify the beginning of abnormal temperature drift.

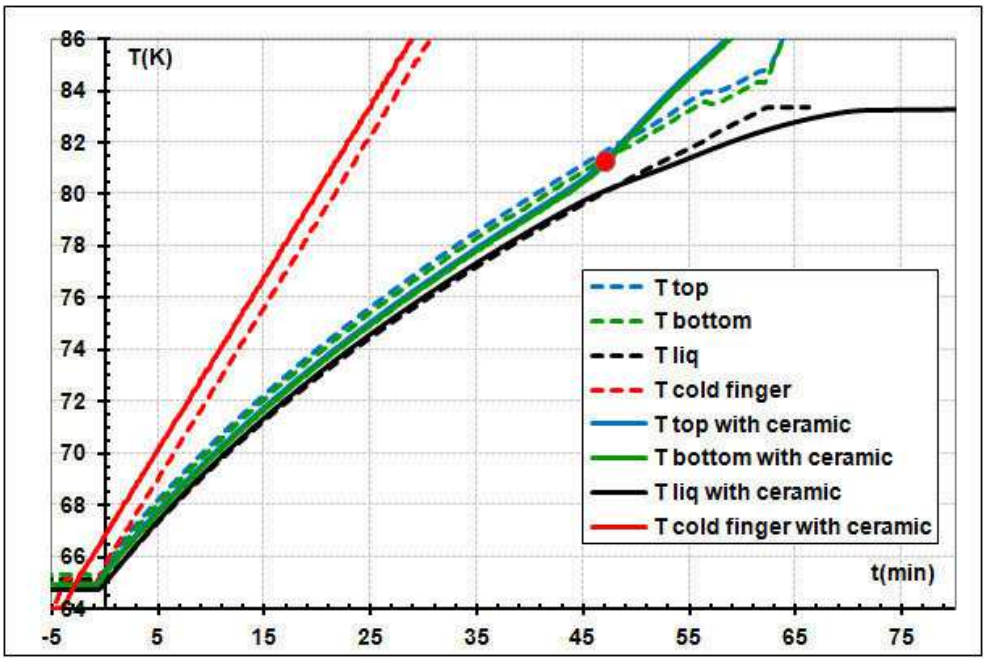


**Figure 2.8: Comparison of the temperature drift with 6 liters expansion volume, 2 bars filling pressure, cryocooler heating up at 0.8 K/min and 1 W applied with ceramic (solid line) and without ceramic (dashed line). The red point signals the beginning of the temperature drift and corresponds to a filling ratio of 13 %.**

Figure 2.9 compares two temperature drifts, one using the upper exhaust (solid line; bottom exhaust blocked) and the other using the bottom exhaust (dashed line, upper exhaust blocked). The temperature drifts for these two configurations are quite coincident indicating a similar thermal behaviour of the whole cell. This result indicates that the liquid is effectively retained by the ceramic: as a matter of fact, if the liquid would accumulate in the bottom part of the cell, it would be rapidly be expelled off the cell through the capillary during the pressure increase, leading to a much faster temperature drift and a very rapid emptying of the cell. In this configuration also, the $T_{top}$, $T_{bottom}$ start to increase in relation with $T_{liq}$ when the liquid filling ratio reaches around 10%-13 %.

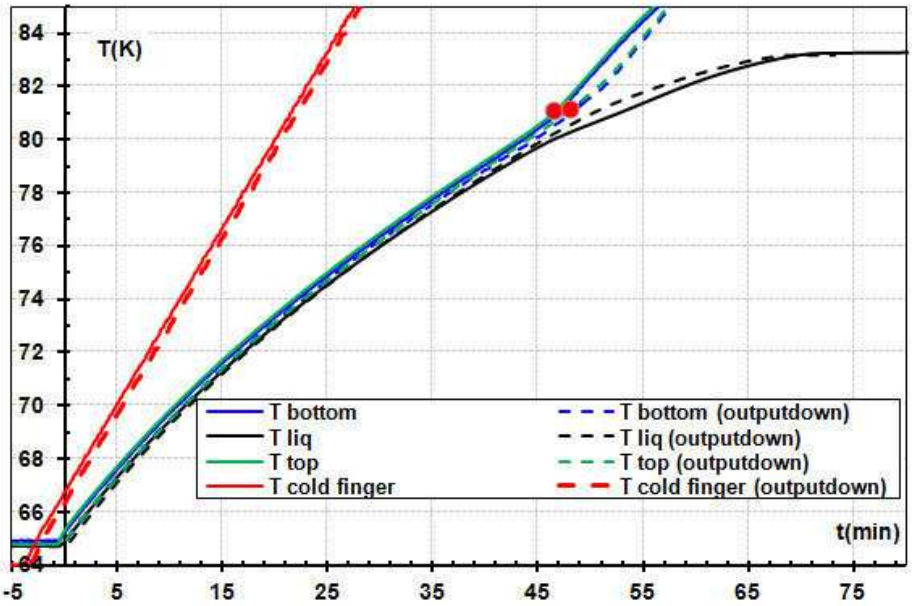


**Figure 2.9: Comparison of the temperature drift with 6 liters expansion volume, 2 bars filling pressure, cryocooler heating up at 0.8 K/min and 1 W applied using the gas exhaust in the top (solid line) and bottom part of the cell (dashed line). The red point signals the beginning of the temperature drift and corresponds to a filling ratio of 10 % and 13 % respectively.**

In all performed experiments (not all shown in this report), below a liquid fraction of 10 %-13 % in the cell, the wall container temperature increases faster than the liquid-vapor interface temperature. To study if these growing temperature difference depends only of the liquid quantity, a test was performed with a larger initial liquid quantity thanks to a higher filling pressure and keeping, as far as possible, the other conditions identical. In Figure 2.10 is possible to see the experimental results of two experiments in the same conditions but with different filling pressure: 1.5 bar and 2.5 bars (corresponding to an initial liquid filling of ≈ 38 % and 50 % respectively). For the higher liquid percentage, $T_{liq}$ and $T_{top}$ remain effectively close together during more time and the significant divergence between $T_{liq}$ and $T_{top}$ started for a liquid amount below ≈13 % in the test 1.5 bar at t = 46.5 min and at ≈14 % in the 2.5 bars test at t = 60 min. This critical value of liquid filling ratio was also found in other tests performed with different initial liquid percentage.

To study if these critical values of liquid filling ration depend on the position of the exhaust, experiments using the upper exhaust (bottom exhaust blocked) were compared with those using the bottom for different filling pressure. For all the tests, the results are very similar and the divergence between the temperatures appears systematically for a liquid fraction between 10% and 15 %.

To test the influence of heating power, some experiment with a lower heating power (0.5 W) were performed and they showed that this critical value of liquid filling ratio is very similar to that obtained in the 1 W experiment. At first sight, the threshold values seem to not depend of heating power.

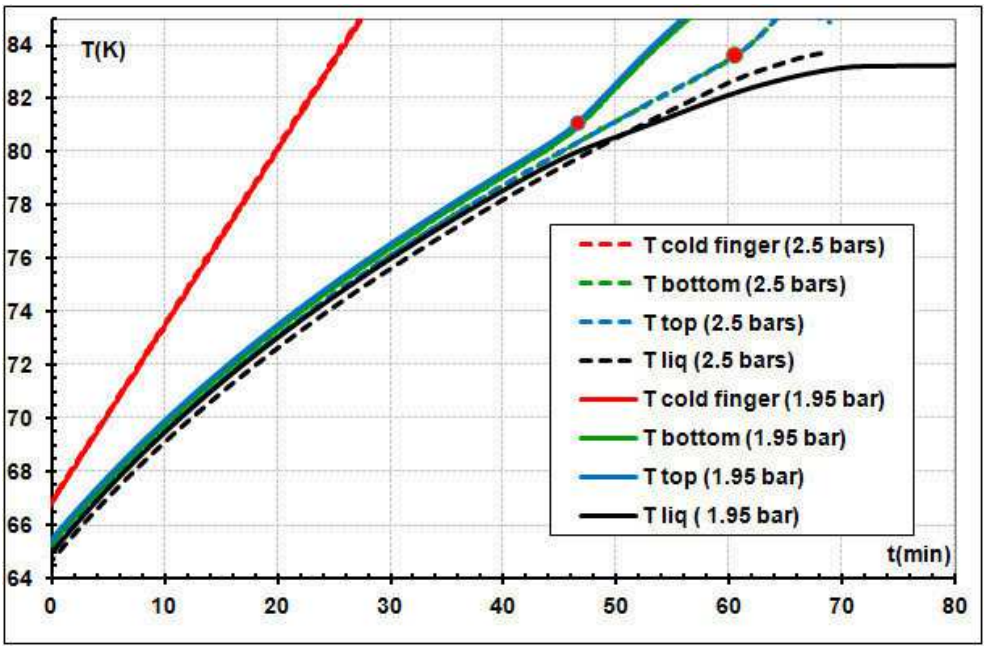


**Figure 2.10: Comparison of the temperature drift with 6 liters expansion volume, cryocooler heating up at 0.8 K/min and 1 W applied with two different filling pressures (1.95 bar solid line and 2.5 bars dashed line). The red points signal the beginning of the abnormal temperature drift and correspond to a filling ratio of 13 % and 15 % respectively.**

#### 2.2.2.2 Volume expansion of 24 liters

In order to store energy with a smaller temperature drift or to work with a higher initial liquid filling ration (then increasing the energy stored with the same temperature drift), tests with 24 liters expansion volume were performed.

In Figure 2.11 two results are displayed: one with ceramic (solid line, corresponding to results of Figure 2.4) and other without (dashed line). In both test, the system was filled with 1.52 bar, corresponding to an initial liquid filling of ≈ 60 % (≈ 22.8 $cm^3$) (without ceramic) and 64 % (with ceramic due to the 8% of ceramic solid fraction). As already seen, the ceramic reduces significantly the temperature difference between $T_{top}$ and $T_{liq}$ as far as the liquid filling is not too small (lower than ≈ 16 %). Without ceramic $T_{top}$ - $T_{liq}$ ≈ 1 K (in the beginning of the experiment) and with ceramic decreases for 0.3 K. In the experiment with ceramic, at t ≈ 48.8 min, when the liquid fraction reaches ≈16 %, the difference between the cell walls and $T_{liq}$ starts to increase as in the experiments with 6 liters expansion volume.

Gravity effect was also studied with this 24 liters expansion volume and no significant difference appeared. With such an expansion volume it is possible to fill the cell with more liquid than with 6 liters, so the ceramic must retain more liquid. For example one test was performed with an initial filling ration of 96 %, and the tests in gravity or antigravity configurations showed similar results.

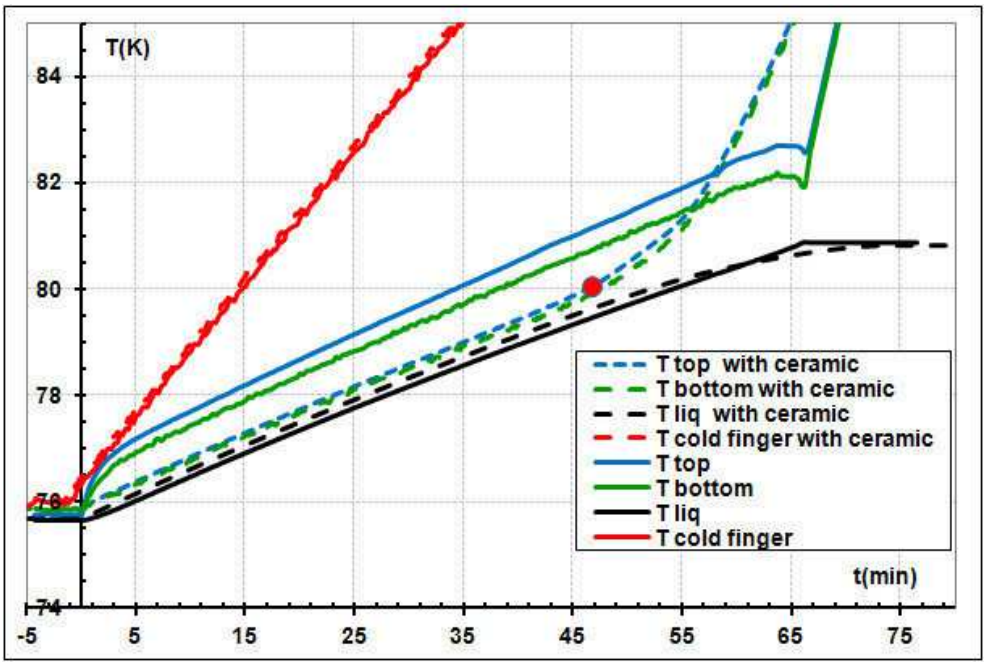


**Figure 2.11: Comparison of the temperature drift with 24 liter expansion volume, 1.52 bar of filling pressure, cryocooler heating up at 0.3 K/min with and without ceramic (dashed line and solid line, respectively). The red point signals the beginning of the abnormal temperature drift and corresponds to a filling ratio of 16%.**

With this volume, to verify again that the critical value is independent of the filling pressure, tests with different filling pressure was realized. Figure 2.12 shows a comparison between one test with filling pressure of 1.52 bar and another with 1.72 bar (corresponding to an initial liquid filling of ≈ 64 % and ≈ 83 %). The conclusion is that to maintain the wall cell temperature close to $T_{liq}$ during a longer time, it is needed to fill the system with more nitrogen.

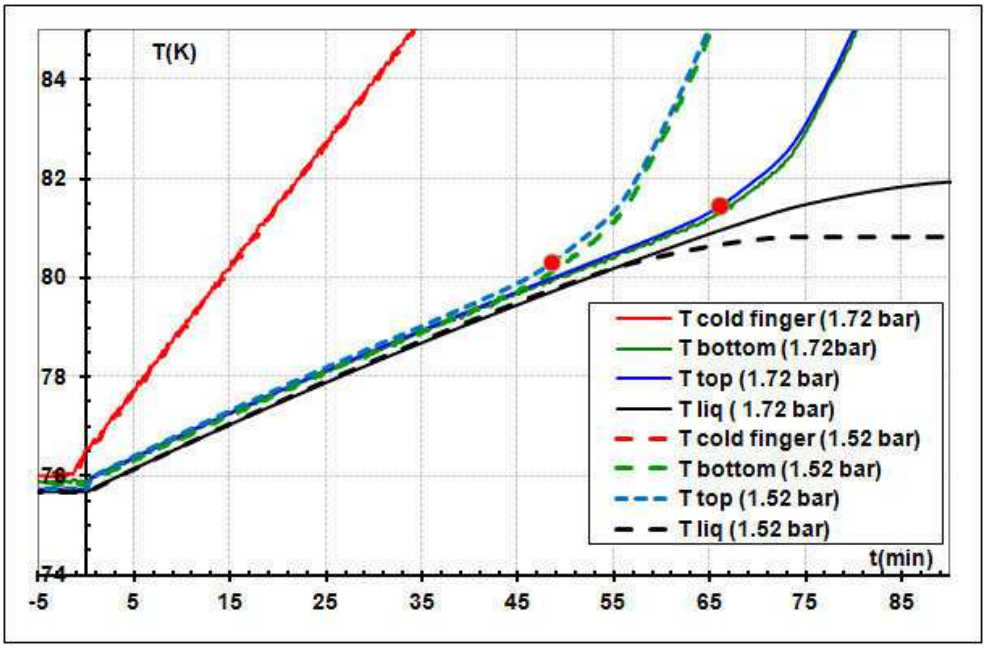


**Figure 2.12: Comparison of the temperature drift with 24 liters expansion volume, cryocooler heating up at 0.3 K/min, 1 W applied load, with different filling pressure 1.52 bar (dashed line) and 1.72 bar (solid line). The red points signal the beginning of the temperature drift and correspond to a filling ratio of 16 % and 17 % respectively.**

The advantage of the system as described in this first part of this chapter is its simplicity: one (eventually large) volume at room temperature and a (rather small) volume at

low temperature. The heat is absorbed by the latent heat of evaporation and by the liquid and solid sensible heat leading to a slow temperature drift. This drift can be reduced using larger expansion volume or working with a gas having a higher dP/dT along the saturation curve in the temperature range desired. As a matter of fact, as dP/dT increases, the expansion volume is able to store more gas for the same temperature drift. It has to be noticed that at low temperature, choice of fluid with a two phase co-existence in the required range of pressure and temperature are not numerous, and sometimes just doesn't exit (range of 5.2 K to ≈ 14 K and 44 K to ≈ 53 K). However, in certain cases, this temperature drift is not acceptable and then a new solution must be found eventually susceptible to compete with triple point ESU.

In conclusion, the ceramic allows turning the system insensitive to gravity and improves the thermal contact between the liquid and the cell wall. However, below a liquid fraction of ≈ 17% in the cell, the wall cell temperature starts to increase very fast. This happens because no more liquid wets the walls and heat conduction becomes ensured by the gas, so the liquid confined in small pore has difficulties to evaporate. So, it is necessary to fill the cell with 17 % of extra liquid added to the necessary amount to store the required energy. This ratio, below which the liquid retained in the ceramic becomes more difficult to evaporate, may depends on the pore size, on the distance from centre of the ceramic to the wall (e.g diameter of the cell), of fluid properties (viscosity, densities) and maybe on the power applied density. This fact might be studied in more detail on the future to optimize cell geometry, and to allow choosing the good porous media.

## 2.3 Controlled temperature Liquid-Vapor Enthalpy Reservoir (without ceramic)

In the previous section, a system in which a temperature drift occurs during the fluid evaporation was presented. This can be an inconvenient for some applications where the temperature stability is a requirement. So, a liquid- vapor system maintaining a constant temperature by pressure control was developed. In this section, this system will be explained and some tests will be displayed.

### 2.3.1 Modus operandi

Experimental set-up (Figure 2.13) is basically identical to that presented in section 2.1.1. The difference is the insertion of a second pressure sensor in the gas circuit at room temperature and a computer controlled valve[3]. In this set-up, the second pressure sensor will measure the pressure in the low temperature cell ($P_{ESU}$), and the first one the pressure in expansion volume ($P_{EXP}$). The computer controlled valve was installed between the cell and the expansion volume (i.e. between these two pressure sensors) in order to control $P_{ESU}$: along the saturation curve, maintaining a constant pressure $P_F$ in the cell will lead to a constant temperature in the enthalpy reservoir ($T_F$). The pressure control was obtained by an ON-OFF control of the valve: if $P_{ESU} > P_{F,\,MAX}$, the valve opens, if $P_{ESU} < P_{F,\,min}$ the valve closes. $P_{F,\,MAX}$ and $P_{F,\,min}$ are defined by the user according to the desired stability. As an example, to maintain $T_F \approx 81$ K, $P_{F,\,min}$ would be 1.525 bar (corresponding to 81.0 K along the saturation curve) and $P_{F,\,max}$ 1.541 bar (81.1 K).

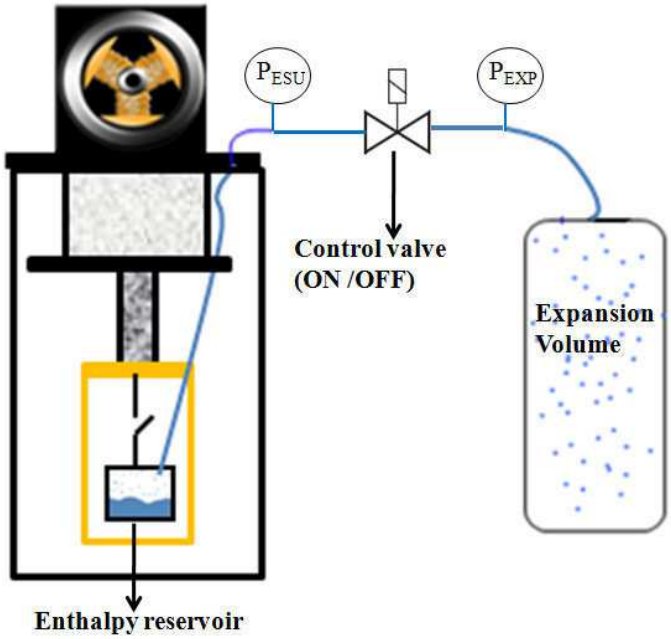


**Figure 2.13: Schema of the controlled temperature liquid-vapor ESU set-up.**

In Figure 2.14 the different phases to run the ESU at constant temperature are displayed. To start the experiment, the expansion volume and the cell are filled at room temperature with a given pressure that determines the fluid quantity during whole experiment. In the first phase, (ESU cooling) the nitrogen is condensed inside the low temperature cell. The low temperature cell acts as a pump for the expansion volume because it is opened to low temperature cell. When

[3] The valve use is needle valve (Pressure and Flow Control Valve Type 148J) fabricated to MRS JAPAN.

the lowest pre-cooling temperature ($T_{PC}$) is reached the expected liquid quantity is condensed in the cell at the lowest pressure, ($P_{min}$) is obtained in the whole system, corresponding to the saturation pressure at $T_{PC}$. At that time, the control valve is closed and the heat switch is opened.

In the second phase, the ESU is heated up from $T_{PC}$ up to $T_F$ with the control valve closed, $T_F$ being the temperature to be maintained constant during the "ESU mode". During this phase, the pressure in the ESU also increases up to $P_F$ (Saturation pressure at $T_F$). So, the pressure in the ESU is larger than the pressure in the expansion volume, and this one will act as a pump during the ESU mode. From this point on, the system is ready to work, i.e. ready to store energy at controlled temperature.

During the ESU mode, a heat load is applied to the ESU, the evaporation leads to a pressure increase: the control valve is briefly open and closed (order computer control) in order to maintain the pressure between $P_{F,\,min}$ and $P_{F,max}$ i.e $T_{ESU}$ almost constant. During this phase, the pressure in the expansion volume $P_{exp}$ increases from $P_{PC}$ up to $P_F$. When the pressure in the expansion volume reaches $P_F$, the pressure control is no more possible ("no more gas pump") and the temperature control ends.

The energy in the ESU is absorbed at "constant" pressure ($P_F$) and temperature ($T_F$). From a thermodynamic point of view, this system works at constant pressure and temperature: the energy stored is simply given by $L\,\Delta n$ where L is the Liquid-Vapor latent heat and $\Delta$n the number of mole evaporated during the ESU mode. The knowledge of the volumes, $T_{PC}$ and the filling pressure, the vapor and the liquid densities and specific energies allows calculating the liquid quantity that will be evaporated during the ESU mode and then the energy stored in the ESU.

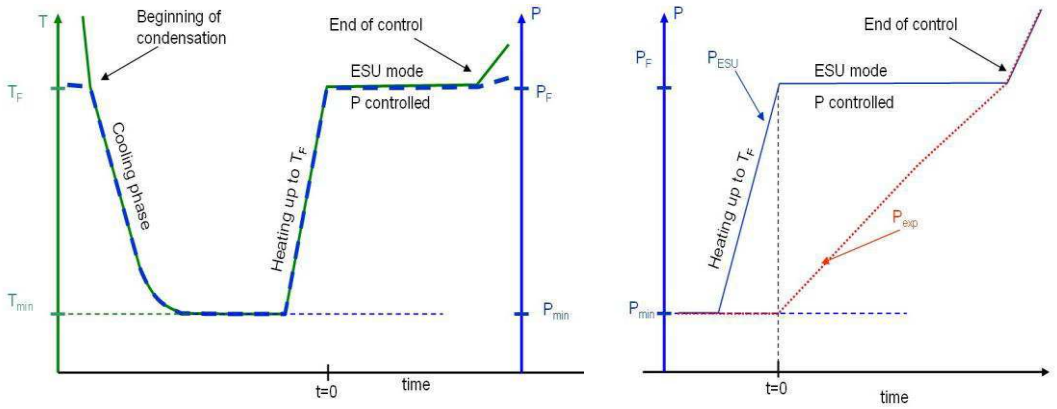


**Figure 2.14: Schema of timing of operation on temperature and on pressure.**

### 2.3.2 Results

To verify if this systems work as expected, tests were carried out, varying some parameters. Knowing the filling pressure, $T_{PC}$ and $T_F$ and the the different volumes, it is possible to calculate the mole number $\Delta n$ that will be evaporated at $T_F$ and then the "theoretical" energy that can be stored.

Figure 2.15 displays one typical experimental result obtained by controlling the pressure. In this experiment, the system with an expansion volume of 6 liters was filled with 2 bars at room temperature. After cooling the low temperature cell down to 65 K ($P_{PC}\approx$ 0.17 bar), the valve was closed and the ESU was heated up to $T_F \approx$ 81 K. At 2 min, the ESU reached $T_F$ =81 K with 38 % of liquid. The pressure in the ESU was 1.52 bar and 0.17 bar in the expansion volume. This pressure difference across the valve turns the pressure control possible and the ESU mode can start.

At t ≈ 3 min, the cold finger temperature (red line) was swept up at a rate of 0.8 K/min for mimicking a natural warming up after stopping the cryocooler.

A constant heating power ($\dot{Q} = 1W$) was applied at t =4 min on the cell, so the temperature measured in the cell increases and the control valve starts the ON/OFF control. In these experiment, $T_F$ = 81 K and the stability for temperature was set to + 100 mK hence the control valve was open for T > $T_F$ + 100 mK and closed if T< $T_F$ (at this temperature such a $\Delta$T corresponds to a $\Delta$P ≈ 0.15 mbar). The black solid line ($T_{liq}$) was obtained from pressure measurement at room temperature and indicates the temperature at the liquid-vapor interface as far as liquid and vapor coexist. The observed oscillations in the $T_{liq}$ have peak-to-peak amplitude of 0.36 K and were caused by the imperfect ON/OFF control.

The blue ($T_{top}$) and green ($T_{bottom}$) lines represent the temperature of the cell walls as measured by the thermometers. The $T_{top}$ and the $T_{bottom}$ increase until to 82.5 K and 82.7 K, respectively, taking 5 min to stabilize. After this phase, the temperatures, $T_{top}$ and $T_{bottom}$ had a small drift approximately (19 mK/min and 11 mK/min), respectively. This drift can be explained by the fact that the liquid evaporates during the ESU mode, consequently the contact area between the housing and liquid reduces, increasing the thermal resistance.

The small difference between $T_{top}$ and $T_{bottom}$ increases with time. This indicates that a small temperature gradient exists along the cell. The $T_{top}$ is higher than $T_{bottom}$ because this thermometer is closer to the electronic resistor used to heat the cell.

The difference between liquid temperature, $T_{liq,}$ and the ESU ($\Delta T \approx$ 1.5 K) is caused by the thermal contact between the liquid- vapor nitrogen and the ESU housing as already explained. An increase of the contact area inside the cell and the fluid should solve this problem. This difference of temperature was also observed in simple enthalpy reservoir results shown in Figure 2.5.

The Figure 2.16 shows the pressures in the cell and in the expansion volume during this experiment. At 27.6 min, the control pressure stopped because the pressure in the expansion volume $P_{EXP}$ aproaches $P_{F,}$ the $\Delta P$ =0.2 bar across the system is too small to allow the necessary $N_2$ gas flow (≈1.8 $10^{-4}$ l/s) to maintain the pressure at $P_F$: the valve stayed open and the pressure and the temperature started to increase in whole system. At that time, calculation shows that inside the cell, 12 % of liquid still exists corresponding to ≈ 4.6 $cm^3$ of liquid. The red point displayed a simple way to determine the time where ESU mode stops

During the ≈ 25 min of ESU mode, an experimental energy ≈1540 J was absorbed.

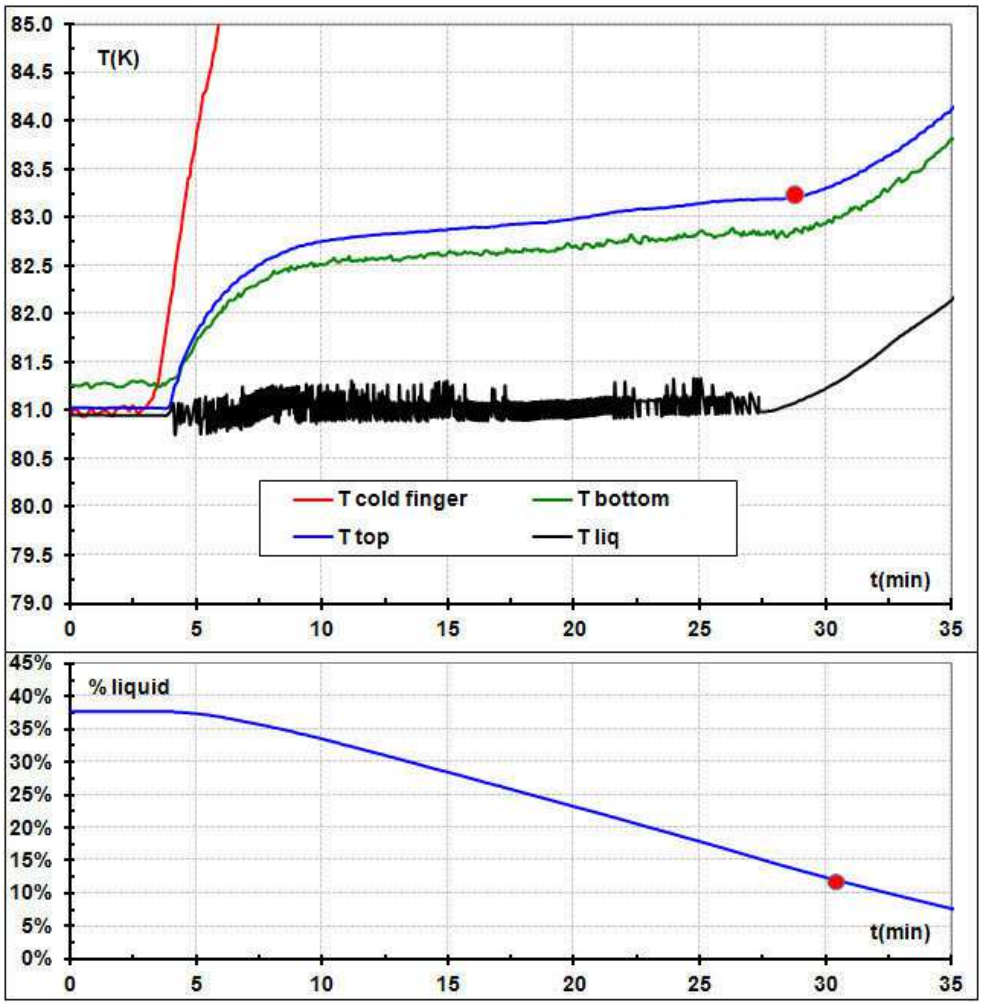


**Figure 2.15: Upper graph: Temperatures versus time for a control at 81 K, 6 liter expansion volume, 1 W applied load, cryocooler heating up at 1.63 K/min. The red point signals the end of the control and corresponds to a filling ratio of 12 %). Bottom graph: Variation of liquid ratio in the cell with time**

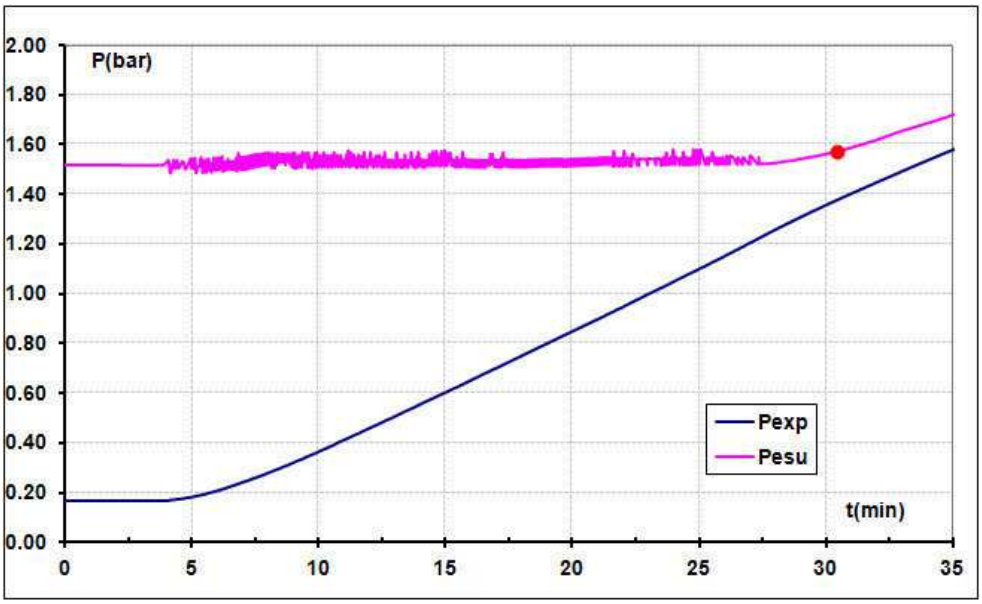


**Figure 2.16: Pressure variation in the expansion volume (blue line) and ESU cell (rose line) during the experiment showed in the Figure 2.15.**

In Figure 2.17, an experiment very similar to the one illustrated in Figure 2.15 is displayed. The difference is that the ESU is connected to an expansion volume of 24 liters. The system was filled at room temperature with 1.52 bar. The low temperature cell was cooled down to $T_{PC} \approx 72$ K.

A constant heating power was applied in the cell at 11 min with 89% of liquid thermalized at 81 K. At that time, the liquid starts to evaporate and the gas is stored in the expansion volume. At the beginning, the ESU mode, the pressure in the expansion volume is 0.5 bar and progressively reached 1.37 bar. When the pressure difference between the expansion volume and the ESU, $\Delta P$, reached 0.21 bar, at 81 min, no more control was possible. This final $\Delta P$ depends on the applied power, the higher the applied power the higher is the $\Delta P$: for example, the $\Delta P$ observed at 1 W is 0.21 bar while at 0.5 W is 0.1 bar. This $\Delta P$ is linear with applied lower indicates a laminar regime in the valve (Re lower than 2300). From this point, the temperature of the cell and the liquid temperature increased while 13 % of liquid leftover. At 93 min, there is no more liquid inside the cell, no more evaporation occurs and all the energy must be absorbed by the cell walls and the gas: $T_{top}$ and $T_{bottom}$ both increase very fast. From this point, the $T_{liq}$ curve is not correct because the system is no longer in the saturation regime.

During the ESU mode, this system stored 4260 J (including parasitical heat leaks) with a drift approximately of 7 mK/min ($T_{top}$) and 4 mK/min ($T_{bottom}$). This experimental energy is in agreement with the calculated within 5 %.

In conclusion, we showed by these results that the small modification introduced in our experimental set-up (a computer controlled valve) allows storing energy at constant temperature. The performed tests showed that our system is able to store energy in a quite reduced cold volume: Taking into account the liquid volume evaporated during these two experiments, ≈ 1542 J and ≈ 4260 J would be stored at 81 K in a ≈ 30 $cm^3$ cell with a 6 liters and 24 liters expansion volume, respectively. Obviously, the 24 liters expansion volume allows storing more gas and then allows storing more energy and/or a lower pre-cooling temperature than the 6 liters expansion volume.

As the system work as expected, a strategy to dimension a controlled liquid- vapor enthalpy was developed. For a given $T_F$ and energy is possible to calculate the volume of enthalpy reservoir, and the expansion volume versus the $T_{PC}$. This calculus are presented in more details in section §2.4.5.

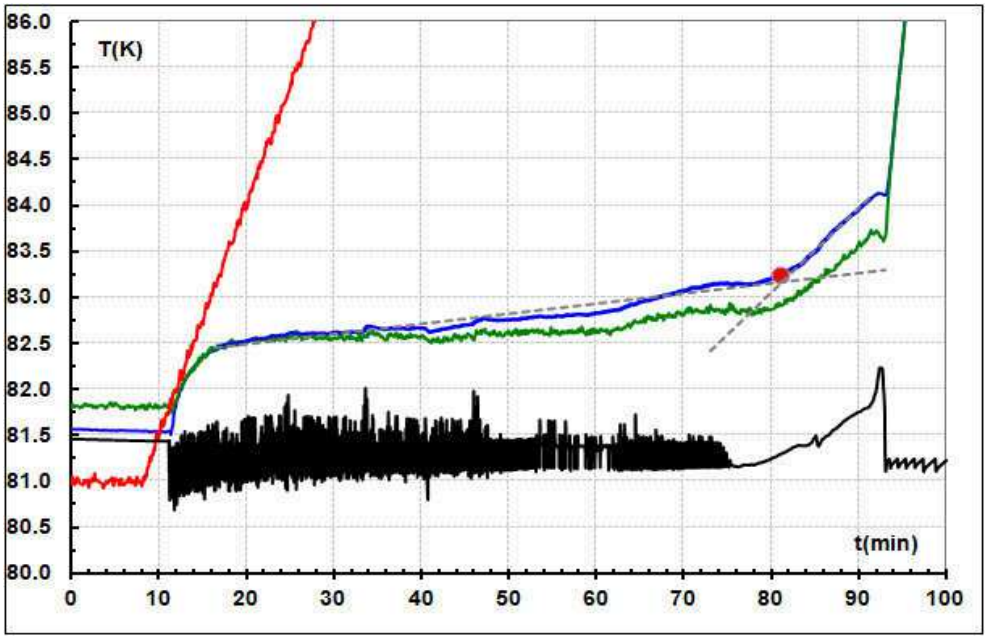


**Figure 2.17: Temperature control at 81 K, 24 liters expansion volume, filling pressure of 1.52 bar, 1 W applied load, cryocooler heating up at 0.3 K/min. The red point signals the end of the control and corresponds to a filling ratio of 13 %.**

## 2.4 Controlled temperature Liquid – Vapor Enthalpy Reservoir (with ceramic)

To transform this system insensitive to gravity, the same ceramic (Procelit P160) as in the test presented in section 2.2 was fitted in the same low temperature cell to perform tests with temperature control.

### 2.4.1 Results

In Figure 2.18, it is possible to see two superimposed experiments: one with ceramic (dashed-line) inside the cell and another without ceramic (solid-line), the same experiment showed in Figure 2.15. In both experiments, the cell was pre-cooled down to 65 K. So, at the beginning the experiment the cell with ceramic has 41 % of liquid and the cell without 38 %, this difference being due to space occupies by ceramic. During the ESU mode 1 W was applied and the gas flows out of the cell by the upper exhaust.

The ceramic inside the cell causes some differences similar to those detected in the "simple ESU" configuration. The main contrast is that the ceramic significantly reduced the temperature difference between the liquid interface ($T_{liq}$) and the thermometers ($T_{top}$ and $T_{bottom}$). With ceramic, this difference grows from 0.5 K up to 1 K during the ESU mode whereas it was 1.5-2 K without ceramic. As already observed, the initial thermal time constant of the cell housing with ceramic is shorter than without ceramic and the difference between $T_{top}$ and $T_{bottom}$ is decreased. In relation to the control, without ceramic the $\Delta T_{liq}$ is 0.36 K ( i.e 0.06 bar), but with ceramic the control is more efficient, the temperature can be controlled within 0.18 K (i.e 0.03 bar).

As previously discussed, all these novelties occurring in the presence of ceramic are a consequence of the better thermalisation between the liquid and the cell housing thanks to the capillarity effect that allows a larger wetting of the cell walls. Also it is possible that the ceramic increases nucleation sites and decreases the natural convection.

In the experiment with ceramic, as in the 6 liters test, the $T_{top}$ and $T_{bottom}$ start to drift when there is 14 % of liquid inside the cell (≈ 28 min, this value take into account the ceramic volume, 13 % is the volume occupies by liquid without ceramic). The cell temperature and the pressure control with ceramic finished when the $T_{top}$ and $T_{bottom}$ are ≈ 2 K higher than the control temperature. This behavior indicated that the last 14 % of liquid did not enter in contact with the cell walls and they are more difficult to evaporate from the ceramic. More detailed these experiences are in Table A.1 in Appendix A:.

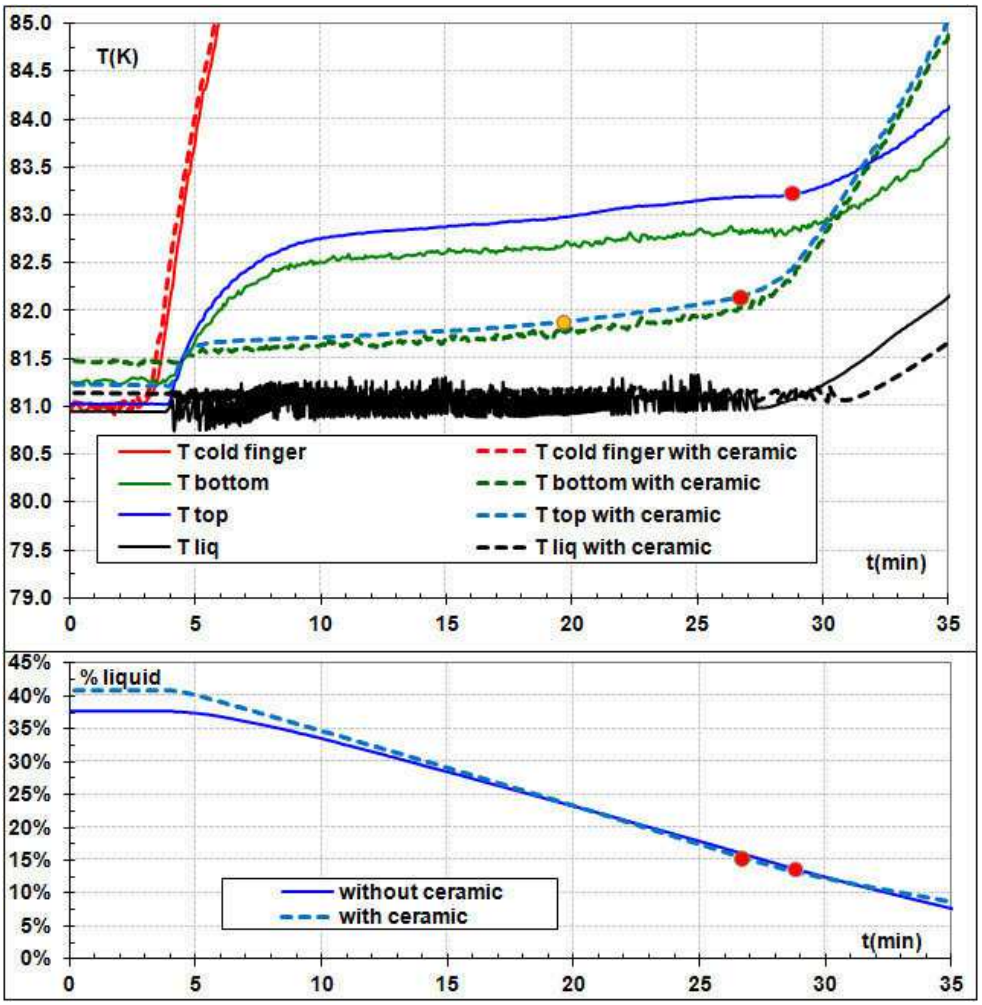


**Figure 2.18: Upper graph: Comparison of the temperature drift with 6 liters expansion volume, 2 bars filling pressure, cryocooler heating up at 1.63 K/min, 1 W applied load with ceramic (dashed line) and without ceramic (solid line). The red points signal the end of the control and correspond to a filling ratio of 12 % and 14 % of liquid respectively. Bottom graph: Variation of liquid quantity with the time.**

### 2.4.2 Tests with Ceramic

The following tests were made to analyze if the ceramic causes the same three main effects observed in the simple liquid enthalpy reservoir configuration: system insensible to gravity, heat exchange improvement until a certain "critical" liquid percentage where the liquid becomes more difficult to evaporate.

To verify that the threshold of this growing temperature difference depends only on the liquid quantity, a test was carried out with a higher initial liquid percentage. During these tests the exhaust is on the top of the cell.

For that, the system was filled with higher filling pressure, 2.5 bars (6 liters volume, corresponding to an initial liquid filing of ≈ 54%) instead of 2 bars (corresponding to an initial liquid filing of ≈ 41%). The other initial conditions were identical. In Figure 2.19, the results of these two tests are shown: solid line is the test with a filling pressure of 2 bars and dashed line is the test with filling pressure of 2.5 bars).

To noticeable results appear in the case of the test with higher pressure (2.5 bars) in comparison with the test at 2 bars. The first is, for 2.5 bars, there is not divergence between $T_{liq}$ and $T_{top}$, until the end of the ESU-mode: when the control reaches its limit of feasibility ($P_{ESU} \approx P_{EXP}$) there is still 26 % of liquid inside the cell. In relation of experiment for 2 bars, it is possible see in comparison with the plateau of experiment of 2.5 bars that the "abnormal" temperature drift starts at 15.3 min when 26 % of liquid still exists in the cell. But, if analyzed

the Figure 2.18 at 15.3 min nothing seems to indicate the beginning of this effect. This shows that the method to determine the "critical filling ratio" can be not quite accurate. A study of this critical ratio was beyond the scope of this work, where the goal was to determine the effect of the ceramic in such a device. After detecting this drift temperature a more precise study was started with helium. This work is presented in the Chapter 4. Then this "critical percentage" used in this chapter must be considered as indicative and not as a rigorous determination.

The second remark is that $T_{top}$ and $T_{bottom}$ during the test with 2.5 bars were closer than in the test with 2 bars because more quantity of liquid was in the cell and this improves homogeneity of the cell.

Another test was performed varying this initial liquid percentage and when the liquid fraction becomes lower than 20%-26%, the divergence between $T_{liq}$ and $T_{cell}$ systematically starts. To avoid this divergence it is necessary to fill the cell with higher pressure, so that, when the control finishes, the liquid quantity inside the cell is still greater than 26 %. In respect to simple liquid enthalpy reservoir systems (no pressure control), it seems that in the control liquid enthalpy reservoir experiment the temperature drift occurs for higher liquid percentage (20%-26% instead of 10-16%). Actually, we think that these higher values are a consequence of a more objective criterion in which we compare a temperature change in respect to a quite constant temperature behavior whereas in the simple ESU experiment we try to localize a slope change during the temperature drift.

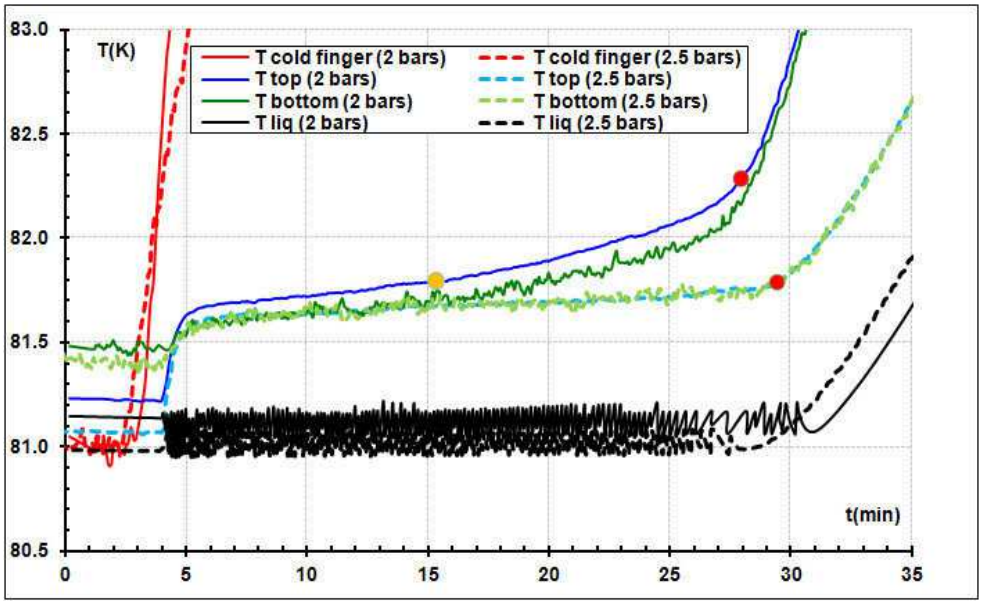


**Figure 2.19: Comparison of the temperature drift with 6 liters expansion volume, with ceramic, cryocooler heating up at 1.63 K/min, 1 W applied load and with filing pressure of 2 bars (solid line) and 2.5 bars (dashed line). The capillary was in top of the cell. The red points signal the end of the control and correspond to a filling ratio of 14 % and 26 % respectively. And the yellow points the beginning of the temperature drift and corresponds to a filling ratio of 26 %.**

In Figure 2.20 it is also possible to see the superimposed results of two tests in similar conditions as in Figure 2.19 but with 0.5 W applied load, this time with the capillary in the bottom of the cell. The results of these tests show that the cell retains the liquid. Otherwise the liquid would have been expelled when the cell was heated. As is possible to see, in the experiment with more quantity of liquid (dashed line in Figure 2.20), the cell temperature was kept stable during the whole ESU mode. At the beginning and at the end of the ESU mode the percentage of liquid is 53% and 24% for 2.5 bars, respectively. In the test with 2 bars (with 42 % of liquid in the beginning) at 43 min the cell temperature started to increase: it corresponds to the mentioned reaching of the critical values of liquid quantity (21 %). In both tests, the temperature measured at the bottom and at the top are the same which is due to the lower applied load and the higher quantity of liquid in respect to the test with 1 W applied in

cell, so the cell was is thermally more homogenous. Figure 2.19 and Figure 2.20 illustrate the same effects. So, the position of the capillary is irrelevant when there is ceramic inside the cell.

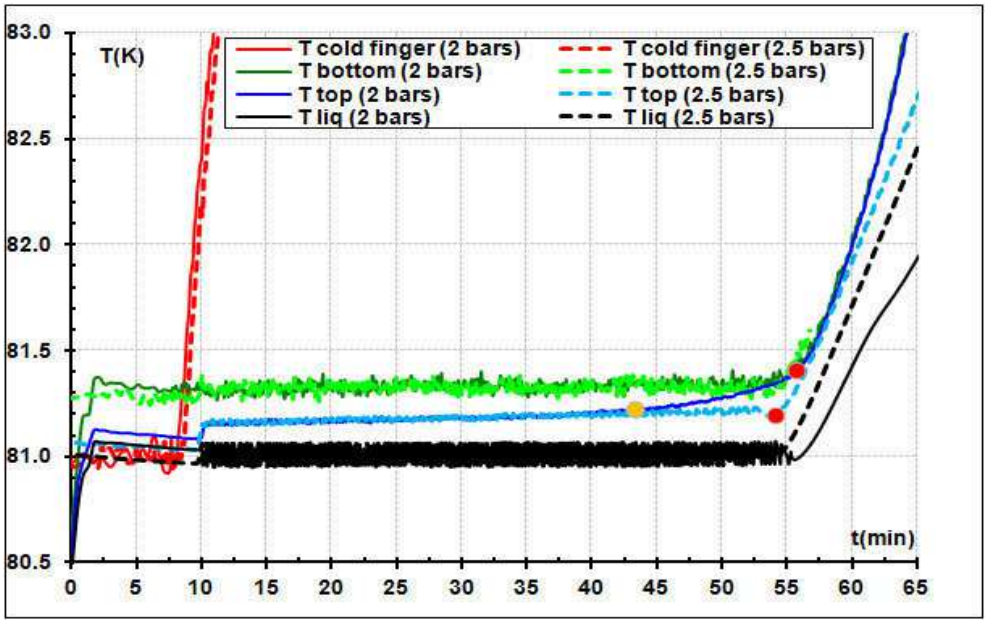


**Figure 2.20: Comparison of the temperature drift with 6 liters expansion volume, with ceramic, cryocooler heating up at 0.8 K/min, 0.5 W applied load and with filling pressure of 2 bars (solid line) and 2.5 bars (dashed line). The capillary was in bottom of the cell. The red points signal the end of the control and correspond to a filling ratio of 24 % and 12 % respectively. The yellow point the beginning of the temperature drifts and corresponds to a filling ratio of 21 %.**

Figure 2.21 depicts two tests performed in same conditions with ceramic: one with the gas exhausting by the bottom output (solid line) and the other by top output (dashed line). The filling pressure was 2.5 bars and the $T_{PC}$ was 64 K. However, between the two experiments, a small modification was made in the cell: a copper grid was introduced between the ceramic and the cell walls with the intention of improving thermal contact between the cell walls and the ceramic. This can explained the different behavior when 1 W was applied in the cell with and without the copper grid. In the cell without the copper grid, $T_{top}$ and $T_{bottom}$ increase 0.5 K and 0.2 K, respectively and both stabilized at 81.6 K. In the cell with the copper grid when the heating power is applied only the $T_{top}$ increases, and stabilizes at 81.3 K. The $T_{bottom}$ kept stable at 81.4 K. During the ESU mode, the $T_{top}$ and $T_{bottom}$ differed by 0.1 K more that in the case without grid of copper. The copper grid decreases the difference between the cell temperature ($T_{bottom}$ and $T_{top}$) and $T_{liq}$ from 0.6 K to 0.4 K.

Beside this small difference, these two tests reinforce the demonstration that the insertion of the ceramic turned this cell insensitive to gravity effects.

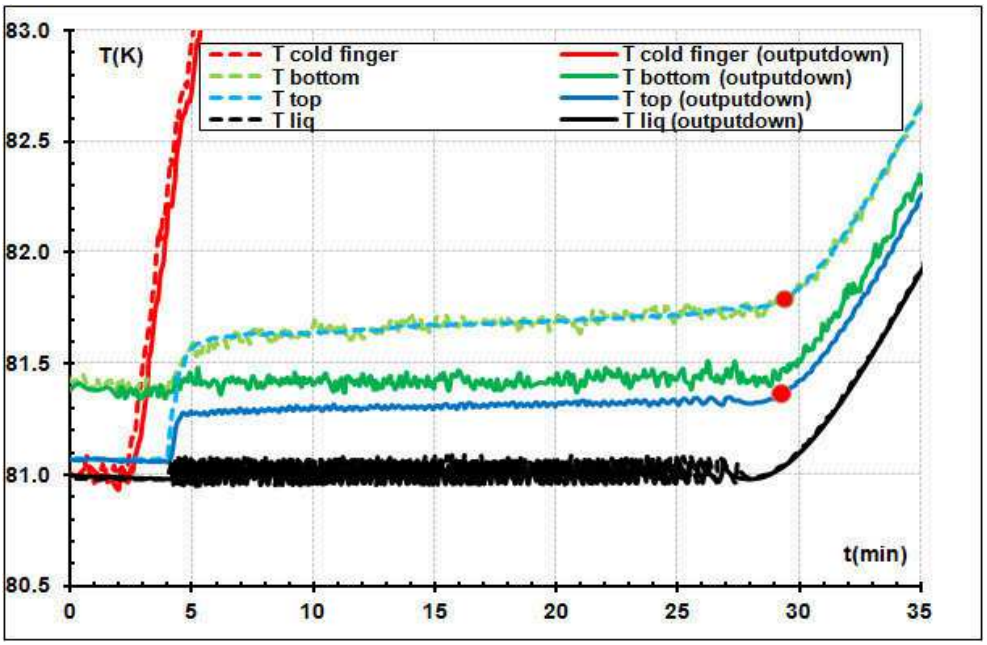


**Figure 2.21: Comparison of the temperature drift between the cell with and without the copper grid (solid line and dashed line, respectively) with 6 liters expansion volume, with ceramic, cryocooler heating up at 0.8 K/min, 1 W applied load with filling pressure of 2.5 bars The capillary was in the bottom of the cell. The red points signal the end of the control corresponds to a filling ratio of 26 %.**

Tests with 24 liters expansion volume were also carried out. Figure 2.22 displays the temperature control at 77.1 K with a 0.5 W applied power and using the upper exhaust. The low temperature cell was pre-cooled down to 70 K. The ESU mode started with 81 % liquid ratio and stopped at 35% when the pressure drop between the cell and the expansion volume decreased down to 0.12 bar, turning impossible any further pressure control. As depicted in Figure 2.22, $T_{top}$, $T_{bottom}$ and $T_{liq}$ were very stable during the whole ESU mode, maybe because of the relatively high liquid filing.

Let us insist again on the advantage of using a 24 liters expansion volume: it allows storing a large amount of gas then a large energy with a pre-cooling temperature, $T_{PC}$, relatively near $T_F$. For example, in this run, the energy stored was ≈ 2436 J at 77 K and, for this energy, the system only needed to be pre-cooled at 70 K, only 7 K below $T_F$.

The disadvantage of using a 24 liters expansion volume is the difficulty to integrate it in a spatial system because of its size. However, as mentioned in the previous chapter, let us note that the Swales Aerospace built and tested a ESU operating near 35 K connected to a 23 liters expansion volume to store 5670 J. This ESU was partially tested on shuttle flights STS-95 [19].

### 2.4.3 Other tests

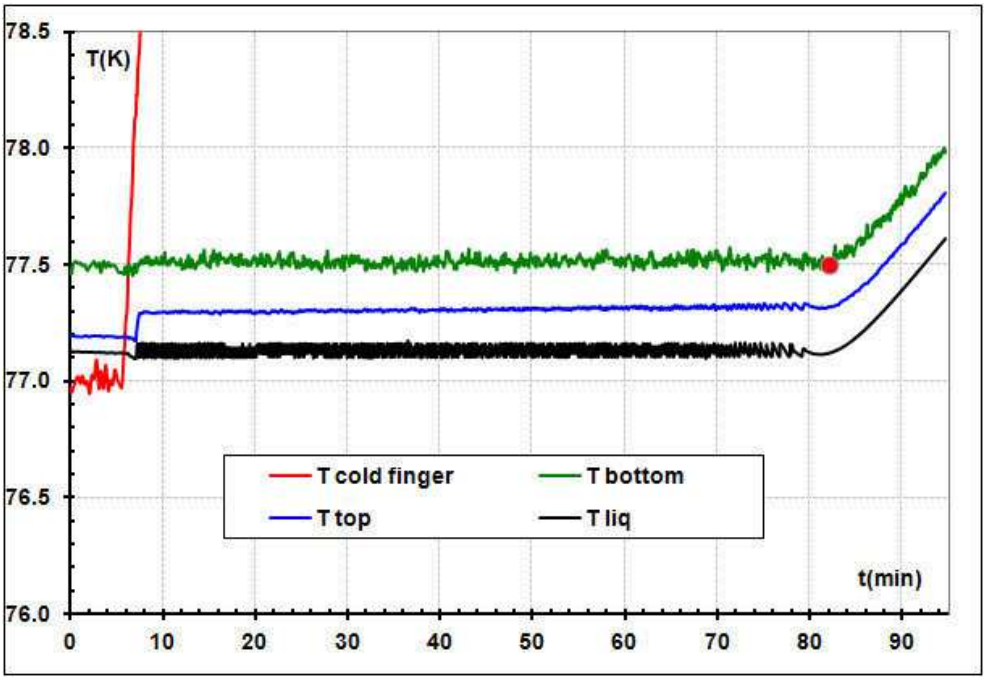


**Figure 2.22: Temperature control at 77.1 K using the bottom gas exhaust of the cell with ceramic with 24 liter expansion volume, cryocooler heating up at 0.8 K/min, with filling pressure of 1.25 bar. The red point signal the end of the control corresponds to a filling ratio of 35 %.**

In all experimental results so far presented, the applied load was constant during the ESU mode, the main goal being to mimic a sensor that dissipates a constant power during its operation. However, the ESU can be also used to absorb energy in systems where some heat bursts are released during short time intervals. Figure 2.23 displays the results for an applied load varying suddenly between 0 W and 2 W. For this experiment, the filling pressure was 2.5 bars, $T_{PC}$ =64 K and controlled at 81 K. During the ESU mode, different heating powers of different durations were applied on the top of the cell. Independently of this different applied loads, $T_{bottom}$ and $T_{liq}$ (green and black lines) remained constant within 0.1 K. These tests confirmed that the ESU can be used to attenuate some heat bursts released in a system. Let us note that because the thermometer measuring $T_{top}$ and heating were thermalized very close one of the other, the temperature in the top of the cell is more heating power dependent: $T_{top}$ varied between 81.1 K and 81.4 K for applied load between 2 W and 0 W.

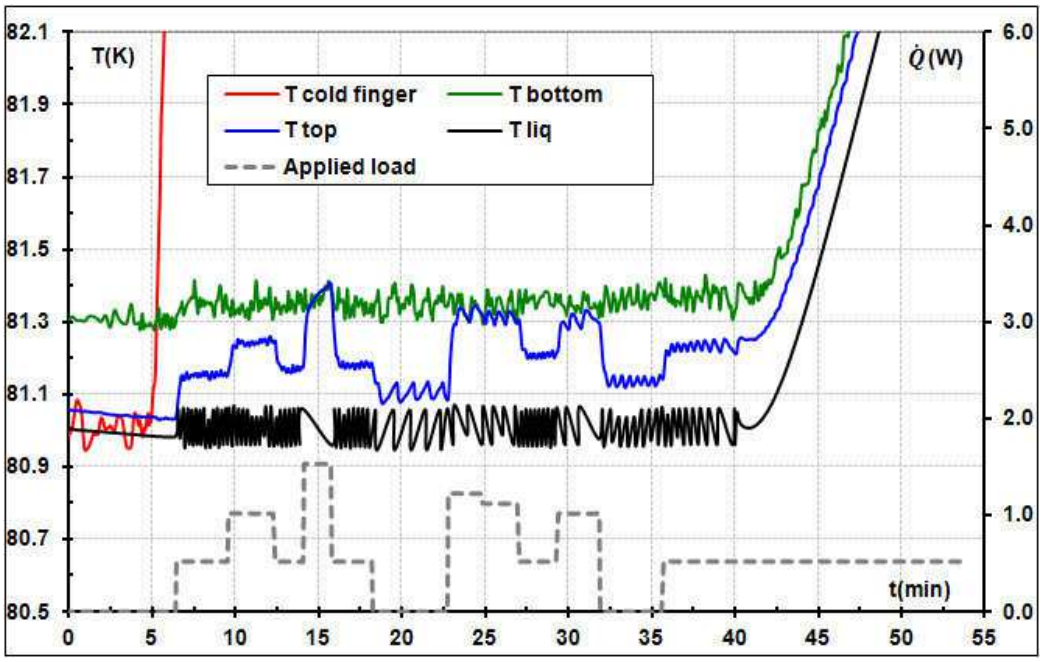


**Figure 2.23: Temperature control at 81 K when heat burst are released using the bottom gas exhaust of the cell with ceramic with 6 liters expansion volume, cryocooler heating up at 1.63 K/min, with filling pressure of 2.5 bars.**

### 2.4.4 ESU working in "Power booster mode"

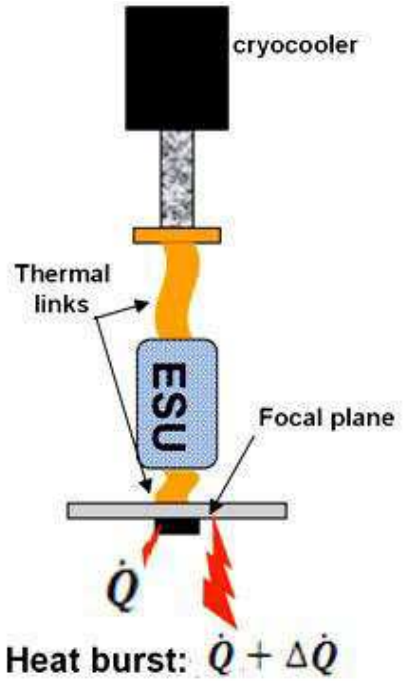


**Figure 2.24: Schematic of the "cooling power booster" mode.**

In some application an ESU directly thermally coupled to the cold finger (Figure 2.24) can be also used as a "cooling power booster" [2] if heat bursts are from time to time released to the cryocooler cold finger. As a matter of fact, if a "constant temperature ESU" is connected to the cold finger, when a peak heat load happens, the thermal energy is absorbed by liquid evaporation, avoiding any temperature increase: during the heat burst, the cooling power is temporarily increased. After the heat burst is over, the evaporated liquid must be recondensed to be able to absorb the next heat peak.

In the case of our tests, to avoid removing the heat switch between the cold finger and the ESU, the heat switch is still present but it is filled with helium, for higher ON conduction. For the temperature range used in these tests, the switch is always in the ON state with a thermal conductance evaluated to ≈ 650 mW/K.

Some tests were performed in these conditions; a typical result is illustrated in Figure 2.25. In this experiment where the system was filled with 2 bars, the cell without ceramic has pre-cooled down to approximately 64 K.

For $t<0$, a constant heating power was applied on the cold finger of the cryocooler, leading to a constant temperature (≈ 79.2 K) characteristic of the cooling power of the cryocooler. At $t=0$, an extra external constant heating power (0.5 W) was applied on the cell walls. The fluid was exhausted by the upper top part of the cell. The ESU temperature increases of about 0.5 K (due to thermal contact between fluid and ESU housing) and stabilizes: a nearly constant temperature is obtained during 55 min. During this time, the cold finger temperature increases slowly of about 0.3 K. At t ≈ 56 min, the pressure in the expansion volume becomes almost equal to the ESU pressure and the pressure control is no more possible: The ESU succeeded to increase by 0.5 W the cooling power of the cryocooler during 55 min.

In same figure, the symbols curves represent the temperature drift obtained in same conditions but with no fluid in the ESU: a configuration mimicking a cold finger without ESU. For $t>0$, the temperature increased with time, up to the new cold finger equilibrium temperature for this new heating power. Despite this relatively small temperature drift due to the high thermal inertia of this system (cold finger + ESU) and to the relatively high cooling power of the cryocooler at this temperature (1W @ 4 K), these results show how can a ESU in the power booster mode be used to increase the temperature stability in the case of sudden heat bursts: such an ESU can avoid the utilization of oversized cryocooler only to limit temperature drifts due to heat burst occurring very rarely. For space applications, it can imply a very appreciable gain in weight.

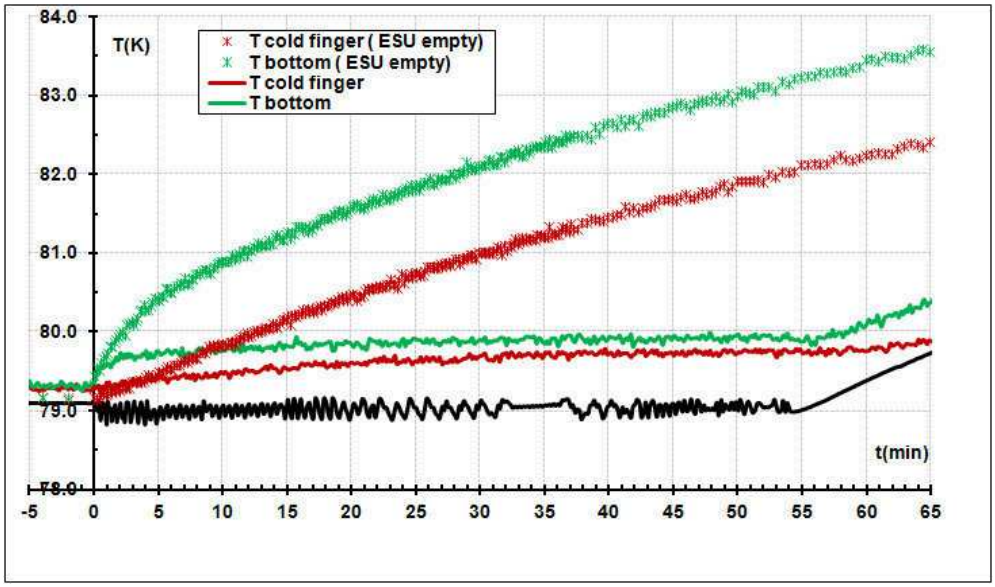


**Figure 2.25: Temperature drift in cooling power booster mode with an ESU filled with nitrogen (solid line) and the empty ESU (crosses).**

### 2.4.5 Software for controlled temperature Liquid-Vapor Enthalpy Reservoir

A pre-dimensioning tool was written in JAVA language to allow dimensioning an ESU working at constant temperature as described in this last sections § 2.3. This software calculates for a given energy stored at a functional temperature $T_F$, the pre-cooling temperatures ($T_{PC}$) (called $T_{min}$ in this software) as a function of the expansion volume size. The inputs are (the numbers corresponding to indication in Figure 2.26):

1. The cryogenic fluid (nitrogen, propane, argon, ethane, hydrogen, neon, oxygen, methane)
2. The functional temperature $T_F$, the temperature at which the system will be controlled.
3. The maximum acceptable size for the expansion volume.
4. The required stored energy.

The thermophysical properties obtained by the NIST on-line data base [33] were used to the calculations.

For example, to store $E_{stored}$, the software calculates the amount of mole liquid ($n_{liq}$) to be evaporated at $T_F$ to absorb this energy (see equation (2.1)). From this value, the minimum volume of the cell is calculated: the cell is considered full of 100% liquid at $T_F$ at the beginning of the ESU mode and empty at the end. The expansion volume must be able to store the amount of gas produced during the liquid evaporation: equation (2.2) using simple perfect gas law approximation gives the relation between the value of the expansion volume and $P_{min}$ (pressure at $T_{PC}$), and $T_{min}$ is calculated as the saturation pressure at $P_{min}$. From these equations, $T_{min}$ is calculated for various expansion volume data regularly spaced between 0 and the maximum expansion volume indicated by the user.

$$n_{liq} = \frac{E_{stored}}{L} \tag{2.1}$$

$$n_{liq} = \frac{(P_F - P_{min})V_{exp}}{RT_{exp}} \tag{2.2}$$

Figure 2.26 displays the graphical interface of this software. This pre-dimensioning tool returns the following outputs (the number refer to the number indicated in Figure 2.26):

5. The functional pressure at $T_F$
6. the minimum volume of the low temperature cell to store the energy required
7. A plot of $T_{PC}$ versus the size of the expansion volume
8. A table with the plotted data and the initial the filling pressure
9. The tab “Gas” gives some properties of the usual cryogenic fluids at the triple and critical point in order to help an adequate choice.
10. The tab “File” gives the densities and the enthalpies (data and plot) of the chosen gas in the gaseous and liquid phases along the saturation curve.

For instance, in the graph zone (n°7), the red curve gives $T_{PC}$ versus expansion volume to store 1500 J (n°4) at 81 K (n°2) using a 9.8 $cm^3$ cell (n°6)

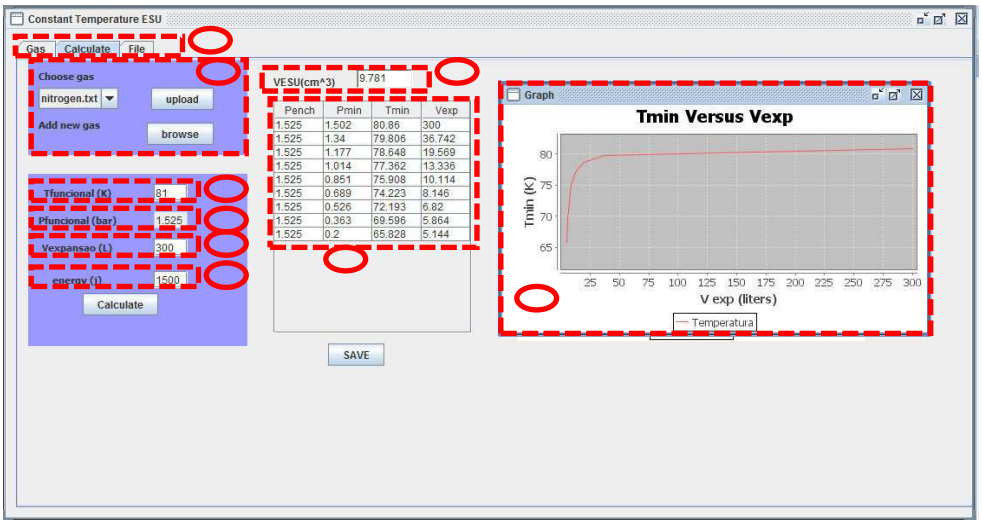


**Figure 2.26: Interface of the software for constant temperature liquid enthalpy reservoir. The encircled numbers are identifying parameter explained in the text.**

This software was tested in comparison with experimental results in order to discard programming and/or reasoning errors.

## 2.5 Conclusion

In this chapter, two different types of energy storage unit connected to an expansion volume at room temperature were presented.

In the first system, the high latent heat of a cryogenic liquid is used to decrease the temperature drift when a thermal load is applied to the ESU while the cryocooler was stopped. Tests with two different expansion volumes (6 liters and 24 liters) were performed. With 6 liters expansion volume, the ESU stored approximately 3 kJ while drifting between 64 K and 83 K. But in some cases this temperature drifting maybe unacceptable. So, a solution to limit this drift was to increase the expansion volume. A test with the ESU connected to a 24 liters expansion volume between 72 K and 80 K stored 4 kJ. Increasing the expansion volume allows to store the same energy with a reduced temperature drift or for the same temperature drift to increase the energy stored. The lower is $T_{PC}$, the lower is the pressure in the expansion volume and, then, more efficient is the expansion volume to store gas nitrogen during the ESU mode. The energy stored in our different systems in various experimental conditions was in agreement within few percent with those calculated from simple thermodynamics models without any adjustable parameters.

The second system presented is composed by the energy storage units connected to the expansion volume through a computer controlled pressure valve. This back-pressure control allowed building a liquid-vapor ESU working at constant temperature. This system allowed choosing the working temperature as far as it corresponds to a temperature at which liquid and gas may coexist. Such a system can compete with the “Triple point” ESU (see section §1.3): the constraint to work exactly at the triple point temperature disappears and the latent heat liquid-gas is significantly higher than the solid-liquid one. A priori, not to close of a critical point where the latent heat vanishes, the energy stored by volume unit is higher than at the triple point.

To turn these systems insensible to gravity, a ceramic was inserted inside the low temperature cell. The ceramic retained the liquid and helps to homogenize temperature. However, we detected that the last 15%-26% of liquid are more difficult to evaporate. Below to this somewhat “critical” liquid percentage, a quite high temperature gradient can exist inside the cell. This problem will be studied in more details in Chapter 4:

# Chapter 3: Study of Energy Storage Unit at 4.5 K

In this chapter, the dimensioning of an ESU using helium and able to absorb 300 J at 4.5 K with a drift temperature of approximately 0.2 K is presented. The reason why the helium is a good candidate compared to other fluids and solid materials is discussed. A study was also carried out to analyse the sensibility of the initial temperature and the acceptable temperature drift.

## 3.1 Context

Some astrophysics missions require the use of very low temperatures (< 1 K) for detectors cooling. To obtain this low temperature different architecture are available. For example to obtain 300 mK on Herschel satellite, an adsorption refrigerator with $^3$He is pre-cooled by a bath of liquid helium maintained at 1.7 K thanks to the free pumping resource available in space. The disadvantage of helium bath is the limited lifetime. Therefore, to overcome this, the tendency is to replace baths by cryocoolers (as on Planck satellite). In the future mission of astrophysics in the field of infrared radiation, SPICA, the detectors need to be cooled to 50 mK. One way to achieve this temperature level is to use for the sub-kelvin stage a $^3$He adsorption refrigerator coupled with a stage of adiabatic demagnetization refrigerator (see Figure 3.1). This sub-kelvin cooler is pre-cooled with a $^3$He and a $^4$He Joule Thomson refrigerators, themselves pre-cooled around 20 K by two-stage Stirling refrigerators [11].

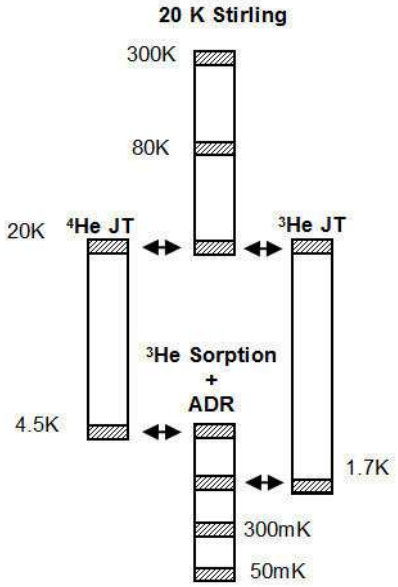


**Figure 3.1: Schema of the SPICA cryogenic chain [11].**

Studies carried out at CEA/SBT [32] have shown that the cooling power required for recycling the adsorption refrigerator which presents an important peak power at 4.5 K cannot be absorbed entirely by the $^4He/^3He$ Joule-Thomson cooler [11]. The adsorption refrigerator as well as the adiabatic demagnetization refrigerator is one shot system that needs to be periodically recycled. During recycle, this sub-kelvin cooler rejects some thermal loads on the upper temperature stages (1.7 K and 4.5 K stages). To prevent the dry out of the J-T cooler, it is necessary to limit the peak power. This means in practice a slow recycling of the adsorption refrigerator which limits the duty cycle efficiency of the cooler. Therefore, there is a reduction of the low temperature observing phase duration which leads to a reduction for science data acquisition. The recycling phase of the refrigerator lasts approximately 11 h. This phase was analyzed in order to identify solutions for minimizing its duration. One way to shorten the recycling time is to use an ESU which allows absorbing one part of energy rejected at 4.5 K.

The results of the study performed at CEA/SBT demonstrate than the recycling time can be reduced using an ESU. In Table 3.1 it is possible to see how much the recycling time can be reduced as a function of energy absorbed by ESU and the temperature drift allowed.

**Table 3.1: The reduction of the recycling time as function of the energy stored in the ESU and the temperature drift.**

| E (J) | Recycling time | $\Delta T$ |
|---|---|---|
| Without ESU | 11 h | |
| 260 | 6.5 h | 4.52 K-6 K |
| 360 | 5.3 h | 4.57 K-6 K |

To store the energy in this range of temperature, one can use the latent heat of a cryogenic fluid or the sensible heat of a solid material. As far as fluids are concerned, only helium have a fluid transition is this temperature range. In this chapter a generic study of an ESU using helium is presented and compared with a solid ESU.

## 3.2 Analyze an 1 liter ESU using Helium

Helium is the only fluid that could be liquid below 13.95 K (hydrogen triple point) and so the only candidate if we want to use the liquid vapor transition to store some energy at low temperature. Helium has 2 isotopes, the helium 4 which is the most common and the helium 3. The helium 3 has its critical point at 3.33 K and could not be used to address needs around 4.5 K. So the only fluid remains the helium 4 which has a critical temperature of 5.2 K. The latent heat associated with the liquid -vapor transition is presented in the Figure 3.2.

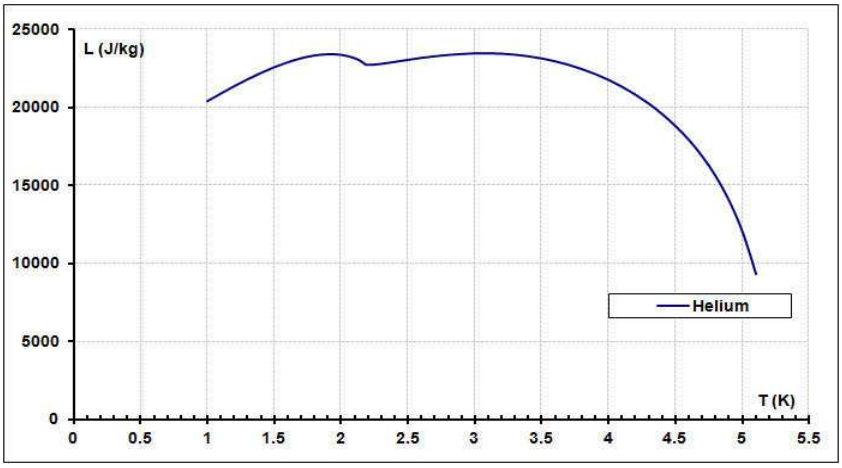


**Figure 3.2: Helium's latent heat as a function of temperature.**

To facilitate the integration of the ESU in the system, a single volume ESU is more adequate. For the first study, the ESU was considered to be a volume of 1 liter of helium. This

volume is the good order of magnitude to address the needs of a space mission like the SPICA mission. The initial objective of this study is to analyze the variation of the stored energy with the filling pressure. This room temperature filling pressure is used to size the thickness of the reservoir which in turn allow to calculate the overall associated cold mass

The single volume ESU is filled at room temperature with a given pressure and after it is sealed. To liquefy the helium inside the ESU, it is necessary to cool it down. After, a heat load can be applied on the ESU and some energy is absorbed with a limited temperature drift.

The energy stored in the ESU can be calculated from the first law of thermodynamic, i.e:

$$\partial Q = dU + \partial W \tag{3.1}$$

Since the volume of the cell is constant, the work applied to the system is zero. So, any heat energy transferred to the ESU will be absorbed as internal energy. From the filling pressure at room temperature and the volume of the ESU, the density can be calculated using real gases properties. Knowing the overall density, which remains constant in all phases (the cell is closed so volume and total mass are kept constant if we neglect the very small thermal contraction), and the temperature, it is possible to calculate the percentage of liquid and vapor inside the ESU (with the assumption of isothermal cell and thermodynamic equilibrium).

Starting from an isothermal point at 4.5 K, it is possible to see the quantity of energy that could be stored for a given temperature drift depending of the quantity of helium sealed inside the volume (filling pressure).

In Figure 3.3 it is possible to see the energy stored when the volume is heated and the evolution of the volume of liquid percentage for different filling pressure. Each line represents the evolution of liquid percentage when the stored energy increases. Table 3.2 gives the helium density for a given filling pressure. For example, when the ESU is filled with 500 bars at room temperature (orange solid line) it corresponds to a density of 65.3 kg/m$^3$, which is lower than the critical density. At 4.5 K, the volume of ESU contents 44.6 % of liquid helium and 55.4 % of vapor of helium. Afterwards, if we suppose that a thermal load is applied on the ESU, the volume of liquid slowly decreases (as the two-phase density is lower than the critical density) to adsorb one part of the energy in the liquid-vapor transformation. But, in the final part of curves in order to continue to adsorb the energy, the quantity of liquid decrease very fast.

In Figure 3.3 it is possible to define three different situations: one where the volume of liquid decreases when the applied heat load or the stored energy increases (left side of Figure 3.3- solid line), this is like the standard evaporation we experience each day. One, where the volume of liquid increases as energy is stored (right side of Figure 3.3 -dashed line), we are less familiar with this behavior. Finally there is a third situation, in-between, where the volume of liquid is constant with the stored energy. These different behaviors depend on the density. If the density of helium inside the ESU is equal to the critical density, 70 kg/m$^3$, it adsorbs 300 J maintaining a constant volumetric liquid vapor ratio; approximately 50 % of each. With a density less than the critical density, all the liquid is evaporated to store the energy. But if the density is higher than the critical density, the maximum energy of diphasic ESU is reached when the cell is completely filled with liquid.

The maximum energy is stored when the liquid volume is close to 50%.

In the Figure 3.3 it is also possible to see the quantity of energy stored for different temperature drifts allowed 0.1 K, 0.2 K and 0.3 K.

The results obtained in the Figure 3.3 are the same results as obtained in the experiment called “the Natterer tube” [34].This experiment consists in determining the critical temperature of a compound that is inside sealed glass tubes. From one tube to the other, the filling varies as in the calculation presented in Figure 3.3 and the quantity of liquid and vapor are different. By increasing of temperature, if the filling corresponds exactly to the critical density, the liquid-vapor interface remains at an almost invariant level. And when the temperature is higher than critical temperature, the interface disappears, giving rise to the “critical opalescence” phenomenon. By observing when the interface disappears, Natterer measures the critical temperature.

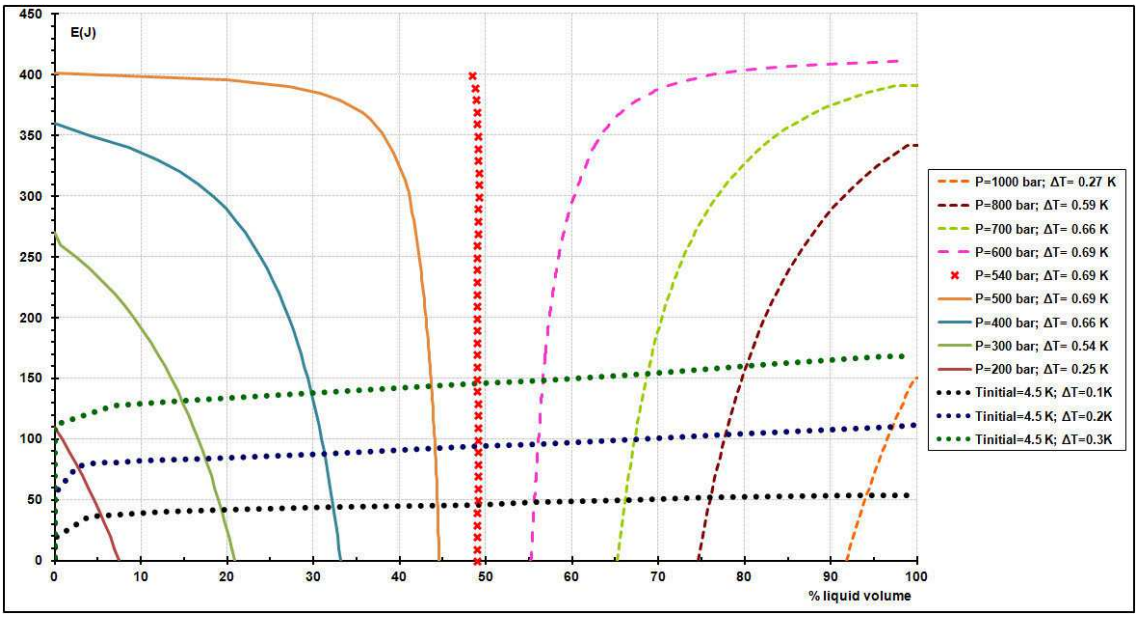


**Figure 3.3: Variation of energy as function of liquid volume for different filling pressure (vertical curves). The $\Delta T$ is the thermal difference between the starting point at 4.5 K and the temperature of saturation curve The energy stored for different temperature drifts ( 0.1 K, 0.2 K, 0.3 K) is also plotted ( horizontal curves).**

**Table 3.2: The density of helium as function of filling pressure for an ESU of 1 liter. The deviation from ideal behavior was calculated (Z- compressibility factor).**

| P(bar) | $\rho$ ($kg/m^3$) | Z |
|---|---|---|
| 1000 | 111.0 | 1.45 |
| 800 | 94.3 | 1.36 |
| 700 | 85.2 | 1.32 |
| 600 | 75.6 | 1.27 |
| 500 | 65.3 | 1.23 |
| 540 | 69.5 | 1.25 |
| 400 | 54.2 | 1.18 |
| 300 | 42.3 | 1.14 |
| 200 | 29.4 | 1.10 |

Another representation of the curves of Figure 3.3 is proposed in Figure 3.4, where the temperature evolution is plotted as a function of the total fluid density. The same curve than the one of Figure 3.3 are traced. In the same graph the saturation line was plotted: the blue line represents the saturated liquid and the pink line is the saturated vapor. The red vertical line corresponds to the experiment where the ESU is filled with the critical density. So, this line passes through the point where the liquid saturation curves and gas saturation curve touch.
During the heating up phase it is possible to see in the Figure 3.4 than for a constant density below the critical density, the quantity of vapor increases. When the temperature is equal to the saturation temperature, the line passes through the vapor saturation line, the cell is full with gas. At this point the pressure is lower than the critical pressure and the temperature higher. Increasing a little the temperature or the pressure inside the cell (constant density or vertical line on Figure 3.4) will result in superheated vapor, i.e. pure gas.

When the density is higher than the critical density the liquid quantity increases during the heating until the cell is full of liquid at saturation temperature. At this point the pressure and the temperature are largely lower than their critical values. A small increase in temperature/pressure will result in subcooled (i.e. pressurized) liquid. But, as this case is less common and more difficult to understand, the vapor mass was calculated during the heating up.

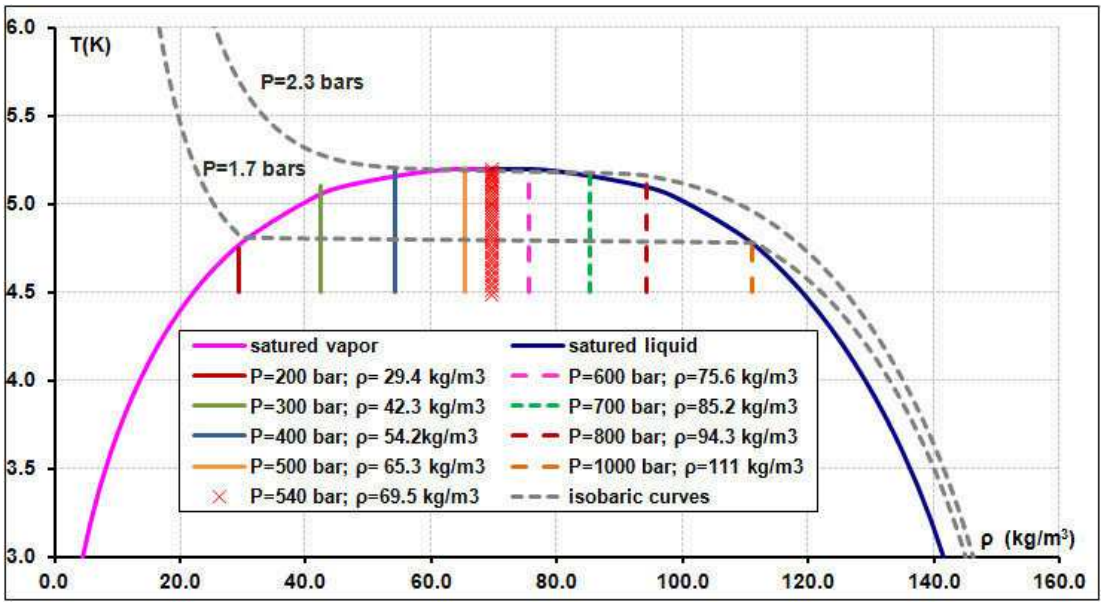


**Figure 3.4: The saturated liquid curve (pink solid line) and the saturated gas curve (blue solid line) of helium as a function of density. The vertical lines are the lines plotted in Figure 3.3 The grey dashed line are the isobar curves.**

In Figure 3.5 it is possible to see the gas mass (top graph) and gas volume (bottom graph) as a function of temperature. The curves above the red line are the case when the ESU is filled with density lower than the critical density, the vapor mass increases when the temperature increases as expected. The curves below red line are when the density is higher than critical density. When temperature increases the liquid is evaporated and therefore the vapor mass starts to increase. However, as the density of vapor increases and liquid density decreases with temperature, the vapor volume decreases and the liquid volume increase. The entire vapor starts to liquefy quickly just before the saturation temperature achieved.

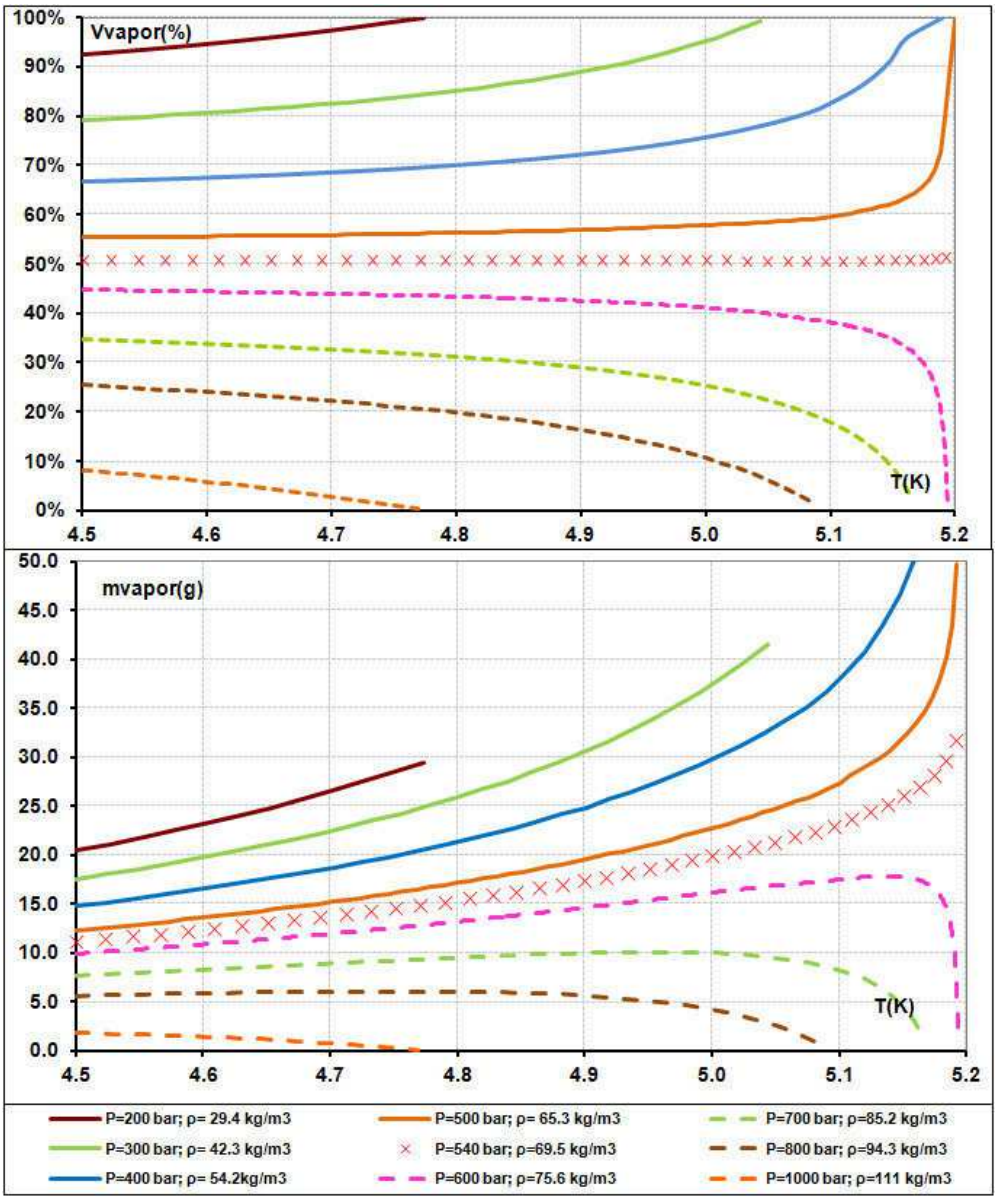


**Figure 3.5: The top graph shows the gas mass as a function of temperature and in the bottom graph shows gas volume as a function of temperature. These lines represent the same data than the one plotted in Figure 3.3 and Figure 3.4.**

With a cell of 1 liter, if we would like to store around 300 J at 4.5 K, a quite high pressure is required (around 350 bars). This is an important constraint leading to thick walls and associated mass which is not welcome for space application.

The other problem with a single volume ESU using latent heat is the temperature drift necessary to store the energy. Of course, the smaller this $\Delta T$ is, the better it is and even if a larger temperature drift is acceptable at cooler level, a temperature drift of 0.2 K to store 300 J is probably more appropriate for the whole spacecraft. In the Figure 3.6 it is possible to see the quantity of energy stored for different temperature drifts allowed 0.1 K, 0.2 K and 0.3 K. The quantity of energy for three different $\Delta T$ is well below 300 J. According to this study, in order to store 300 J a volume higher than 1 liter is necessary. It is also worthwhile mentioning that except for low filling pressure, the filling pressure has a limited impact on the stored energy.

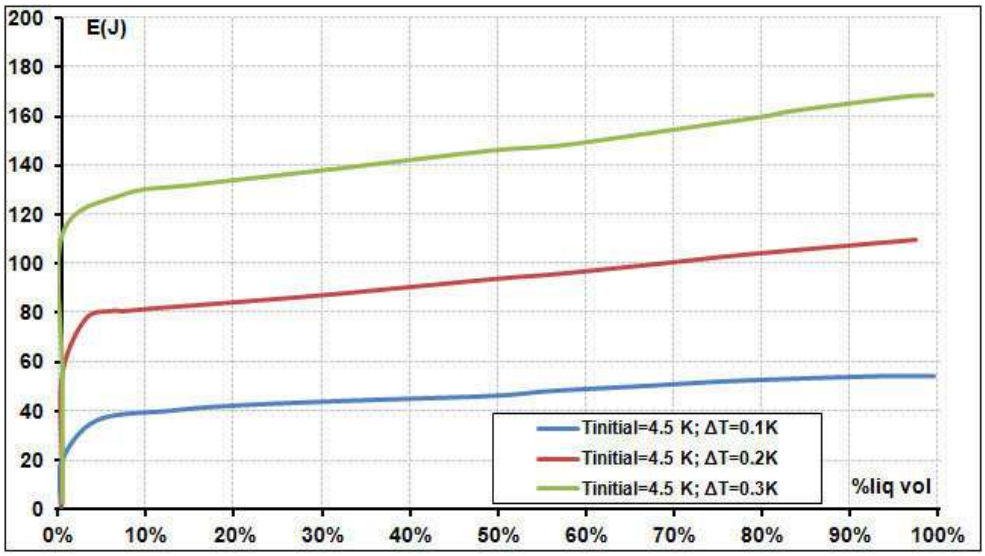


**Figure 3.6: Stored energy as function of the final % of liquid volume at 4.8 K, 4.7 K and 4.6 K. In all the cases the initial temperature is 4.5 K. For each percentage of liquid volume corresponds to a determined filling pressure.**

### 3.3 Dimensioning the ESU with Helium

Based on a requirement of 300 J absorbed between 4.5 K and 4.7 K, a study was performed to define the volume and the filling pressure that allows achieving this goal. The Figure 3.7 shows the variation of the filling pressure as a function of the volume which allows to store 300 J with a drift temperature of only 0.2 K. The filling pressure is an input parameter, which allows calculating the density of helium inside the ESU. Using the density ($\rho$) and the expression (3.1) it is possible to define the ESU volume:

$$V = \frac{E}{\rho(P_{fill})[\mathrm{u_f}(\mathrm{T_f} + \Delta T) - \mathrm{u_i}(\mathrm{T_f})]} \tag{3.2}$$

Where E is the energy, in this case, equal to 300 J, and $u_f(T_f + \Delta T)$ and $u_i(T_f)$ are the internal energy at initial temperature and final temperature. Internal energy is the sum of vapor and liquid internal energy affected by their massic percentages which are different at initial and final stage. The initial and final temperatures, in this case, are equal to 4.5 K and 4.7 K.

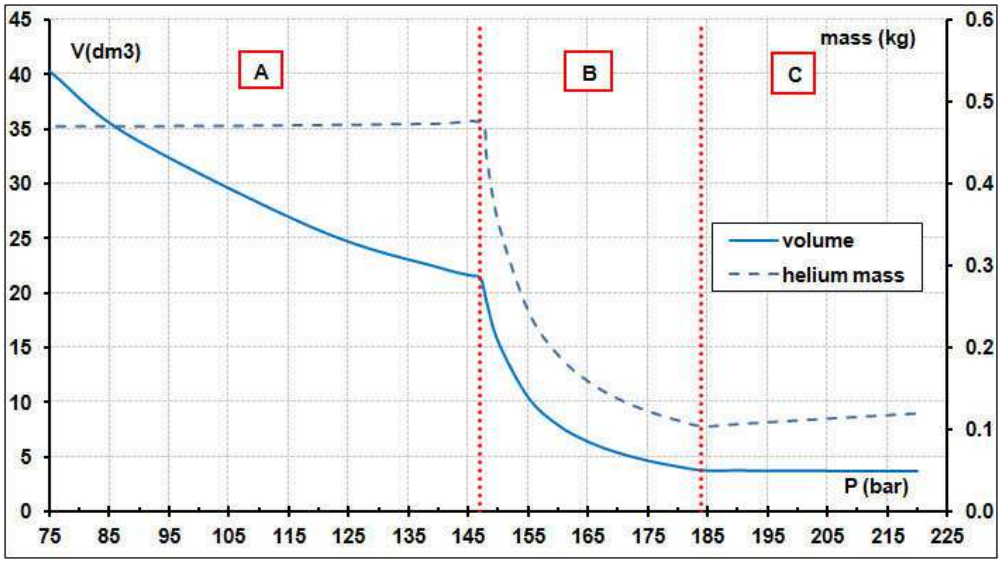


**Figure 3.7: Volume (left axes) and helium mass (right axes) necessary to store 300 J with 0.2 K drift as a function of the filling pressure.**

In Figure 3.7 three regions can be distinguished: in the phase A there is only gas inside the ESU whatever the temperature is; in the phase B, all the liquid is evaporated between 4.5 K and 4.7 K and in the phase C there is still some liquid at 4.7 K.

In Phase A, the volume decreases as the filling pressure rises. At 4.5 K, with a room temperature filling pressure between 75 bars to 148 bars, there is only gas inside the cell. For a closed volume, the energy is equal to internal energy

$$E = \Delta U = m\int_{Ti}^{Tf} CvdT + (L - P)dV \tag{3.3}$$

And for an ideal gas:

$$E = \Delta U = m\int_{Ti}^{Tf} CvdT \tag{3.4}$$

With for monatomic gas like helium $C_v$= 3120 J/kg/K. So the energy is equal to:

$$E = \Delta U = mCv\int_{Ti}^{Tf} dT \tag{3.5}$$

In this range of temperature and pressure, the volumetric specific heat capacity of helium gas is almost constant like for ideal gas. Therefore during this phase the amount of helium gas need to stored the 300 J for a minimum drift of 0.2 K is almost constant (m = E/CvdT) and equal to 0.47 kg. As the volumetric specific heat capacity is low, a large volume is needed to store the helium gas. As in this phase the energy is stored only in the gas, the higher the filling pressure is (i.e the higher the density of helium inside the ESU is), the smaller the volume is. Between 75 and 148 bars at room temperature, the gas can be considered as an ideal gas. Therefore, the PV is constant if the stored mass is constant, so the variation of the volume as function of the pressure is an hyperbole $\left(V = \frac{\alpha}{P}\right)$ with α = constant as it is possible see in Figure 3.7

Phase B is between a filling pressure of 148 bars and 184 bars at room temperature. In this phase, after cooling down, the cell contains some liquid at 4.5 K. The fact that there is a certain quantity of liquid inside the cell allows storing energy in the liquid–vapor transformation. Therefore the mass of helium necessary to store 300 J reduces drastically. If the helium mass reduces, then the volume need is also drastically reduced. The higher the filling pressure is, the higher the rate of liquid at 4.5 K is and the smaller the volume required is. In all cases this liquid level is well below the 50 % so critical density is never reaches. In this region, the quantity of liquid present at 4.5 K is all evaporated before reaching the 4.7 K temperatures. At 184 bars it is possible to see a minimum in the mass of the helium because at this filling pressure the quantity of helium liquid at 4.5 K is the maximum quantity of liquid that is possible to evaporate before the temperature reach 4.7 K.

With a filling pressure higher than 184 bars, region C, there is still some liquid inside the cell at 4.7 K. In other words, if all the liquid is evaporated the ESU stores an energy greater than 300 J, but with a drift temperature higher than 0.2 K. So, in this region, the mass of helium increases with the filling pressure, because the quantity of liquid also increases. The volume with filling pressure remains more or less constants, because the quantity of liquid does not increase much.

According to this study, in term of volume and mass, the optimal ESU has a volume of 3.82 liters and is filled with 184 bars, which corresponds to 104 g of helium. One problem with this design point is the high filling pressure. To study its impact on the wall cell, the thickness of the wall was calculated with the assumption that the ESU shape is a sphere. The metals currently used to build an ESU are: aluminum, titanium alloy (Ta6V) and stainless steel. The material chosen for our analysis are the titanium and stainless steel because they present good mechanical characteristics (yield and ultimate tensile strength) and can be easily welded (see Table 3.3). For the calculation of the dimension, the safety factors recommended by ESA

(European Spatial Agency) were taken into account [35]. The safety factor is 1.25 for yield strength and 1.5 for ultimate strength. To calculate the minimum wall thickness, the stress is set to the minimum values obtained by applying the safety factor to the yield and to the ultimate strength. In the case of stainless steel, the yield strength is used with a value of 156 MPa whereas for the titanium the ultimate strength is used with a value of 597 MPa.

**Table 3.3: Some properties of stainless steel and titanium (alloy Ta6V).**

| | Stainless steel | Titanium (alloy Ta6V) |
|---|---|---|
| Density(kg/m$^3$) | 7900 | 4507 |
| $\sigma_{yield\ strength}$ (MPa) | 195 | 827 |
| $\frac{\sigma_{yield\ strength}}{1.25}$ (MPa) | 156 | 662 |
| $\sigma_{ultimate\ strength}$(MPa) | 490 | 896 |
| $\frac{\sigma_{ultimate\ strength}}{1.5}$ (MPa) | 327 | 597 |

To see the impact of the material choice for the construction of the cell, the mass of cell was calculated for both materials. The mass of the cell depends on the thickness of the wall cell and the density of the material. For a sphere, the stress $\sigma$ in the wall depends of the filling pressure $P_{fill}$, the inner diameter D and the thickness $t_{hic}$ with the following equation [36]:

$$\sigma_{stress} = \frac{P_{fill} D}{4 t_{hic}} \tag{3.6}$$

In Figure 3.8 it is possible to see the thickness of cell wall as a function of the filling pressure for two materials (titanium alloy Ta6V and stainless steel). The volume size is optimized with pressure according to the above sub section. As the titanium alloy is more resistant than stainless steel, the cell made in titanium alloy has a thinner wall than the cell made of stainless steel. In the region A, as mentioned previously the gas behaves approximately as an ideal gas, (PV =constant) and so P.D$^3$ is constant. $PV = P\left(\frac{1}{6}\pi D D^2\right) = a$ where D is the diameter and a an constant. Using equation (3.6), it comes that the thickness is inversely proportional to $D^2$ $\left(t_{hic} = \frac{b}{D^2}\right)$ where b is constant. When the volume decreases the thickness increases. If we assumed that the thickness of the wall is low compared to the sphere radius, the mass of the wall can be approximate by the product of the sphere surface by the thickness. mass = $\pi D^2 t_{hic} = \pi b$ is constant. When the cell wall is too thick, mass is no more fully constant as it can be seen for the stainless steel sphere (see Figure 3.9).

In the region B, given that the volume decreases a lot with the filling pressure growth, the thickness of the cell wall decreases. For a filling pressure higher than 184 bars, the thickness of the cell wall starts to increase slowly So, there is a minimum of thickness for 184 bars (5.8 mm for stainless steel and 1.5 mm for titanium). Furthermore, this minimum thickness corresponds also to a minimum of volume. Obviously, there is a second minimum in thickness for low pressure, but this minimum corresponds to a pressure that tends to zero and to an infinite volume. The same thickness than the one obtained at 184 bars is obtained at 89 bars but with a volume of 34 liters instead of 4 liters

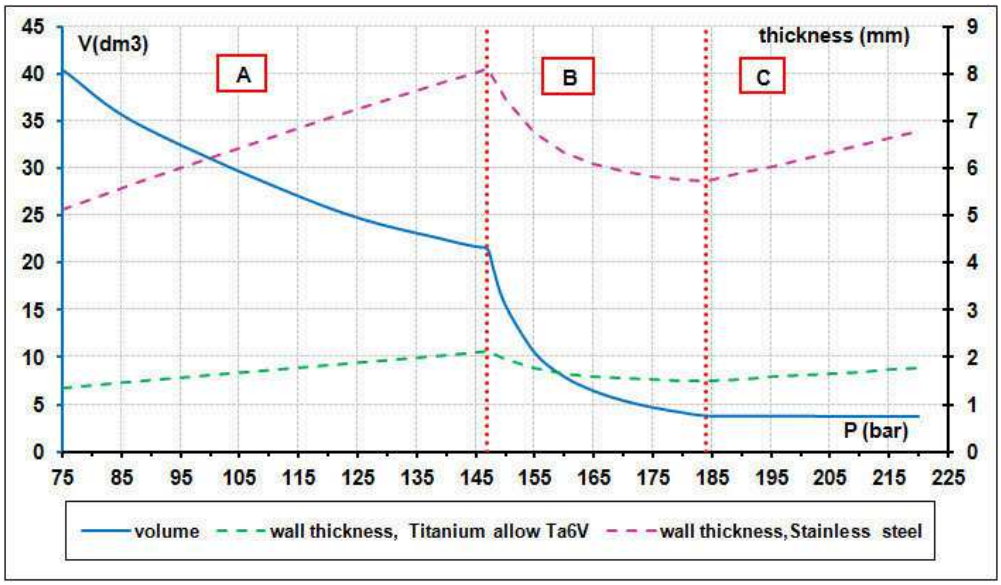


**Figure 3.8: Volume (left axes) and thickness of cell wall (right axes).necessary to store 300 J with 0.2 K drift as a function of filling pressure.**

Knowing the helium mass, and the volume and the thickness of the cell wall, it is possible to calculate the total mass of the ESU (Figure 3.9) which is a key parameter for space application.

The cell made of titanium alloy is lighter than the one made of stainless because this material has better structural properties and is lighter than stainless steel. The minimum of mass is at 184 bars is 0.91 kg for titanium and 5.8 kg for stainless steel. The ESU mass is essentially due to the cell wall; the helium mass is only 0.104 kg. Obviously, it is more interesting to build the ESU with titanium alloy for space applications

.

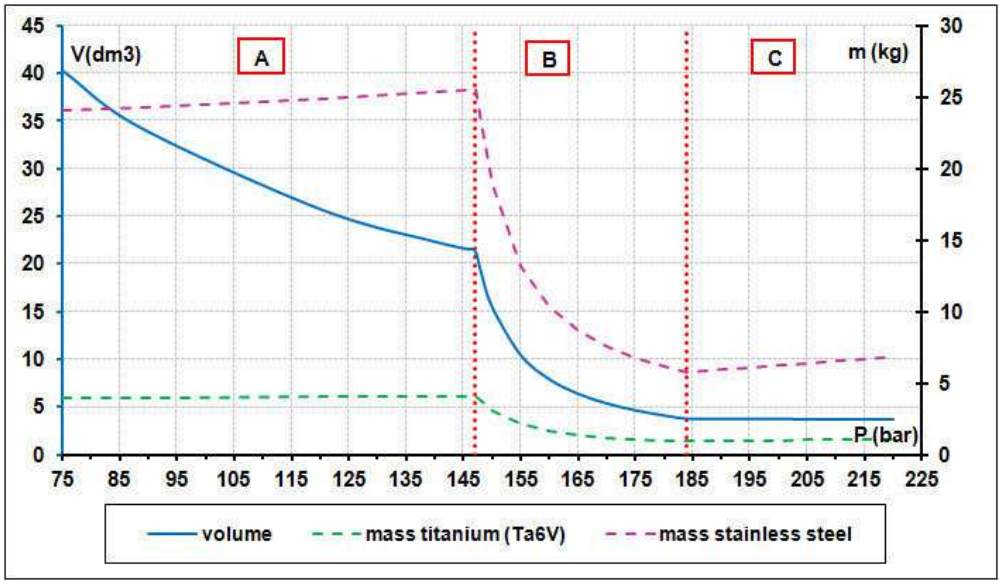


**Figure 3.9: Volume (left axes) and mass cell (cell + helium mass) (right axes) necessary to store 300 J with 0.2 K as a function of filling pressure**

### 3.3.1 ESU with a porous medium

If we want to use the ESU for space applications it is necessary to demonstrate that it could operate in a microgravity environment. One way to demonstrate this on ground is to performed test with and against gravity and to compare the results. If we use a simple cell, the liquid will be always at the bottom of the cell due to gravity. In space, it is more difficult to

predict the position of the liquid. One possible way to turn the ESU gravity-independent is to put inside the volume a porous medium where the capillary force is higher than the gravity force.

Another important aspect is the temperature drift during the use of the stored energy. When a small drift is allowed, like in our case (0.2 K), the thermal path from the external surface to the liquid gas interface should be very good. So, it is necessary that the liquid always wet the heat exchange surface avoiding the heat transfer via the gas which has a very bad thermal conductivity. In a simple design, the heat exchange could be the cell wall itself.

One way to ensure that the liquid is in contact with the cell wall independently of gravity is to use a porous medium. Owing to the capillary force, this porous media retains the liquid and maintains it in contact with the cell wall. When the load is applied, the first liquid that evaporates is the one which is in contact with the cell wall and a liquid/vapor interface appears at the cell wall. Due to the porous media, a capillary force is generated that allows the fluid circulations, i.e. pumps the liquid. In the previous chapter, the results of the nitrogen ESU with and without ceramic prove that the ceramic decreases the difference between wall and fluid temperature. To better understand the behaviour of liquid and the vapor during the evaporation in a porous medium, a dedicated experimental set-up has been designed and built and tests were carried out with helium. This will be described in the next chapter.

The analysis below shows the impact of using a porous medium for the design of the cell. The ceramic chosen, Procelit P160–Kapirok, is the same that the one used in the evaporator of the adsorption refrigerator built for the Herschel mission [32], very similar to Procelit-RATH. The characteristics of the ceramic are:

- Composition: 9 % $SiO_2$, 91% $Al_2O_3$,
- Porosity :0.92,
- Density : 300 kg/m$^3$

The results of dimensioning for titanium alloy (Ta6V) with a ceramic are plotted in Figure 3.10 and in Figure 3.11.With a ceramic inside the cell, the volume of the cell increases because 8% of the space is occupied by the ceramic. As the volume increases, the wall thickness also increases to withstand the pressure. So there is an extra mass due to the larger volume, the larger thickness and the ceramic itself. It can be shown in Figure 3.11 that the mass has been doubled by the use of a ceramic (2.39 kg). This is mainly due to the mass of the ceramic itself. The ceramic is only necessary in region B and C, because in the region A there is no liquid and so nothing to confine. As the ceramic mass is an important contributor to the total mass, it is interesting to use a ceramic with the density as low as possible. On way to achieve this is to increase the porosity. For example, increasing the void fraction of the ceramic from 0.92 to 0.96 would decrease by a factor 2 the ceramic mass and have a large impact on the overall cell mass.

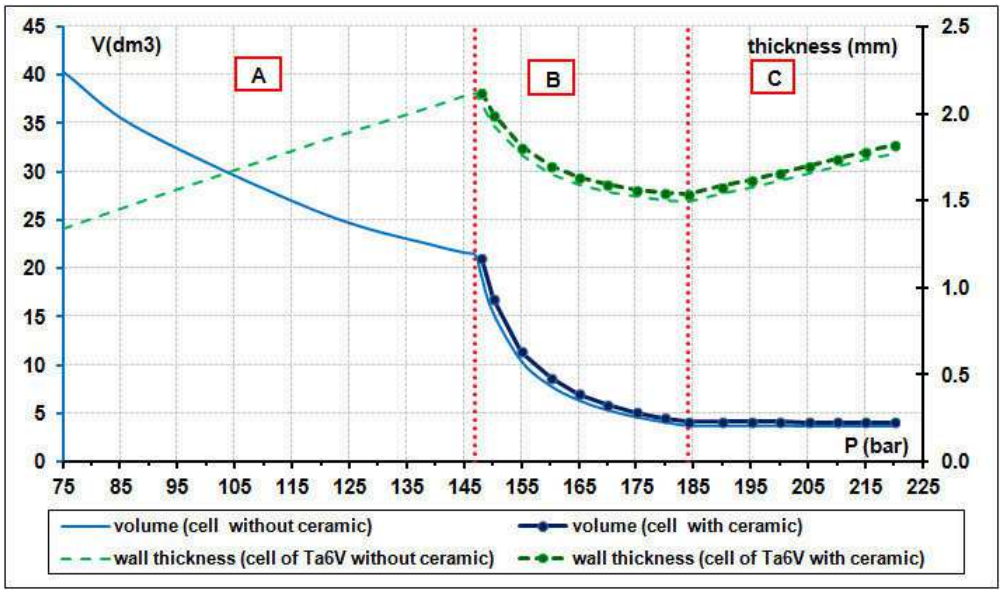


**Figure 3.10: Volume (left axes) and thickness of cell wall made of titanium alloy (right axes) necessary to store 300 J with 0.2 K as function of the filling pressure. Cell with or without ceramic.**

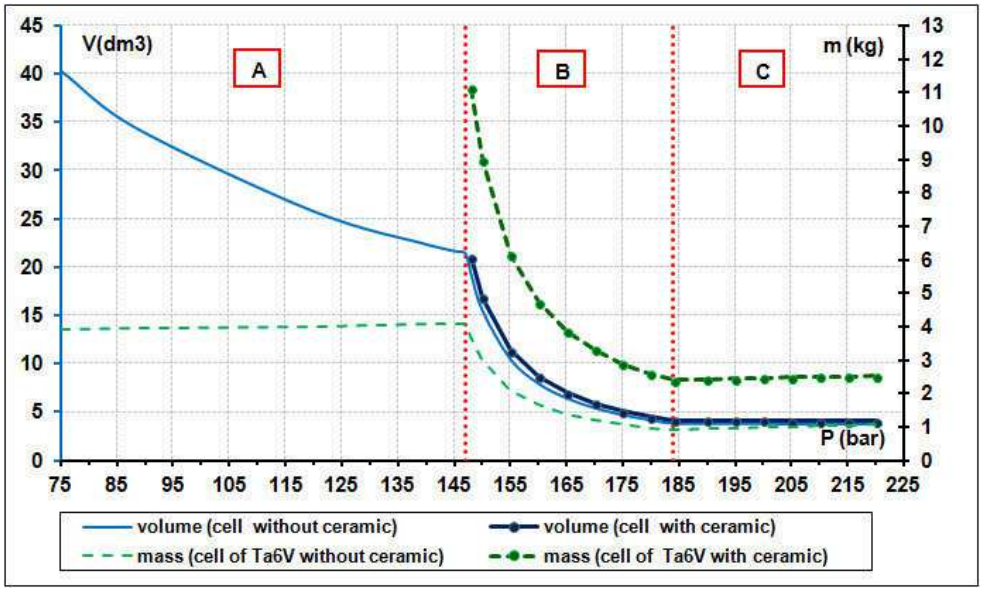


**Figure 3.11: Volume (left axes) and total mass (helium, cell made of titanium alloy and ceramic mass) (right axes) necessary to store 300 J with 0.2 K as a function of the filling pressure. Cell with or without ceramic.**

### 3.3.2 Sensibility study to the initial temperature $T_I$ and $\Delta T$

To analyse the influence of $T_I$ a study for three different temperatures (4.4 K, 4.5 K and 4.6 K) was carried out. Similar analysis was also carried out for different thermal drift. The goal was to analyse whether by modifying the $T_I$ of only 0.1 K or by allowing a different drift temperature, the energy stored could be higher, or the system mass could be lowered.

#### 3.3.2.1 Study of different $T_I$

In Figure 3.12 it is possible to see the volume as a function of the filling pressure for three different initial temperatures. The big difference is that the drop in volume, corresponding to the apparition of liquid inside the cell, occurs at lower pressure when the temperature is lower (due to saturation pressure). It can also be seen that the optimum volume is obtained for lower

pressure when the $T_I$ is lower but the impact on the volume value remains limited (see Table 3.4).

On the mass side, the Figure 3.12 shown that the impact on mass is negligible. The values are reported in Table 3.4. In conclusion, the parameter $T_I$ allows a limited change in term of volume but does not allow a large change in term of mass.

**Table 3.4: Values of ESU for three different initial temperature $T_I$.**

| $T_I$(K) | $P_{fill}$(bar) | V($dm^3$) | thickness (mm) | m(kg) |
|---|---|---|---|---|
| 4.4 | 164 | 4.50 | 1.41 | 2.48 |
| 4.5 | 184 | 4.15 | 1.54 | 2.39 |
| 4.6 | 208 | 3.81 | 1.69 | 2.31 |

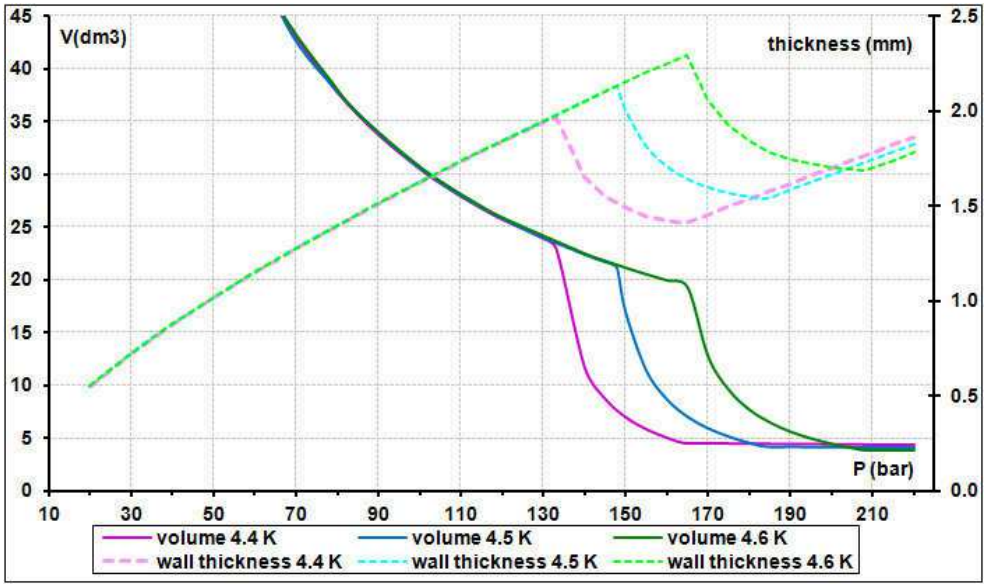


**Figure 3.12: Volume (left axes) and wall thickness of a cell made of titanium alloy (Ta6V) (right axes) necessary to store 300 J with 0.2 K for three different $T_I$ as a function of the filling pressure.**

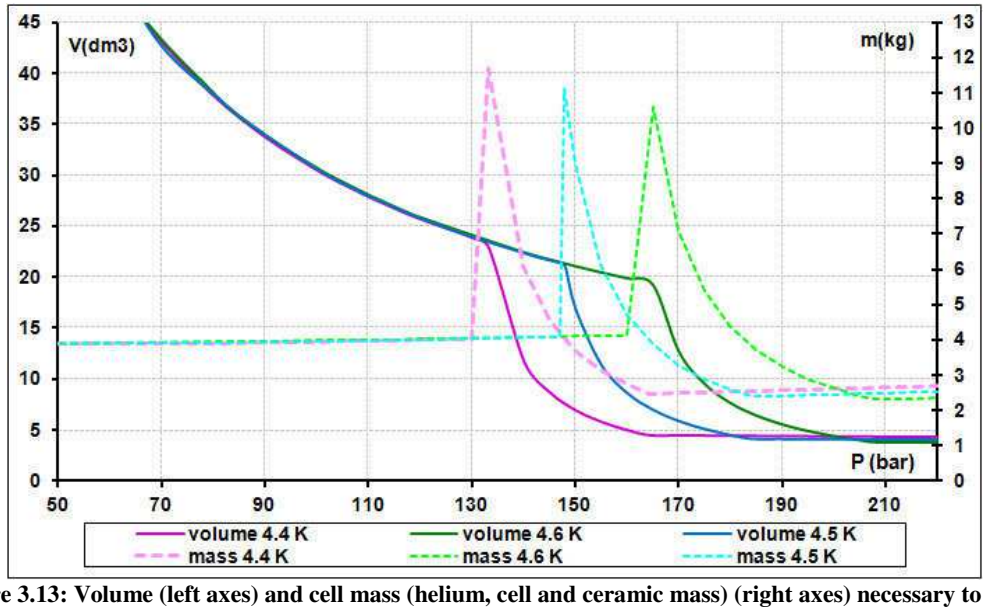


**Figure 3.13: Volume (left axes) and cell mass (helium, cell and ceramic mass) (right axes) necessary to store 300 J with 0.2 K for three different $T_i$ as a function of the filling pressure.**

#### 3.3.2.2 Study different $\Delta T$

Another parameter that was studied is the temperature drift during the evaporation. Three different values were analysed: 0.1 K, 0.2 K, and 0.3 K.

The higher the $\Delta T$ is, the smaller the volume of cell is, because it is possible to use the energy of the fluid along a larger temperature drift and less mass of fluid is needed.

The sudden drop in volume occurs for the same pressure (Figure 3.14) because it corresponds to the apparition of the first amount of liquid. The optimum volume value is reported in Table 3.5.

As the larger drift allow for lower volume, it also lead to smaller mass (Figure 3.15). Values are shown in Table 3.5.

In conclusion, the higher the allowed temperature drift is, the lighter and the smaller the ESU is but the higher the optimum filling pressure is.

**Table 3.5: Values of ESU lighter for three different $\Delta T$.**

| $\Delta T$(K) | P(bar) | V(dm$^3$) | $t_{hic}$ (mm) | m(kg) |
|---|---|---|---|---|
| 0.1 | 164 | 8.72 | 1.76 | 4.80 |
| 0.2 | 184 | 4.15 | 1.54 | 2.39 |
| 0.3 | 208 | 2.62 | 1.49 | 1.59 |

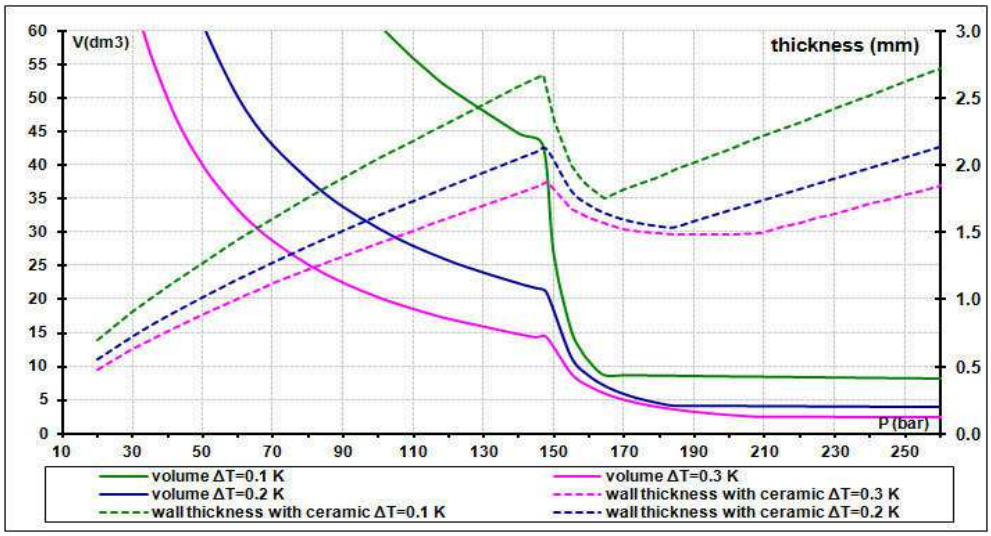


**Figure 3.14: Volume necessary to store 300 J for three different $\Delta T$ as a function of filling pressure (left axes) and thickness of cell wall made of titanium (right axes). Initial temperature 4.5 K.**

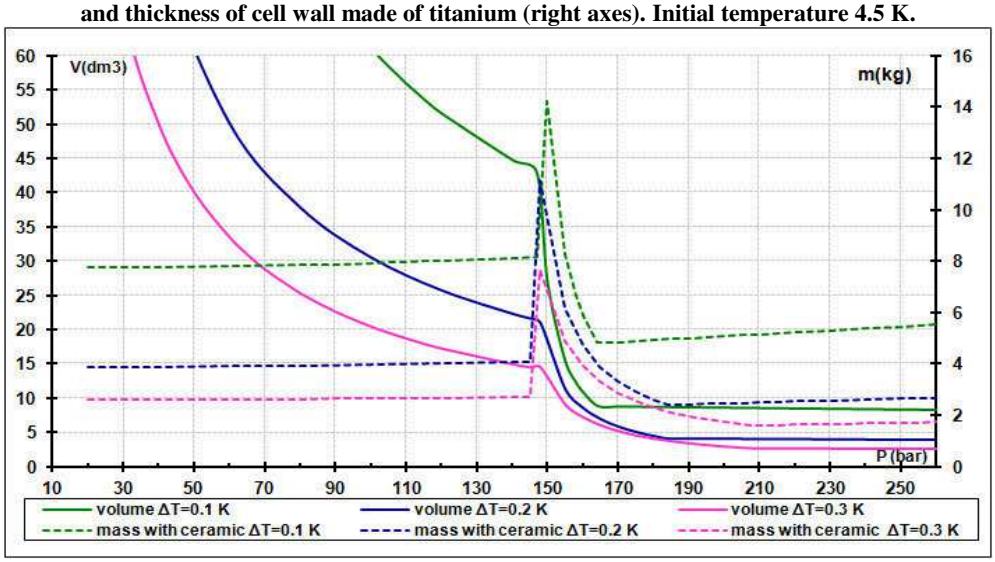


**Figure 3.15: Volume necessary to store 300 J for three different $\Delta T$ as a function of filling pressure (left axes) and mass cell (helium mass, cell mass and ceramic mass) (right axes). Initial temperature 4.5 K**

### 3.4 Comparison between Solid ESU and Fluid ESU

The other possibility to store energy at low temperature is to use a material with a specific heat anomaly that allows storing energy with a little temperature change. In Figure 3.16 it is possible to see the volumetric heat capacity for various materials as a function of temperature. Around 4.5 K, there are two potential materials that are good candidates: the GOS ($Gd_2O_2S$) and the Ho Sb.

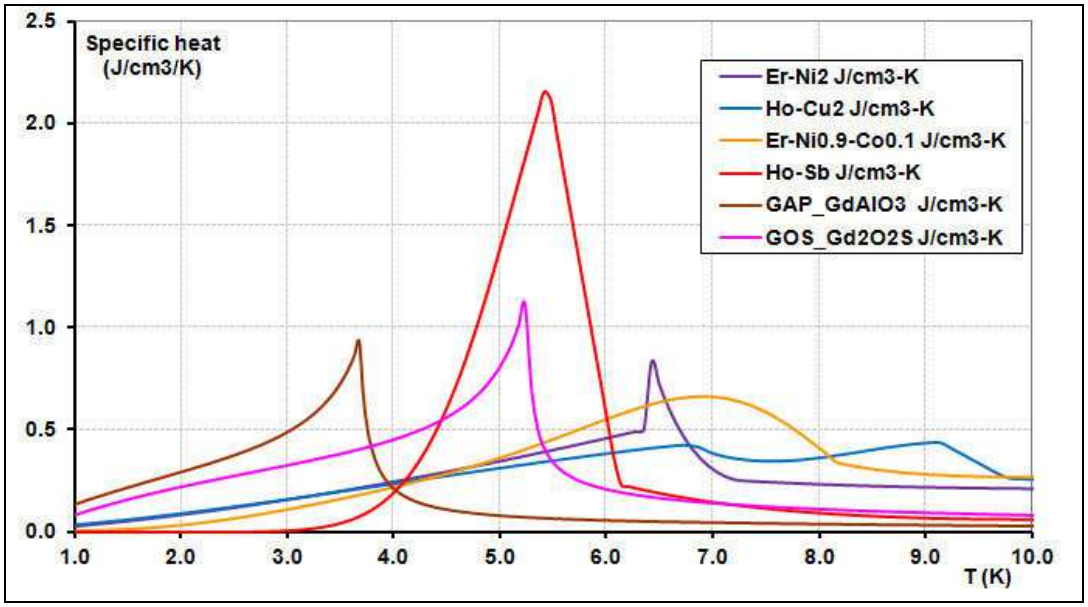


**Figure 3.16: The volumetric heat capacity for various materials as a function of temperature [37].**

The Ho-Sb has a peak of specific heat at 5 K. This material contains antimony which is toxic. This characteristic could be problematic for qualification in order to use it for space applications. The other solution is to use GOS which presents a lower peak of specific heat but has been already implemented in prototype. I have used this material to design and test an ESU to store 36 J between 3 K and 6 K, see section §1.2.2. The ESU using helium is compared with an ESU using GOS as a function of drift temperature. For the volume and the mass of GOS the reservoir has not been accounted. The volume and mass of ESU using helium was calculated as explained in section §3.3 . Knowing the specify heat (see Figure 1.5) and the density of GOS (7.6 g/cm$^3$), it is possible to calculate the mass and the volume of GOS necessary to store 300 J at 4.5 K for a 0.2 K temperature drift.

$$E = m \int_{Ti}^{Tf} c \, dT \tag{3.7}$$

$$V = \frac{m}{\rho_{GOS}} \tag{3.8}$$

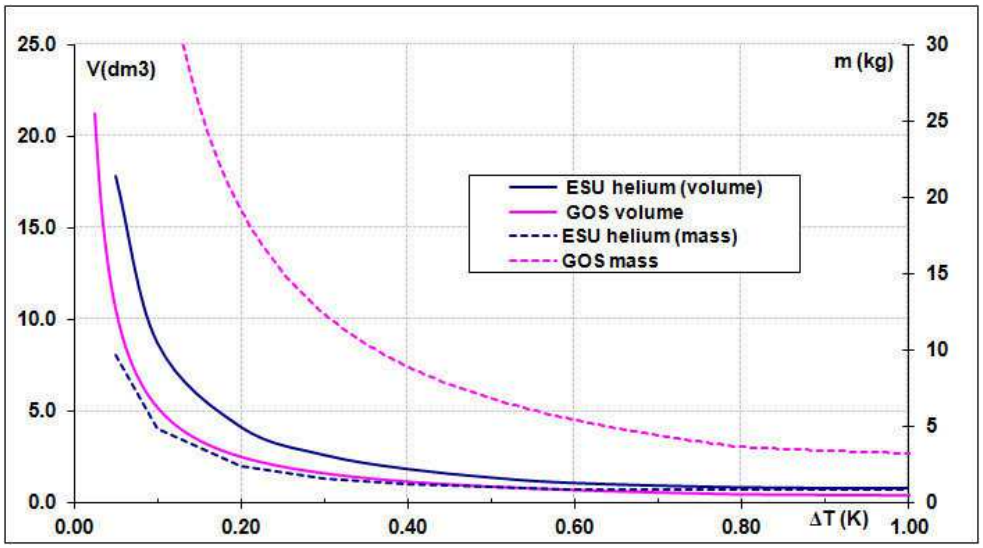


**Figure 3.17: The volume and the mass of an ESU using either helium or GOS as a function of drift temperature. The heat exchanger mass has not been account for.**

The difference between the ESU using helium and GOS volume decreases with $\Delta$T. The volume of the helium ESU is higher than volume of GOS for low temperature drift but the volume tends to have the same value when the temperature drift increases.

In terms of mass, the GOS mass is always higher than the helium ESU mass. The difference decreases with the increase of $\Delta$T. At 0.2 K the mass of GOS is seven times higher than the mass of the helium ESU and is still four times for a 0.8 K temperature drift. For a $\Delta$T higher than 0.62 K, the critical point is exceeded so the helium ESU is less suitable.

In conclusion, helium is a good candidate for ESU that required operating with a low temperature drift at 4.5 K.

## 3.5 Dual volume

For ESU using fluid, there are two different architectures that are possible: single volume (only a cold volume) or dual volume (two volumes, one at low temperature and the other one at room temperature). The dual configuration is more difficult to integrate because there is a need to implement some piping between the two volumes. The volume at room temperature is usually larger than the one at low temperature and as a consequence allows decreasing the filling pressure. This volume is also used to store the vapor during the evaporation limiting the pressure increase. This way, the volume of cell at low temperature can be decreased and can have thinner walls leading to a mass reduction of this cold part.

With the goal to verify if an expansion volume at room temperature can decrease the cold volume of an ESU using helium, a study was carried out to analyse the impact of the expansion volume. The results are presented in Figure 3.18. The cell volume decreases with the filling pressure increase. Two different zones can be distinguished: one where the cell volume decreases very fast with the increase of the filling pressure and another one where the decrease is slower. In the first zone, there is only gas inside the cell and in the second some liquid is condensed at the nominal temperature. This second zone can be achieved only if the pressure is above the saturation pressure when the volume is cold. As already seen before, less volume is needed once conditions to condensate some helium have been achieved.

Higher is the volume at room temperature, lower is the required filling pressure. When liquid exists inside the cell at low temperature, the volume reduces drastically. The point where the curve changes of behavior is when the liquid inside the cell is the quantity necessary to store 300 J. In the case of single ESU, this point corresponds to the minimum mass presented with the single ESU in Figure 3.9.

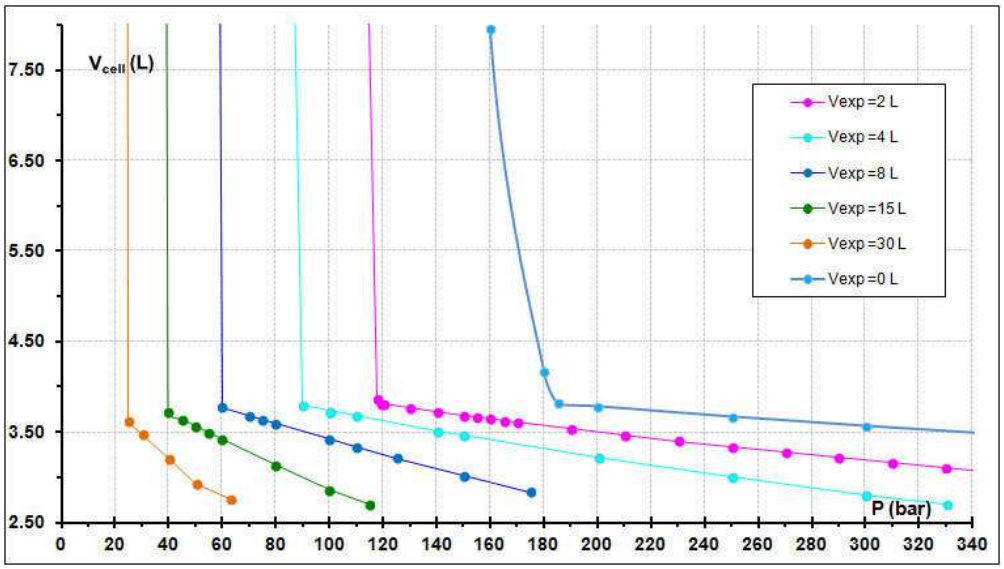


**Figure 3.18: The cell volume at 4.5 K in function of the filling pressure for different size of expansion volume.**

To reduce the filling pressure to half in comparison with an ESU without expansion volume it is necessary to add at room temperature a volume of 4 liters and the cold volume will have a volume of 3.8 liters. The expansion volume allows a filling pressure reduction but does not impact too much the volume at low temperature. So, in our conditions with helium an expansion volume at room temperature does not allow a big advantage in term of cold volume compared to the difficulty induced by the integration of a dual volume configuration. In term of cold mass, the quantity of mass helium inside the cold volume is the same for the case single volume and 4 liters of expansion volume. However the wall cell of single volume is thicker because the filling pressure is higher.

Another interesting aspect of the single volume configuration is that the gas is maintained at cold temperature, i.e inside cold volume. On the contrary, in the dual volume configuration the gas is stored in the expansion volume at room temperature. In this case, to fill the ESU with liquid it is necessary to cool down the gas from 300 K to approximately 4 K, so more time and energy are necessary to liquefy the liquid in comparison with the single volume.

In conclusion, the single volume looks like a suitable configuration for our system.

## 3.6 Conclusion

The aim of this study was to demonstrate the capability of using the latent heat associated with a liquid –vapor transformation of helium to adsorb 300 J at around 4.5 K with a drift temperature of 0.2 K. To store this amount of energy, a volume of approximately 4 liters weighting 2.4 kg is necessary. This volume has to be filled with 185 bars. With the goal to decrease the mass, the volume or the filling pressure, the influence of the initial temperature, the drift temperature allowed and the configuration (single/dual volume) were analysed. To absorb energy at 4.6 K or 4.4 K instead to 4.5 K does not allow large gains. But, if the drift temperature can be increased to 0.3 K the volume and the mass of ESU can be decreased significantly.

An expansion volume connected to the low temperature cell in this temperature range does not seem to be the best solution because it requires a large expansion volume at room temperature to have a significantly reduction of the cold volume.

In this diphasic ESU using helium it is useful to put a porous medium in order to make it less depend to gravity and suitable for space applications.

Beside this function, the porous media can also reduce the temperature gradient between the cell wall and the fluid.

When a heat load is applied on a cell wall, the liquid in contact with the wall evaporates but some other liquid can be pumped due to capillary effect in the porous media. But how much

liquid can be pumped to the wall cell when some heat load is applied? To answer this question and to better understand how the thermal transfer is affected by applied head load, helium properties and porous media, experimental set-ups and measures were necessary. In the following chapter this subject is discussed in more detail.

# Chapter 4: Two phase normal helium behavior in a porous medium with applied heat flux

The Energy Storage Units (ESUs) are units that use the latent heat associated to the liquid-gas phase transition as enthalpy reservoir. One of the aims of this study is to investigate their potential use for space applications. Before being integrated into a satellite, the device, using a two phase fluid, should demonstrate their capability to operate in a micro gravity environment without performance degradation. This is not an easy task and on ground demonstration using test against gravity represents a conservative approach to fulfil this requirement. One solution to make this ESU, in practice a reservoir filled with two phase fluid, less dependent to gravity is to confine the liquid in a porous medium, for example a ceramic foam.

## 4.1 Objectives

Fluid phase change mechanism is a very efficient way to transfer heat from a solid surface to a fluid. For space application, the use of fluid phase change mechanism is usually associated with a porous medium to maintain the phase separation at a given position.

The goal of the study presented in this section was to procure a better understanding of what could be the two phase fluid behaviour in microgravity when heat is applied. This gives us guidelines for the design of energy storage unit dedicated to space environment. For this purpose, tests with and against gravity has been performed that show the importance of capillarity effect to retain and to bring the liquid up against gravity.

## 4.2 Principle of experience

We are interested in studying the heat transfer in a cell filled with porous media and with a two phase fluid. Our main question is to know how gravity can affect the heat exchange between the fluid and the cell walls. One of the related questions is how the liquid separation will be in the cell. For example, if we performed an antigravity test, i.e. heating the cell on its top end, what is the maximum liquid we can evaporate keeping the cell isothermal and how this amount of liquid could be affected by the heat flux imposed (Figure 4.1). If liquid is evaporated at the top of the cell, due to capillary effect of the porous media, some liquid from the lower part of the cell will replace the evaporate liquid and fill the void pores. This will remain true to some extend depending on fluid and porous media properties, cell height and applied power.

A small experiment has been built in order to have a better understanding of the porous media capillarity effect to retain the liquid and to bring it up against gravity. This experiment is also a useful tool to understand the liquid/vapor motion in a porous medium when heat is applied. A good understanding of the heat transfer in porous media will allow optimizing the design of these kinds of system for space applications.

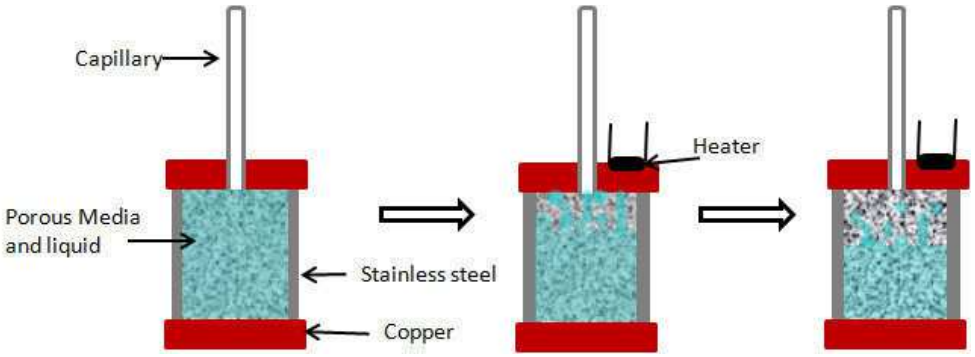


**Figure 4.1: Scheme of an antigravity test. At first, the cell with ceramic is full of liquid (left side). After, the top end of the cell is heating so we start to evaporate liquid (middle) and liquid is pump by capillarity effect towards the top cell end. However, after some time it is impossible to evaporate more liquid (right side).**

The purpose of the experiment is to study the effect of capillarity inside one cell with ceramic using helium as working fluid.

The Jurin's Law allows calculating the maximum height that a liquid is able to climb in a capillary tube. If we assume the porous material is made of small capillaries of diameter Ø and we know the surface tension ($\sigma$) and the liquid and gas density the fluid ($\rho_L$, $\rho_V$, respectively) it is possible to calculate the capillary height (h) from the equation (4.1). For helium, the contact angle θ is close to 0º [38]

$$h \leq \frac{4\,\sigma\,cos\theta}{(\rho_L - \rho_V)g\emptyset} \tag{4.1}$$

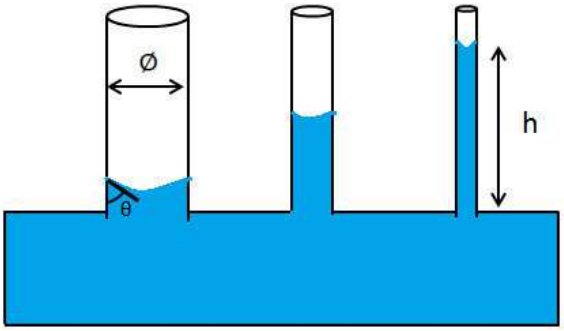


**Figure 4.2: Scheme representing the capillarity effect in three different tubes.**

The capillary effects are predominant at a scale smaller than the capillary length ($l_c$). The capillary length is a characteristic dimension of a liquid when the capillary force and gravitational forces are equal in magnitude. The capillary length is defined by:

$$l_c = \sqrt{\frac{\sigma}{(\rho_L - \rho_V)g}} \tag{4.2}$$

We built an experimental set-up to measure the capillary height and see how it can be affected by applied heat load. In this experiment, we had one cold cell that contains ceramic foam. This cell is filled with liquid helium. Heat power was applied on the top of the cell to see how much liquid was climbing in the porous media.

In view of the above equation (4.1), the capillary height depends on parameters that change with temperature (densities and surface tension) (Figure 4.3). So, it is important to maintain a constant temperature during heating to avoid variation in capillary height and check independently the heat flux influence.

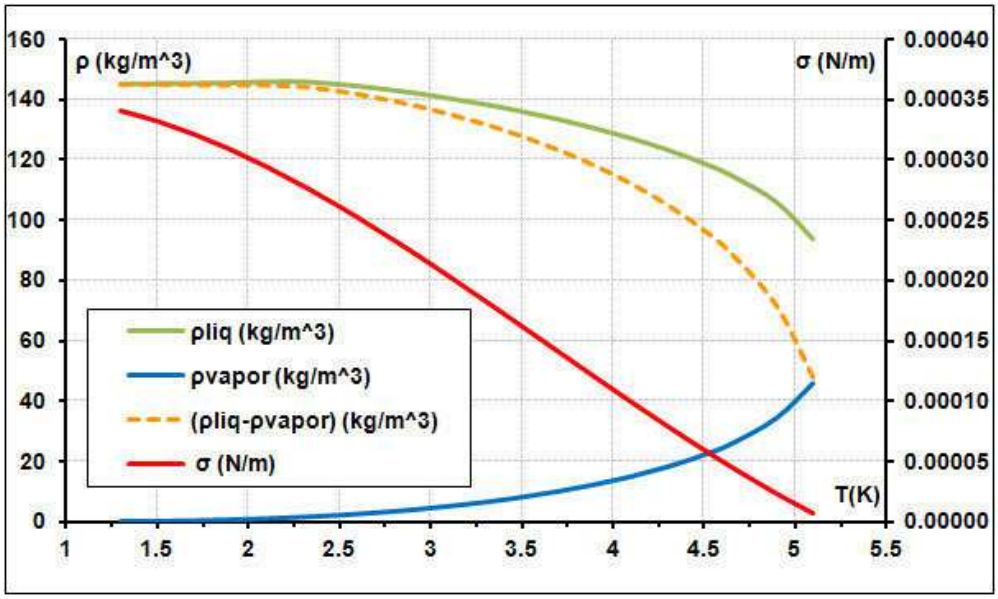


**Figure 4.3: Variation of liquid density, vapor density, difference between density (left axis) and surface tension (right axis) with temperature.**

## 4.3 The Experimental set-up

The experimental set-up was composed by a low temperature cell connected to an expansion volume at room temperature by a capillary (ESU dual volume configuration). The cell was attached to a cold plate of an helium cryostat through a gas gap heat switch (Figure 4.4).The cell is protected from radiation by a 4 K thermal shield. The helium bath can be pumped to achieve a minimum temperature of 1.2 K, if needed.

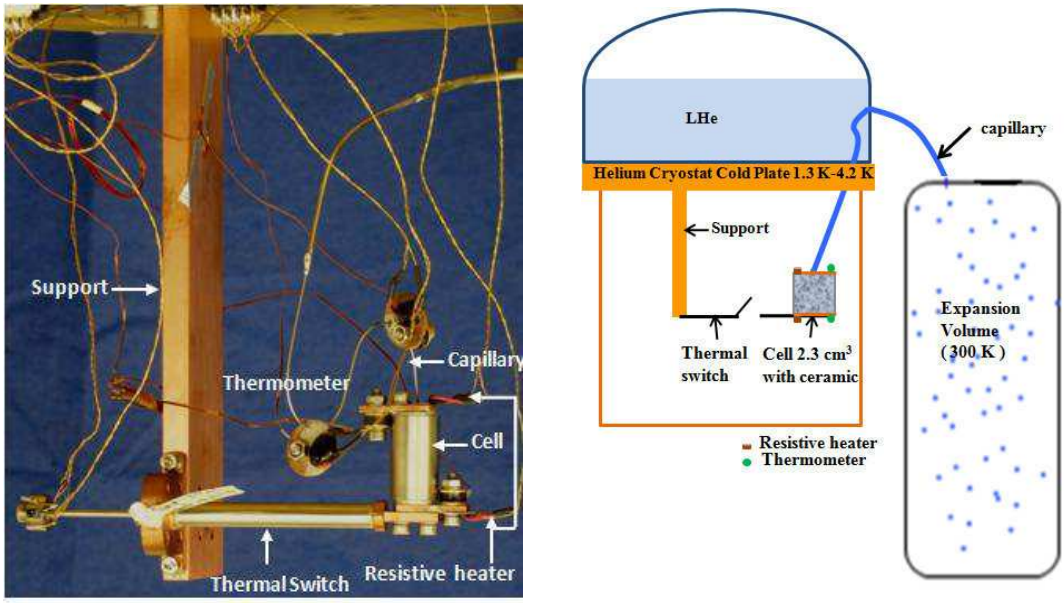


**Figure 4.4: Picture of the cell mounted on cold plate of a helium cryostat through a gas gap heat switch (left). Schema of the experimental set-up (right).**

### 4.3.1 The cell

The cell has a cylindrical shape and is made with two copper tips connected by a thin stainless steel tube. Each copper tip weighs 10 g .The tube has a 13.8 mm inner diameter with a

wall thickness of 0.1 mm. The effective length of the connecting tube is approximately 14.3 mm which leads to an inner cell volume of 2.1 $cm^{3.}$ This is the total volume without taken into account the volume filled by the porous media. Copper tips assembly with stainless steel tube was made by tin base brazing [39].

The cell was filled with the porous media which has been adjusted to the cell shape. The porous media will retain the liquid.

For the assembly of the cell, a procedure was followed to adjust the ceramic to the cell. First the copper tips (without capillary hole) is assembled with the stainless steel tube by brazing. The ceramic is made of plate, in which the sample will be cut. It is important that both faces are plane parallel. To cut the ceramic cylinder that we want to use in the cell, a stainless stain tube with the same inner diameter than the cell is used with a thin wall thickness of 0.1 mm is used. Due to the small tube thickness, it can be used as a tool to cut the ceramic simply by pushing it. The tool tube is longer than cell height, so that it can be easier to hold it and the ceramic sample remains inside the tube. Once the ceramic inside the tube the following phase is to transfer the ceramic to the cell. For this action, a piece was built to make the two tubes concentric (the tool tube with ceramic and the cell tube). Once, the tubes are aligned; the ceramic is pushed into the cell until the ceramic comes in contact with the copper tip. After that, the other copper tip, with the capillary already brazed is pushed until it comes in contact with the ceramic. Then, it is possible to braze and finish the assembly of the entire cell.

The Figure 4.5 illustrates the thermal resistance contributions between the two cell ends for wall, full gas and full liquid for a cell without ceramic and without taking into account natural convection ($T_{bottom}$ lower than $T_{top}$).

It can be noted that the cell wall and the gas have similar total thermal conductivities which are well lower than the one of the liquid helium.

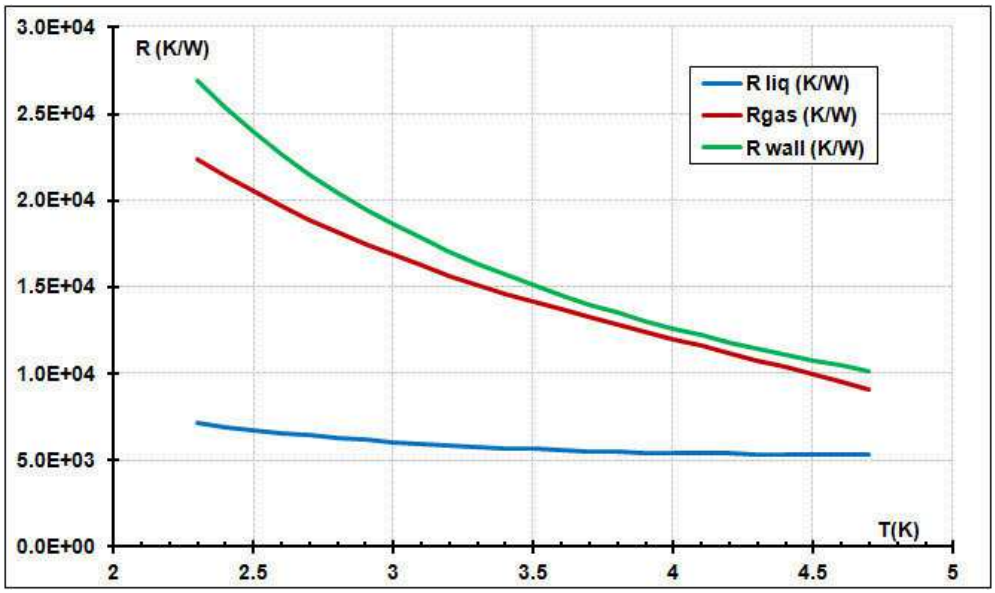


**Figure 4.5: Thermal resistance contributions between the two cell ends for wall, full gas or full liquid.**

The temperatures are measured in the two copper tips with a Cernox sensor.

Two resistive heaters were attached to the cell: one on copper top and the other on copper bottom. But during the heating up, we only used one resistor as heat source.

The thermal gradient induced by the heat flux at the thermometer location has been estimated to be 1 mK for a applied heat load of 10 mW (the RRR of the cooper part is assumed to be 100).

The wires of heaters and thermometers were thermalized to the helium bath. From this location the wires are made of manganin with a diameter of 0.2 mm and a length around 30 cm) to avoid significant parasitic load on the cell.

This cell is equipped with a stainless steel capillary (0.5x0.7 mm diameter and 200 mm length) which is connected on the top end of the cell and allows the filling of the cell during the

cool down and the release of the vapor during heating up. So, the gas comes in and gets out from the cell top. Two other capillaries are mounted in serial to the first one up to the cryostat cold plate. This two capillary are made of copper-nickel alloy and have the following dimensions 1 mm inner diameter and 70 mm length and 2 mm inner diameter and ≈ 100 mm length. The end of the third capillary is thermally connected to the cryostat cold plate.

From the cryostat cold plate to the volume expansion at room temperature a copper capillary (1 mm inner diameter and ≈ 900 mm length) is used. Note that another thermal contact is ensured on the liquid nitrogen cryostat reservoir.

The dimensions and materials of the capillaries used between the cell and the cryostat cold plate leads to negligible conduction load on the cell. The thermal anchoring of the capillary to the helium bath allows removing most of the enthalpy flow of the gas when it comes from room temperature during the filling phase. A heater and thermometer is attached at the thermal anchoring of the capillary with the cryostat cold plate and is used to avoid condensation of superfluid helium inside the capillary when pumped helium bath is used (temperature around 1.3 K).

To measure pressure in the system, there is a pressure sensor Keller type (Leo 1 Ei with a range of 0 to 4 bars) installed at room temperature in the piping that connects the expansion volume to the cold cell.

The bottom of the cell is clamped to the gas gap heat switch which is used as a thermal link in ON position. So, the cell is mainly cooled down by the bottom part.

#### 4.3.1.1 Ceramic

Kapirok ceramic

Inside the cell, we put a porous medium (ceramic). Most of the tests were performed with the ceramic Procelit P160 manufactured by Kapirok Company[4]. Some other tests have been realized with Altraform KVR 164/502 manufactured by RATH [5] In this section only the Procelit P160 (Kapirok ceramic) is described.

This ceramic, Procelit P160, was the one used in the sorption space cooler's evaporator built at SBT/CEA[32] and is very similar to Procelit P160 – RATH (using in nitrogen ESU) Procelit P160 is made of 9% silica and 90 % alumina with a density of about 300 kg/m$^3$ and a void volume in order of 90%. To estimate the wicking height during the experiment design phase, it was considered that the ceramic is composed of pores with average diameter around 50 μm. The evolution of the capillary height (using equation(1) with θ=0) with temperature is plotted in (Figure 4.6) for a 50 μm pore size.

The internal geometry in this porous material is not structured. The silica fibbers are stacked randomly and it is difficult to define a pore size from a geometrical analysis. In Figure 4.7 is possible to see one SEM picture of the ceramic.

The permeability of ceramic was measured in two different ways. The first consists in measuring the pressure drop of helium through the ceramic at 300 K. This measure has been realized at the CNRS/Néel Institut by Gerard Vermeulen and the value obtained is 3.8 x $10^{-12}$m$^2$ In CEA/SBT an higher value of 2.4 x $10^{-11}$ m$^2$ was obtained by measuring the pressure drop of liquid ethanol in the ceramic at room temperature (measurement done by Philippe Gully).

The difference between the two values (factor 6) can be due to two different measurement methods and also by the fact that two different samples of the same ceramic were used. It is also suspected that the higher value found by measurement with ethanol can be due to some destruction of the pores caused by ethanol flow leading to a more permeable sample.

[4] Ceramic P160, Kapirock Company,ZA LES COMPAS, 76170, LILLEBONN."
[5] Ceramic 164/502, RATH GmbH, Hafnerstraβe 3, A-3375 Krummnußbaum, Austria

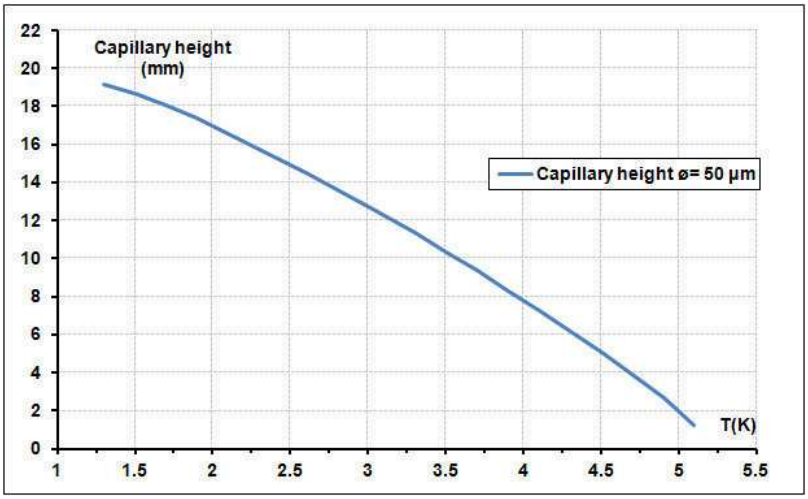


**Figure 4.6: Capillary height versus temperature calculated for Ø=50 µm.**

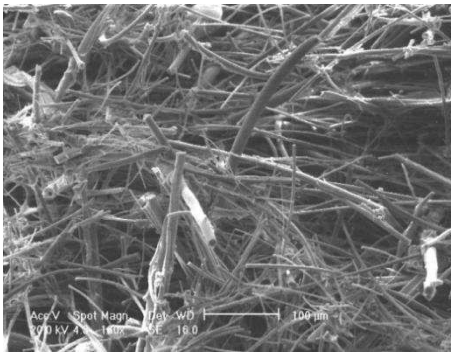

**Figure 4.7: SEM picture of Procelit P160 ( photographic Record- CEA/DTA/CEREM/DEM).**

### 4.3.2 The expansion volume

During the heating phase, the cell's temperature must be kept almost constant in order to have the same capillary height throughout all the phase duration. With this condition, it is possible to study the heat transfer process for a given and known capillary height.

As the experiment is performed on the saturation curve, the control of the interface temperature is the same that the control of the pressure. So, one solution to maintain a constant temperature in the cell is to connect the cell with a large expansion volume at room temperature in order to reduce pressure variation during helium evaporation.

A room temperature expansion volume was sized in order to completely fill the cell with liquid helium at low temperature and to limit the capillary height variation at a maximum value of 10 % during the evaporation of all the liquid contained in the cell. The evolution of the variation of the capillary height and the variation of the temperature with expansion volume size is represented in Figure 4.8.

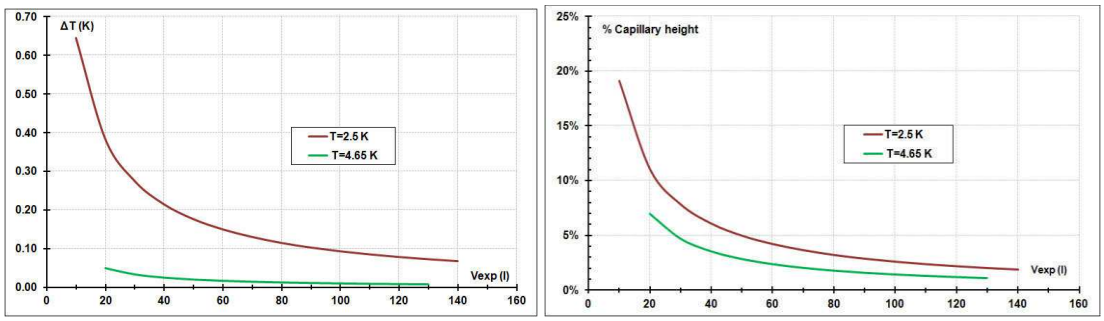


**Figure 4.8: Variation of the variation of the temperature (left) and capillary height (right) during evaporating process in function of the size of expansion volume for 2.5 K and 4.65 K initial temperature conditions.**

If all the liquid in the cell is vaporized at 4.65 K, with an expansion volume of 20 liters the variation of temperature is only 0.05 K and this corresponds to a 5 % variation of the capillary height. But at 2.5 K the evaporation of all the liquid with the same 20 liter expansion volume implies an increase of temperature of 0.65 K and a capillary height variation of 11 %.

So, we mainly use an expansion volume of 30 liters which is enough to achieve the 10 % criteria for temperatures between 4.65 K and 2.5 K. For some experience at 2.5 K a larger expansion volume of 100 liters was used to minimise the capillary height variation even more.

By adjusting the pressure in the expansion volume before the run, we can perform experiments (condensation/evaporation) at different temperatures with different fluid properties and study their impact on capillary height.

Before dealing with the main topics of this study which is the energy storage and heat transfer in porous media filled with a two phase flow, the heat transfer in simpler condition has been studied and is being presented in the following section.

### 4.3.3 Heat transfer

When a surface in contact with liquid is maintained at a temperature above the saturation temperature of the liquid, boiling could occur. In this section a brief review on boiling process is presented. The so-called Nukiyama's boiling curve is plotted in Figure 4.9. It shows the relationship between the heat flux and the temperature difference between the heated surface and the saturation temperature of the liquid. In the curve depicted, four distinct trends of heat transfer regimes can be distinguished:

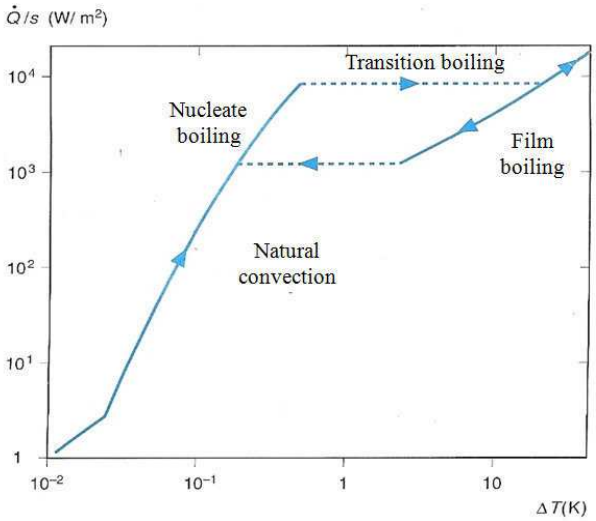


**Figure 4.9: Boiling curve of helium liquid at 4.2 K. ΔT is the temperature difference between the heated surface and the saturation temperature adapted from [40].**

- **Natural convection**- This happens when the temperature surface is heated above the saturation temperature. The liquid in contact with surface is slightly superheated and rise by natural convection due to the expansion of the heated liquid. In this regime there is no vapor bubbles formation.

- **Nucleate boiling –** The first bubbles are formed at preferential sites on the heated surface. By increasing the heat flux, more and more nucleation sites become activated until the surface is covered with the bubbles that grow and depart in rapid succession. At $\dot{Q}_{critical}$, the rate of vapor generation is such that it is starting to impede the flow of liquid onto the surface. The critical heat flux is reached and corresponds to a maximum possible liquid flow rate in the counter flow of vapor flowing away from the surface. A film of vapor is created between the heated surface and the liquid bulk. The value of the critical heat flux depends of the temperature as shown in Figure 4.10. At 4.2 K, the critical heat flux is around 8 kW/m$^2$. It is evident that the critical heat flux depends of others factors as: surface finishing, surface orientation versus gravity and geometry.

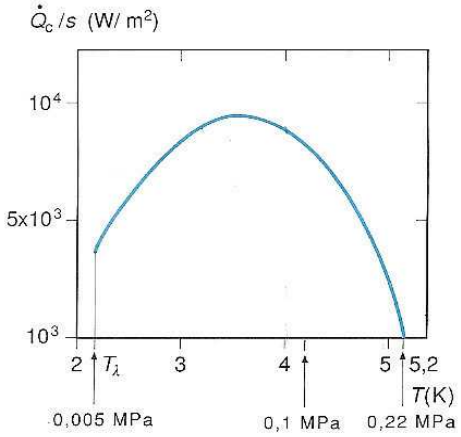


**Figure 4.10: Critical flux in function of the liquid helium temperature [40].**

- **Transition boiling (sometimes called unstable film boiling) -** In this regime there is a transition between the near –complete liquid contact with the surface in nucleate boiling to near- complete vapor contact in film boiling.

- **Film boiling-** In this region (for a heat flux above critical heat flux) the heated surface is completely covered by a continuous stable film of vapor because departing bubbles coalesce into a vapor jet. This vapor film impedes the heat transfer.

By reducing the heat flux, the process follows the film boiling curve until arriving at a heat flux for which the film boiling process become unstable (transition boiling). At this unstable transition the film boiling is completely replaced by nucleate boiling.

During our experience, heat flux applied are between 6 W/m$^2$ and 67 W/m$^2$ well below the critical flux. The thermal response of the cell is affected by the presence or the absence of ceramic as it will be presented hereafter.

Some tests were carried out to study the conduction and the convection in a cell filled with or without ceramic and with an empty cell.

#### 4.3.3.1 Conduction with ceramic

The aim of this experience is to analyze the influence of ceramic in the heat transfer by conduction.

In this section the study carried out to analyse the heat transfer by conduction in two configurations will be presented:

- cell filled with ceramic – to analyze the ceramic conductivity
- cell filled with ceramic and liquid- to analyse the conduction of liquid inside the ceramic.

In all these tests the cell was heating on the top, on the copper tip, and the temperature of the bottom of the cell was controlled with a heater so that the temperature of the bottom of the cell was maintained constant for all the power applied on the top, in Figure 4.11 it is possible to see a schema of the experimental set-up.

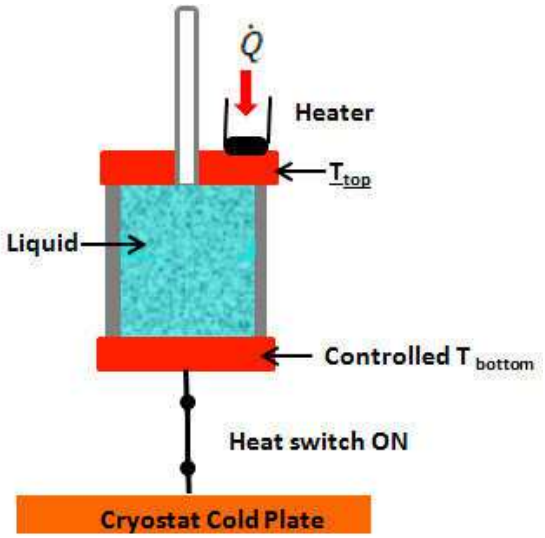


**Figure 4.11: Schema of the experimental set-up to measure conduction.**

**Cell filled with ceramic without fluid**

In the first test the cell with ceramic was tested with vacuum inside. In this case, the heat transfer from the top to the bottom is done only by the stainless tube and the ceramic. Test at 4.2 K and 2.5 K was carried out. The experimental points (square point) at 2.5 K (red) and 4.2 K (green) are plotted in Figure 4.12. The theoretical values for stainless tube wall is calculated using the integral of conductivity of 304 L stainless steel [41] and is also plotted in this graph (lines). It can be seen that the experimental values fit well with the theoretical value of stainless steel and so that the contribution of ceramic is negligible.

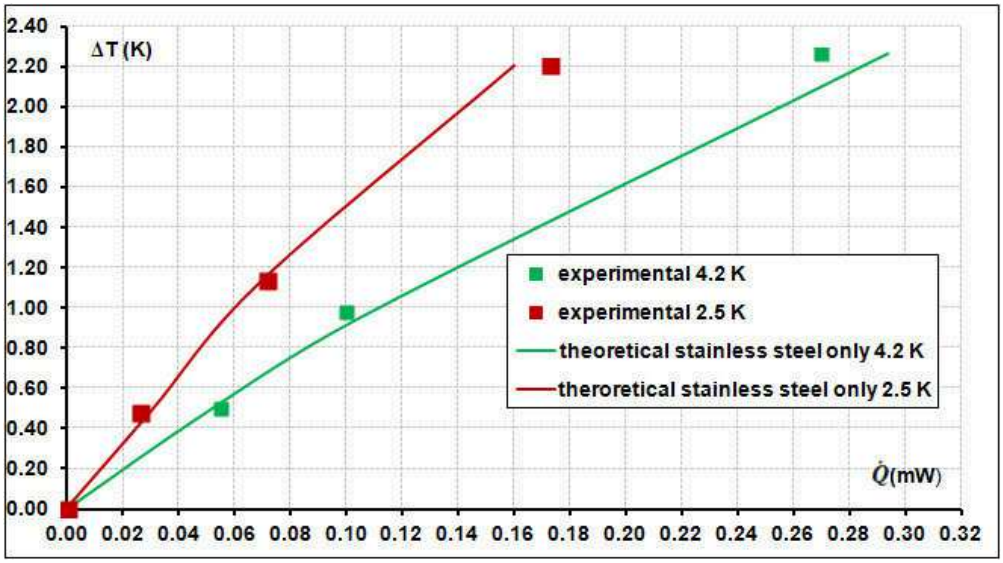


**Figure 4.12: Load applied on the top of the cell with ceramic and with vacuum inside as function of $\Delta T$ ($T_{top}$-$T_{bottom}$) at 4.2 K (green square) and 2.5 K (red square). The theoretical values for the cell wall made of stainless steel are represented by lines.**

## Cell with ceramic filled with liquid

To measure the conduction of liquid at 2.5 K and 4.65 K the cell with ceramic was filled with 2.23 bars of helium ($T_{sat}$ =5.18 K), a pressure above the saturation pressure for 2.5 K and 4.65 K. So, when the cell is heated on the top, the cell remains filled of liquid because the liquid will not be in saturation regime.

In Figure 4.13, the square points are experimental data at 4.65 K (green) and 2.5 K (red) and the lines are theoretical values. The theoretical values take into account the conduction of the stainless steel tube and the conduction of the liquid. For the liquid conduction, the cross section has been assumed to be the cross section of the tube multiplied by the porosity (0.92).

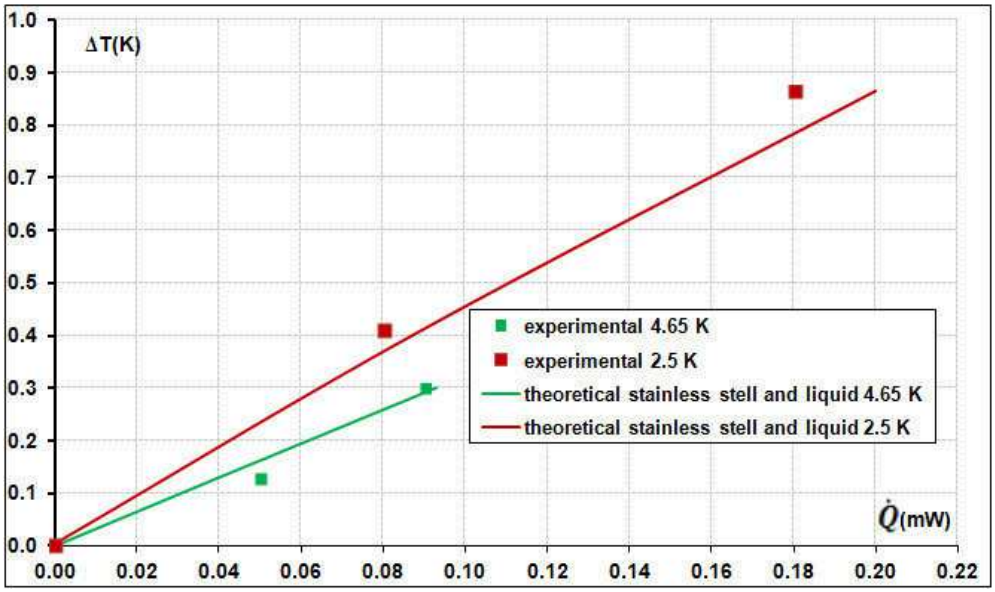


**Figure 4.13: Load applied on the top of the cell with ceramic and liquid as function of $\Delta T$ ($T_{top}$-$T_{bottom}$) at 4.65 K (green square) and 2.5 K (red square). Theoretical values taking into account liquid and cell wall contributions are represented by lines.**

Comparing these results with those obtained without liquid, we can deduce that heat conduction through liquid helium is roughly 2/3 of the global heat conduction. Furthermore, theses experiences allow concluding that the ceramic inside the cell don't change the

conductivity of the liquid as the measurements obtained are in good agreement with the theoretical values. Moreover, it has been shown that the conductance of the ceramic (cylinder Ø =13.8 mm and length =14.3 mm) is well lower than the conductance of the cell walls (the stainless tube wall ($Ø_{int}$=13.8 mm and $Ø_{ext}$=14 mm)) which is more than twice as lower as the conductance due to liquid in the temperature range between 4.65 K and 2.5 K.

#### 4.3.3.2 Convection with and without ceramic

Another test was performed to measure the natural convection inside the cell filled with liquid. This test was carried out with and without ceramic for 2 levels of temperatures: 4.65 K and 2.5 K.

To study the natural convection in the liquid, the cell was always filled with liquid and the temperature is measured on the top and the bottom of the cell. The cell was inverted in the cryostat (see Figure 4.14), in other words the cell is attached to the heat switch by the top (where the capillary is connected). To create the natural convection the bottom of the cell is heated with different powers and the top of the cell is maintained at a constant temperature of 4.65 K or 2.5 K. The top of the cell is cooled via the heat switch and its temperature is automatically controlled with a heater.

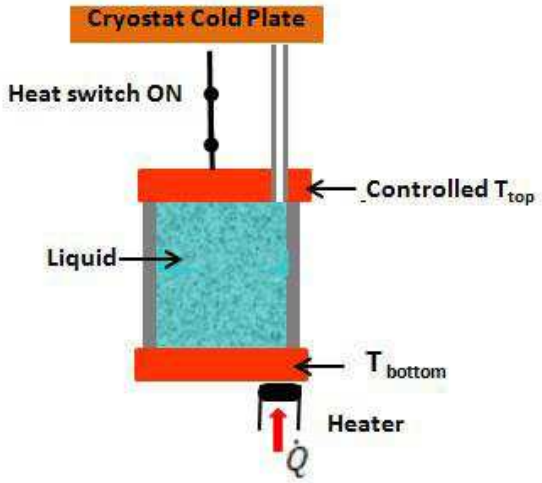


**Figure 4.14: Schema of the experimental set-up to measure convection.**

To avoid evaporation while the cell is heated on the bottom, the system was filled with a pressure of 2.15 bars, higher than the saturation pressure at 4.65 K and 2.5 K.

The results of the experiment are plotted in Figure 4.15 and Figure 4.16 respectively for 4.65 K and 2.5 K. The square points correspond to the measurements when there is no ceramic inside the cell and circle points when the cell is filled with the ceramic. The solid line is the theoretical value for natural convection without ceramic and the dashed line is the theoretical value for conduction taking into account the space occupied by ceramic.

The theoretical values for natural convection are calculated using a formula dedicated to horizontal rectangular enclosure with isothermal surfaces [42].

To deal with heat transfer caused by natural convection, the dimensionless number of Rayleigh is used. This number is the product of the Grashof number and Prandtl number (Pr). The Grasholf number represents the radio of the buoyancy force to the viscous force acting on the fluid and the Prandtl number is the ratio of the momentum diffusivity to thermal diffusivity.

With the horizontal rectangular geometry, natural convection occurs when the Rayleigh number is higher than the critical Rayleigh number (1708). For Rayleigh number between 1708 and $5x10^4$ fluid motions consist of regularly spaced roll cells, while for larger Rayleigh numbers, the cells break down and fluid motion is turbulent.

For helium, in our working conditions, the $Ra_l$ is higher than $5x10^4$ even for very low dT so we are in a turbulent regime.

For Rayleigh number between $3x10^5$ and $7x10^9$ the following expression can be used to calculate the Nusselt number (Nu) [42]:

$$Nu = 0.069\, Ra_l^{1/3} P_r{}^{0.074} \tag{4.3}$$

The Pr is defined as:

$$P_r = \frac{\mu\, C_p}{\lambda} \tag{4.4}$$

Where $\mu$ is the dynamic viscosity, $C_p$ is specific heat and $\lambda$ is the thermal conductivity of the liquid in the cell.

Where the Rayleigh number [42] is:

$$R_{a_l} = \frac{\rho^2 \beta C_p g (T_h - T_c) L_c{}^3}{\mu\, \lambda} \tag{4.5}$$

Where $L_c$ is the characteristic length, in our case the distance between the hot and the cold surface, $T_h$ and $T_c$ is the temperature of the hot and cold surface, $\beta$ is the volume coefficient of expansion.

When the Nusselt number is known, the rate of heat transfer [42] though the enclosure can be determined from:

$$Q = \lambda \quad Nu \frac{A_T}{L_c} (T_h - T_c) \tag{4.6}$$

Where $A_T$ is area of the cell.

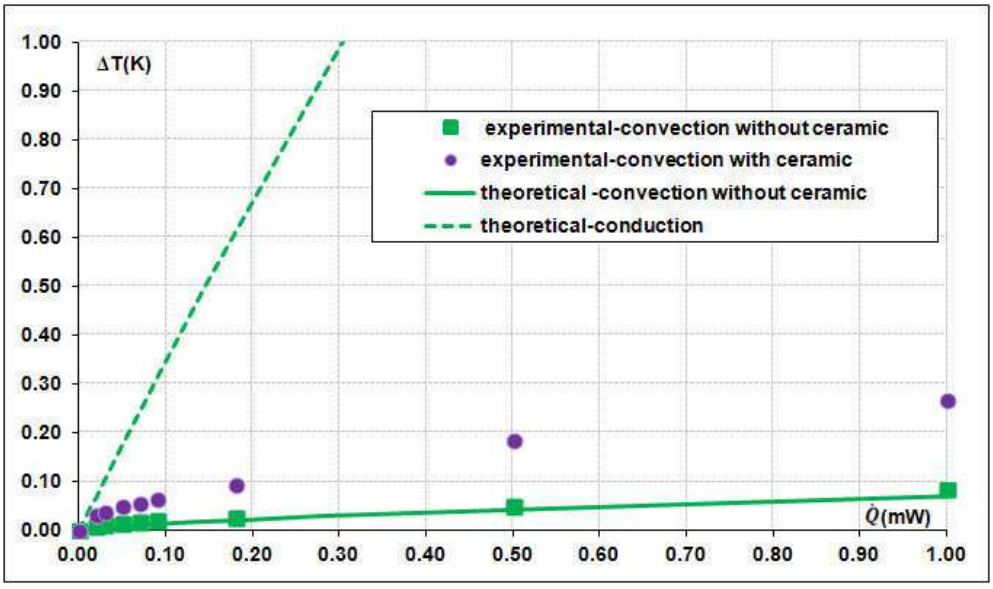


**Figure 4.15: Load applied on the bottom of the cell filled with liquid helium, with ceramic (purple circle point) and without ceramic (green square point) as function of $\Delta T$ ($T_{top}$-$T_{bottom}$) at 4.65 K. The theoretical values for natural convection without ceramic are represented by green solid line. $\Delta T$ is the difference of temperature, obtained after removing the difference without applied heat flux, which was 0.001K.**

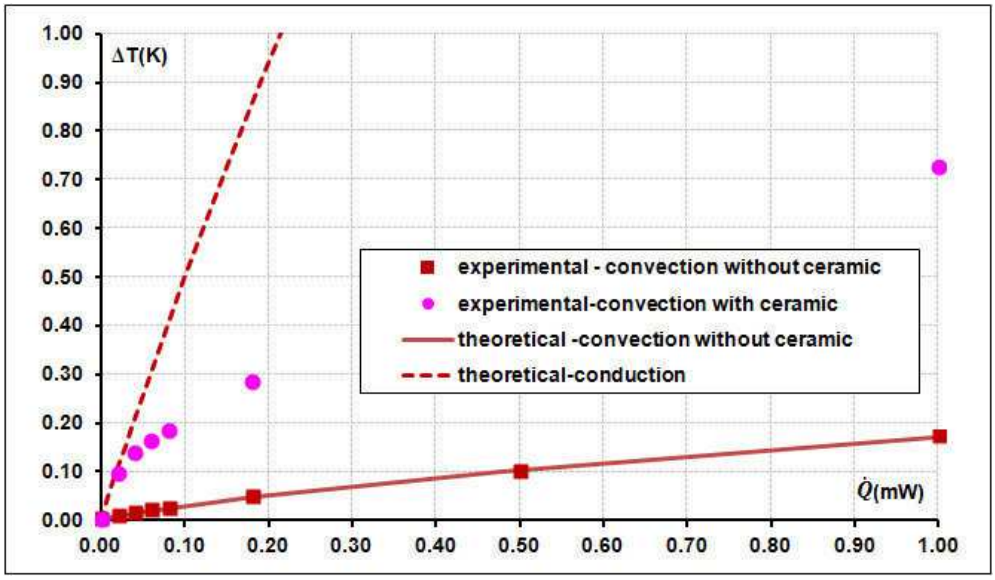


**Figure 4.16: Load applied on the bottom of the cell filled with liquid helium, with ceramic (pink circle point) and without ceramic (red square point) as function of $\Delta T$ ($T_{top}$-$T_{bottom}$) at 2.5 K. The theoretical values for natural convection without ceramic are represented by red line. $\Delta T$ is the difference of temperature, obtained after removing the difference without applied heat flux, which was 0.001K.**

There is a good agreement between the experimental values obtained and the theoretical value even if the law used should not directly applied to the shape of this study (different aspect ratio, cylindrical and not rectangular shape). This is probably due to high Rayleigh number for which the fluid motion is turbulent. The convection leads to a higher heat transfer (around 3 times) at 4.65 K than 2.65 K due to the fact that at high temperature the liquid is more compressible and thus the coefficient of volumetric expansion is higher inducing a higher Rayleigh number. But also the specify heat at 4.65 K is higher than at 2.65 K, so the Prandtl number is higher too, that means that the convection is more efficient.

The ceramic inside the cell strongly reduces the natural convection. For a dT=0.1 K, the heat transfer is reduced by a factor 5.5 at 4.65 K and by a factor 25 at 2.5 K.

In porous media heated by the bottom, it is possible to use a filtration Rayleigh number (Ra) to know whether the energy is transferred by conduction or convection. This filtration Rayleigh number (Ra) is:

$$R_a = \frac{k\,\rho_L g \beta \Delta T H}{\mu[\lambda^*/(\rho_L \mathrm{Cp_L})\ ]} \qquad (4.7)$$

Where k is the permeability of ceramic; H is the height of cell; $\Delta T$ is the difference between $T_{top}$ and $T_{bottom}$; $\lambda^*$ is the effective thermal conductivity, $Cp_L$ is the specific heat capacity of liquid. As shown in the §4.3.3.1, the presence of the ceramic does not affect the thermal conductance of the cell filled with liquid. So, the effective thermal conductivity is equal to the thermal conductivity of the liquid taking into account that the height of the cell and multiplied by the porosity of the ceramic (0.92).

Depending on hydrodynamic and thermal boundary conditions of the experiment there are values tabulated for critical filtration Rayleigh number (see in Table 4.1). Our configuration is the first in the Table 4.1, the bottom of the cell is isothermal (ISO) and impermeable (IMP) as well as the top of the cell. In this case, the critical filtration Rayleigh number is equal to $4\pi^2$ (39.4). When the filtration Rayleigh number is less than $4\pi^2$ the transfer in the cell is purely conductive. Above $4\pi^2$ there is a transitory regime from conduction to convection. When the filtration number is three times higher than the critical filtration number, the heat transfer increases much. In Figure 4.15, it is possible to see isothermal and convection cell representation for different filtration Rayleigh number in the case where the ratio between the width and height of the cell is 5.

**Table 4.1: Values of critical filtration Rayleigh number in function of hydrodynamic and thermal boundary conditions of the cell [43].**

| Surface inférieure | Surface supérieure | $Ra^*_c$ |
|---|---|---|
| ISO, IMP | ISO, IMP | $4\pi^2$ |
| ISO, IMP | FLC, IMP | 27,10 |
| FLC, IMP | FLC, IMP | 12 |
| ISO, IMP | ISO, LIB | 27,10 |
| FLC, IMP | ISO, LIB | 17,65 |
| ISO, IMP | FLC, LIB | $\pi^2$ |
| FLC, IMP | FLC, LIB | 3 |
| ISO ou LIB FLC | ISO ou LIB FLC | 0 |

ISO : isotherme, IMP : imperméable

FLC : flux constant, LIB : libre

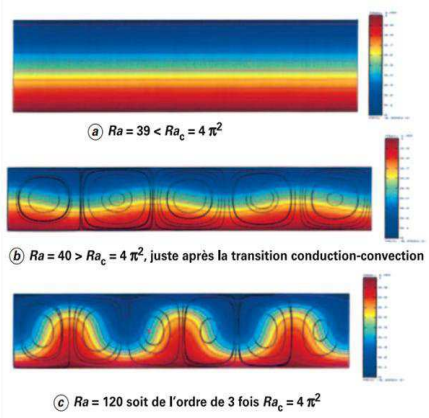


**Figure 4.17: Isothermal and convection cells representation in the case where the ratio between the width and the height of the rectangular cell is 5 for different filtration Rayleigh number [43].**

From the experimental results of cell with ceramic, it is possible to calculate the Nusselt number using the equation (4.6) and the filtration Rayleigh number from the equation (4.7). The results can be compared with literature results (shown in the Figure 4.18) for horizontal porous layer heated from below and defined by impermeable surfaces. For each experimental point there is a value of Nu and Ra, these values are plotted in Figure 4.19: red line is the experimental point calculated for 2.5 K with the k=2.4 x $10^{-11}$ $m^2$ (triangle date) and k= 3.4 x $10^{-12}$ $m^2$ (circles date) and the green line is the experimental point calculated for 4.65 K with k=2.4 x $10^{-11}$ $m^2$ (triangle date) and 3.4 x $10^{-12}$ $m^2$ (circles date). The black line in the Figure 4.19 is the blue line in Figure 4.18.

The curves for a given permeability are superimposed as expected (adimensionnal Numbers). The results are higher than literature data and can become closer if we use higher permeability (which is not consistent with other results presented into this manuscript). The higher Nusselt value found in our experiment could probably be attributed to the fact that the geometry of our system (cylinder cell) and the ratio aspect (H equal Ø) is different of literature (parallelepiped cell, H/width <<1).

For information only, the critical Rayleigh below which no convection occurs is represented in Figure 4.19 with a black solid line.

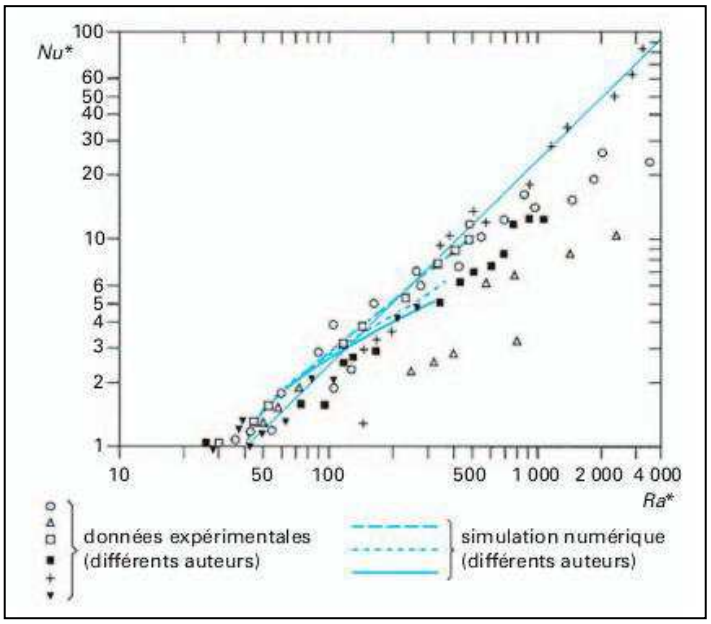


**Figure 4.18: The Nusselt number as function of filtration Rayleigh number for horizontal porous layer heated from below and defined by impermeable surfaces[43].**

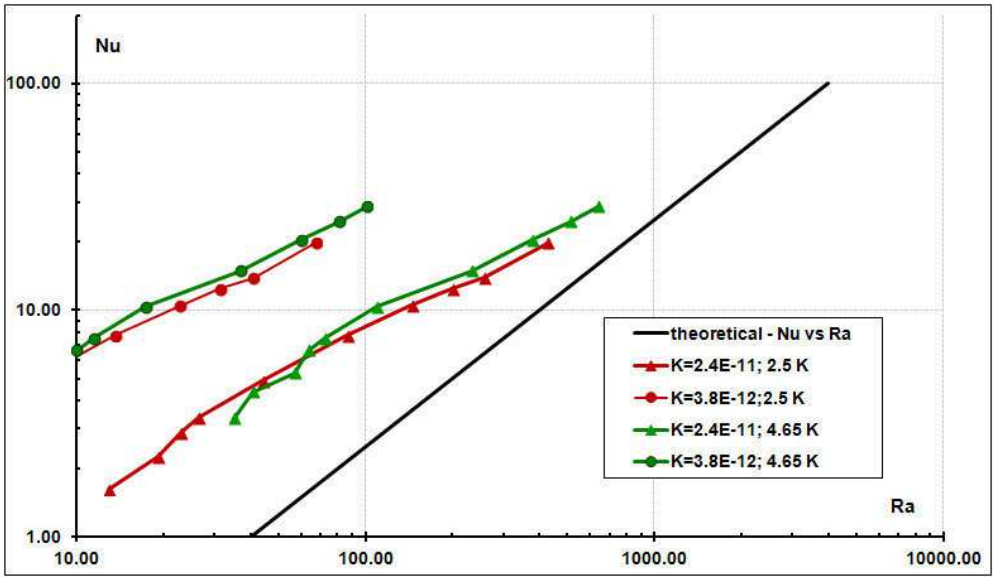


**Figure 4.19: The Nusselt number as function of the filtration Rayleigh number. The black line is the blue line in Figure 4.18. The line curve with data is calculated from the experimental results.**

In conclusion, without ceramic the natural convection in liquid helium at 4.65 K is higher than at 2.5 K due to fluid properties. The main effect of the ceramic is to delay the onset of the natural convection. It can be noticed that the convection effect is more reduce for 2.5 K than for 4.65 K, so the ceramic difficult more the convection at 2.5 K

## 4.4 Modus operandi

In the following chapter, the energy stored inside the cell and the heat transfer process in a two phase fluid will be studied. First the standard modus operandi will be described.

To start the experiment, the expansion volume and the cell are filled at room temperature with a given pressure. This pressure value will determine the cell temperature for which the condensation/evaporation will occur.

In the first phase, the helium cryostat is cooled and the cell is cooled down with the gas gap heat switch which is in ON state. Since the cell is connected to the gas gap heat switch by its bottom, the poor heat conduction of lateral wall and the gas enters by the top, condensation mainly occurs at the base.

At the beginning, the cell ends tips temperatures decrease fast due to large thermal gradient between cell and helium bath. The cell bottom tip reaches $T_{sat}$ and helium gas starts to liquefy at this position. Then, the helium continues to liquefy until the cell is full of helium. At this stage, liquid at the bottom of the cell is slightly subcooled.

In the second phase, when the cell is completely filled with liquid, the gas gap heat switch is used to thermally decouple the cell from the cold plate of the cryostat. This is done by toggling OFF the gas gap heat switch.

In the third phase, a constant heating power is applied to the cell; it can be on the top or on the bottom. The energy dissipated is absorbed thanks to the progressive liquid evaporation. The helium evaporated is stored in the expansion volume that is connected to the cell, avoiding a significant increase of pressure inside the cell. While the liquid is evaporated and the gas is stored in the expansion volume at constant pressure, the cell temperature remains constant. During this phase, temperature evolution of the top and the bottom is measured. Until there is liquid in contact with copper tip heated, copper's temperature remains almost constant and equal to saturated temperature of liquid/vapor. Using this plateau (almost constant temperature versus time during a certain amount of time), it is possible to estimate the stored energy or more precisely the energy stored in the cell that could be recovered at the saturated temperature. This energy is simply the power applied multiplied by the duration while the temperature is constant.

When all the liquid is evaporated, no more latent heat is available so the temperature drifts increase dramatically and the heating power is stopped.

To start a new cycle, it is necessary to cool down again the cell and this is achieved by turning ON the gas gap heat switch.

## 4.5 Cooling process

### 4.5.1 Cooling of the cell without ceramic

Figure 4.20 shows typical cooling of the cell without ceramic. In this experiment, the 30 liters expansion volume and the cell were filled with helium gas at 1.53 bar at room temperature. The cell was cooling down by a cold plate of the helium cryostat (yellow line) approximately at 4.2 K. The temperatures, measured by the thermometers, thermalized at the bottom $T_{bottom}$ and the top $T_{top}$ of the cell are representing by green line and blue line, respectively. It can be seen that the bottom of the cell which is connected to the cold plate via the heat switch, cool down very quickly whereas the top cell temperature decreases slowly and present two regimes.

When $T_{bottom}$ is at 4.65 K which corresponds to saturated temperature at 1.48 bar (here at time ≈ 3min), the first drop of helium was formed in the bottom of the cell. Then, when helium is liquefied inside the cell, the liquid level increased. The liquid is liquefied at the liquid gas interface and the cooling power available to liquefy the gas will depend on the thermal gradient through the liquid height. The contribution from the wall is negligible as shown in §4.3.1. At the liquid-vapor interface, the temperature is always 4.65 K (saturation temperature) and the base of the cell is at a temperature close (thanks to the good conductance of the heat switch) to the cryostat cold plate, 4.2 K for the case presented.

The top of the cell cools down more slowly than the bottom cell because is cooling only by a stainless steel tube and the gas conduction inside the cell. When the top of the cell indicates 4.65 K, that means that the liquid helium touch the cell's top and that the cell is full (after 7 hours). However, for the example shown, we cooled the cell below the saturation temperatures until the cell reaches the bottom temperature.

The capillary used to fill the cell has a small section in the cold area (close to the cell) to avoid the storage of a large amount of liquid in the capillary at the end of the condensation phase.

Once the whole cell is at the same temperature (after 10 hours) and the heat switch was in OFF state we can start the experiment.

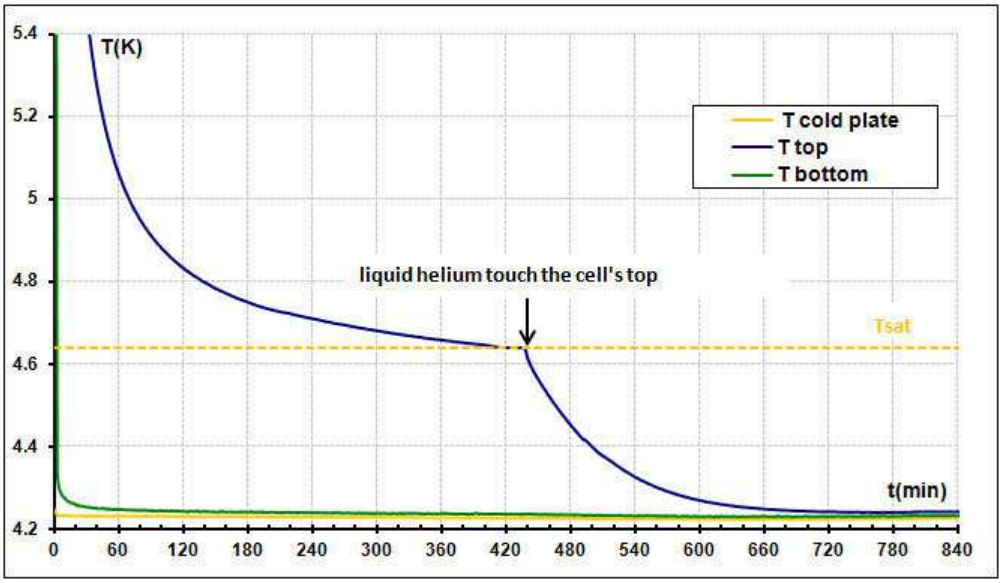


**Figure 4.20: Evolution of the top and the bottom temperatures of the cell and cold plate temperature when the cell without ceramic is cool down.**

### 4.5.2 Cooling of the cell with ceramic

In another experiment, we perform a cooling test with ceramic. In the Figure 4.21, $T_{bottom}$ and $T_{top}$ of the cell with ceramic are represented by green and blue lines, respectively.

As in previous case, the $T_{bottom}$ of the cell reached the saturation temperature faster than $T_{top}$ because the cell is cooling down by the bottom of the cell. So, the first droplet is created at the bottom when $T_{bottom}$ reach the saturation temperature (4.65 K). Then, liquefaction continues and the amount of liquid impregnated in the ceramic increases with time. There is not a liquid level well defined in the cell, the liquid spreads inside the ceramic.

At 180 min the $T_{top}$ is equal to 4.65 K, and remains constant during approximately 180 additional minutes. When $T_{top}$ indicates the saturation temperature (4.65 K) this means that some liquid reaches by capillary the top of the cell but the cell is not full. During the plateau, the gas continues to liquefy inside the cell until to fill up.

After 6 hours, the $T_{top}$ of the cell starts to decrease because all the vapor has been condensated: the cell is full of liquid.

The thermal gradient between the top and the bottom of the cell is due to a poor liquid conduction, as seen in section §4.3.1.

Once the cell is full, we continue to cooling down the cell below the saturation temperature until the top temperature reaches the bottom temperature to be sure that the cell is full of liquid.

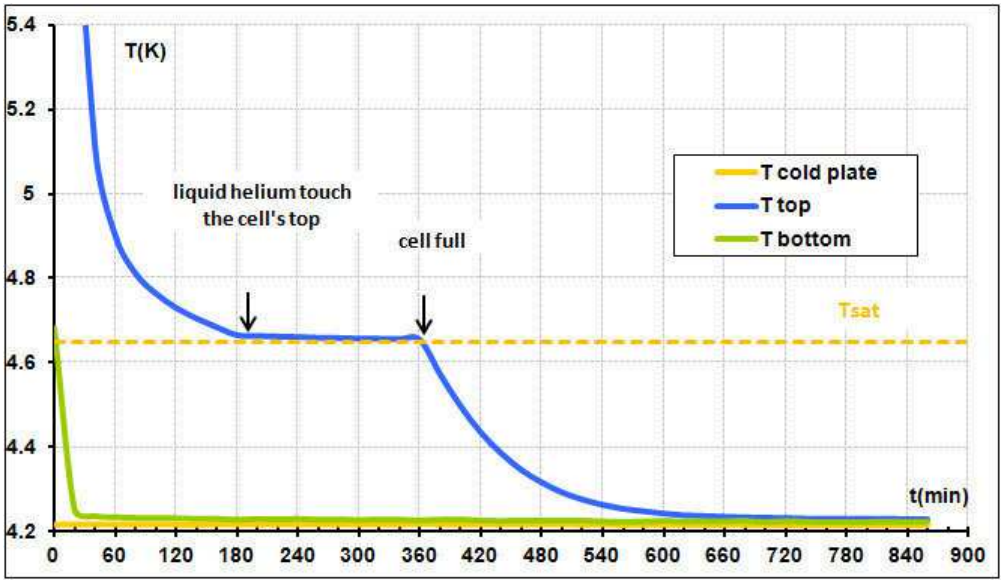


**Figure 4.21: Evolution of the top and bottom temperatures of the cell and cold plate temperature when the cell with ceramic is cool down.**

### 4.5.3 Comparison between cooling down with ceramic and without ceramic

There are four differences between cooling downs with and without ceramic (Figure 4.22).The first one is that the cell with ceramic fills faster than a cell without ceramic. The reason is probably due to the fact that ceramic which is impregnated by liquid helium increases vapor/liquid interface. Although ceramic occupies approximately 10 % of the cell volume, a cell with ceramic takes less than 22% less time to fill up than a cell without ceramic.

The second one is the evolution of the bottom temperature ($T_{bottom}$) of the cell. When the cell with ceramic is cooled down, the $T_{bottom}$ decreases slower than if the cell has no ceramic. This can probably be attributed to the fact that when helium starts to condensate the liquid rise through the pore of the ceramic, increasing the vapor-liquid interface, and so, the liquefaction rate is larger when the cell is filled with a ceramic and the cool down via the limited conductance of the heat switch takes more time.

The third difference is $T_{top}$ of the cell with ceramic reached the saturation temperature faster than cell without ceramic. This is due to capillary effect in the ceramic, which allow some liquid to reach the top of the cell before the cell is completely full.

When the $T_{top}$ in the cell with ceramic reached the saturation temperature, it remains constant during 6 hours at 4.65 K. In the experiment without ceramic, there is no plateau. This is the forth difference. The first liquid in contact of the top defines the first point of the plateau. During the plateau the cell continues to fill. When the plateau finished, the cell is full.

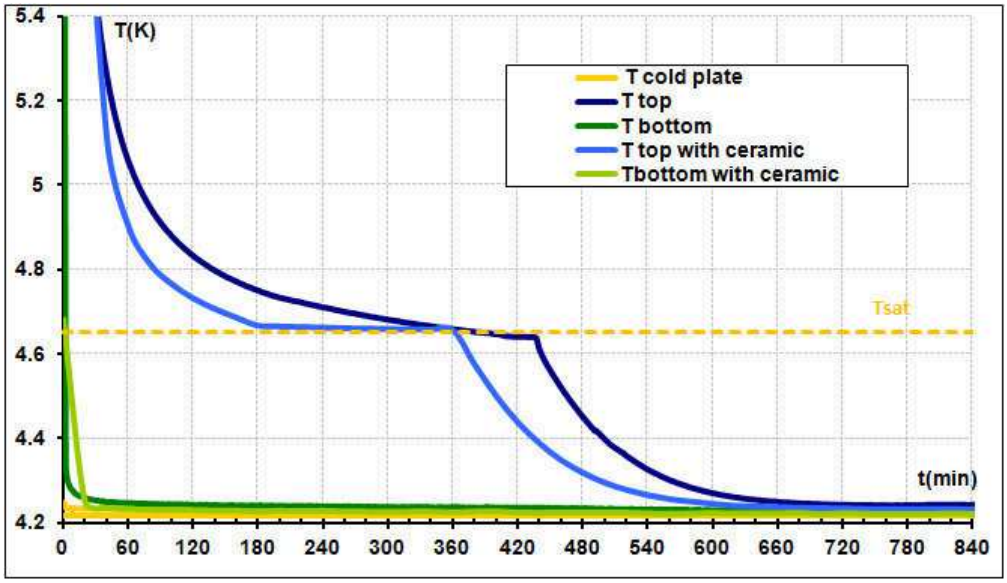


**Figure 4.22: Comparison between the cooling down tests with and without ceramic.**

### 4.5.4 Cooling down of the cell with ceramic in superfluid.

When the cryostat cold plate is at 4.2 K, the cell with ceramic takes 6 hours to be filled with helium liquid. To reduce the cool down time, the cold source temperature can be decreased. For that, we pumped on the cryostat helium bath and its temperature achieves a low temperature of 1.3 K (yellow line).

In Figure 4.23, the evolutions of the temperatures are shown during a cool down process of the cell.

At the beginning, before 3.6 min, another experience had been done and the cell had bee, heated up to reach approximately 5.2 K with the switch in OFF state. So, at 0 min, the cell is at 5.2 K and the switch is commuted to the ON state. During the time that the switch takes to commute between OFF to ON (3.6 min), the $T_{bottom}$ and the $T_{top}$ remains approximately at 5.2 K and the pressure of the cell is approximately 1.5 bar; meaning that there is no liquid inside the cell.

At 3.6 min, the $T_{bottom}$ decreases rapidly until reaching 2.17 K, the superfluid temperature. This fact happens because the heat switch is toggled to the ON state, meaning that the conduction between the bottom of the cell and the cryostat cold plate is set to its best value (40 mW/K). This way, the cell starts to cool down. As the heat switch is attached in the bottom of the cell, this part of the cell is the first to achieve the superfluid temperature. The bottom cell remains at 2.17 K during approximately 20 min.

In parallel, the $T_{top}$ increase fast until 11.5 K and after the temperature start to decrease slowly until it reaches 4.65 K. At this temperature, the saturation temperature, the $T_{top}$ makes a plateau (same behaviour as previously) of 2 min and after decreases quickly to $T_{bottom}$ .The temperature of the bottom of the cell stays at the helium superfluid temperature because it is not possible to subcool the superfluid helium (like in “bain Claudet”) with the cross section of the cell. So, there is a fixed and large thermal gradient inside the heat switch that leads to a large cooling heat flux that drives the liquefaction rate. The large liquefaction rate induces an increase of the “hot” helium mass flow rate passing through the cell top end which is almost thermally decoupled from the bottom of the cell. This leads to the quick increase of the $T_{top}$.

When there is superfluid helium inside the cell, the thermal resistance inside the liquid helium is no longer the limiting factor for the condensation. The limiting factor is due to the heat switch conductance which is quite good.

The cell is filled with a certain quantity of superfluid helium and normal helium up to the liquid/gas interface at 4.65 K.

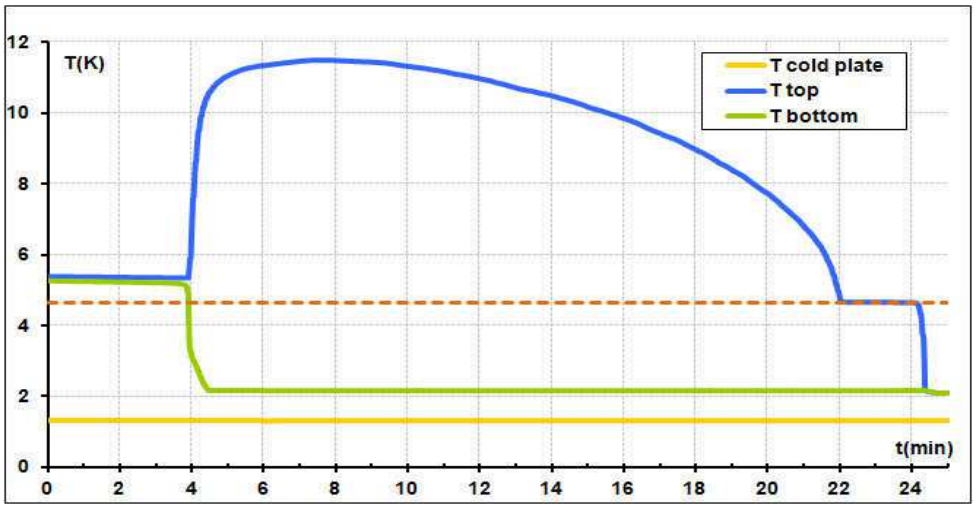


**Figure 4.23: Evolution of the cell top and bottom temperature and cold plate temperature when the cell is cool down.**

The cell is filled with a certain quantity of superfluid helium and above there is a limited thickness (approximately 0.17 mm) of normal helium up to the liquid/vapor interface at 4.65 K. In the Figure 4.24 is it possible to see a scheme of the cell fill with superfluid and normal helium. This small thickness of normal helium depends of course of the helium properties (conductivity) but also of the cooling power generated by the thermal gradient inside the heat switch. The heat flux crossing the normal helium layer is equal to the heat flux passing through the heat switch. The thickness of normal helium was calculated using the follow expression (assuming that the conduction in the ceramic and the tube wall tube are negligible):

$$W_{CD} = C_{HS}\,(T_{CF} - T_{botton}) = \frac{A_T}{t_{hic}}\,\varepsilon \int_{2.17K}^{4.65K} \lambda\, dT \qquad (4.8)$$

Where $C_{HS}$ is the conductance of heat switch, $T_{CF}$ is the cold finger of cryostat, $A_T$ is the section of the cell, $t_{hic}$ is a thickness of normal helium up to the liquid/vapor interface at 4.65 K and $\varepsilon$ is the porosity of ceramic.

At approximately 8 min, $T_{top}$ starts to decrease, this mean than the heat power released by the thermalization of the gas entering in the cell becomes lower than the heat flux than can be evacuated by the stainless steel cell wall and conduction of the vapor inside the cell. This is due to the fact that the level of liquid inside the cell increases and that the distance between the liquid/vapor interfaces becomes smaller.

There is a short plateau of 2 min at the saturation temperature. When the top of cell indicates the saturation temperature of 4.65 K, there is some liquid on the top of the cell due to capillarity effect but the cell is not yet full. The temperature $T_{top}$ remains constant up to the cell is filled completely with liquid. Then $T_{top}$ start to decrease until the whole cell is at the $T_{bottom}$.

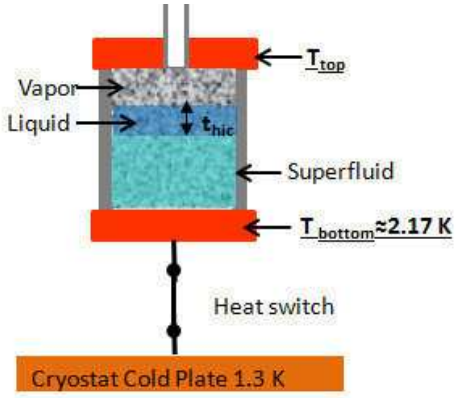


**Figure 4.24: Scheme of the cell with helium in superfluid, liquid and vapor. Above the superfluid, there is a limited thickness (t of normal helium up to the liquid/vapor interface at 4.65 K.**

## 4.6 The effect of wicking height variation when the cell is heating on the top end

In this section the results of the experiment in which the cell with and without porous media is heating on top end will be presented. One model has been developed to understand how the heat flux affects the amount of liquid that evaporates.

### 4.6.1 Results when cell is heating on the top end

#### 4.6.1.1 Heating the top of the cell without ceramic

In this section, the effect of heating the cell without ceramic on the top of the cell is analyzed. In Figure 4.25 the evolution of $T_{top}$ and $T_{bottom}$ when 5 mW (3.3 mW/cm$^2$) is applied are plotted as a function of time for an experiment with a saturation temperature of 4.65 K ($P_{sat}$=1.48 bar is the pressure imposed by the large volume located at room temperature and connected through the capillary to the cell). When the top of the cell with a temperature slightly lower than the saturation temperature is heated, the temperature increases to the saturated temperature and then a short plateau occurs. It takes only 12 seconds before the $T_{top}$ of the cell starts to increase again quickly. We can evaporate only the liquid that is in contact with the copper top end. Then a vapor film is formed, leading to a large thermal gradient inside it. This happen because helium vapor has a poor heat conductivity and as there is no possibility for convection (lower vapor density is in contact with the heated plate located at the top of the cell). Thus, the amount of liquid to evaporate is small, leading to the short plateau. Obviously, $T_{bottom}$ remains constant because there is still a lot of liquid inside the cell.

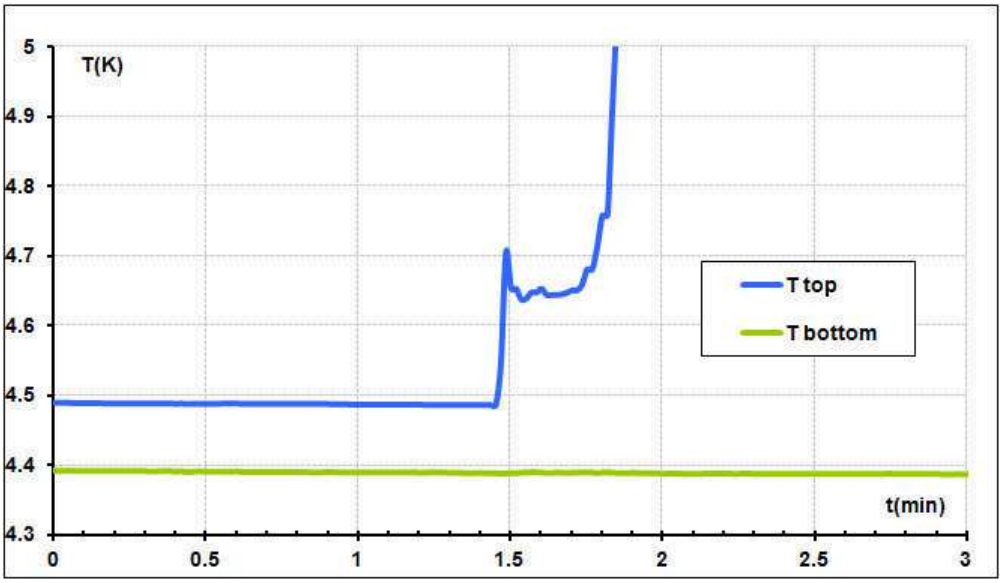


**Figure 4.25: Evolution of the top and bottom temperatures with 5 mW applied on the top of the cell - cell without ceramic.**

#### 4.6.1.2 Heating the top of the cell with ceramic

With ceramic inside the cell, the top of the cell was heated. The results of this test are presented in this section.

A test where heat is applied on the top of the cell with ceramic was made at 4.65 K (pressure of 1.48 bar imposed as in the previous case). The Figure 4.26 shows the results obtained with 5 mW, blue and green lines are $T_{top}$ and $T_{bottom}$, respectively.

After the whole cell was completely filled at 1.2 K, the bottom of the cell was heated up until the whole cell reached a temperature of about 4.55 K. After the temperature of the whole cell was stabilized, we could begin the experiment. During the experiment, we wanted to quantify the quantity of liquid that can be pumped to the top of the cell thanks to the ceramic

and be evaporated at saturation temperature. To have a precise measurement it is required that most of the applied heat is used to evaporate the liquid. So, it was necessary to heat the whole cell close to saturation temperature. Otherwise, a thermal gradient will appear between the top and the bottom of the cell and one part of the applied load which is difficult to determine will be used to heat up the liquid located in the bottom to the saturation temperature. It is also necessary to limit the heat leak towards the cryostat and so the heat switch was in OFF position.

At 1.5 min, a heat power of 5 mW (same as previously) is applied on the top of the cell. The $T_{top}$ increases up to the saturation temperature and then remains constant during 2.6 min. The existence of a plateau at saturation temperature demonstrates that the ceramic allows the liquid to be pumped when the top of the cell is heated up. The liquid that is evaporated at the top of the cell is replaced by another liquid coming from a lower part of the cell.

The end of the plateau is defined by a rapid increase of $T_{top}$, due to the fact that there is no liquid anymore in contact with the top of the cell. In other words, it is impossible to pump more liquid. However, $T_{bottom}$ remains constant which indicates that there is still liquid in the bottom of the cell. If there wasn't any liquid in the bottom of the cell a few seconds would be enough to heat the copper of the bottom from 4.55 K to 5 K. The time constant RC of the copper end linked by the stainless tube is approximately 5 seconds (R =19870.8 K/W ; C = 0.25mJ/K ).

Using the plateau duration, it is possible to calculate the accessible energy which is equal to 0.78 J (156 s with 5 mW power).

The error associated to the heating of the subcooled liquid (4.55 K) up to the saturation temperature (4.65 K) before evaporation could occur will be discussed later.

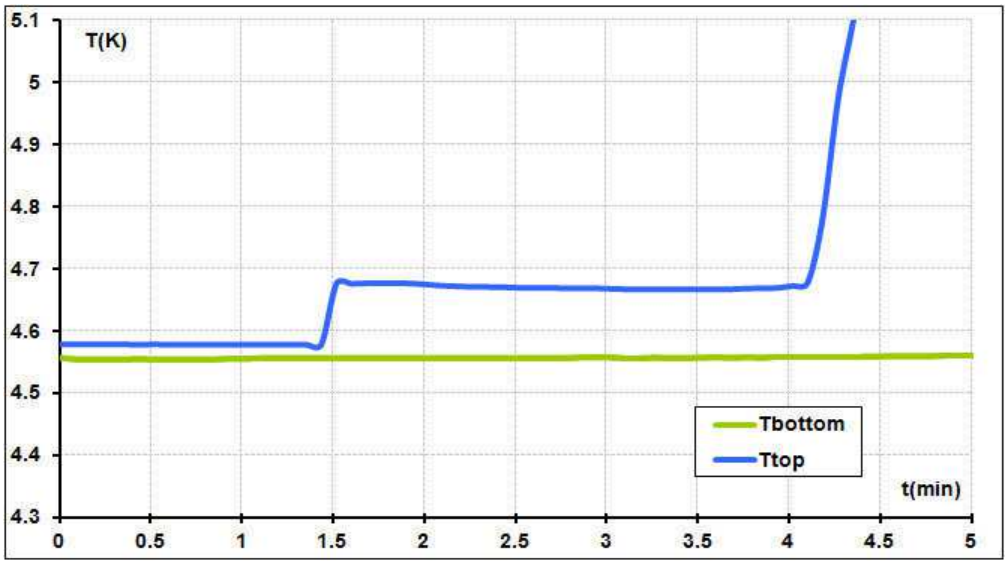


**Figure 4.26: Evolution of the top and bottom temperatures with 5 mW applied on the top of the cell with ceramic, for $T_{sat}$ = 4.65 K.**

#### 4.6.1.3 Heating the top of the cell with ceramic - effect of the load applied at a given temperature

Different loads have been experimented on the top of the cell filled with a ceramic at the same saturation temperature of 4.65 K. In Figure 4.27 accessible energy is plotted as a function of the applied load (green circle). The accessible energy is well lower than the theoretical energy value (calculated using only the void volume of the cell, excluding ceramic). This was expected as the height of the cell (14.3 mm) was chosen in order to be larger than the capillary height for this temperature (≈ 4 mm). Another result is that the higher the applied load is, the lower the accessible energy is. A possible hypothesis to justify this behaviour is that higher applied load leads to higher evaporation rate and so higher liquid mass flow rate through the ceramic. As a consequence the pressure losses due to the increase of the liquid mass flow rate

could not be compensated by the pumping effect due to surface tension. A model was developed to better explain this phenomenon and will be presented in the section §4.6.2. As this model leads to a hyperbolic dependence of the accessible energy with the load applied, the experimental points were fitted with hyperbolic laws.

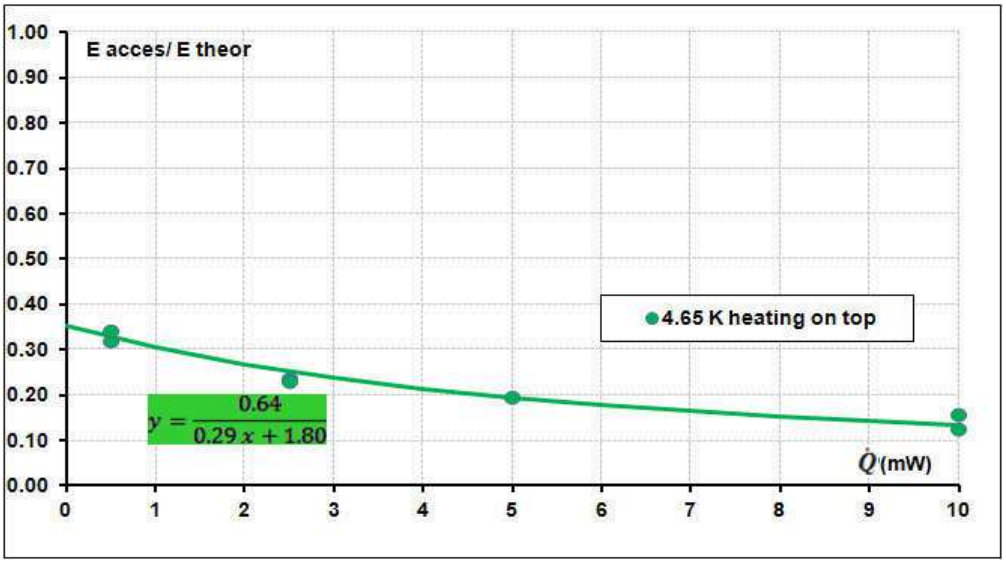


**Figure 4.27: Evolution of ratio between the accessible energy and the theoretical energy with load applied on top of the cell for 4.65 K.**

#### 4.6.1.4 Heating the top the cell with ceramic- effect of the saturation temperature

To see how the change of capillary height could affect the amount of accessible energy, we change the saturation temperature. Experiments similar to the ones carried out at 4.65 K were reproduced at 3.55 K and 2.55 K.

For testing at 3.55 K and 2.55 K, the system (the cell and the 30 liters expansion volume) was filled with 0.52 bar and 0.137 bar respectively, at room temperature leading to a pressure of 0.50 bar and 0.113 bar when liquid helium is present in the cold cell.

For lower temperature, the shape of the curve obtained when a load is applied is not always as nice as the one presented in Figure 4.26. At 2.55 K, the experimental temperature plateau shows a temperature drift (see Figure 4.28) due to the finite expansion volume and due to the large $dT_{sat}/dP$ for this temperature than for the higher ones. In addition, a short peak temperature above the setting saturation temperature is observed. We think that this peak temperature is due to an increase of the saturated pressure and can be explained by an extra pressure drop in the capillary connecting the cold cell to the expansion volume. Once again, due to the large $dT_{sat}/dP$ at this temperature, the saturation temperature is very sensitive to small pressure variation. What could explain this extra pressure drop? When we start the experiment, i.e. putting some heat load at the top cell, there is probably still some liquid in the exhaust capillary although the capillary was heated up at some distance of the cell to avoid storage of liquid helium in the capillary. There could be also some liquid expulsed from the cell when the cell is heated up to the saturation temperature due to helium dilatation. This liquid in the exhaust capillary (small diameter: 0.5 mm) could act as a plug and generate an extra pressure drop. This liquid helium is evaporated when it reaches “hot” section of the connecting tube given an extra mass flow rate that can also explain an extra pressure drop. To analyse the experimental data, when a peak power has been seen, the time defining the beginning of the plateau has been set to the first time the temperature reaches the plateau. This is represented by a red point in the Figure 4.28.

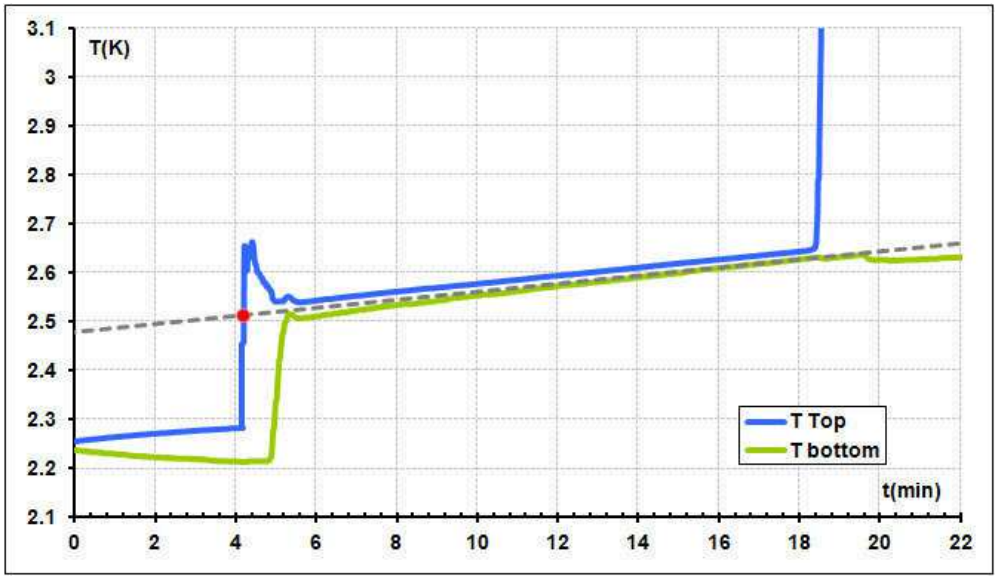


**Figure 4.28: Evolution of the top and bottom temperatures with 5 mW applied on the top of the cell with ceramic, for $T_{sat}$ = 2.55 K. The red point represents the time chosen to estimate the accessible energy.**

In Figure 4.29 the accessible energies are shown as a function of the applied load for each temperature (4.65 K green line, 3.55 K blue line, and 2.55 K brown line) when heat is applied on the cell top.

The accessible energy increases when the temperature decreases. This is explained by the fact that the capillary height increases when the temperature decreases (Figure 1.6). A similar tendency to the one observed at 4.65 K temperature level was also observed for the colder temperatures, i.e. the accessible energy decreases when the applied load increases. In order to obtain the maximum accessible energy, it is necessary to heat the cell more slowly, i.e at a low evaporation rate enabling more liquid to reach the cell top.

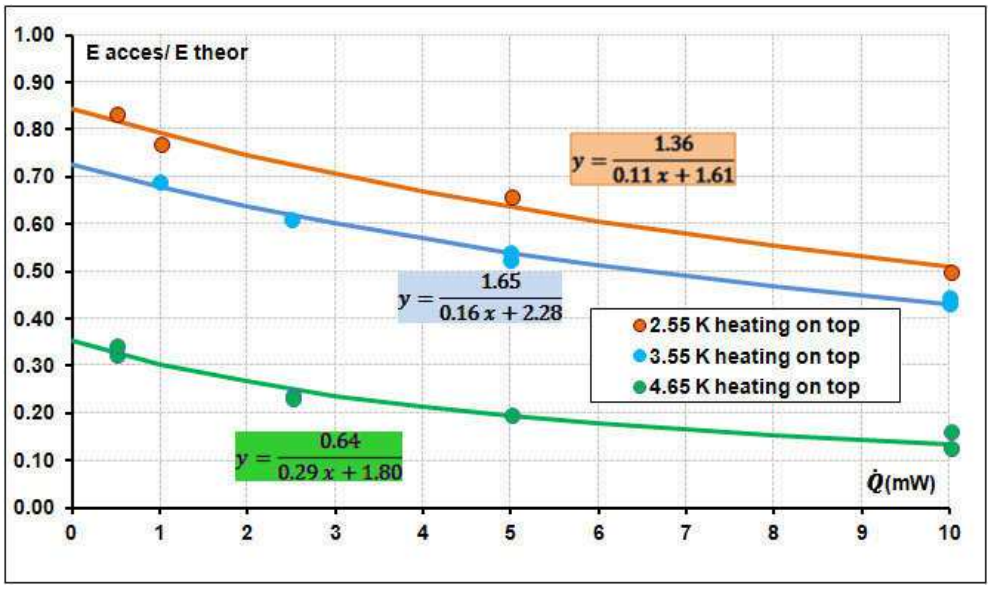


**Figure 4.29: Evolution of ratio between the accessible energy and the theoretical energy with load applied on top of the cell for three different temperatures (4.65 K. 3.55 K and 2.55 K).**

To better understand why the accessible energy becomes lower as the applied heat load is increasing, an additional experiment was performed (Figure 4.30). First, we applied 10 mW in the top of the cell and when $T_{top}$ increases rapidly, we stopped the applied load. The $T_{top}$ drops to $T_{sat}$. Then, we applied 2.5 mW and $T_{top}$ remained constant during approximately 1 min. This

result shows that there is still liquid inside the cell that could reach the top, but this should be done with a smaller mass flow rate. The liquid´s capability to reach the cell top depends on the capillary effect, the gravity effect and the pressure drop inside the ceramic which depends of the mass flow rate. The pressure drop that prevents the liquid to reach the cell top depends of the mass flow rate (proportional to the applied heat load) and the length on which the liquid has to be pumped. The experiment shows that even if it is not possible to pump more liquid with 10 mW, the reduction of the applied heat load allows pumping liquid from a lower level in the cell. A model will be presented in the section §4.6.2 to explain this phenomena.

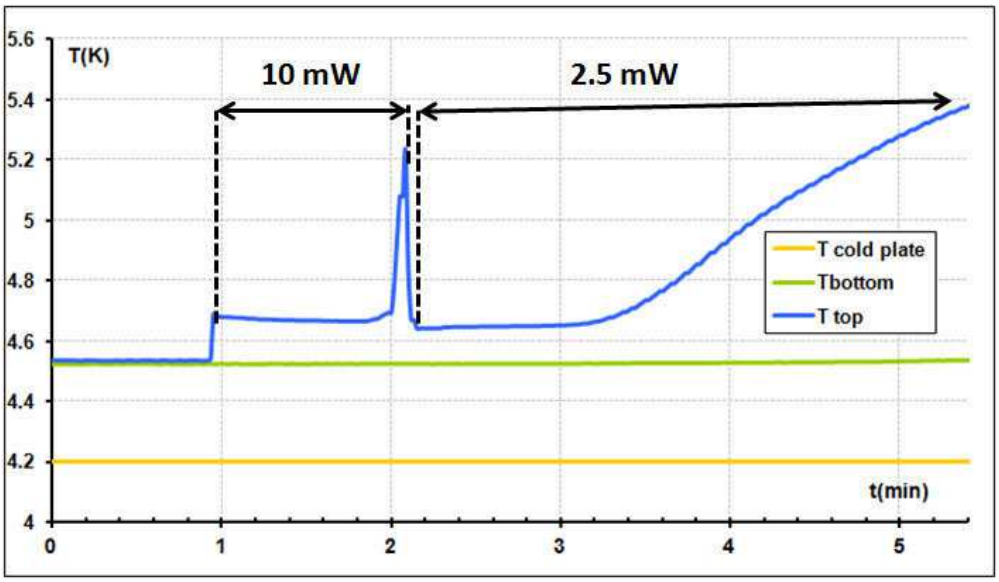


**Figure 4.30: Evolution of top and bottom temperatures when 10 mW is applied on the top between 0.95 min and 2 min. At 2 min the heating is stopped and at 2.3 min, 2.5 mW is applied on the cell top.**

#### 4.6.1.5 Discussion about heating on top of the cell

During the heating of the cell, there is evaporation of liquid and so the quantity of liquid and the level of liquid inside the cell decrease. The volume of liquid that is evaporated is replaced by helium gas. We can imagine that there is a zone at the bottom of the cell that is occupied only by liquid, like a "lake" we can call it the "liquid zone". This assumption is reinforced by the fact that liquid at the bottom remains subcooled, which means that there is only pure liquid at the bottom. Above this zone there is a zone where there is vapor but also some liquid: filament or column that brings the liquid from the top of liquid zone to the top of the cell. We can call this zone the "diphasic zone". This diphasic zone grows from the top to the bottom when the power is applied. A scheme is present in Figure 4.31. The vapor inside the diphasic zone corresponds to the volume of liquid that has been evaporated.

For a given liquid/ceramic void ratio ($\alpha$) in the ceramic above the "lake" and when no more liquid reaches the cell top, the "dynamic capillary height" can be determined: it is the difference between the internal height of the cell and the height of the lake. This is equivalent to the height of the diphasic zone. The parameter $\alpha$ represented the part of liquid helium that is stored inside the capillary path connecting the liquid bath interface to the top of the cell.

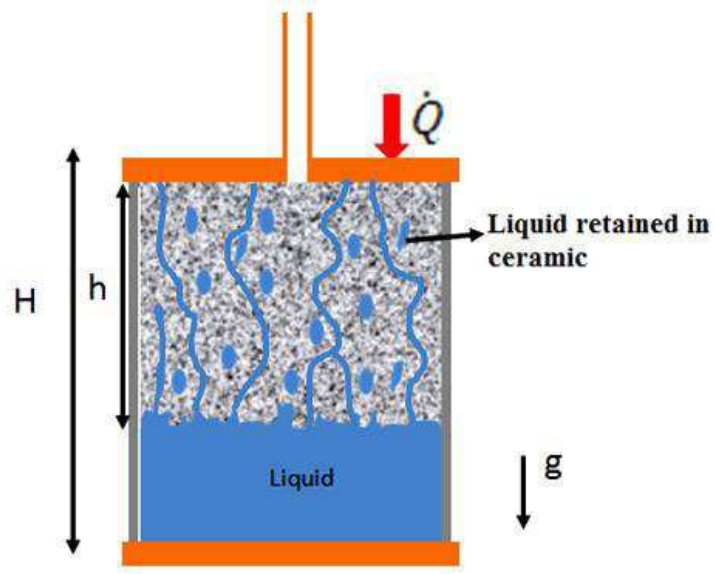


**Figure 4.31: Scheme of the two zones in the cell when the heating power was applied on the top of the cell. In the bottom there is only liquid. In the diphasic zone there is vapor and a small quantity of liquid due to capillary effect.**

When no load is applied, the dynamic capillary height should be equal to the capillary height and can be calculated from the amount of liquid evaporated at constant temperature in the saturation phase. The capillary height is equal to the height of the diphasic zone. To calculate the volume of the diphasic zone, not only the volume of evaporated vapor should be taken into account but also the quantity of liquid that is above the lake(α) and the porosity (ε) of the cell. The volume of this diphasic zone is equal to the sum of the volume of the evaporated liquid, the volume of the liquid present in this diphasic zone and the volume of the ceramic inside this zone.

The volume of evaporated liquid needed to estimate the capillary height can be determined using the accessible energy at the y-intercept point (ordinate of the fit found with applied load reported in Figure 4.29). At this position, as no load is applied, only the capillary effect generates the rise of the liquid. The energy is equal to

$$E_{origin} = \rho_L(T_{sat}) A_T \, h \, L(T_{sat}) \, \varepsilon \, (1-\alpha) \tag{4.9}$$

The capillary height can be calculated using the Jurin's Law (express in equation 1.1 and recall here equation (4.10)):

$$h = \frac{2\sigma}{(\rho_L - \rho_V) g \, r} \tag{4.10}$$

So the energy is equal to:

$$\Leftrightarrow E_{origin} = \frac{2\rho_L(T_{sat}) \, A_T \, \sigma \, L(T_{sat}) \, \varepsilon}{(\rho_L - \rho_V) \, g} \, \frac{(1-\alpha)}{r} \tag{4.11}$$

For a given temperature:

$$E_{origin} = constant \times \frac{(1-\alpha)}{r} \tag{4.12}$$

We can see that the energy is proportional to $\frac{(1-\alpha)}{r}$. There is an infinite numbers of couple (1-*α)* and r that gives the same energy.

The choice of alpha, which is an unknown value, will determine the radius of the pore and the capillary height. For example, if the value of alpha is set at 10%, we can plotted the capillary height using the accessible energy at the origin in the equation (4.9), and then use the equation (4.10) do determine the best pore radius to minimize the gap between the experimental data and the fit. This minimization is done by minimizing the sum of $\left(h_{Jurin} - h_{exp}\right)^2$. The minimization gives a radius of 25 µm (α = 10%).

To analyse the sensibility of radius pore, two curves with the same $\alpha$ and different radius pore are traced.

As can be seen in Figure 4.32 the capillary height calculated from Jurin's law (dashed line) is lower than the calculation from the accessible energy at 4.65 K and 3.55 K but higher for 2.55 K. This point will be discussed in more detail later in this chapter.

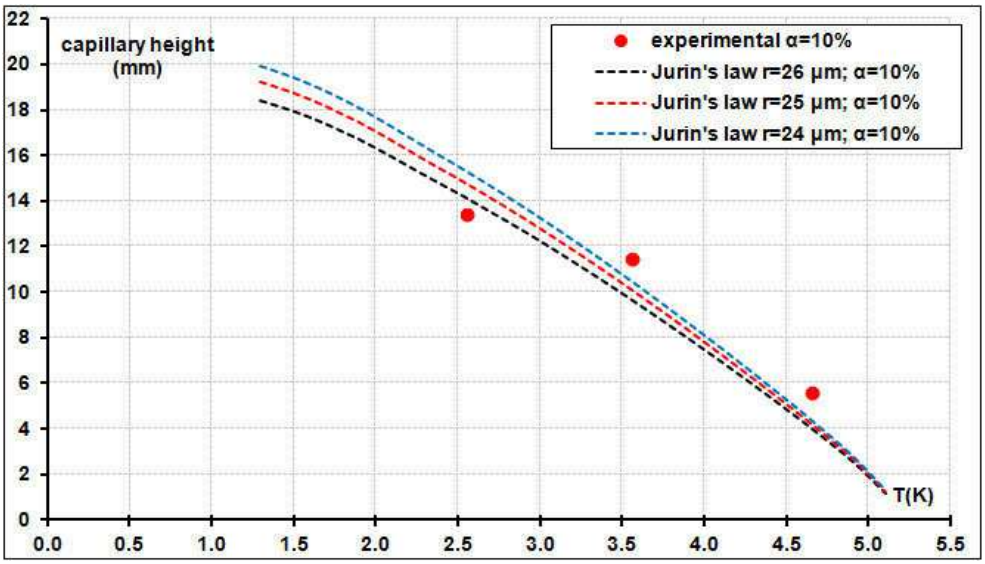


**Figure 4.32: The capillary heights calculated from the experimental results (ordinate of the fit found with applied load) (round point). In dash lines the capillary heights calculated for the three different radius pore.**

It is possible to see in Figure 4.33 the evolution of the pore radius and the capillary heights obtained at different temperatures tested as a function $\alpha$.

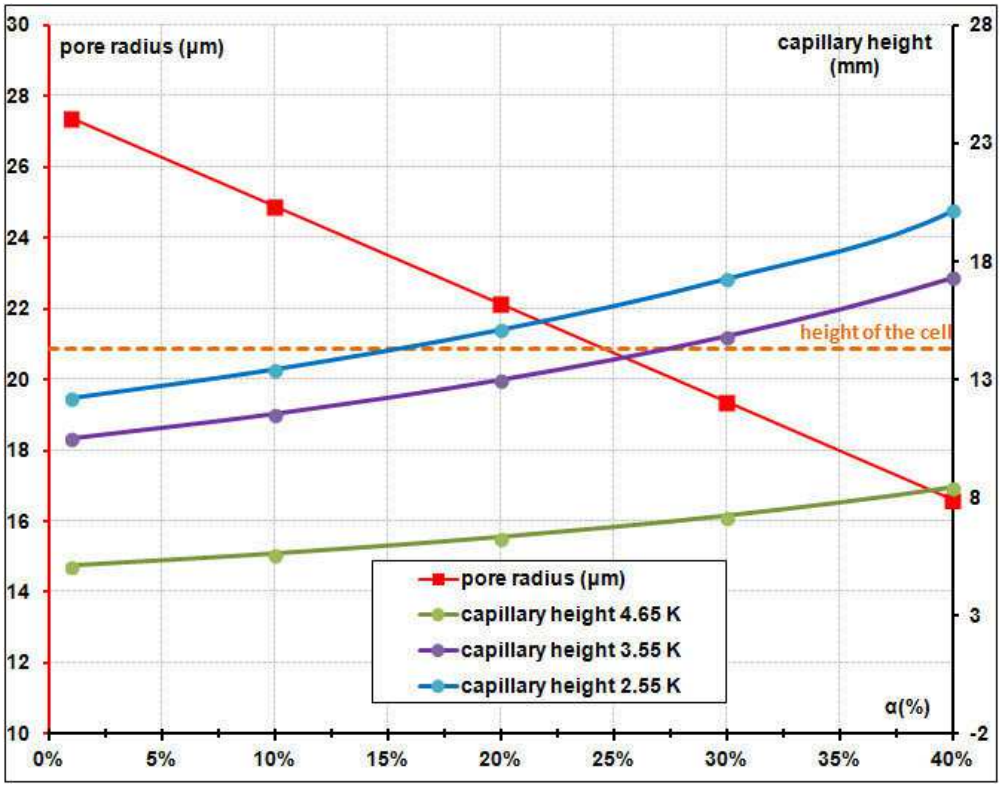


**Figure 4.33: The evolution of the pore radius and the capillary heights for the different temperatures tested for different value of *α*.**

For the same quantity of liquid evaporated, the higher the quantity of liquid retained in the diphasic zone of the ceramic ($\alpha$) is, the smaller the liquid zone is. And therefore the lower the liquid-vapor interface is, leading to a higher capillary height. To increase capillarity effect, the pore radius should be smaller. So the higher $\alpha$ is, the higher the capillary height and smaller the pore radius are.

It can be seen in Figure 4.33 that experimental data gives 2 different capillary heights for the 2.55 K and 3.55 K temperatures, so we can affirm that there is not limitation of the capillary height for the case 3.55 K and that the capillary height should be lower than the cell height. Using the curve obtained for this temperature, it can be deduced that the $\alpha$ should be lower than 27 % and the pore radius should be higher than 20 microns. The $\alpha$ could not be equal to 0% because the ceramic always retained approximately 10% of liquid in some experiments at the end of plateau of the heating phase (these results are presented in the section dedicated to heating by the bottom). The value assumed for the rate of liquid in diphasic zone is based on quantity of liquid that cannot be evaporated at saturation temperature in the most favourable conditions. This is why, in the calculation that follows $\alpha$ is set at 10%. In addition, $\alpha$ is assumed to be constant with the temperature.

In the Figure 4.34, the derivatives of the ratio between the accessible energy and the theoretical energy fit versus the heating power applied presented in Figure 4.29 are plotted as function of the temperature. For each temperature the derivatives slopes were calculated in three positions: at 0 mW, at 5 mW and at 10 mW. The curves of slopes at 5 mW and 10 mW have the same tendency: when the temperature decreases, the accessible energy becomes more dependent of the applied load. The curves of slopes at 0 mW has a shape different than the others curves. We will see that the model presented in the next section could predict its behaviour.

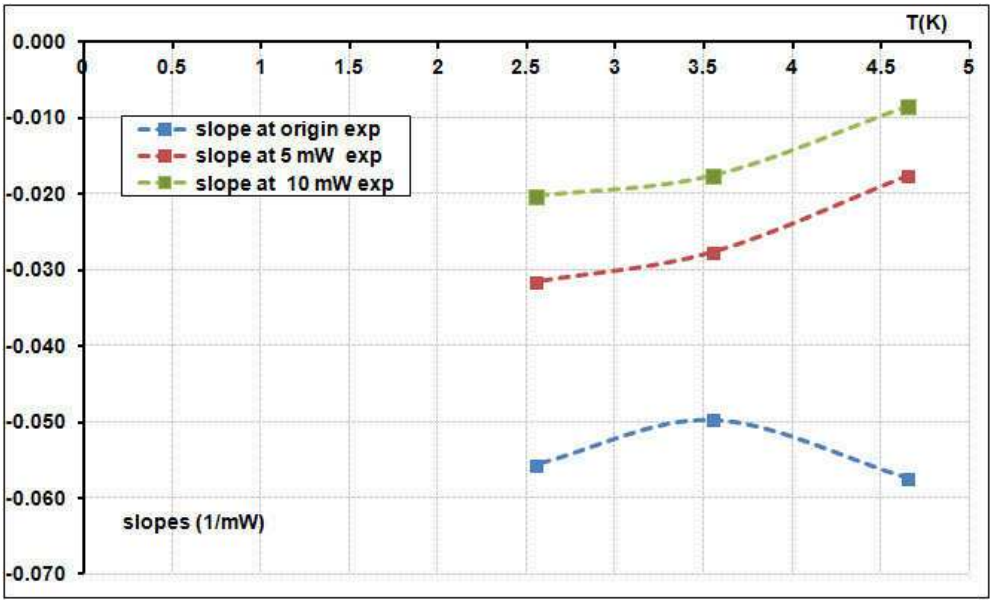


**Figure 4.34: Evolution of the slopes of the ration between the accessible energy and the theoretical energy fit versus the heating power applied reported in Figure 4.29 as a function of temperature and for different applied loads (cell with ceramic).**

To sum up what we know until that point, when the applied load is null, the accessible energy (equation (4.9)) is defined by the fluid properties, the cross section of the cell and the ratio between (1-*α)* and pore radius. The only unknown parameter that is the ratio (1-*α)* by radius pore was set in order to minimize the difference between the experimental accessible energy and the theoretical one over the 3 temperatures tested. The pore radius and the quantity of liquid above the lake are link and could take an infinite number of values. Due to some results obtained in the experiences that will be shown in the section dedicated to the heating of the cell by its bottom, a realistic value for alpha seems to be around 10 %. With this value, the pore radius is equal to 25 µm and the capillary height is known for each temperature. So, the value of the y intercept at x=0 of all experimental curves in Figure 4.29 can be determined. We will now try to predict the shape of these curves when load is applied.

## Error associate to initial subcooling

At the beginning of the experiment the cell is thermalized at a temperature lower than the saturation temperature. Then, when the heat load is applied on the top of the cell, the top reached the saturation temperature and the bottom remains at a temperature lower than the saturation temperature. This is due to the fact that the characteristic time of the cell (14.3 mm) is large (76 min at 4.55 K) and so stratification occurs in the cell. Before evaporation, the subcooled liquid has to be warm up to the saturated pressure which has a cost in term of energy. Another error is coming from the fact that the subcooled liquid has a higher density than the liquid at saturated temperature. It means that the void volume at the end of the vaporization was filled with subcooled liquid at the beginning heating phase and so more liquid was stored than if this liquid was already at the saturated temperature. The experience performed at 4.65 K (Figure 4.26) will be used to illustrate the error.

In the Pressure- Enthalpy diagram it is possible to see the evolution of enthalpy of the experience at 4.65 K performed at constant pressure. The energy necessary to go from point A to B is equal to:

$$E = m\,(H_{en_B} - H_{en_A}) \qquad (4.13)$$

Where m and $H_{enA}$ are the mass of liquid and the enthalpy at point A and $H_{enB}$ is the enthalpy at point B. This energy could be compared with the total energy put inside the cell, which is the difference of enthalpies from A to C.

$$error\_enthalpy = \frac{(H_{en_C} - H_{en_B})}{(H_{en_C} - H_{en_A})} \tag{4.14}$$

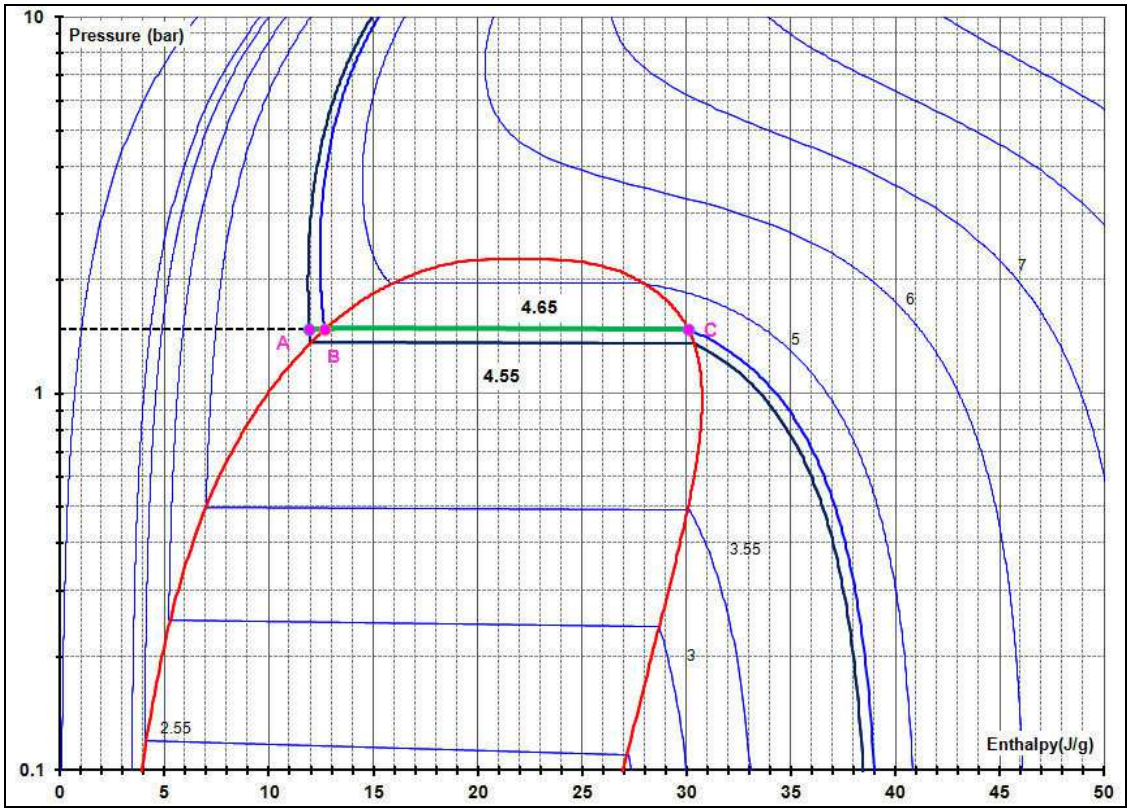


**Figure 4.35: The Pressure-Enthalpy diagram for helium. The green line represents the 4.65 K experience.**

To estimate the error due to density, we should compare the density of the subcooled liquid ($\rho_A$) and the density at liquid at saturated temperature ($\rho_B$) (see Figure 4.36). The error made by using the density of the saturated liquid is:

$$error\_density = \frac{\rho_B}{\rho_A} \tag{4.15}$$

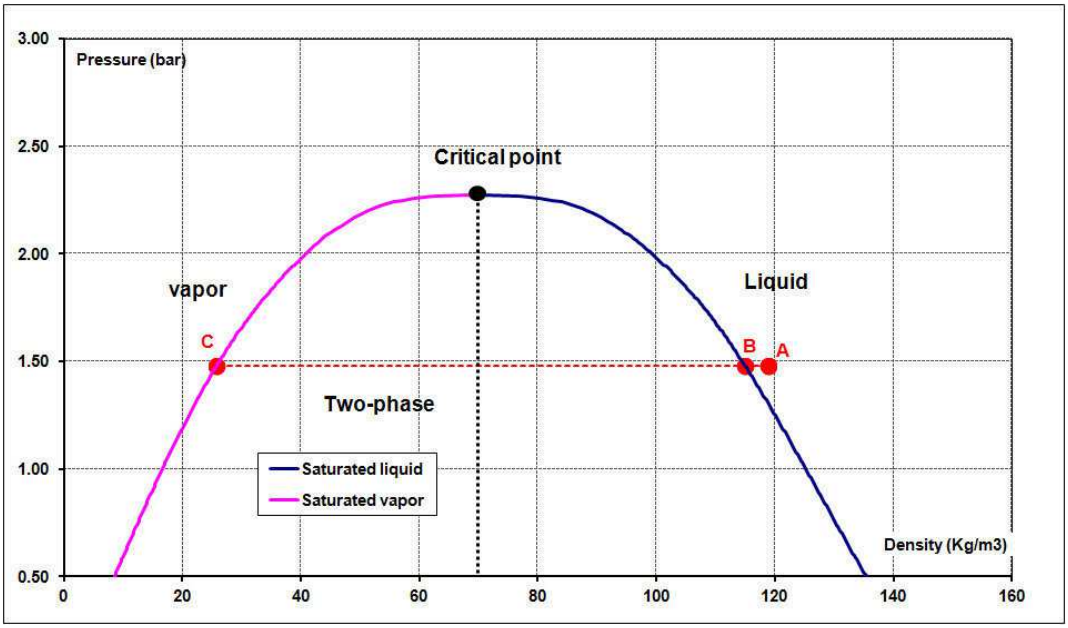


**Figure 4.36: The Pressure-Density diagram for helium. The red line represents the 4.65 K experience.**

The total error made by neglecting the path between A and B is:

$$error = \frac{(H_{en_C} - H_{en_B})}{(H_{en_C} - H_{en_A})} \times \frac{\rho_B}{\rho_A} \tag{4.16}$$

In Figure 4.37, it is possible to see the errors obtained for different saturation temperature if we consider an initial subcooling of 0.1 K which is more a less the level of subcooling we have chosen in our experiment.

It can be seen that the errors increase when the saturated temperature increase. For our experiment, the maximum error is around 7 % (saturated temperature of 4.65 K). No systematic correction of this error has been made in the results presented in this manuscript.

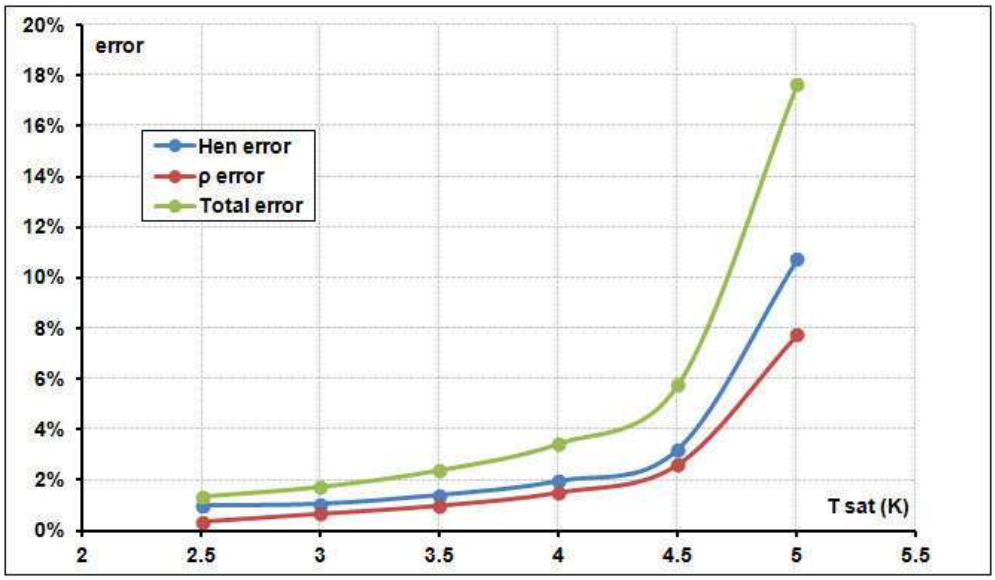


**Figure 4.37: The error for different saturation temperatures for an initial subcooling of 0.1 K.**

### 4.6.2 Model when the cell is heating on the top end

A model was developed in order to describe the behaviour of the cell when it is heated on the top. This model consists of a one-dimensional approximation of force balanced on the top of the porous media in the vertical direction.

In the beginning, the porous media inside the cell is full of liquid. When the copper tip is heated, the load is transferred to the liquid in the upper part of the cell.

The heating causes the evaporation of the liquid in the end wall and the appearance of meniscus in the porous media. This generates a capillary force that leads to the circulation of the fluid (rising of liquid and delivery of the vapor). However, there are three forces that act against the flow of the liquid, the gravity forces, and the pressure drop of liquid and vapor.

During the transient drain of the cell, it is possible to distinguish two areas inside the cell. The inferior area, where the liquid occupies the totality of the pores and where there is no vapor. The upper area, the two phase area, where liquid is climbing and where the vapor is closed to a stationary state. Most of the vapor coming from liquid evaporation is released to the warm expansion volume and only a small fraction is used to compensate the decrease for the level of the "lake". In our model, we assume that the liquid flows vertically in parallel pipes having the same radius without tortuosity.

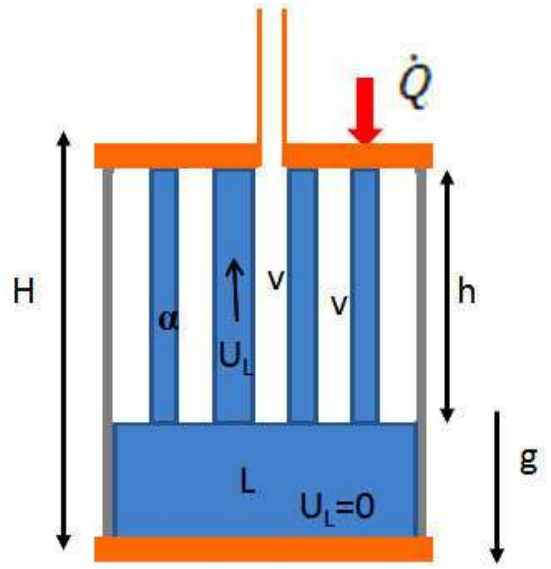


**Figure 4.38: Scheme of the cell when the heating power is applied on the top of the cell. The $U_L$ is the filtration velocity, v is the vapor, α is the rate of liquid in the two phase zone.**

When the capillary force balances the pressure drop induced by the flow and the gravity forces, in contact with the copper no evaporation takes place. So, if we express the force as a balance in pressure, we can summarize:

$$\Delta P_{cap} = \Delta P_g + \Delta P_{FL} + \Delta P_{FV} \quad (4.17)$$

Where $\Delta P_{cap}$ is the capillary pressure, $\Delta P_g$ is the gravitational force and where $\Delta P_{FL}$ and $\Delta P_{FV}$ are the pressure drop induced respectively by the liquid flow and the vapor flow.

The capillary pressure is given by

$$\Delta P_{cap} = \frac{2\sigma}{r} \quad (4.18)$$

where $\sigma$ is the surface tension.

The gravitational force is given by:

$$\Delta P_g = (\rho_L - \rho_V) g\, h \quad (4.19)$$

where h the capillary height.

The pressure drop of vapor is neglected in this model because most of the vapor produce by the evaporation is going out of the cell by the exit located at the top of cell to reach the warm expansion volume. Only a small fraction will flow against the liquid that climb into the ceramic and will counter the capillary effect.

When the liquid flows through a porous medium and the flow is laminar, the pressure drop induced by the liquid flow can be determined by Darcy's law as:

$$\Delta P_{FL} = \frac{\mu_L\, U_L\, h}{k} \quad (4.20)$$

Where $\mu_L$ is the dynamic viscosity, $U_L$ the filtration velocity

The filtration velocity also called superficial velocity or Darcy velocity is a fictitious velocity since it assumes that flow occurs across the entire cross-section of the porous media. Flow actually takes place only through pores and it is called the interstitial velocity. The interstitial velocity ($u_L$) is related to the superficial velocity ($U_L$) by the porosity $\varepsilon$:

$$U_L = \varepsilon u_L = \varepsilon \left( \frac{D_{vol-L}}{A_L} \right) \quad (4.21)$$

Where $D_{vol-L}$ is the volumetric flow rate and $A_L$ is the fraction occupied by the liquid and are defined as:

$$D_{vol-L} = \frac{\dot{Q}}{L\,\rho_L} \qquad A_L = \alpha\varepsilon A_T \tag{4.22}$$

Where $\alpha$ the rate of presence of liquid and $A_T$ the total section area.

Thus, equations (4.21) and (4.22) used in the equation (4.20) give:

$$\Delta P_{FL} = \frac{\mu_L\ h\,\dot{Q}}{k\,L\,\rho_L \alpha A_T} \tag{4.23}$$

By substituting (4.18), (4.19) and (4.23) into (4.17) and rearranging the yield, it is possible to calculate the position of the liquid "lake" interface when the liquid meniscus disappears at the top of porous media, i.e, when the pumping action ends.

$$h = \frac{\frac{2\sigma}{r}}{\left[\frac{\mu_L\,\dot{Q}}{k\,L\,\rho_L \alpha A_T} + (\rho_L - \rho_V)g\right]} \tag{4.24}$$

In this situation, the position of the liquid interface is equal to the capillary height. From the position of the liquid-vapor interface, h, we can estimate the volume of evaporated liquid, using expression (4.9), which is proportional to the accessible energy found during the experiments.

By substituting (4.9) into the (4.24) the accessible energy can be defined as:

$$\frac{E_{acces}}{E_{theor}} = \frac{2\sigma\frac{(\mathbf{1}-\boldsymbol{\alpha})}{\boldsymbol{r}}}{\left[\frac{1}{\boldsymbol{\alpha k}}\frac{\mu_L\,\dot{Q}}{L\,\rho_L A_T} + (\rho_L - \rho_V)g\right]H} \tag{4.25}$$

The equation (4.25) allows calculating the accessible energy as a function of the applied load. The results of the model should fit with the experimental measurements presented in Figure 4.29.

In the equation (4.25) there are three parameters $\alpha$, k and r for which it is difficult to define a value because they depend on the structure of ceramic and of the behaviour of the liquid inside the ceramic that is not well known. The ration between the (1-$\alpha$) and the pore radius has been already discussed in the previous section and even there are an infinite numbers of couple ($\alpha$, $r_{pore}$) that gives the same accessible energy, this ratio can been determined by the energy when no load is applied ((y-intercept point of the model curve). It was decided to set the value of alpha at 10 % and by consequence fixed the value of the pore radius to 25 µm. The only free parameter is then the permeability.

The shape of the model curves versus applied heat load can be adjusted using the permeability. To find the value of permeability that minimizes the difference between the experimental points and the model results, the method of least square was used. First, for each temperature the average of the points with the same power was done, to have only one point by temperature and by applied power. The weighted average for each temperature was done. After that the minimization was done using:

$$\left[\frac{\sum(x_m - x_{exp})^2}{n\,point}\right]_{4.65K} + \left[\frac{\sum(x_m - x_{exp})^2}{n\,point}\right]_{3.55K} + \left[\frac{\sum(x_m - x_{exp})^2}{n\,point}\right]_{2.55K} \tag{4.26}$$

Where $x_m$ and $x_t$ is the ratio between the accessible energy and the theoretical energy respectively for experimental points and points calculated by the model.

The values of $k = 9.86 \times 10^{-13}\ m^2$ allows to adjust the model simulation to the experimental results. The results obtained with the model using this permeability are displayed

in Figure 4.39 (dashed line). This permeability value is closed to the values measured by CNRS ($k = 3.8 \times 10^{-12} m^2$)

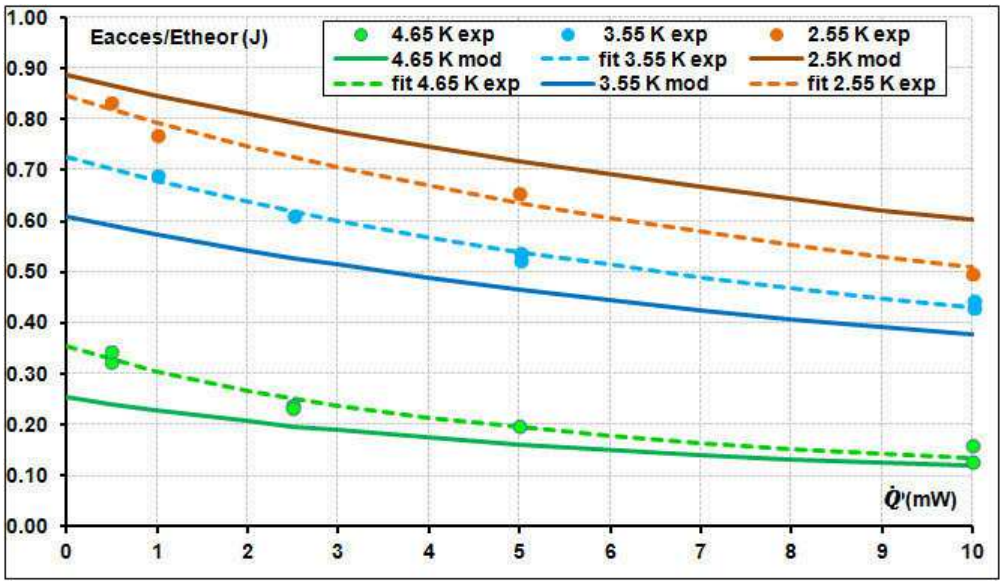


**Figure 4.39: Comparison of the ratio between the accessible energy and the theoretical energy with load applied on top of the cell for three different temperatures (4.65 K. 3.55 K and 2.55 K). The points are experimental results and the solid lines are results obtained from the model with $k = 9.86 \times 10^{-13}\ m^2$.**

The accessible energy calculated by the model at 4.65 K and 3.55 K is lower than that of the experimental results, but higher at 2.55 K. At 2.55 K with $\alpha$= 10% the capillary height calculated (13.4 mm) is very close to the height of cell (14.3 mm) If the value of $\alpha$ is 16%, the capillary height is 14.3 mm equal to the effective cell height. Therefore, depending of the real value of the alpha, the cell can be smaller than the capillary height, and so the amount of the evaporated liquid calculated by the model at 2.55 K could be greater than the total amount of the liquid available inside the cell. This could explain why the accessible energy calculated by the model at 2.55 K is greater than the experimental value.

Since at 2.55 K the capillary height is almost equal to, or maybe greater than the height cell, the experimental results at 2.55 K in Figure 4.39 and Figure 4.32 show a different behaviour in comparison with the ones at 4.65 K and 3.55 K. Since the height of the cell can be a physical limitation for the comparison between the experiments and the model at 2.55 K, the point done at this temperature has been suppressed to redo the analysis. In the Figure 4.40 it is possible to see the same analysis that the one performed for Figure 4.32 The results give for the same $\alpha$ (10 %), a higher capillary height (i.e. pore radius is smaller) because the cancelled experimental point at 2.55 K gave results smaller than expected.

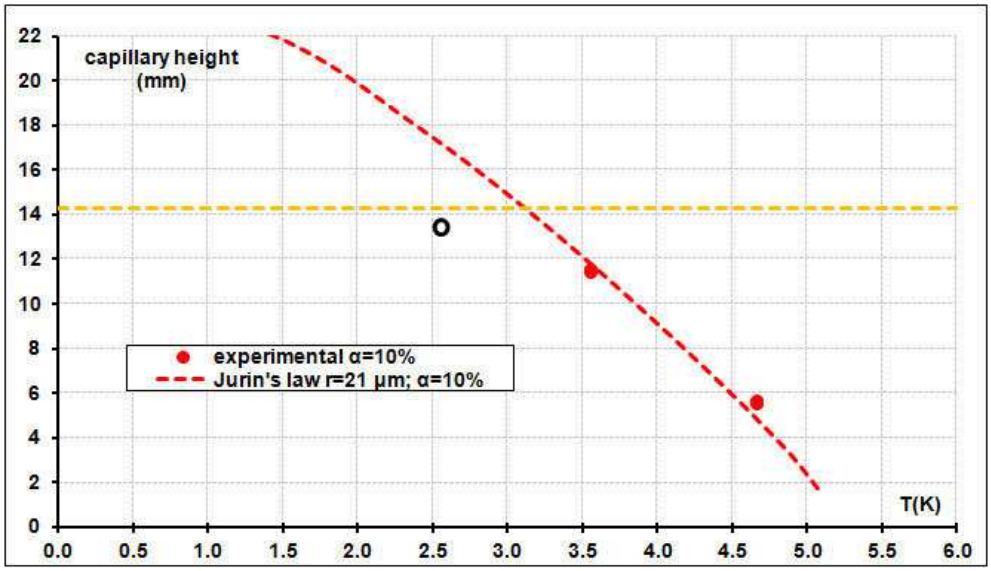


**Figure 4.40: The capillary heights calculated from the experimental results without the point at 2.55 K (ordinate of the fit found with applied load) for $\alpha$ equal to 10 %(circle point). The dashed line is the capillary height calculated for Jurin's law.**

With these new ratios (1-$\alpha$) by r, with alpha still set at 10 % it is possible to calculate the new values of permeability that allows to adjust the model curve to the experimental curve at 3.55 K and 4.65 K. In Figure 4.41 the new model curves calculated with optimum $k = 8.50 \times 10^{-13}\ m^2$are displayed .As expected, the model curves better simulate the experimental curves at 4.65 K and at 3.55 K. At 2.55 K, the model predicts that it is possible to evaporate more helium than the quantity stored in the cell. This is due to the fact that with the new pore radius (21 µm) smaller than (25 µm), the capillary height is higher than the cell's height. It should be noted that the permeability have not been strongly affected by removing the experimental results at 2.55 K, around 15% variation.

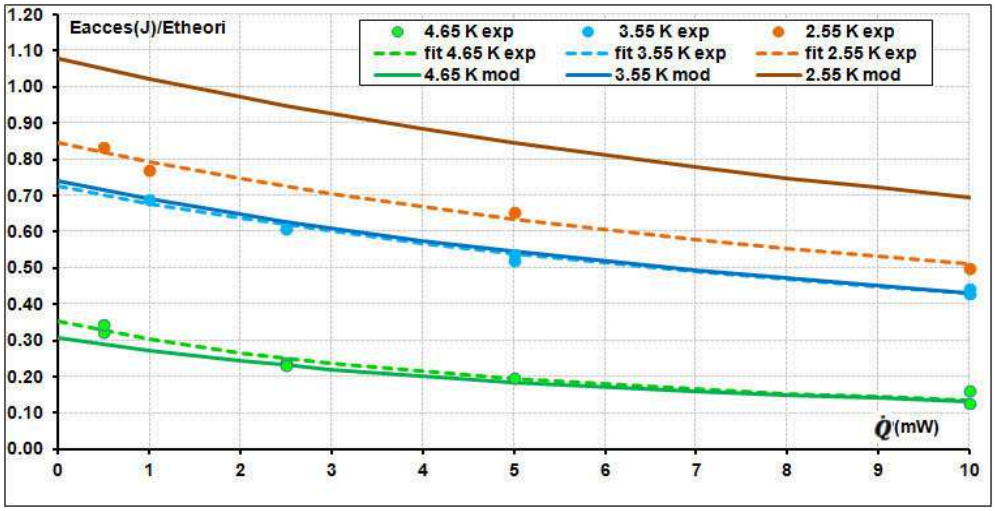


**Figure 4.41: Comparison of ratio between the accessible energy and the theoretical energy with load applied in top of the cell for three different temperatures (4.65 K, 3.55 K and 2.55 K). The points are experimental results and the solid lines are results obtained from the model with $k = 8.50 \times 10^{-13}\ m^2$.**

To see the influence of permeability, for the same radius pore and $\alpha$, two different values of permeability was traced for 3.55 K (see Figure 4.42), two times higher and two times lower $8.50 \times 10^{-13}\ m^2$ .

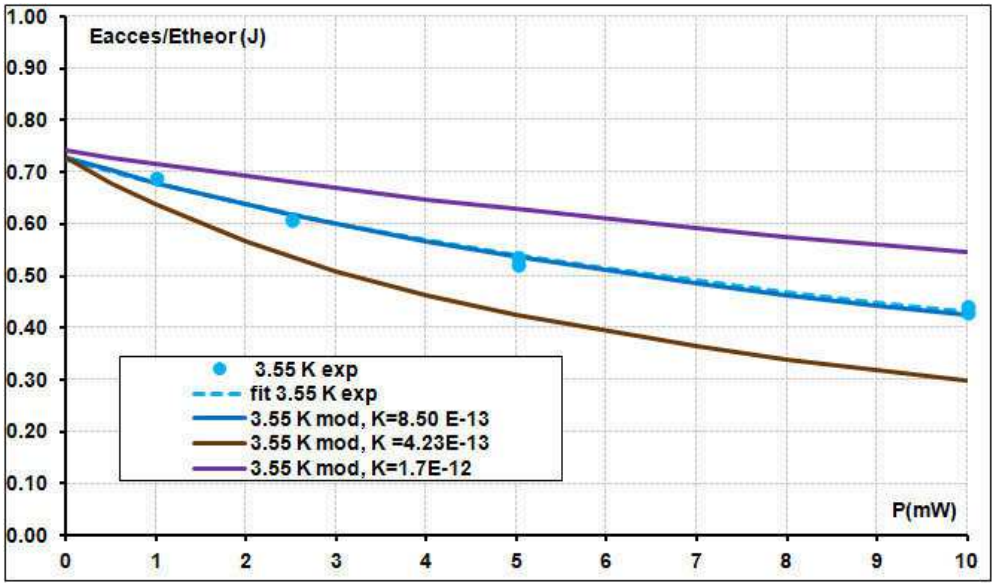


**Figure 4.42: Comparison of ratio between the accessible energy and the theoretical energy for three different permeability with load applied in top of the cell for 3.55 K. For permeability above $k = 1.2 \times 10^{-11}\ m^2$ the accessible energy is almost constant for applied loads between 1 mW and 10 mW.**

In the Figure 4.43, the evolution of $\alpha$ and of the permeability is plotted as a function of pore radius. A pore radius was chosen and as previously explained, the $\alpha$ varies linearly with pore radius $\frac{(1-\alpha)}{r} = a$ (a represent a constant). Once alpha is determined and knowing that the permeability is inversely proportional to the $\alpha$ ($k\alpha$= b) (b represent a constant), the permeability is an hyperbolic function of the pore radius $k = \frac{b}{1-a\,r}$.

Permeability changes more significantly after the pore radius is higher than 22 µm. The value of permeability measured by CNRS corresponds approximately to a $\alpha$ of 3%, lower than value estimated from experiment. The value measured by CEA is impossible to achieve with any value of $\alpha$ .

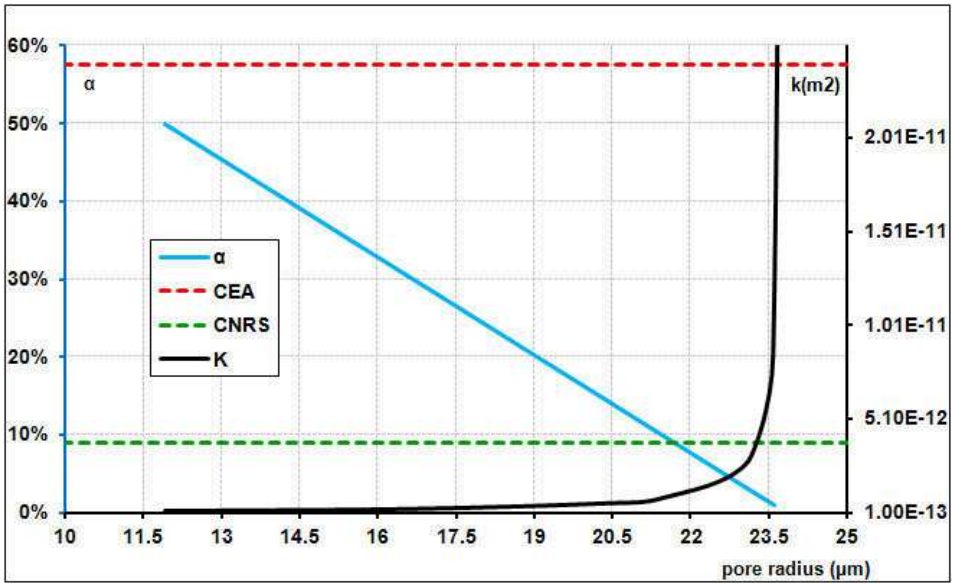


**Figure 4.43: The $\alpha$ (blue line) and permeability (black line) versus pore radius. The green and red dashed lines represent the permeability measured respectively by CNRS and CEA.**

If we compare the slopes of the curves obtained by the model from equation (with α=10% and $k = 8.50 \times 10^{-13}\ m^2$) and experimental results, (Figure 4.44) we observe that the slopes at 10 mW and 5 mW decrease with temperature. There are a good agreement between the

model curve and the experimental curve at 4.65 K and 3.55 K. For 2.55 K the slopes obtained with the experimental points are lower than the one obtained with the model because the experimental at 2.55 K are not taken into account in the model as described above. For the slope at the origin, it can be notice that the model and the experiment give none monotonous evolutions with the temperature. This is due to the fact that helium properties are not monotonous in the temperature we have explored.

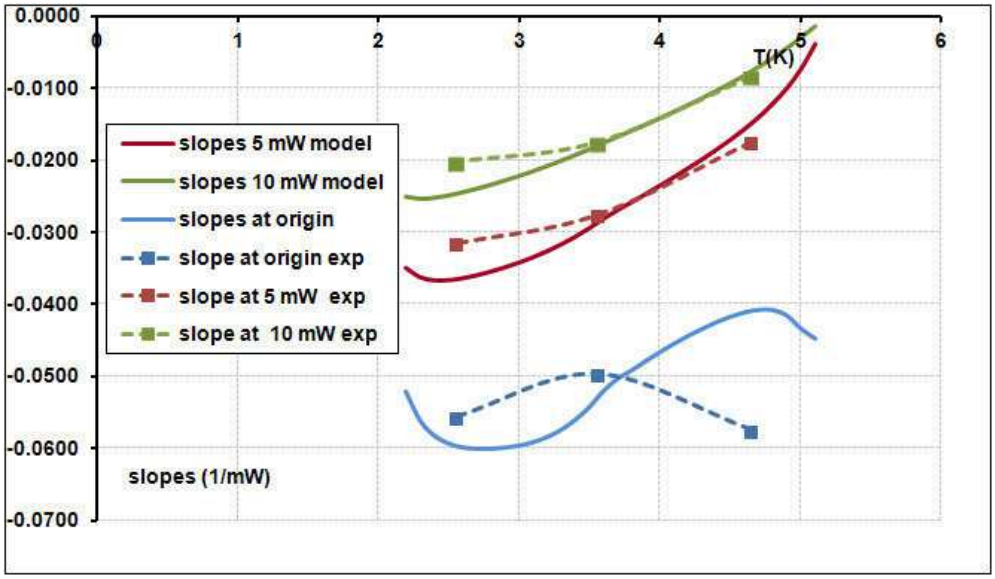


**Figure 4.44: Evolution of the slopes in three different load applied (model and experimental) as function of temperature.**

### 4.6.3 New cell with an extended height

With the aim of verifying that the height of the cell could explain the discrepancy for the points at 2.55 K, we decided to build a new cell having an effective height (30.6 mm) twice larger than the one use in the experiments describe up to now. All the other parameters of the cell have been kept constant.

Number of runs was limited due to the available time of the cryostat. The main goal here was to have a cell that remained higher than the capillary height for low temperature, so experiments at 2.65 K were obviously mandatory. Some cross checks with the smaller cell are also important and it was decided to perform them at 4.65 K and to cancel the tests at 3.55 K to respect the cryostat schedule. Some typical rough values obtained at 4.65 K are compared on the following plot. Clearly the result is a little surprising. Normally with the same ceramic one would expect to see the same plateau duration as the heating and the exhaust for the vapor are located on the top of the cell: liquid vaporized should not be influenced by the cell depth. Looking in more detail is needed to confirm if this difference is significant.

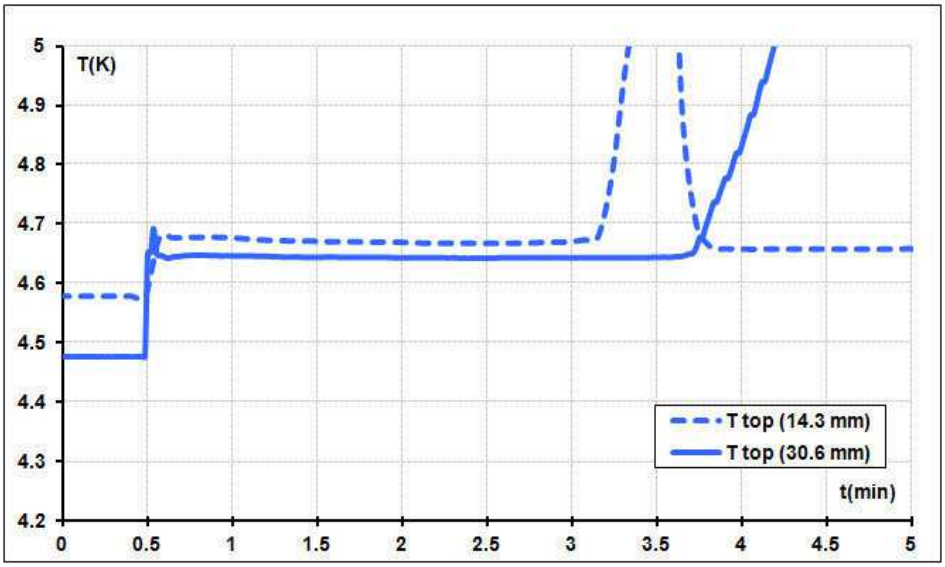


**Figure 4.45: Evolution of the top and bottom temperatures with 5 mW applied on the top of the cell of 30.6 mm and 14.3 mm with ceramic.**

The plateau last 23 % more with the highest cell, but experimental conditions were also slightly different: subcooling was higher and the plateau temperature was slightly lower. Using equation (4.16) it is possible to calculate the correction due to the subcooling: plateau duration would be reduced by a factor of 0.93 for the 14.3 mm cell and by of factor of 0.88 for the 30.6 mm cell if no subcooling was applied. Thus 4.5 % must be subtracted to the previous 23 %. A higher temperature level for the plateau as two consequences: it reduces the latent heat and it reduces the capillary height. Change from 4.67 to 4.645 K increases the latent heat by 1.6 %. Concerning the capillary effect, a simple linear extrapolation of the results obtained at 3.55 K and 4.65 K (see Figure 4.29) gives an increase of 4% of the plateau duration in the case of the 30.6 mm height cell. Finally some 13 % of difference (23% - 4.5% - 1.6% - 4%) between the two cells remains unexplained. Part of this difference can be due to the ceramic samples which may not have exactly same polydisperse repartition of "pores". Anyway, same procedure of analysis was employed for the 30.6 mm ceramic for data obtained at 2.55 K and 4.65 K. The results obtained (see Figure 4.46) are consistent with the results obtained with a cell of 14.3 mm. The accessible energy decreased as the applied power increased and the lower the temperature is, the higher the energy accessible is.

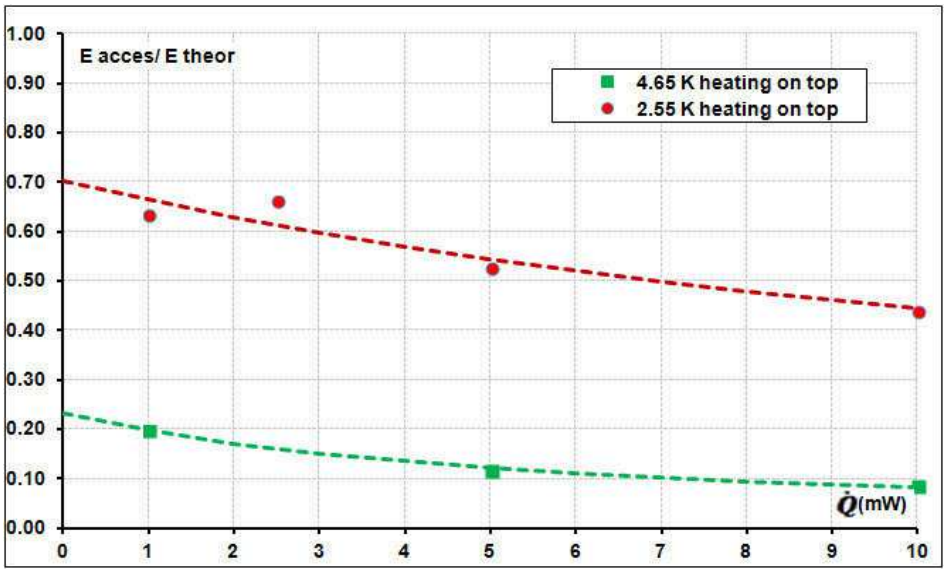


**Figure 4.46: Comparison of ratio between the accessible energy and the theoretical energy with load applied on top of the cell of 30.6 mm for two different temperatures (4.65 K. and 2.55 K).**

The capillary height estimated from the accessible energy at 0 mW (y-intercept point) with α equal to 10 % gives the black point represented in Figure 4.47. These points correspond to a capillary height for a pore radius of 15 µm and shown that with the same type of ceramic (not the same sample) it is possible to climb a height well higher than the height of the first cell. For first cell (14.3 mm height), when the value of pore radius is calculated without the point at 2.55 K a pore value of 21 µm was found. The value of pore radius in the new cell (15 µm) is smaller than the one measured in old cell (21 µm). This could be explained by the fact that the two samples of ceramic even if they are coming from the same ceramic type are different. It is possible that there is dispersion in term of pore sizes in the same ceramic type.

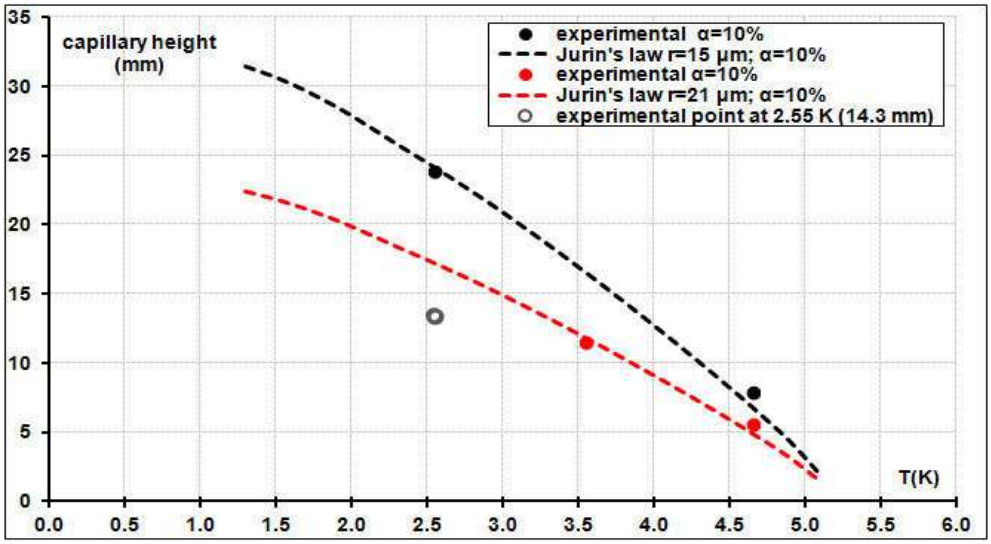


**Figure 4.47: The capillary heights calculated from the experimental results with cell of 14 mm height without point at 2.55 K (red dashed line) and with cell of 30.6 mm height (black dashed line).**

Using the model presented in the section§ 4.6.2, it is possible to calculate the curves of accessible energy as a function of the applied load at 2.55 K and 4.65 K. The model curves are calculated for a pore radius of 15 µm, values obtained from the results with this cell. The permeability is calculated using the method of least square, and the value found is $= 7.97 \times 10^{-13}\ m^2$ . This value of permeability is slightly lower than the values obtained with a first cell (14.3 mm) ( $k = 8.50 \times 10^{-13}\ m^2$)around 6 % less and there is a qualitative accordance with the lower pore diameter found for this cell.

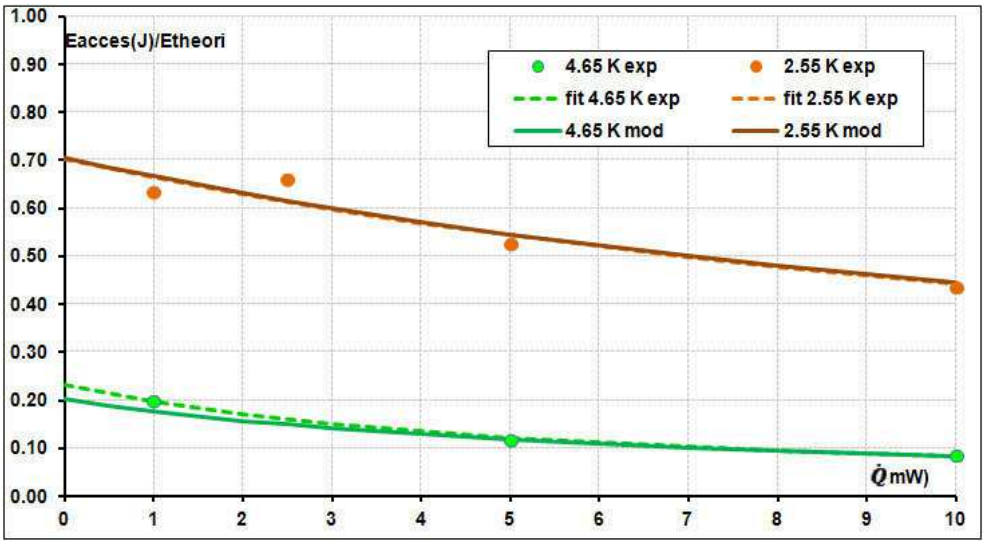


**Figure 4.48: Comparison of ratio between the accessible energy and the theoretical energy with load applied on top of the cell of 31 mm for two different temperatures (4.65 K and 2.55 K). The points correspond to experimental results and the dashed lines are results obtained from the model *with* $k = 7.97 \times 10^{-13}\ m^2$.**

### 4.6.4 Synthesis of heating the top of the cell with ceramic

When some heat is applied at the top of the cell, the accessible energy that could be recovered at saturated temperature could be explained by Jurin's law and as such increased when temperature decreased. However, for the same temperature saturation, the accessible energy depends on the applied load.

Based on a first cell, using the Jurin's law and the experimental results it was determined that the pore radius of ceramic is around 21 µm for a liquid vapor ratio above the lake of α=10 %.

A model was developed to explain qualitatively the experimental results. The model consists in a balance of three forces: capillarity force, gravity force and pressure drop induced by the liquid flow. The model allowed us to determine the permeability of ceramic ($k = 8.50 \times 10{-}13\ m2.$

The liquid reach the cell top due to capillary force, but the gravity force and the pressure drop of liquid made difficult the liquid ascension. The pressure drop is proportional to the mass flow rate (i.e. proportional to the applied load) and causes a variation in accessible energy with applied heat load. Higher the applied load is, lower is the accessible energy.

A second cell with a larger height (30.6 mm instead 14.3 mm) was tested and exhibited different parameters than the first one. The pore radius was 15 µm (21 µm for the first cell) and, the permeability was $k = 7.97 \times 10^{-13}\ m^2$ ($k = 8.50 \times 10^{-13}\ m^2$ for the first cell). This seems to be due to $k = 7.97 \times 10^{-13} m^2$dispersion in term of pore radius in the samples coming from the same ceramic type.

## 4.7 The effect of porous media when the cell is heating on the bottom end

With the goal to verify if all the liquid inside the cell is evaporated when the cell is heated on the bottom, tests were carried out at 4.65 K, 3.55 K and 2.55 K with and without ceramic and will be presented in this section. The results obtained also allow us to analyse the effect of the saturation temperature and of the different loads applied in the bottom of the cell. In these tests, it was also possible to observe if the last 10% of liquid helium are retained in the ceramic as it happened with nitrogen.

### 4.7.1 Results when the cell without ceramic is heating on the bottom end

In this section, the behaviour of the temperature of the cell ends without ceramic has been studied for different saturation temperatures and for different loads applied on the bottom of the cell.

#### 4.7.1.1 Heating the bottom of the cell without ceramic for a given temperature

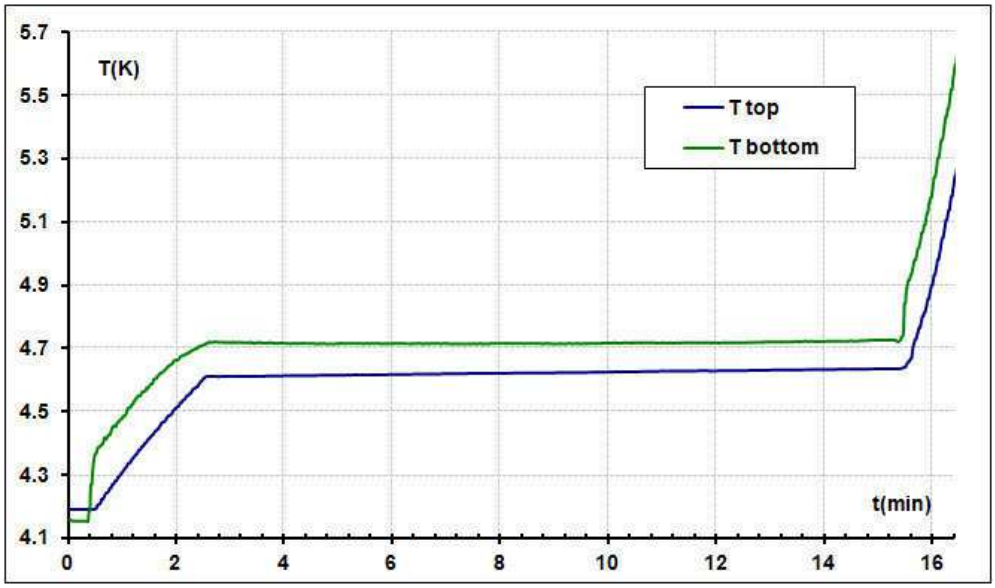


**Figure 4.49: Evolution at the top and bottom temperatures of the cell without ceramic when 5 mW is applied on the bottom of the cell.**

Figure 4.49 shows the evolution of temperatures when 5 mW (3.34 mW/cm$^2$) is applied at the bottom of the cell (cell without ceramic). At t =0, the switch is off and all the liquid inside the cell is subcooled and stratified: temperature at the bottom (initially connected to the cold end) is slightly below temperature at the top. At t= 1 min the power is applied. When we started to heat the cell, the temperatures of the top and the bottom increase up to the saturation temperature. At the beginning, $T_{bottom}$ increases to allow heat transfer through the small heat resistance between the copper end and the liquid. This first increase is very sharp as the bottom end has almost no heat capacity. The 10 g of copper in bottom tip needs only 0.2 mJ to bring the temperature from 4.2 K to 4.4 K. Then, $T_{bottom}$ and $T_{top}$ increase at the same rate because there is a good thermal coupling between them (natural convection occurs as the heating comes from the bottom).

After 2 minutes, $T_{top}$ and $T_{bottom}$ reach a constant temperature indicating that liquid from the cell is being evaporated. Between $T_{top}$ and $T_{bottom}$ there is a 0.1 K difference. This difference between $T_{top}$ and $T_{bottom}$ is analysed in more detailed in the section§ 4.7.2.3

A sudden acceleration of the $T_{top}$ and $T_{bottom}$ drift occurs after 20 min when all the liquid has been evaporated.

During the plateau, the system absorbed an energy of 3.8 J (temperature was constant during 12.7 min while 5 mW was applied). This accessible energy could be compared with the theoretical energy which is the product of the latent heat by the mass of liquid inside the cell. The mass of liquid in the cell used to determine the theoretical energy depend of the void volume of the cell and has been determined experimentally at room temperature. The volume at low temperature decreases due to thermal dilatation of copper and stainless steel that is approximately 3.3 mm per meter. So, the volume of the cell decreases by 1 % at low temperature. The accessible energy has been estimated to be 4 % less than the theoretical energy in the present experiment.

The slight difference between the theoretical value and the measured value can be due to the difficulty to define the onset and the end of the plateau. In the experience shown in the Figure 4.49 boundaries of the plateau are easy to define but in some experiences (mainly at low temperature) it is more difficult.

The energy stored in the cell depends on the temperature as the latent heat and the density of helium vary with temperature. This is illustrated in Figure 4.50. The latent heat, such as other properties of helium, is obtained by the Hepak ® [44]. However, the latent heat values given by Hepak ® are different of latent heat calculated by the difference between the enthalpy of the liquid and the vapor using the same Hepak® code. As it is difficult to know the most relevant value, direct value of latent heat was arbitrary chosen and the associated uncertainty (roughly 1 %) is presented in Appendix C:.

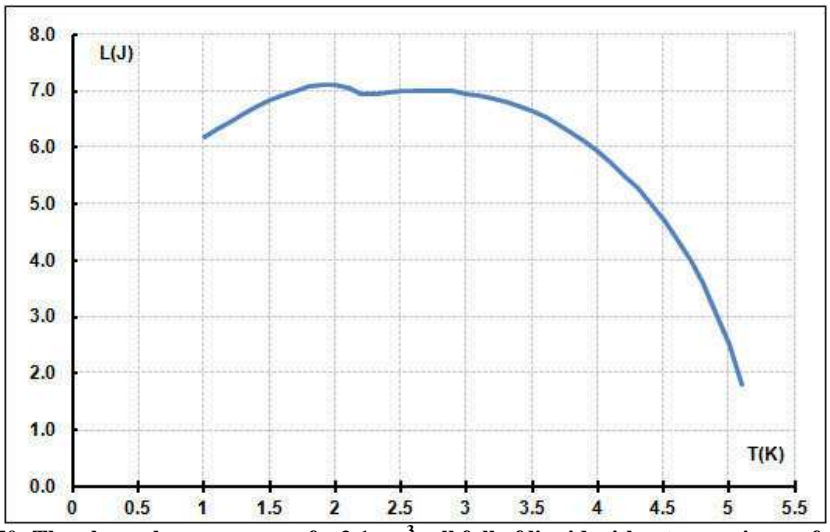


**Figure 4.50: The phase change energy of a 2.1 cm$^3$ cell full of liquid without ceramic as a function of temperature.**

#### 4.7.1.2 Heating the bottom of the cell without ceramic – effect of the applied load and of the saturation temperature

In Figure 4.51, it is possible to see the ratio between accessible and theoretical energy when the cell is heated with different loads and at different temperatures. In the test at 4.65 K and 3.55 K the cell was connected to a 30 liters expansion volume, while for tests at 2.66 K a 100 liters expansion volume was used.

At 4.65 K, the accessible energy is the same from 1 mW up to 10 mW and is approximately equal to theoretical energy. In other words, all the liquid inside the cell is evaporated at a constant temperature when load is applied on the bottom of the cell.

The same test was performed at 3.55 K and 2.55 K, respectively the blue points and brown points in Figure 4.51. Whatever are the applied heat loads, we can get around 95% and 92 % of the theoretical energy respectively at 3.55 K and 2.55 K.

In conclusion, the accessible energy is closed to the theoretical value and is not affected by the applied heat load in the 0 mW-10 mW range. This demonstrates that there is no liquid entrained by the vapor in the exhaust capillary. It looks like that as the temperature decreases, the accessible energy slightly decreases. No evident reason was found to explain this tendency.

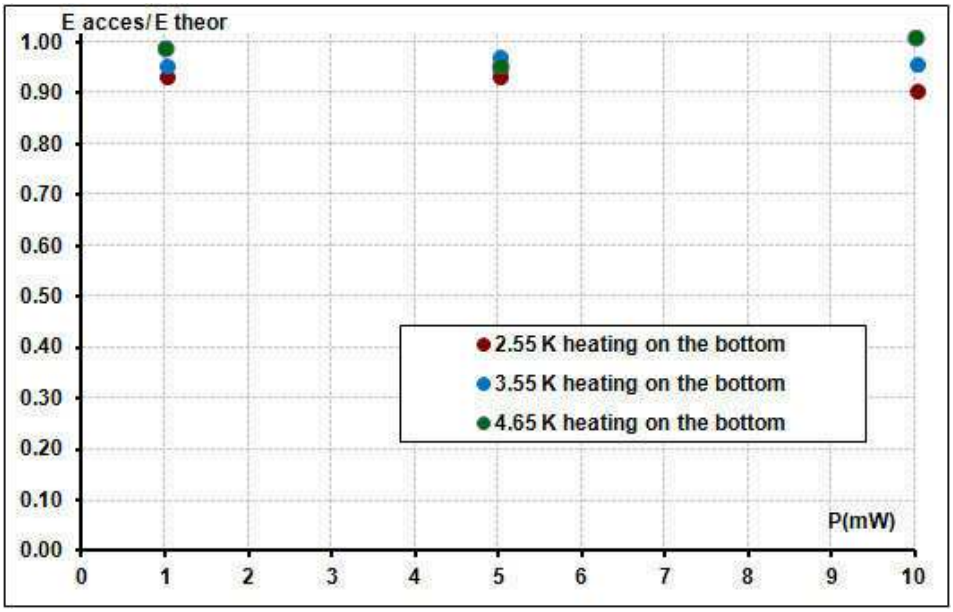


**Figure 4.51: Evolution of ratio between the accessible and the theoretical energy for different loads applied at the bottom of the cell for 3 different temperatures. (4.65 K, 3.55 K, 2.55 K) – cell without ceramic.**

#### 4.7.1.3 Synthesis of heating the bottom of the cell without ceramic

When the cell without ceramic is heated at the bottom, the accessible energy is constant with the applied load. The accessible energy is approximately equal to theoretical energy even if it looks like that a small difference appears as far as the saturation temperature decreases.

### 4.7.2 Results when the cell with ceramic (P160 – Kapirock) is heating on the bottom end

In this section, the effect due to a ceramic put inside the cell is investigated. In particular, the behaviour of the temperature of the cell ends has been studied for different saturation temperatures and for different loads applied on the bottom of the cell.

#### 4.7.2.1 Heating the bottom of the cell filled with ceramic (P160 – Kapirock) for a given temperature

In the Figure 4.52, the evolution of $T_{top}$ and $T_{bottom}$ is shown when 5 mW is applied on the bottom of the cell filled with ceramic.

At the beginning of the heating phase, the $T_{bottom}$ increases quickly. In 18 seconds the temperature reaches $T_{sat}$. This is faster than for the test performed with the cell without ceramic (2.26 min). This behaviour is due to the fact that the ceramic makes difficult to create a natural convection as shown in the section § 4.3.3.2.

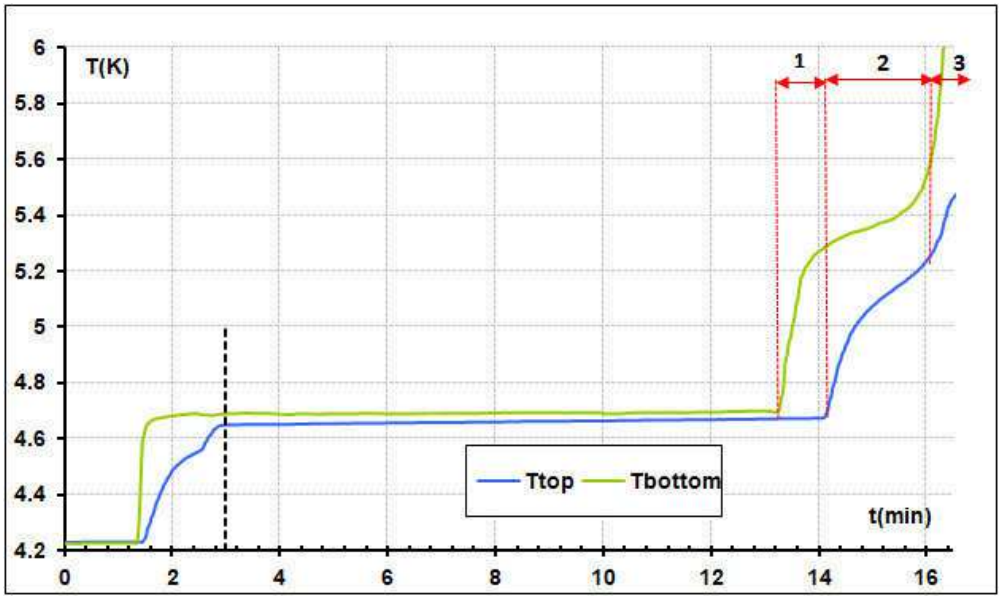


**Figure 4.52: Evolution of top and bottom temperatures when 5 mW is applied at the bottom of the cell (cell with ceramic).**

At first look, it seems easy to define the accessible energy by using the duration of the bottom temperature plateau (green curve), but one part of this energy is due to the heat needed to warm up the subcooled liquid that is inside the cell and therefore should be removed from the energy estimated taking into account the whole plateau. When helium dilatation is neglected, this energy can be approximated by the product of the liquid mass inside the cell at the beginning of the plateau by the difference of the liquid enthalpy at $T_{sat}$ and at initial temperature (subcooled liquid). The mass of the liquid is estimated by the product of the helium density (at $T_{sat}$) by the volume of the cell once cold. Neglecting the liquid helium dilatation already permits a good approximation of the energy required for the subcooling liquid present in the cell to reach the saturation, but to be more precise, liquid dilatation should be taken into account. One part of the mass that is present at the beginning of the experiment (during subcooled phase) will be heated before being expulsed. The liquid will be expulsed at the temperature (and enthalpy) of the top cell. In case of a rapid warm up of the bottom temperature with the top cell temperature remaining cold (this is the case for the plot 5 mW at 4.65 K presented in Figure 4.52) there is some liquid expulsed before being heated. Assuming a linear thermal gradient inside the cell, this liquid quantity is one half of the total liquid that will be expulsed. At first order, the second half will be expulsed at an average temperature comprise between the subcooled temperature and the saturated temperature. So we can propose the following simplified formula to estimate the energy associated to the warm up of the subcooled liquid to the saturation temperature.

$$warm\ up\ energy = \rho(T_{sat}).V_{cell}\left[H_{en_L}(T_{sat}) - H_{en_L}(T_{subcooled})\right] + \left(\left(\rho(T_{subcooled}) - \rho(T_{sat})\right)\right).\frac{V_{cell}}{2}\left[H_{en}\left(\frac{(T_{sat} + T_{subcooled})}{2}\right) - H_{en}(T_{subcooled})\right] \quad (4.27)$$

The time (duration from the starting of the heating phase) associated to this energy is plotted on the Figure 4.52 (dash vertical line). It can be seen that this time is close to the time (1.5 min) when the top temperature of the cell reach the saturated temperature. This confirms that the duration between the times that the bottom temperature and the top temperature reach the saturated temperature should not be taken into account for the estimation of the accessible energy. In other word, starting from a temperature closer to the saturated temperature will reduce the length of the bottom temperature plateau. It can be noticed that the duration needed for $T_{top}$ to reach the saturated temperature is almost the same for the case with and without ceramic, respectively 1.5 min and 2 mim.

What happen in practice in the cell? It is possible that bubbles are formed at the bottom of the cell at the beginning of the plateau made by the bottom temperature, because the fluid reaches the saturated temperature. But the bubbles are probably condensate during their progression through subcooled liquid towards the output capillary located at the cell top end leading to the heating up of the helium until all the helium of the cell reaches the saturated temperature.

As described above, to estimate the accessible energy, the beginning of the plateau is set when the $T_{top}$ reaches the saturated temperature. The end of the plateau is set when the $T_{bottom}$ starts to increase rapidly. This fixes the duration. This duration is multiplied by the latent heat of evaporation. This works well to analyse the experiment done at 4.65 K but things are less simple at lower temperature because the shape of the plateau is less regular. This point will be discussed later.

The duration taking into account for the calculation of the accessible energy is around 10 minutes, allowing us to use 3.1 J of energy (78% of theoretical energy). The difference between $T_{top}$ and $T_{bottom}$ is only 0.05 K, smaller than in the case of a cell without ceramic (0.1 K) (Figure 4.49).

The final part of the curves shown on the graph can be divided into three regions. The first one (indicated in Figure 4.52 with 1), starting at 13 min where $T_{bottom}$ raised quickly, while $T_{top}$ remains at $T_{sat}$. As we heat from below, this part dries first while there is still some liquid at the top end confined by capillarity.

One minute after, (region 2 in Figure 4.52), $T_{top}$ increases quickly and then the cell ends show a kind of "plateau" after the first strong increase and before increasing quickly again. The $T_{top}$ increases when there is no more liquid (inside the ceramic) in contact with the top of the cell. In the "second plateau region", we can suspect that there is still some liquid retained in the ceramic which prevents from a quick increase of temperature.

The third region (region 3 in Figure 4.52) is when the temperatures ($T_{top}$ and $T_{bottom}$) rise faster and there is probably no more liquid inside the ceramic.

Analysing the end of the curves after the plateau at saturated temperature, we can infer that a part of the liquid remains trapped in the ceramic and will not contribute to the accessible energy (energy that can be recovered at the saturated temperature). This is confirmed by the balance of energy.

#### 4.7.2.2 Heating the bottom the cell with ceramic (P160 – Kapirock) - effect of the applied load at a given temperature

At 4.65 K, other loads were applied at the bottom of the cell, and the results of those tests are plotted in Figure 4.53. The accessible energy decreases with loads and is always lower than the theoretical energy. We can observe that minimum inaccessible energy is 15 % of theoretical energy. Obviously the theoretical energy is estimated by removing the place taken by the ceramic. The fit plotted in the figure is done using a hyperbolic law as in the previous section even we cannot affirm that this kind of low is still valid in this case.

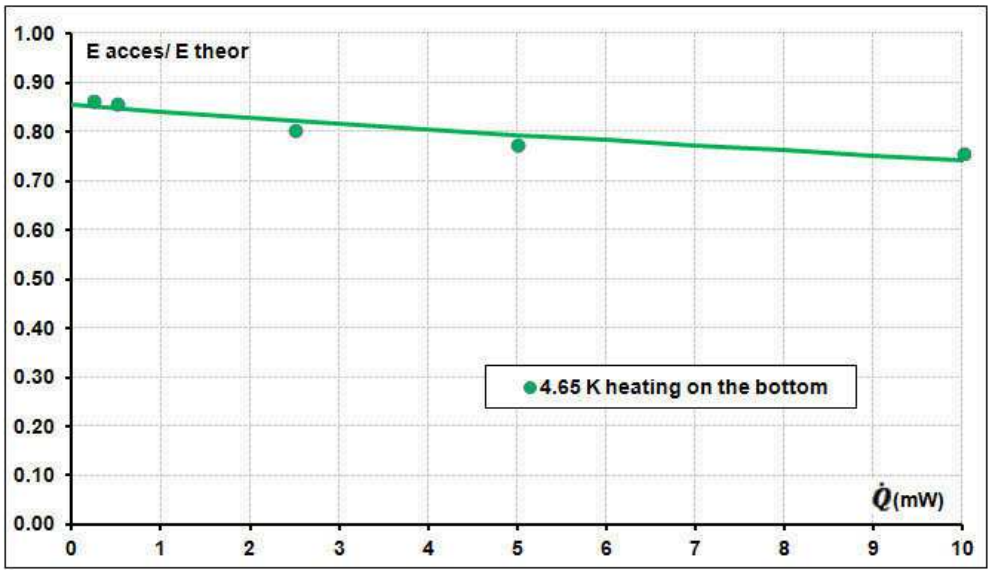


**Figure 4.53: Evolution of the ratio between accessible energy and theoretical energy for different loads applied on bottom of the cell at $T_{sat}$ = 4.65 K.**

One possible hypothesis to justify this discrepancy is that at the beginning of the experiment the cell is not fully filled with liquid. This hypothesis is based on the fact that the ceramic is a porous medium with bad thermal conductivity and one could have doubt about the fact that all the pores are filled with liquid during the cooling down process. To check this hypothesis, we decide to cool down the cell below the superfluid transition temperature. It is expected that the superfluid helium could fill every pores even the very small ones. Another interest of using the helium superfluid properties is to fasten the cool down of the cell as presented in the section §4.5.4.The accessible energy obtained with the 2 cooling down modes is compared in Figure 4.54. In both modes, after the filling, the cell was thermalized at a temperature close to the saturated temperature before the beginning of the run, in any case above 4.2 K.

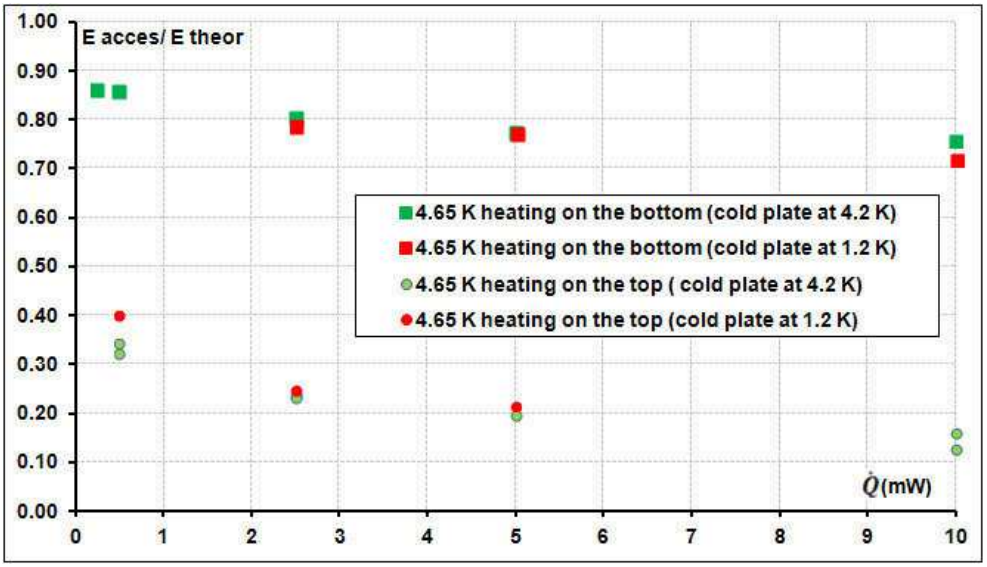


**Figure 4.54: Comparison of the ratio between the accessible energy and the theoretical energy with applied load on the bottom of the cell for 4.65 K. The results obtained when the cell if heated on the top are also presented. The green points are obtained when the cell was cooling down with a cold plate at 4.2 K and the red points with a cold plate at 1.2 K.**

As shown , when the cell is heated in the bottom of the cell the accessible energy is the same if the pre-cooling is performed at 4.2 K or at 1.2 K (superfluid) . So, we can conclude that

all ceramic is full with liquid and that the missing energy is not due to a lack of helium in the cell.

Another hypothesis to justify this discrepancy is that the ceramic retains one quantity of liquid which is more difficult to extract.

The accessible energy is estimated by considering only the energy absorbed at a constant temperature, i.e. during the plateau or more precisely during the $T_{bottom}$ plateau once the $T_{top}$ has reached the saturated temperature. The liquid that stays trapped into the ceramic and was evaporated after the $T_{bottom}$ increase is not taken into account because this remaining liquid is evaporated when the $T_{bottom}$ is higher than the saturation temperature. It is possible to estimate the quantity of liquid that remains trapped in the ceramic using the discrepancy between the accessible energy and the theoretical energy. When the cell is heating by the bottom, the part of the ceramic in contact with the copper bottom end dries up while the copper top end remains wet (constant temperature). Using the experiences performed at 4.65 K, if we assumed that all the missing energy is due to trapped liquid inside the ceramic, there are around 15 % of liquid inside the cell at the end of the plateau of the bottom temperature, which is away from the bottom of the cell. But, approximately 5 % are already missing in the tests without ceramic (section § 4.7.1.1 ), so we can estimated that the ceramic retains around 10 %. We think that this liquid is trapped into the ceramic and could not migrate easily to the heated surface (it is only evaporated by superheated vapor). This difference in energy also happens in the nitrogen ESU (Chapter 2:) where a ceramic very similar to ceramic P 160- Kapirok was used. In this nitrogen case, the ceramic retains between 15 % - 25 % of liquid.

#### 4.7.2.3 Heating the bottom the cell with ceramic (P160 – Kapirock) - effect of saturation temperature.

Other tests have been performed at 3.55 K and 2.55 K. The treatment of these data is more complex, because they do not present a shape as regular as the ones measured at 4.65 K. As an example, the data obtained for a saturated pressure of 2.55 K and an applied heat load of 5 mW is presented in the Figure 4.55

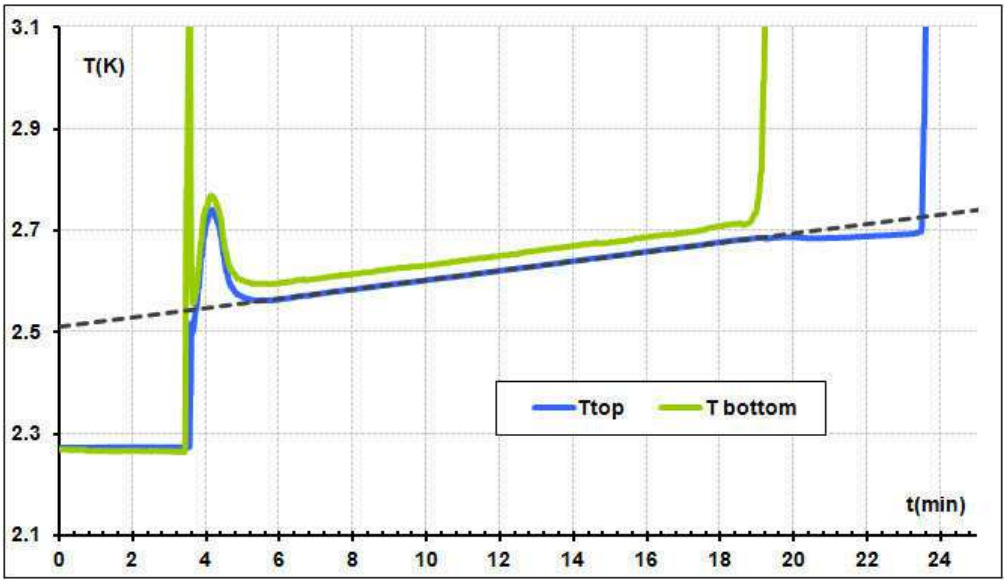


**Figure 4.55: Evolution of top and bottom temperatures when 5 mW is applied at the bottom of the cell (cell with ceramic) at 2.55 K.**

We can see that there are 2 peaks above the saturated temperature before the bottom temperature achieve the plateau: the first one is short in duration but leads to high temperature above 3 K; the second is lower in term of intensity but takes a longer time. We think that these peaks are the signature of extra pressure drop in the connecting pipe between the cold cell and

the expansion volume and could be due to a liquid plug or large liquid evaporation taking place in the pipe. It should be noted that there is a siphon in the connecting pipe at the cold cell exit and that the capillary diameter (0.5 mm) is quite small at the cell output.

It is easy to define the end of the plateau, but less easy to define the beginning. We would like to use the time when the temperature of the cell top reach the saturated temperature. Even this value is not so easy to define due the limited expansion volume and the associated temperature drift. It is possible to linearly extrapolate the plateau towards the beginning of the experiment to define the saturated temperature at each time. Then there are several choices to set the beginning of the plateau. It could be the first time that the $T_{top}$ cross the saturated temperature (red mark on Figure 4.56). It could be when the $T_{top}$ comes back to the saturated temperature after the second temperature peak (yellow mark on Figure 4.56). The third solution is to define a time corresponding to the energy needed to warm up the helium from the subcooled to the saturated temperature (pink mark on Figure 4.56). This point is not on the $T_{top}$ temperature curve but presents the advantage to be "operator" independent, which is not the case for points where the $T_{top}$ curve reaches smoothly the saturated temperature (yellow mark situation). For all the data treated in the section related to the heating by the bottom with ceramic, this third solution has been adopted.

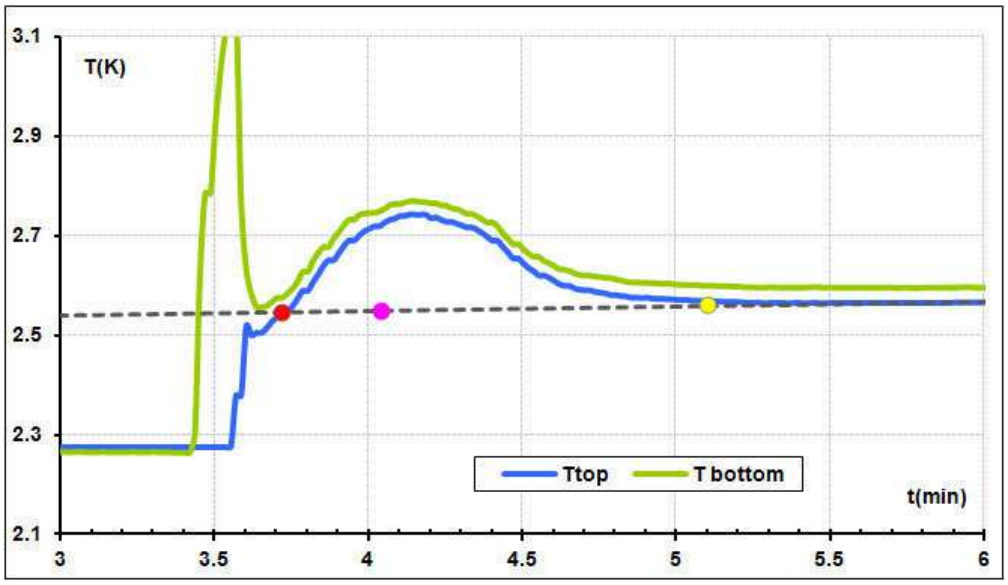


**Figure 4.56: This figure is a zoom of the Figure 4.55. The red mark is the first time that $T_{top}$ crosses the saturation temperature. The pink mark corresponds to the time necessary to warm up the helium from the subcooled to the saturated temperature. The yellow point is when the $T_{top}$ comes back to the saturation temperature after the second temperature peak.**

We can see in Figure 4.57 the variation of the accessible energy with the saturation temperature. The first result is that the accessible energy is approximately the same at low applied load. The hyperbolic fit extrapolation intercept the Y axis (Figure 4.57) at respectively 0.86, 0.86 and 0.84 for 4.65 K, 3.55 K and 2.55 K. We have around 15 % (or 10 % if we take into account for the offset for the cell without ceramic) of liquid that could not be removed easily from the ceramic.

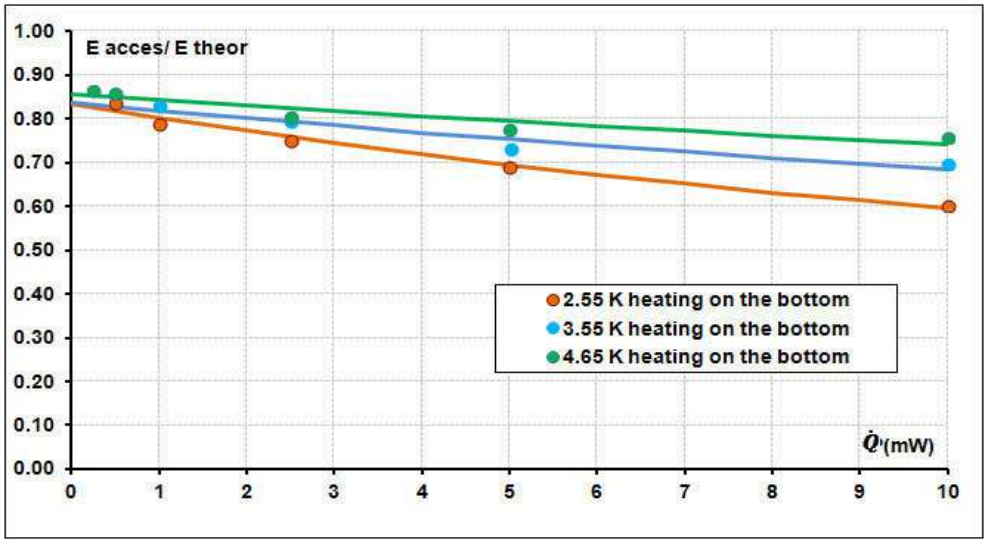


**Figure 4.57: Comparison of the ratio between accessible energy and theoretical energy as function of the applied load on bottom of the cell with ceramic for three different temperatures (4.65 K, 3.55 K, and 2.55 K).**

The results show also a dependence of the accessible energy with the applied load for all temperature tested. Furthermore, the variation of the accessible energy with applied load is more pronounced at low temperatures (slope of the hyperbolic fits increases with decreasing temperature).

When the cell is heated by the bottom, the liquid in contact with the copper in the bottom starts to evaporate. To keep the temperature at the saturated temperature, the vapor due to evaporation has to go away and some new liquid has to wet the copper surface.

For small load the accessible energy is the same for all the temperatures, because the quantity of liquid evaporated is small and consequently, there is no limitation due to pressure drop for the vapor exhaust and for the liquid. The heated copper surface is always wet.

The fact that the accessible energy decreases when the applied load increases and when the temperature decreases (Figure 4.59) means that the liquid has more difficulty to reach the heated surface. As in previous sub chapter (section § 4.6.2), this may be explained by a competition between difference forces acting on the liquid or vapor flow. Hereafter, a list of these forces is displayed.

1) Vapor friction

To go out of the cell, the vapor has to cross the cell because the capillary outlet is on the other side, at the top of the cell. To go up, the vapor has to push the liquid and to create an output path. There is vapor friction (see equation (4.28)) with the ceramic that depends of the filtration velocity, the dynamic viscosity and permeability of ceramic.

$$\Delta P_V = \frac{\mu_V \, U_V \, H}{k} \Leftrightarrow \tag{4.28}$$

Where $\mu_V$ the dynamic viscosity of vapor and $U_V$ the filtration velocity of vapor that can be expressed as:

$$U_V = \frac{\dot{m}}{\rho_V(1-\alpha)A_T} \Leftrightarrow U_V = \frac{\dot{Q}}{L\,\rho_V(1-\alpha)A_T} \tag{4.29}$$

Where $\dot{m}$ mass flow rate, $\alpha$ the rate of presence of liquid equal to 10 % and $A_T$ the total section area is equal to 1.5 $cm^2$.

The filtration velocity depends of the applied load (proportional to mass flow rate), and is inversely proportional to vapor density and latent heat. Taking into account all these behaviors, it quickly increases when temperature decreases. The values of velocity, show in Table 4.2 are calculated for 10 mW and flow section of 1.5 $cm^2$.

To calculate the pressure drop due the vapor flow, the permeability k must be known. However, this value may be different from the value taken for the liquid as it is foreseen that liquid will flow in the smallest pores and vapor in the largest ones. Anyway a conservative approach (i.e. maximizing the pressure losses) consists to take the value found for liquid.

Thus, the rough values of the vapor pressure drop in a ceramic having a length of 14.3 mm and a diameter of 13.8 mm are displayed in Table 4.2. It is clear that values are higher at low temperature.

**Table 4.2: Some properties of vapor helium, the vapor filtration velocity and the vapor pressure drop of three different temperatures for 10 mW of power applied.**

| T(K) | L(J/kg) | $\rho_v$(Kg/m^3) | $\mu_V$ (Pa.s) | Uv (cm/s) | $\Delta P_{FV}$ (Pa) |
|---|---|---|---|---|---|
| 4.65 | 1.73E+04 | 25.80 | 1.46E-06 | 0.017 | 4.07 |
| 3.55 | 2.30E+04 | 8.56 | 9.88E-07 | 0.038 | 6.28 |
| 2.55 | 2.28E+04 | 2.35 | 6.72E-07 | 0.138 | 15.61 |

2) Capillary pressure

The capillary pressure in the ceramic is the responsible to bring the liquid against the gravity but also in the other directions. When a pore is empty because the liquid is evaporated, new liquid came to fill this pore. The new liquid comes because the capillary force pumps liquid from larger pores to smaller ones. This way, the largest pores act as a reservoir for the smallest pores. As the ceramic is composed by large and small pores the liquid circulates due to a capillary pressure. As this force increases with decrease of temperature (see values in Table 4.3), at 2.55 K the liquid tends to be "trapped" by larger pores than for higher temperature and could easily remain located in the top part of the cell.

**Table 4.3: The capillary force of liquid helium (pore radius 21 µm) of three different temperatures.**

| $T_{sat}$ (K) | $P_{cap}$ (Pa) |
|---|---|
| 4.65 K | 4.28 |
| 3.55 K | 14.65 |
| 2.55 K | 23.94 |

However, there are other phenomena that have a negative contribution to explain the dependence of the accessible energy with the temperature

3) Liquid friction

In order to go down to the bottom of the cell, the liquid needs to move through the ceramic causing pressure drop. The pressure drop is proportional to dynamic viscosity and filtration velocity (see equation (4.30)). The filtration velocity is proportional to the applied heat load and inversely proportional to latent heat and liquid density (see equation (4.30)). The dynamic viscosity does not change much in the temperature range of our measurements. The latent heat at 2.55 K is approximately equal to the one at 3.55 K and higher that the one at 4.65 K (when the latent heat increases, liquid mass flow evaporated by given heat load decreases). The liquid density increases slightly as the temperature decreases (so liquid velocity also slightly decreases). As a consequence, the liquid friction is lower at lower temperature. Table 4.4 it is possible to see the values for filtration velocity and the pressure drop when 10 mW is applied in ceramic having a length of 14.3 mm and a diameter of 13.8 mm for three different temperatures.

$$\Delta P_L = \frac{\mu_L \, U_L \, H}{k} \tag{4.30}$$

Where $\mu_L$ the dynamic viscosity of liquid; $U_L$ the filtration velocity of liquid that can be expressed as:

$$U_L = \frac{\dot{m}}{\rho_L \alpha A_T} \Leftrightarrow U_L = \frac{\dot{Q}}{L \, \rho_L \alpha \, A_T} \tag{4.31}$$

Where $\alpha$ the rate of presence of liquid equal to 10 % and $A_T$ the total section area equal to 1.5 $cm^2$.

**Table 4.4: Some properties of liquid helium, the liquid filtration velocity and the liquid pressure drop of three different temperatures.**

| T(K) | L(J/kg) | $\rho_L$(kg/m3) | $\mu_L$ (Pa.s) | $U_L$ (cm/s) | $\Delta P_L$ (Pa) |
|---|---|---|---|---|---|
| 4.65 | 17304 | 114.94 | 2.92E-06 | 0.034 | 16.52 |
| 3.55 | 22956 | 135.45 | 3.52E-06 | 0.022 | 12.72 |
| 2.55 | 22837 | 144.73 | 3.23E-06 | 0.020 | 11.00 |

4) Ratio of density

The ration between liquid density and vapor density increases when the temperature decreases: 4, 16 and 61 for 4.65 K, 3.55 K and 2.55 K, respectively. So, at low temperature, if the liquid is 61 times heavier than the vapor it must go down more easily. So the gravity forces tend to make the accessible energy constant with the applied load.

It is not only worthwhile to see the evolution of the forces in presence but also to have an idea of their magnitude.

At 2.55 K, if we compare the results when the cell is heated at the top or at the bottom (see Figure 4.58), the accessible energy is approximately the same at low heating power, because the capillary height at this temperature is equal to the height of the cell. When a significant heat power is applied a difference occurs between the accessible energy obtained by heating on the top or on the bottom. As expected due to gravity force it is a little bit easier to remove the stored energy by the bottom because the liquid easier goes down to the heated surface. The negative effect of the vapor pressure drop is probably lower than the positive effect of the gravity to recover accessible energy.

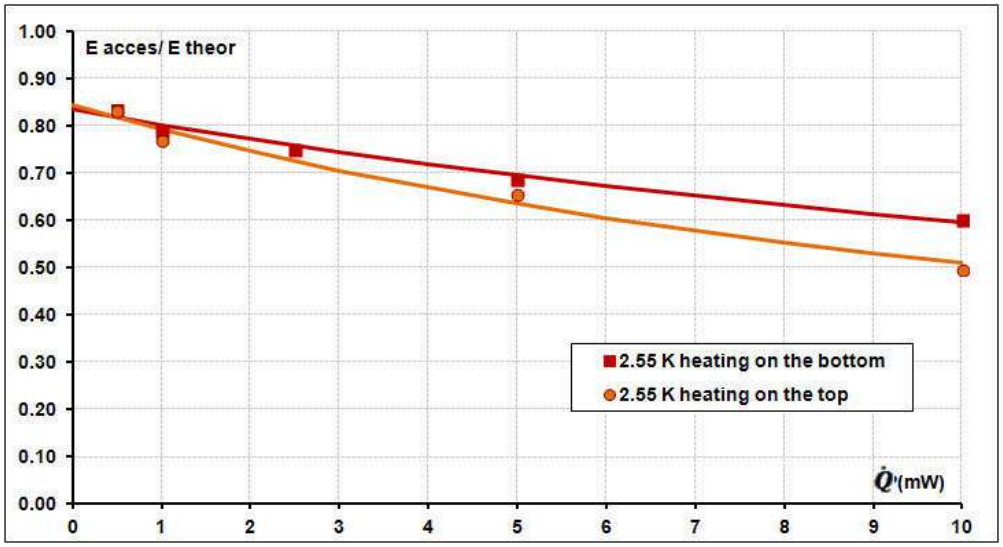


**Figure 4.58: Comparison of the ratio between accessible energy and theoretical energy as function of the applied load on bottom and on top of the cell for 2.55 K.**

The slopes of each hyperbolic fit of the accessible energy as a function of the applied load on the bottom are plotted versus the temperature in Figure 4.59. The slopes at different applied load presents the same behaviors: at low temperature, the variation of accessible energy with the applied load is higher.

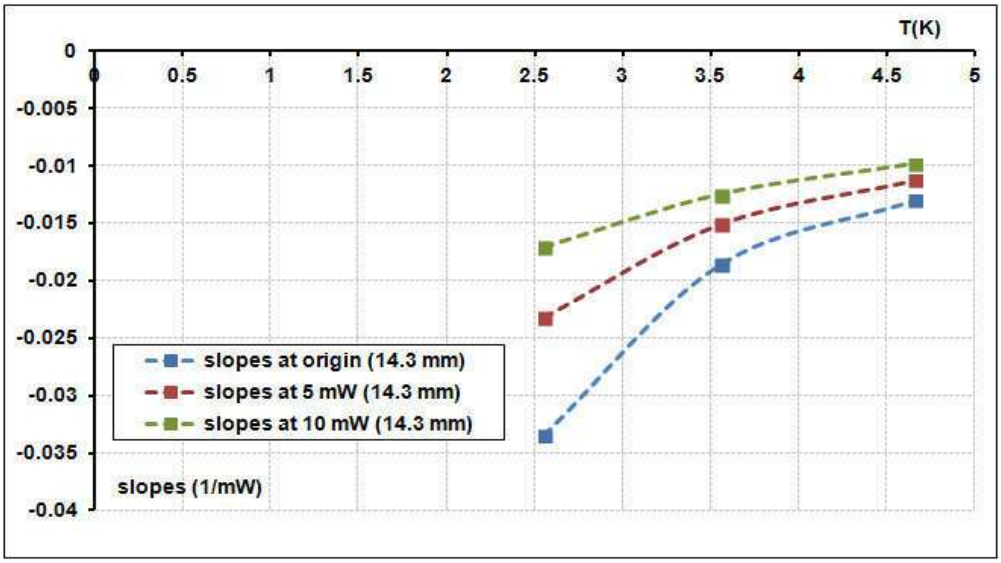


**Figure 4.59: Evolution of the slopes reported in Figure 4.57 as a function of temperature (cell of 14.3 mm with ceramic kapirok-P160).**

Test with the higher cell

To check the behaviour of the higher cell (30.6 mm), a test at 4.65 K was performed. As the cell with a height of 30.6 mm store more energy it was possible to use heat load higher than 10 mW keeping a good accuracy (not too short plateau duration). Figure 4.60 shows that the accessible energy also depends of the applied load.

If we extrapolate the measurements to the low applied heat power, we found a value of 96 % for the accessible energy when not heat power is applied. This value is higher than the one obtained with the smaller cell. For this cell, due to some helium leakage and time constraint, tests with lower applied power than 5mW have not been performed and we cannot exclude that there is some saturation (a kind of plateau in the Figure 4.60) for low applied power and that the

extrapolation of the accessible energy gives a value that is overestimated. If additional tests confirm the high level of accessible energy for this higher cell, then we have to propose some explanation. Two potential explanations are given below.

We still imagine that at the beginning of the plateau corresponding to the saturated temperature ($T_{bottom}$), some bubbles are formed at the bottom and then are condensate when they rise. With such scenario, bubbles are formed in the bottom and decreased exponential with the height (at the beginning of the plateau, when part of the liquid inside the cell is still subcooled). This gas volume, lower in proportion for the higher cell, will lead to some liquid expulsion and could explain why accessible energy is lower for smaller cell.

Another reason can be due to the quantity of liquid inside the cell. In the cell of 30.6 mm, the liquid column weight is higher so it can help to push the liquid down.

Additional tests would have been necessary to confirm these hypotheses.

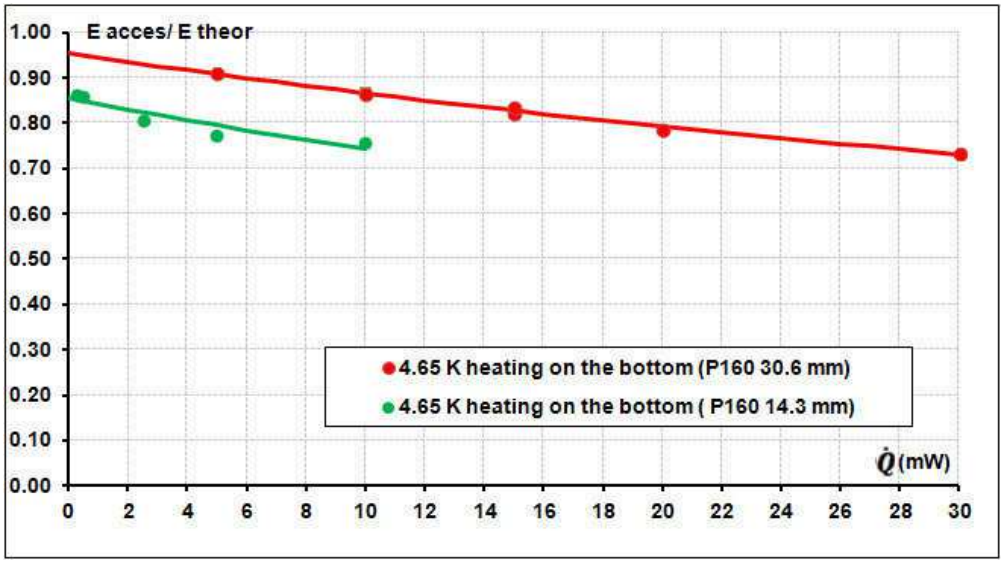


**Figure 4.60: Comparison of the ratio between accessible energy and theoretical energy with the load applied in the bottom of the cell with 14.3 mm and 30.6 mm for 4.65 K.**

The temperature difference between the 2 ends of the cell

During experiments the two temperatures are measured at the bottom and at the top of cell. The temperature of fluid itself is never measured. When the cell is heated at the bottom, $T_{bottom}$ is overheating because of the thermal resistance between the copper and the fluid. The copper of the top is thermalized by the fluid, so the $T_{top}$ is approximately equal to a fluid temperature (no heat flow at this location). For this reason, when in experiments $T_{top}$ and $T_{bottom}$ reach the plateau, the saturation temperature is considered equal to ($T_{top}$). The difference between the heated surface ($T_{bottom}$) and the saturation temperature ($T_{top}$) is defined by $\Delta T$. In the experiment without ceramic (Figure 4.49), the $\Delta T$ is 0.1 K while in the experiment with ceramic (in Figure 4.52), the $\Delta T$ is lower and equal to 0.05 K. So, in presence of ceramic the $\Delta T$ is smaller than in the case of cell without ceramic.

In Figure 4.61 and in Figure 4.62 , the $\Delta T$ measured in each experiment at 4.65 K and at 2.55 K with and without ceramic is plotted as function of the heat flux. The blue dashed line with squares is the values measured for cell with ceramic of 14.3 mm and 30.6 mm. The values obtained for the cell without ceramic are represented by the red dashed line with squares. Comparing the results of this detailed study with ceramic and without ceramic, it is clear that the ceramic decreases the $\Delta T$ for the same heat flux. This confirms the behavior also seen with nitrogen.

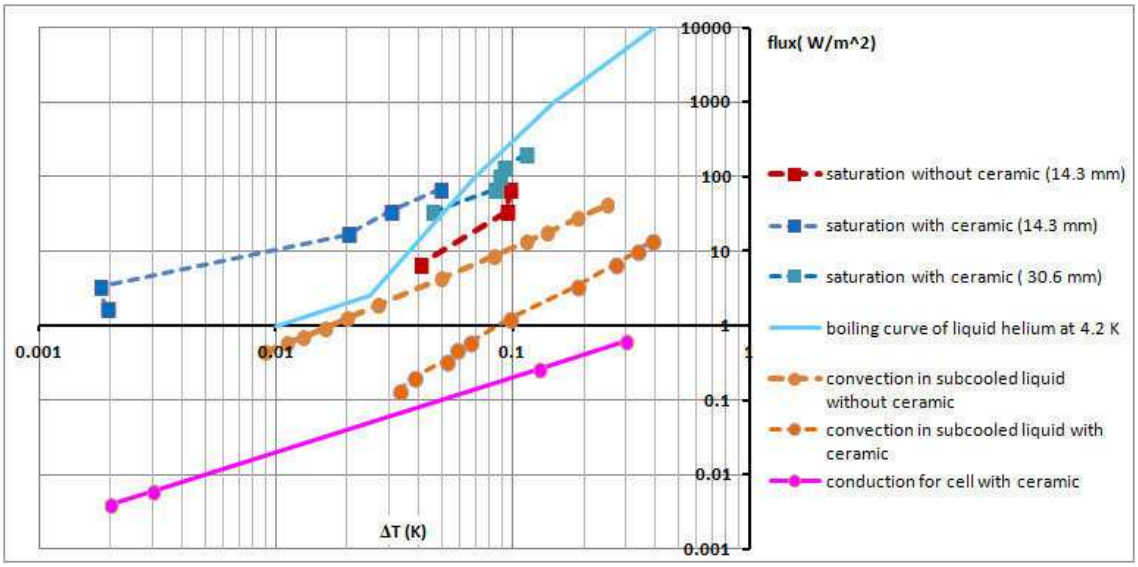


**Figure 4.61: The applied flux as function of the $\Delta T$ for different experimental configuration and operating conditions at 4.65 K.**

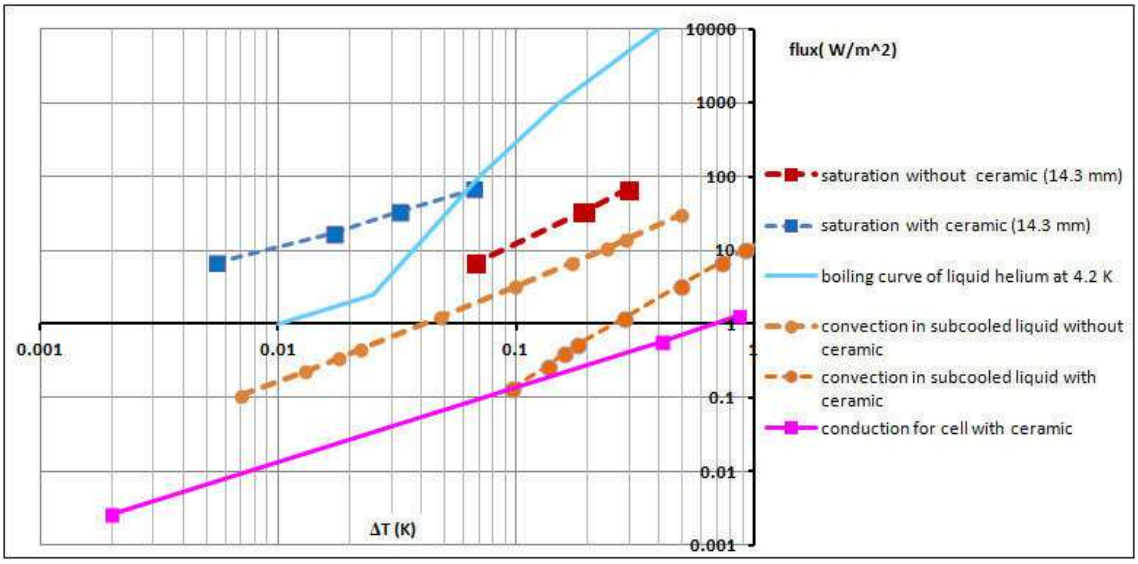


**Figure 4.62: The applied flux as function of the $\Delta T$ for different experimental configuration and operating conditions at 2.55 K.**

In the same figure, it is possible to plotted the values obtained when the convection was measured in the subcooled liquid helium with and without ceramic (orange curves). For the same flux, a higher $\Delta$T was measured during convection tests than at saturation temperature with ceramic. At saturation temperature, the use of ceramic gives more than one order of magnitude on the heat flux for a given $\Delta$T. The convection even without ceramic could not explain the small $\Delta$T obtained during our experiment at saturation temperature.

The small $\Delta$T can be the signature that the nucleation boiling regime with ceramic is reached faster than without ceramic.

The plain blue line in Figure 4.61 and in Figure 4.62 is the boiling curve of liquid helium at 4.2 K (the same that is represented in Figure 4.9). This curve is a rough order of magnitude and depends obviously on conditions, orientation and surface material.

If we compare the values of the boiling curves of helium from the literature with the values obtained in our experiment with ceramic, it seems that the nucleation boiling regime was reached faster than expected. The difference between the literature and our experimental values can be due to a different experimental configuration (not the same temperature, surface quality, or shape of the cell) However, for the cell with ceramic, other factors may have helped the

nucleation boiling regime to be reached earlier than predicted by the literature for experiment without ceramic. In the section § 4.3.3.2 we conclude that the main effect of the ceramic is to delay the onset of convection. So, for the same flux, the cell with ceramic had higher $\Delta T$ than cell without ceramic (see orange curves in Figure 4.61). When we started to heat the bottom part of the cell, the liquid in contact with the copper started to be overheated because there is no convection and the heat flux by conduction is low (see pink curve in Figure 4.61. which represents the conduction of subcooled liquid helium). The quick increase of temperature at the bottom of the cell can help to reach the nucleate boiling.

Another factor that can help the nucleate boiling regime is the ceramic in contact with a heated surface which can allows increasing the number of active nucleation sites, where the vapor is formed. The rate of bubbles formation increases, and this improves the heat transfer between the fluid and the bottom ends. If inside the cell there isn't ceramic and the liquid starts to boil, the bubbles are formed with a diameter roughly equal to capillary length (lc) expressed as:

$$l_c = \sqrt{\frac{\sigma}{g\,\Delta\rho}} \tag{4.32}$$

For example, in these conditions, lc is equal to 0.22 mm at 4.65 K, so the diameter of bubbles is in the order of 0.22 mm. In the test with ceramic, the ceramic probably limit the diameter of the bubbles to pore diameter of the ceramic. So, with the ceramic maybe more bubbles are formed but with smaller dimension. From the expression (4.33) [45], it is possible to determine the limit of nucleation boiling as function of helium properties and the pore radius of ceramic , i.e this expression allows to calculate how much it is necessary to heat the ceramic in order to form bubbles. The $\Delta T$ is the difference between the $T_{sat}$ and the temperature of the fluid (close to surface where it is heated) when the bubbles were formed inside a porous medium with a pore radius equal to r:

$$\Delta T = \frac{2\sigma\, T_{sat}}{L\,\rho_v}\left(\frac{1}{r}\right) \tag{4.33}$$

In our situation, with $r = 21\ \mu m$, it is only necessary to have a $\Delta$T=0.05 mK at 4.65 K to initiate the formation of the bubbles. This expression also confirms that if the fluid in contact with the copper is overheated, the nucleate boiling regime is reached faster.

### 4.7.3 Effect of other ceramic type - ceramic-502

Another ceramic, Altraform KVR/502® (called herafter as the "ceramic 502") manufactured by RATH, with smaller pores than the Kapirok ceramic P 160 was studied to analyse the effect of the pore diameter. In this section are presented the results when the cell is heating on the top and on the bottom.

#### 4.7.3.1 Ceramic description

The structure of the ceramic 502 is very similar to Kapirok Ceramic P160 but there are some differences (see Table 4.5). The ceramic 502 is denser than the Kapirok ceramic with a void volume in same order approximately 90 %. In Figure 4.63, it is possible to see a SEM picture of the ceramic 502 and the ceramic Kapirok P160.

**Table 4.5: Characteristic of Altraform KVR/502 and Kapirok ceramic P 160.**

| | Kapirok ceramic P 160 | Altraform KVR/502 |
|---|---|---|
| Density (kg/m$^3$) | 300 | 500 |
| Porosity (%) | 90 | 88 |
| Composition | | |
| $AlSO_3$ (%) | 91 | 98 |
| $SiO_2$ (%) | 9 | 2 |

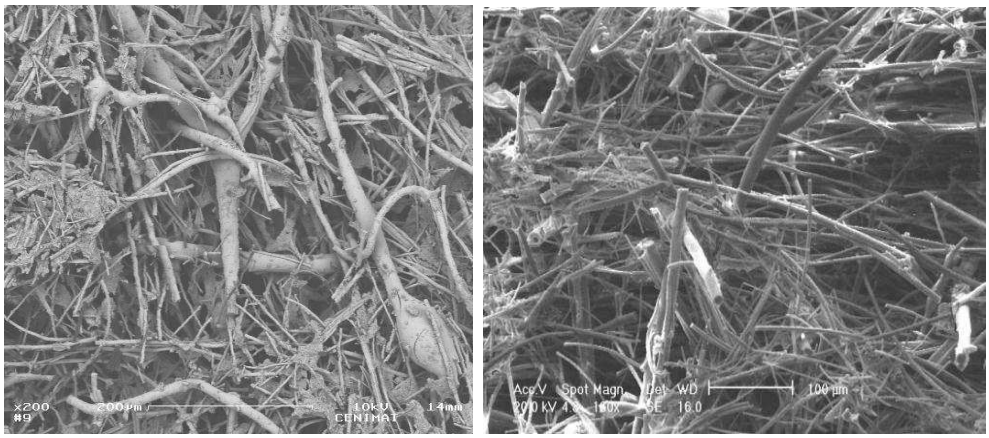

**Figure 4.63: SEM picture of Altraform KVR/502 (photographic Record- CENIMAT/FCT/UNL) (left side) and SEM picture of Procelit P160 (photographic Record- CEA/DTA/CEREM/DEM) (right side). The resolution of two pictures is the same.**

This ceramic was tested inside of a small cell similar to the one describe up to now with a slightly different height of 16.0 mm due to assembly process. This cell was heated on the top in order to determine the pore radius and the permeability of the ceramic. We also heated the cell on the bottom to observe if the accessible energy varies in function of applied load. In the tests at 4.65 K the cell was connected to a 30 liters expansion volume and for tests at 2.6 K, the cell was connected to a 100 liters expansion volume.

#### 4.7.3.2 Heating the top of the cell with ceramic-502

In the first test, the cell was heated on the top at 4.65 K and 2.6 K and the accessible energy was measured. The results obtained are showed in Figure 4.64. The two main phenomena observed with ceramic Kapirok P160 were also observed with ceramic 520: the accessible energy increases when temperature decreases and the accessible energy decreases when the applied load increases.

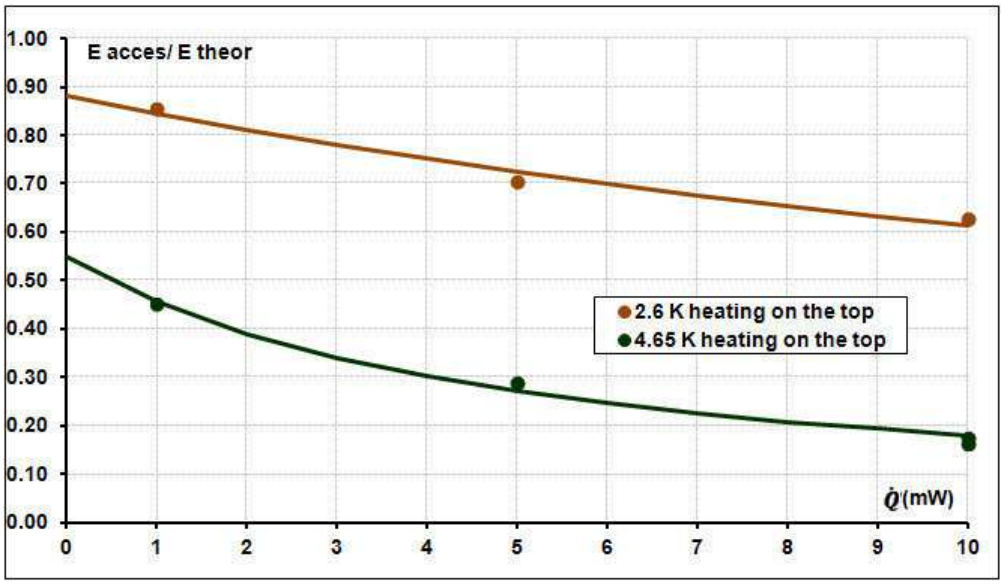


**Figure 4.64: Comparison of the ratio between accessible energy and theoretical energy as function of the applied load on top of the cell with ceramic 502 for two different temperatures (4.65 K and 2.6 K).**

From the y- intercept point it is possible to calculate the value of radius pore if we know $\alpha$. For the radius determination, $\alpha$ is taken at 10 % (same value than the one taken for the Kapirok P160). As it is possible to see in Figure 4.65 the capillary height of the point at 2.6 K is

approximately equal to the height of the cell. So, it's obvious that the cell is too small to use the experimental point at 2.6 K to determine the pore radius. That's why this point was not taken into account in the calculations. The radius pore equal to 11 µm was calculated only with the point at 4.65 K. Using the model described before in this chapter, we could determine that the permeability should be equal to $k = 5.82 \times 10^{-13}\ m^2$.

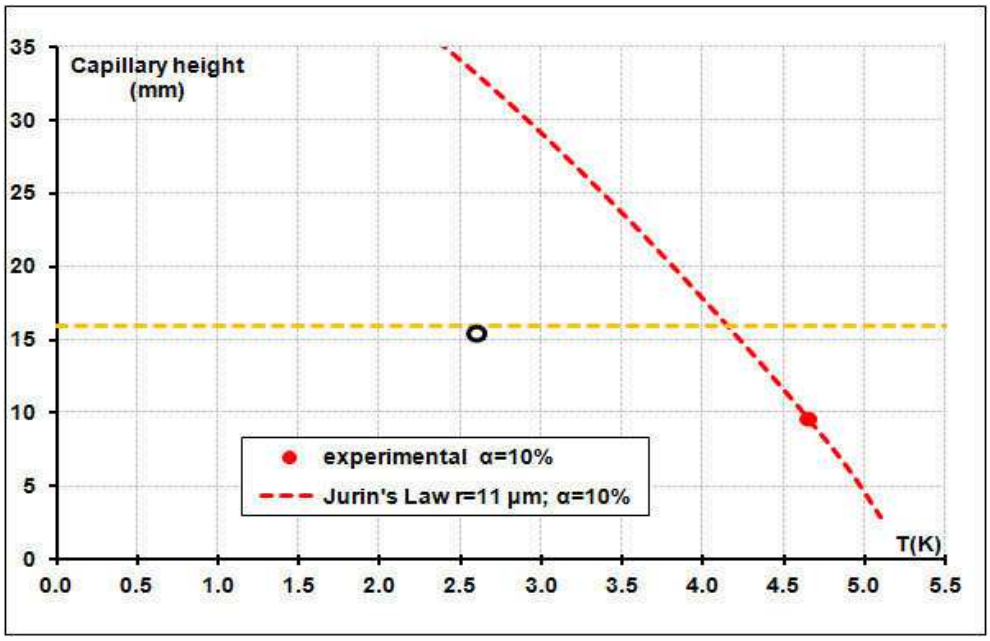


**Figure 4.65: Comparison of the ratio between accessible energy and theoretical energy as function of the applied load on top of the cell with ceramic 502 for two different temperatures (4.65 K and 2.6 K).**

#### 4.7.3.3 Heating the bottom of the cell with ceramic-502

Tests were performed heating the cell on the bottom at 2.6 K and 4.65 K in order to study the behavior of liquid helium inside the 502 ceramic. The results are illustrated in Figure 4.66. The accessible energy depends on saturated temperature and on the applied heat load.

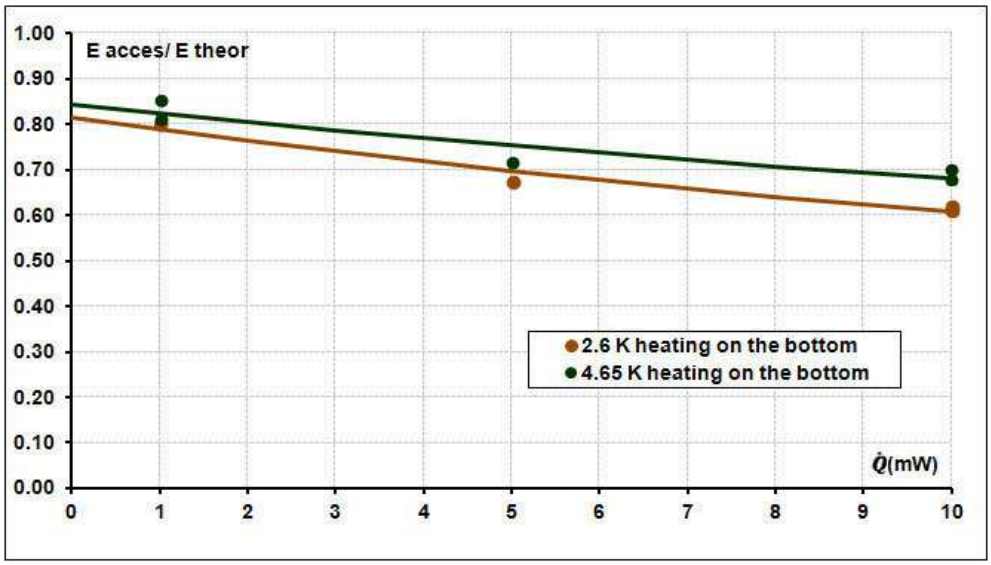


**Figure 4.66: Comparison of the ratio between accessible energy and theoretical energy as function of the applied load on bottom of the cell with 502 ceramic for two different temperatures (4.65 K and 2.6 K).**

It can be noticed that even the ceramic is not the same for this cell (16.0 mm height) than for the other small cell (14.3 mm height) tested before; the accessible energies when no

heat power is applied are very similar: 85% instead of 86% at 4.65 K and 82 % instead of 84 % at 2.6 K. The same is true for the variation of accessible energy with applied load (Figure 4.67). So, in spite of different values determined for the pore radius (11 µm and 21 µm), the behavior of this two cell when are heated by the bottom are very similar. This tends to prove that the capillary effect is not a predominant factor when the cell is heated by the bottom.

In regards with the results (higher accessible energy/theoretical energy, that needs to be confirmed) obtained with the larger cell (30.6 mm height) for which an intermediate pore radius was found, it looks like that the height of the cell is a more important parameter than the pore radius to describe the accessible energy behavior when the cell is heated by the bottom.

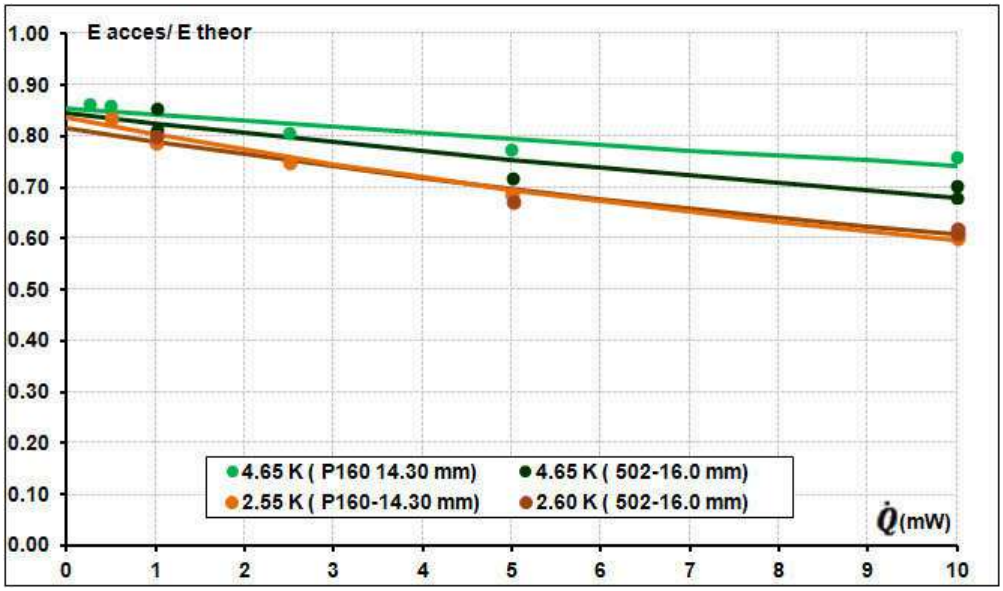


**Figure 4.67: Comparison of the ratio between accessible energy and theoretical energy as function of the applied load on bottom of the cell with 502 ceramic and P 160 ceramic for two different temperatures.**

The accessible energies found with the different cell are summarized in the Figure 4.68.

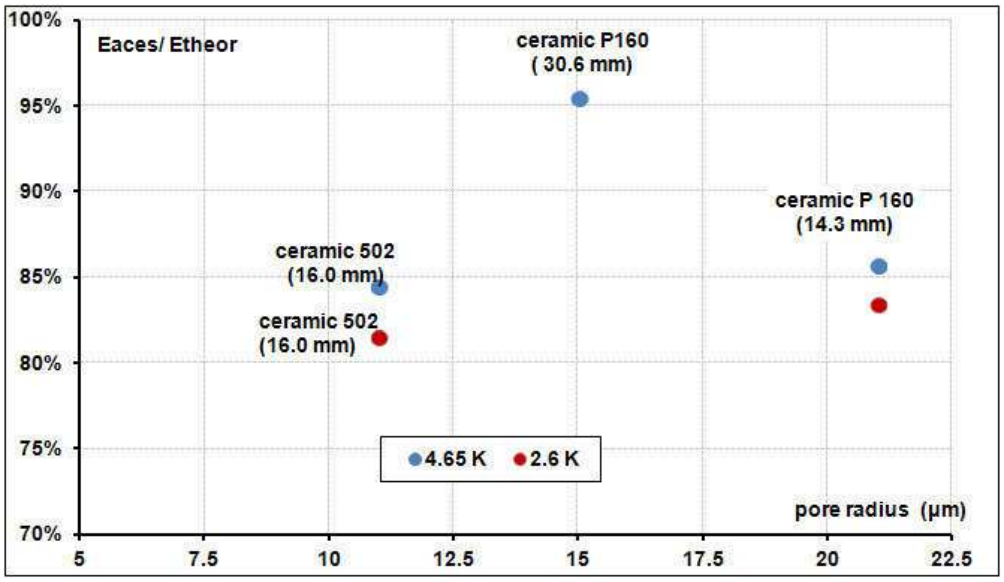


**Figure 4.68: The ratio between accessible energy and theoretical energy for the different cells when the cell is heated by the bottom. The accessible energies are plotted in function of the pore radius estimated using measurement performed by heating the cell by the top.**

### 4.7.4 Synthesis of heating up the bottom of the cell with ceramic

Three different cells were tested: two cells with P160 ceramic with different height (14.3 mm and 30.6 mm) and one cell with 502 ceramic (16.0 mm).The analysis of the results obtained, when the cell was heated up by the bottom, showed three important aspects.

The first one is that the ceramic decreases the temperature difference between the bottom and the top of the cell. This is probably due to the decrease of the thermal contact resistance between the heated surface and the liquid. This may be due to the fact that the ceramic allow the starting of the boiling regime for lower heat flux and that the ceramic increases the nucleation sites.

The second one is that the accessible energy is dependent of the applied heat load. This is probably due to the pressure drop of liquid and vapor in the ceramic. This dependence to the applied heat load increases when the temperature decreases. This is probably due to vapor pressure drop increase.

The third one is that a certain amount of liquid remains trapped in the ceramic and could not join the heated surface in order to be evaporating at saturated temperature. This quantity of liquid helium seems to be dependent of the height of cell and not of the pore radius. The quantity of helium is comprised between 16 % and 4.5 % in the configurations we have tested.

To have a perfect horizontal symmetry and check only the influence of gravity, the capillary tube allowing the vapor exit should have been moved from top to bottom, closed to the heated surface. In that case, equations of the previous model (see chapter 3.2) remain identical with the opposite sign in front of the gravity term. Analytical solution for accessible energy versus applied power would also lead to a hyperbolic dependence and it would have been nice to verify if same couple (e.g. pore size and permeability) can be used to fit with the experiments. Comparing this test with the one we have performed by heating the cell by the bottom would show the impact of the vapor pressure drop. Unfortunately, due to lack of time and cryostat availability these tests were not performed. It should be noticed also that if the capillary exit is placed at the bottom of the cell it should not be possible to fill the cell above the capillary height which could make difficult the reproduction of the tests performed heating up the cell by the top.

In the case studied, as the vapor is created at the bottom and released at the top, pressure losses corresponding to this flow path have to be introduced in the model. This will add a new free parameter in the model: distribution of pore size for the vapor flow is not known even if we can infer that vapor may flow along the large pores whereas liquid is pump by capillary effect along the smallest ones. That is why it was decided to present only experimental analysis. Anyway, experimental data fit well with hyperbolic shape and that corresponds to the expected behavior.

## 4.8 Conclusion

The studies performed in this chapter had as objective to understand the heat transfer in cell filled with porous media and with a two phase fluid when heat is applied in the cell walls.

The first conclusion is that the ceramic helps the liquid to climb against gravity but the length is limited with the kind of ceramic we had experienced (radius pore size in the range of 11 -21 μm). Smaller the radius pore is, larger distances the liquid climbs. The ceramic used limits the size of a reservoir fully gravity independent.

The second conclusion is that the accessible energy if ceramic is used dependent of the applied load. This dependence increased when the temperature decreases. So, it is necessary to have low applied load or large heat surface exchange in order to keep a reasonable level of flux. In the case of the Helium ESU dimensioned in Chapter 3, if considered that the sphere de 4 liter should adsorb 300 J during 1 hour using its entire surface, then the heat flux is 0.67 $W/m^2$. This flux corresponds to applied 0.1 mW in cell tested in this chapter. So, the loss due to the applied heat load will be very modest.

It has been shown that it is not possible to recover at saturation temperature all the theoretical energy and that around 10% is missing. This is due, at least for one part, to some helium that remains trapped in the ceramic and cannot reach the wall surface. This leads to the needs to oversize the ESU volume is ceramic is used.

The latest conclusion is the ceramic helps to reduce thermal gradient across the liquid solid interface. This is important for the ESU with stringent requirement in term of temperature drift.

This study gives valuable inputs for optimizing the design of energy storage unit dedicated to space environment.

# Chapter 5: Conclusion and Perspective

The use of cryocooler is very attractive as an autonomous and high longevity cold source. However, for some space applications, highly sensitive sensors require a vibrationless cold source offering a high thermal inertia.

In this thesis, the cryogenic liquid-vapor Energy Storage Units (ESUs) for spatial applications were investigated. In its first part, two systems using the latent heat associated to the evaporation of liquid nitrogen were studied. The main goal of these thermal buffers is to absorb a high quantity of thermal energy with a small temperature drift in a passive way.

The first system consists in a small cold reservoir filled with nitrogen and connected to an expansion volume at room temperature (dual volume configuration). The nitrogen is liquefied by cooling it down and coexists with its vapor. The evaporation of liquid inside the reservoir allows absorbing energy with the pressure increase being limited by the expansion volume. Two different expansion volumes were tested (6 liters and 24 liters) with the same low temperature reservoir. With a 6 liters expansion volume, it was possible to store 3.7 kJ drifting from 65 K to 83.5 K, while 4.0 kJ was stored between 75.7 K and 80.8 K with 24 liters expansion volume.

In the second system, the temperature drift (an inconvenient in particular for some spatial applications) was drastically reduced by installing a control valve between the reservoir at low temperature and the expansion volume. The function of this valve is to keep constant the cold reservoir pressure – and then the temperature - during the evaporation process. This new system allows storing 1.4 kJ at 81 K with a drift in temperature limited to $\approx 0.2$ K. This system allows building an ESU working at constant temperature that can be freely chosen along the saturation curve contrary to the thermal buffer using the triple point of the pure substances that could work only at some discrete constant temperature. Moreover, the latent heat associated to the liquid - vapor phase change is higher than the solid – liquid phase change latent heat (if not too close to the critical point), allowing the liquid – vapor ESU to use a more compact and lighter cold reservoir when compared to a triple point one.

The perspectives that emerged for future developments on this ESU:

- Cold expansion volume: For each run, the gas is pumped from the room temperature reservoir and goes inside the low temperature volume where it is thermalized and partly liquefied. This thermal cost may be avoided or reduced by using an expansion volume at an intermediate temperature instead of room temperature. The energy to cool down the gas and the expansion reservoir size would be reduced. This solution depends on the final application and on the cryogenic chain architecture.

- To avoid an electromagnetic mechanical valve for pressures control that can be a problem in the space due to its limited lifetime, one possibilities is:

    - Pneumatic valve: the electromagnetic valve could be replaced by a pneumatic valve at low temperature, actuated by a cryopump. A cryopump is composed by active charcoal and a control gas. When the cryopump is warmed up, the charcoal releases

the gas and the pressure controlling the valve aperture may increase until the valve becomes fully closed. The contrary happens by cooling down the cryopump, i.e. the control gas is adsorbed in the active charcoal and the valve would permit a smooth and continuous modulation of the flow.

To turn the liquid-vapor ESUs insensible to gravity, the liquid phase is confined inside the reservoir by filling it with an adequate porous material. For spatial application the ESUs should be light and a porous ceramic was used (porosity 90%, $\rho \approx 0.3$ g/cm$^3$).

During this thesis, it was demonstrated that in such a cell, this ceramic helps to homogenize the temperature in a first phase but isolates from the heated surface one part (15 % - 25 %) of the liquid that becomes difficult to evaporate. This last feature leads to a "useless volume". One way to limit this inconvenient would be to test:

- A porous medium with good thermal conduction such as aluminum or copper. However, this solution is difficult because metallic porous media with low density and high porosity are rare and are not available commercially with the small pore size we are looking for.

- A different form of the porous media in order to avoid long distance between the cell walls and the most internal part of the porous piece.

The reasons for the difficulty of accessing the evaporation of a fraction of the liquid needs to be understood or at least the quantity that remains trapped in the porous media needs to be quantified. This quantity has to be taken into account at the ESU design stage in order to fulfill the temperature drift requirements. In general, the impact of the porous media was found in need of being investigated and this is why a dedicated experimental set up was designed and built.

The porous media set-up as investigated was used with helium and allows a detailed analysis of the heat transfer in a liquid-vapor confined in a porous ceramic. It consists of a small cell with 2 potential heated surfaces located at its base and top and thermally isolated from each other. It was possible to measure the liquid quantity pumped thanks to capillarity effects against gravity by heating from the top of the cell. Tests have also been performed with gravity for comparison by heating the bottom of the cell. The set up was equipped with a very large expansion volume allowing operating at a quite constant saturation temperature, i.e. with known and fixed fluid properties. Results obtained at different saturation temperatures (2.55 K, 3.55 K and 4.65 K) and under different heat flux have been analyzed. The main conclusions on the different experiment runs are synthesized below

- When the heat load is applied at the top of the cell (the liquid to evaporate being pumped up against the gravity) the accessible energy increases when temperature decreases. These results can be explained by Jurin's Law: the capillary force increases with temperature decreases. For the same saturated temperature, still heating at the top of the cell the accessible energy depends on the applied load and this fact cannot be directly linked to Jurin's law. In this thesis it is shown that this behavior is due to the pressure drop of the liquid along the ceramic. A model based on a balance of forces has been developed to explain the experimental results. This model takes into account the capillary force, the gravity force and the pressure drop induced by the liquid flow. The results obtained by the model are in good agreement with the experimental results. It is interesting and surprising that such a simple model can describe the physics associated with a thermally driven liquid flow in a porous medium: Indeed, this model is based on a monodisperse pore size defining vertical parallel channels, and this description of ceramic is far from reality. A picture obtained from a SEM of a ceramic sample reveals a structure in the form of tangled "spaghettis" of various diameters.
- The experimental results when the liquid must go down (cell heated at the bottom) show once again that the ceramic retains 10-20% of liquid helium. Due to different constraints, this configuration is not the exact horizontal symmetry of the previous case: the capillary

for vapor exhaust remains at the top of the cell and the vapor must flow across the entire cell. For this reason, the previous model could not be applied by reversing only the gravity term. A model able to describe qualitatively the behavior when the cell is heating on the bottom may have to take into account the pressure drop of the vapor flow: this approach was not implemented here but would be useful to study. Same remark stands for the two cell configurations that haven't been tested yet (heating at the top and vapor exhaust at the bottom or heating and vapor exhaust at the bottom).

Others experiments in the cell with poor conductive side wall would be interesting for clarifying some additional point, for example:

- The influence of the properties of fluid: a test with other cryogenic fluids than helium, such as nitrogen would also be interesting for having different surface tension and liquid-vapor density.

- In terms of the ceramic height: two samples with different heights of the same ceramic were analyzed, showing the same overall behavior, even if the results differ slightly. Anyway, another test with different height is still needed to test whether this difference is relevant or not.

- Pore size of ceramic: two different ceramic samples with different pore sizes were tested but the difference between the sizes of pores was small, and it would be interesting to test another ceramic with a size pore one order of magnitude smaller than the ceramic tested.

The pre-design of ESU using helium and able to provide 300 J with a limited temperature drift has been carried out. This study was focused to a single volume configuration (no expansion volume). It shows that the thermal requirement imposes a quite large filling pressure, around 185 bars, in a significant volume, more than 4 liters leading to a total mass of 2.1 kg. This mass is partially due to mass of the ceramic that counts approximately for the half of the total mass. For use in spatial application a ESUs should be light. To decrease the weight of the helium ESU studied, it is thus necessary to find a ceramic with a density as low as possible or to reduce the ceramic volume inside the ESUs which has been assumed to fill the whole volume in our study. For example, one solution could be to put only a ceramic layer in contact with the cell wall. During the cooling down the liquid is produced close to the cell wall, assuming that the whole wall is cold, so the liquid is retained close to the wall where it will be evaporated later. It would be interesting to test if these ceramic layer configurations or others could work.

In conclusion, an original concept for a liquid-vapor ESU was demonstrated for a nitrogen cell working in the 63-83 K range. The problem of the temperature drift of such ESU was explored as well as the confinement of the liquid nitrogen inside the cell. The heat transfer inside the porous media that is used to confine the liquid was studied and a thermal model built up that fits well the experimental data. Some additional tests were suggested as a result of this study, but this study already gives valuable inputs for the design of ESU using the liquid vapor transition.

The liquid-vapor ESU is now a competitor with the already studied triple point ESU. Both solutions are able to provide a silent temporary cold source with a stable temperature. The choice of the more adequate ESU should be studied case-by-case: a triple point based ESU is only a solution if a triple point exists at the required temperature.

# References


[1] D. C. Bugby, R. G. Bettini, and M. Stoyanof, "60 K Thermal Storage Unit", Space Technology and Applications International Forum (STAIF-96), pp. 781–793, 1996.

[2] D. Bugby and B. Marland, Cryogenic thermal storage units in Spacecraft thermal control handbook- Volume II: Cryogenics, 2th edition, the Aerospace Press 2003, pp. 409–432.

[3] D. Bughy, R. Bettini, C. Stouffer, M. Stoyanof, and D. Glaister, "Development of a 60 K Thermal Storage Unit", Cryocoolers, vol. 9, pp. 747–764, 1997.

[4] V. T. Arkhipov, V. F. Getmanets, A. Y. Levin, and R. S. Mikhalchenko, "Cold Accumulators as a Way to Increase Lifetime and Cryosystem Temperature Range", Cryocoolers, vol. 10, pp. 689–696, 1999.

[5] Y. Ikushima, R. Li, T. Tomaru, N. Sato, T. Suzuki, T. Haruyama, T. Shintomi, and A. Yamamoto, "Ultra-low-vibration pulse-tube cryocooler system – cooling capacity and vibration", Cryogenics, vol. 48, no. 9–10, pp. 406–412, 2008.

[6] A. Rijpma, D. Meenderink, H. Reincke, G. Venhorst, H. Holland, and H. Brake, "A nitrogen triple-point thermal storage unit for cooling a SQUID magnetometer", Cryogenics, vol. 45, no. 3, pp. 231–239, 2005.

[7] G. Bonfait, I. Catarino, J. Afonso, D. Martins, M. Linder, and L. Duband, "20K Energy storage unit", Cryogenics, vol. 49, no. 7, pp. 326–333, 2009.

[8] I. Catarino, J. Afonso, D. Martins, M. Linder, L. Duband, and G. Bonfait, "6K solid state Energy Storage Unit", Cryogenics, vol. 50, no. 2, pp. 102–110, 2010.

[9] B. Wiliams and I. Spradley, "Test Results of a Nitrogen Triple-Point Thermal Storage Unit", Cryocoolers, vol. 10, pp. 697–706, 1999.

[10] L. Duband, J. M. Duval, N. Luchier, and T. Prouve, "SPICA sub-Kelvin cryogenic chains", Cryogenics, vol. 52, no. 4–6, pp. 145–151, 2012.

[11] P. Gully, "R & T CNES Volant thermique basse température Etude de besoin Etude de solutions", final rapport by Services des Basses Température, C.E:A Grenoble, 2011.

[12] J. Afonso, I. Catarino, D. Martins, J. Ricardo, R. Patricio, L. Duband, and G. Bonfait, "Energy storage unit: Solid state demonstrators at 20K and 6K", Cryogenics, vol. 50, no. 9, pp. 522–528, 2010.

[13] R. Levenduski, W. Gully, and J. Lester, “Hybrid 10 K Cryocooler for Space Applications”, Cryocoolers, vol. 10, pp. 505–511, 1999.

[14] R. Levenduski, J. Lester, and E. Marquardt, “A Hybrid Multistage 10K Cryocooler for Space Applications”, Cryocoolers, vol. 12, pp. 579–586, 2003.

[15] R. C. Levenduski and J. M. Lester, “A Thermal Storage Unit For Low Temperature Cryocoolers”, Cryocoolers, vol 13, pp. 583–592, 2004.

[16] I. Charles, A. Coynel, and C. Daniel, “Thermal Storage Unit Using the Triple Point of Hydrogen”, Cryocoolers, vol. 16, pp. 575–582, 2011.

[17] D. S. Glaister, K. D. Bell, M. Bello, and F. Edelstein, “Development and Verification of a Cryogenic Brilliant Eyes Thermal Storage Unit”, Journal of Spacecraft and Rockets, vol. 33, no. 4, 1996.

[18] D. Bugby, B. Marland, C. Stouffer, and E. Kroliczek, “Advanced Components for Cryogenic Integration”, Cryocoolers, vol. 12, pp. 693–708, 2003.

[19] D. Bughy, B. Marland, and C. Stouffer, “Development and Testing of a 35K cryogenic Thermal Storage Unit”, 41st Areospace Science Meeting and Exihibit, pp. 1–9, 2003.

[20] W. Gully, P. Hendershott, D. Glaister, and J. Lester, “Initial Test Results for a 35 K Variable Load Cryocooler”, Cryocoolers, vol. 15, pp. 545–551, 2009.

[21] D. C. Bugby, C. J. Stouffer, and L. M. Rich, “Experimental verification of a 60 K thermal storage unit”, Energy Conversion Engineering Conference, IECEC-97, Proceedings of the 32nd Intersociety, vol. 2, pp. 1427–1432, 1997.

[22] C. J. Stouffer, R. M. Hagood, and D. C. Bugby, “Cryogenic Thermal Storage Unit (CRYOTSU) Flight Experiment”, Energy Conversion Engineering Conference, IECEC-97, Proceedings of the 32nd Intersociety, vol. 2, pp. 1409–1414, 1997.

[23] D. C. Bugby, C. J. Stouffer, R. . Hagood, L. Michael, L. B. J. Tomlinson, M. Davis, and J. Ku, “Development and Testing of the CRYOTSU Flight Experiment”, Space Technology and Applications Internationl Forum,1999.

[24] D. Bugby, C. Stouffer, T. Davis, B. J. Tomlinson, L. M. Rich, J. Ku, T. Swanson, and D. Glaister, “Development of Advanced Cryogenic Integration Solutions”, Cryocoolers, vol. 10, pp. 671–687, 1999.

[25] K. Mizuno, Y. Miyazaki, K. Nagashima, A. Kawano, and T. Okamura, “Cold storage characteristics of mobile HTS magnet”, Cryogenics, vol. 51, no. 6, pp. 321–325, 2011.

[26] J. Afonso, I. Catarino, R. Patrício, a. Rocaboy, M. Linder, and G. Bonfait, “Liquid nitrogen energy storage unit”, Cryogenics, vol. 51, no. 11–12, pp. 621–629, 2011.

[27] J. P. Afonso, “Unidade criogénica de armazenamento de energia com mudança de *fase”*,Physical engineering Master Thesis, Faculdade de Ciência e Tecnologia da Universidade Nova de Lisboa, 2009.

[28] I. Catarino, G. Bonfait, and L. Duband, “Neon gas-gap heat switch”, Cryogenics, vol. 48, no. 1–2, pp. 17–25, 2008.

[29] D. Martins, I. Catarino, U. Schroder, J. Ricardo, R. Patricio, L. Duband, G. Bonfait, and J. G. Weisend, "Customizable gas-gap heat switch", in AIP Conference Proceedings, 2010, vol. 1218, no. 1, pp. 1652–1660.

[30] E. W. Lemmon, M. L. Huber, and M. O. McLinden, "NIST Standard Reference database 23: Reference fluid Thermodynamic and Transport Properties- REFPROP, Version 8.0, National Institute of Standards and Tecnology, standard Reference Data Program, Gaithersburg", 2007.

[31] J. Ekin, Experimental Techniques for Low-Temperature Measurements, Oxford University Press, USA, 2006, p. 62.

[32] L. Duband, L. Clerc, E. Ercolani, L. Guillemet, and R. Vallcorba, "Herschel flight models sorption coolers", Cryogenics, vol. 48, no. 3–4, pp. 95–105, 2008.

[33] NIST web page, "NIST Livro de Química na Web." [Online]. Available: http://webbook.nist.gov/chemistry/. [Accessed: 13-Dec-2012].

[34] G. Bruhat, A. Kastler, and R. Vichnievsky, *Cours de physique générale : à l'usage de* l'enseignement supérieur scientifique et technique. Thermodynamique, 5$^{e}$ édition, Paris: Masson & C, 1933, pp. 210–213.

[35] "ECSS-E-ST-32C Rev. 1,Space engineering Structural design and verification of pressurized hardware", ESA Requirements and Standards Division.

[36] W. Young and R. Budynas, *Roark's Formulas for Stress and Strain*, 5$^{th}$ edition. McGraw-Hill Professional, 2001, p. 832.

[37] "cryogenic material properties." [Online]. Available: http://www.cryogenics.nist.gov/MPropsMAY/RegeneratorMaterials/RegenPlot.htm. [Accessed: 08-Jan-2013].

[38] A. W. Adamson and A. G. Petry, Physical Chemistry of Surfaces, 6$^{th}$ edition, Wiley-Interscience, 1997, p. 354.

[39] "157 | Castolin Eutectic." [Online]. Available: http://www.castolin.com/product/157-0. [Accessed: 28-Nov-2012].

[40] auteur collectif (IIF-IIR), Croyogénie. Ses applications en supraconductivité, Technique de l'Ingenieur, Paris, 1995, p. 108.

[41] "cryogenic material properties 304L Stainless." [Online]. Available: http://www.cryogenics.nist.gov/MPropsMAY/304LStainless/304LStainless_rev.htm. [Accessed: 27-Oct-2012].

[42] Y. Cengel, Heat and Mass Transfer: A Practical Approach, McGraw-Hill, 2006, p. 928.

[43] S. Bories, A. Mojtabi, M. Prat, and M. Quintard, *"Transferts de chaleur dans les milieux poreux"*,Tecniques de L'Ingenieur, Paris,1995, pp. 1–22.

[44] V. Arp, R. McCarty, and F. Jeffrey, "Hepak" version 3.4, Cryodata, Inc, Data Program.

[45] «. V.M. KISEEV, V.A. NOUROUTDINOV, N.P. POGORELOV, “Analysis of maximal heat transfer capacity of capillary loops,” Proc. of 9th International Heat Pipe Conf., pp. 1007–1014, 1995.

# Appendix A: Table of test in the configuration "Controlled liquid enthalpy reservoir"

Table A.1 summarizes the various runs performed in the configuration "Controlled liquid enthalpy reservoir" with ceramic and the gas exhausts located in the upper or bottom part of the cell. The columns of the table are:

**$V_{exp}$:** dimension of expansion volume.

**$T_{CB}$:** temperature of the cold finger during the ESU mode. If ramping, the initial temperature was $T_{PC.}$

**$P_{fill}$:** pressure of filling the system at room temperature.

**$T_{PC}$:** temperature of pre-cooling enthalpy reservoir.

**$P_{min}$:** pressure corresponding to the pre-cooling temperature ($T_{PC}$).

**$T_{liq}$ cont:** is the temperature which the valve opens to maintain the liquid temperature between [$T_{liq}$ cont- 0.1K, $T_{liq}$ cont] and (0.1 K corresponds to 0.016 bar).

**P cont:** pressure corresponding to the liquid control temperature ($T_{liq}$ cont).

**P:** applied load in the enthalpy reservoir.

***Δt*:** duration of plateau.

**Calculated energy**: is calculated from the liquid-gas latent heat multiplied by the number of liquid moles evaporated.

**Useful energy**: is the energy dissipated by the sensor during the ESU mode (= Power x ESU-mode duration).

**Experimental energy**: is the energy dissipated by the sensor during the ESU mode +estimation of parasitical heat ( through the heat swith and by radiation).

**Error:** is calculated between the calculated stored energy and useful energy +parasitical .

**Initial volumic fraction of liquid**: liquid volume fraction at the beginning to the ESU.

**Final volumic fraction of liquid:** liquid volume fraction at the end to the ESU mode.

**Table A.1: Summary of tests. Case of “controlled liquid enthalpy reservoir” with ceramic with gas exhausted located in the upper or bottom part of the cell.**

| | Vexp(L) | $T_{CB\,(K)}$ | $P_{fill}$ (bar) | $T_{PC\,(K)}$ | $P_{min}$ (bar) | $T_{liq}$ cont (K) | P cont (bar) | P(W) | Δt (min) | calculated E(J) | useful E(J) | experimental E(J) | error | initial volumic fraction of liquid(%) | final volumic fraction of liquid(%) | exhaust position | fig |
|---|---|---|---|---|---|---|---|---|---|---|---|---|---|---|---|---|---|
| 1 | | 0.8K/min | 1.98 | 65.0 | 0.174 | 81.1 | 1.54 | 0.5 | 46 | 1522 | 1382 | 1447 | -4.9% | 41 | 13 | upper | |
| 2 | | 1.63K/min | 2.00 | 65.0 | 0.174 | 81.1 | 1.54 | 1.0 | 24 | 1369 | 1424 | 1461 | 6.7% | 41 | 14 | upper | 2.18 |
| 3 | | 0.8K/min | 3.00 | 64.3 | 0.154 | 81.1 | 1.54 | 0.5 | 49 | 1658 | 1460 | 1536 | -7.3% | 65 | 35 | upper | |
| 4 | | 1.63K/min | 2.50 | 64.0 | 0.146 | 81.1 | 1.54 | 1.0 | 25 | 1518 | 1524 | 1543 | 1.7% | 54 | 26 | upper | 2.21 |
| 5 | | 1.63K/min | 2.00 | 64.3 | 0.154 | 81.1 | 1.54 | 1.0 | 21 | 1368 | 1272 | 1304 | -4.7% | 41 | 16 | bottom | |
| 6 | | 0.8K/min | 2.00 | 64.0 | 0.146 | 81.1 | 1.54 | 0.5 | 47 | 1648 | 1370 | 1437 | -12.8% | 42 | 12 | bottom | 2.20 |
| 7 | 6 | 1.63K/min | 2.50 | 64.2 | 0.152 | 81.1 | 1.54 | 1.0 | 22 | 1407 | 1308 | 1339 | -4.8% | 53 | 28 | bottom | |
| 8 | | 0.8 K/min | 2.50 | 64.0 | 0.146 | 81.1 | 1.54 | 0.5 | 44 | 1621 | 1332 | 1394 | -14.0% | 53 | 24 | bottom | 2.20 |
| 9 | | 0.8K/min | 2.50 | 63.7 | 0.138 | 77.1 | 0.98 | 0.5 | 29 | 968 | 862 | 885 | -8.5% | 53 | 36 | bottom | |
| 10 | | 81 K | 2.50 | 65.6 | 0.193 | 81.1 | 1.54 | 0.5 | 58 | 1728 | 1746 | 1745 | 1.0% | 54 | 22 | bottom | |
| 11 | | 81 K | 2.50 | 63.5 | 0.133 | 81.0 | 1.53 | 1.0 | 26 | 1544 | 1576 | 1576 | 2.0% | 54 | 25 | bottom | |
| 12 | | 1.63K/min | 2.50 | 64.0 | 0.146 | 81.1 | 1.54 | 1.0 | 25 | 1524 | 1508 | 1527 | 0.2% | 49 | 24 | bottom | 2.21 |
| 13 | | 65 K | 2.50 | 67.0 | 0.243 | 83.1 | 1.90 | 1.0 | 34 | 1767 | 2040 | 1989 | 12.6% | 49 | 16 | bottom | |
| 14 | | 77 K | 1.26 | 70.0 | 0.385 | 77.1 | 0.98 | 0.5 | 88 | 2868 | 2652 | 2650 | -7.6% | 82 | 32 | bottom | |
| 15 | | 81 K | 1.55 | 71.8 | 0.497 | 81.1 | 1.54 | 0.5 | 127 | 4065 | 3808 | 3806 | -6.4% | 92 | 17 | bottom | |
| 16 | 24 | 0.8 K/min | 1.25 | 70.2 | 0.396 | 77.1 | 0.98 | 0.5 | 75 | 2627 | 2252 | 2436 | -7.2% | 83 | 33 | bottom | 2.22 |
| 17 | | 0.8K/min | 1.25 | 73.3 | 0.610 | 81.0 | 1.53 | 0.5 | 88 | 2868 | 2652 | 2649 | -7.6% | 93 | 5 | bottom | |
| 18 | | 0.18K/min | 1.55 | 73.0 | 0.587 | 81.1 | 1.54 | 0.5 | 127 | 4256 | 3800 | 3902 | -8.3% | 91 | 12 | bottom | |
| 19 | | 0.22K/min | 1.55 | 72.7 | 0.566 | 81.0 | 1.52 | 1.0 | 59 | 3845 | 3560 | 3588 | -6.7% | 95 | 25 | bottom | |

# Appendix B: Nitrogen Properties

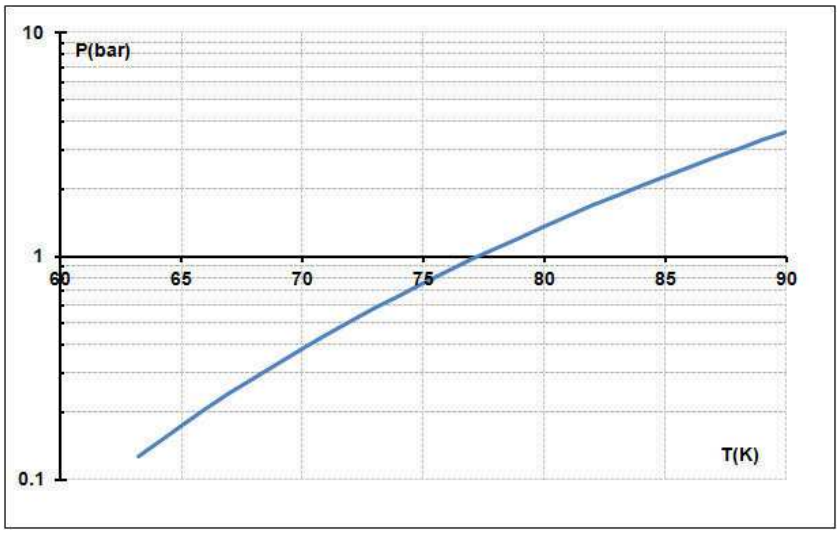


**Figure B.1: Saturation curve of nitrogen.**

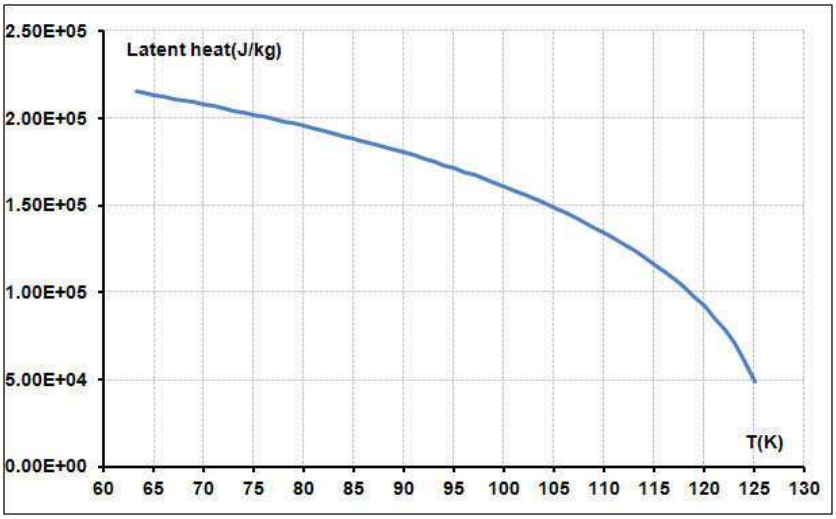


**Figure B.2: Latent heat of nitrogen in function of temperature.**

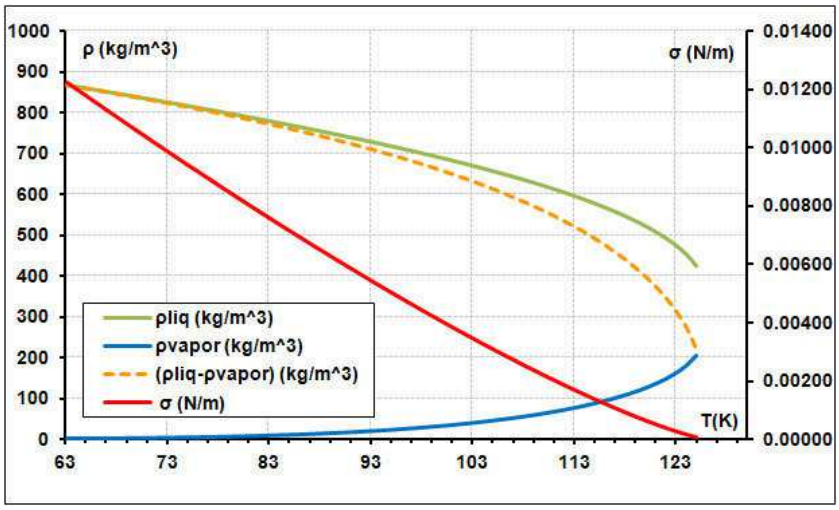


**Figure B.3: Variation of liquid, gas density, difference between density (left axis) and surface tension (right axis) with temperature.**

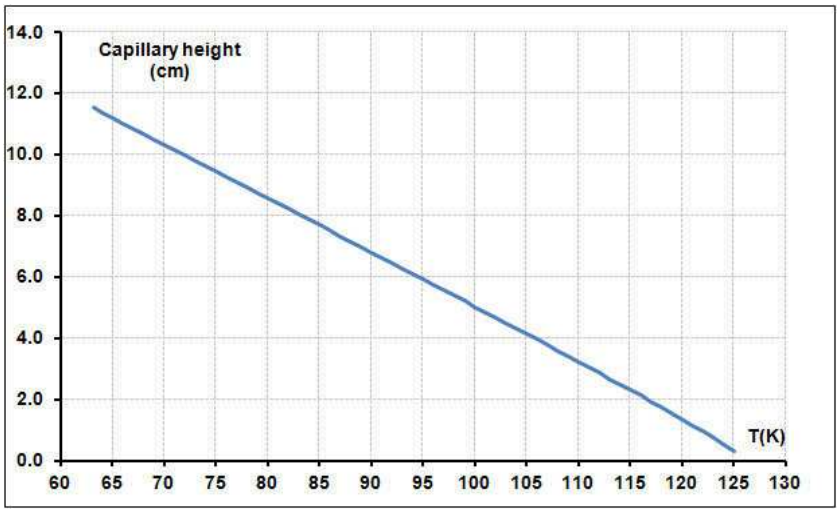


**Figure B.4: Capillary height versus temperature calculated for $\phi$= 50 µm.**

# Appendix C: Helium Properties

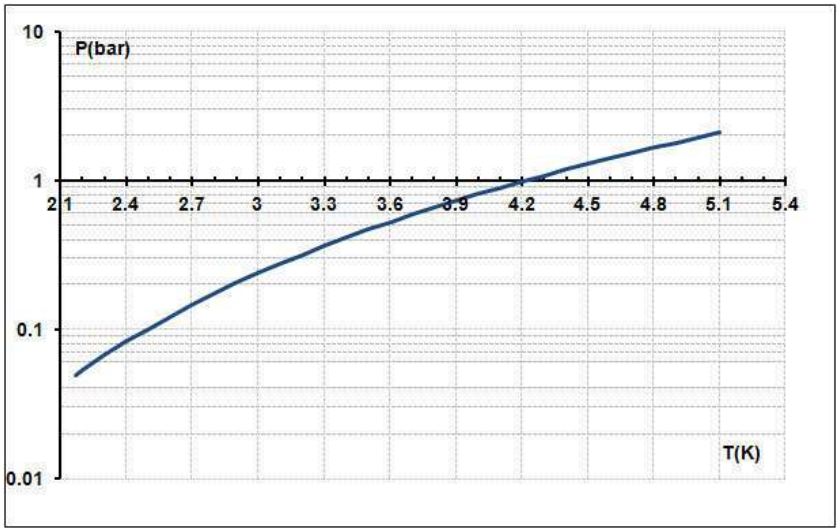


**Figure C.1: Thermal resistance contributions between the two cell ends for wall, full gas or full liquid.**

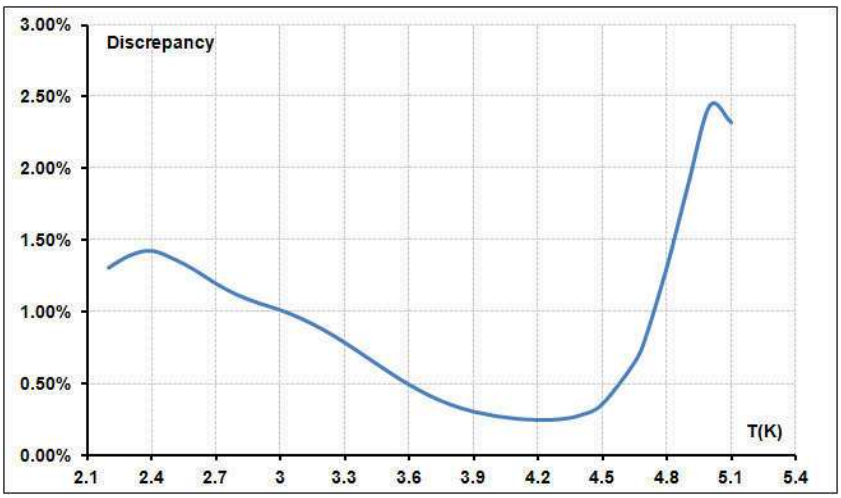


**Figure C.2: Discrepancy between the latent heat and the difference between the enthalpy of the liquid and the vapor from Hepak.**